Shear Flow Behavior and Molecular Structure of High Melt Strength Polypropylenes

by

Chunxia He

Department of Chemical Engineering

McGill University, Montreal

March 2003

A thesis submitted to the Faculty of Graduate Studies in partial fulfillment of the requirement of the degree of Doctor of Philosophy

Library and
Archives Canada

Published Heritage
Branch

395 Wellington Street
Ottawa ON K1A 0N4
Canada

Bibliothèque et
Archives Canada

Direction du
Patrimoine de l'édition

395, rue Wellington
Ottawa ON K1A 0N4
Canada

Your file Votre référence
ISBN: 0-612-88607-7
Our file Notre référence
ISBN: 0-612-88607-7

The author has granted a non-exclusive license allowing the Library and Archives Canada to reproduce, loan, distribute or sell copies of this thesis in microform, paper or electronic formats.

The author retains ownership of the copyright in this thesis. Neither the thesis nor substantial extracts from it may be printed or otherwise reproduced without the author's permission.

L'auteur a accordé une licence non exclusive permettant à la Bibliothèque et Archives Canada de reproduire, prêter, distribuer ou vendre des copies de cette thèse sous la forme de microfiche/film, de reproduction sur papier ou sur format électronique.

L'auteur conserve la propriété du droit d'auteur qui protège cette thèse. Ni la thèse ni des extraits substantiels de celle-ci ne doivent être imprimés ou aturement reproduits sans son autorisation.

In compliance with the Canadian Privacy Act some supporting forms may have been removed from this thesis.

While these forms may be included in the document page count, their removal does not represent any loss of content from the thesis.

Conformément à la loi canadienne sur la protection de la vie privée, quelques formulaires secondaires ont été enlevés de cette thèse.

Bien que ces formulaires aient inclus dans la pagination, il n'y aura aucun contenu manquant.

Canada

In memory of my grandparents

何永桥 宣美花
你们永远活在我的心中

Abstract

Linear shear flow behavior and molecular structure studies were carried out on linear polypropylenes produced using Ziegler-Natta catalysts and sets of branched polypropylenes produced from these linear precursors.

A method combining dynamic and creep measurements was employed to obtain a complete picture of the linear viscoelastic behavior of these polypropylenes. It was found that all samples in a set of polypropylenes have the same linear viscoelastic behavior in the high-frequency range, but display dramatic differences at low frequencies. Increasing branching level results in a steep increase of the zero-shear viscosity, an increase of the steady-state compliance, and a broadening of the relaxation spectrum whose shape changes dramatically and peaks shift to longer times.

Molecular models were tested and applied to the linear polypropylenes to predict linear viscoelastic properties from the molecular weight distribution (MWD). The parameters obtained from the best fit of predicted and experimental data of linear polypropylenes were used to calculate a fictive relaxation spectrum for branched polymers from their MWDs as if they were linear. The comparison between this predicted result and the experimental spectrum showed the separate effects of polydispersity and branching on rheology.

To obtain detailed structural information, the branching process of polypropylenes was simulated using a Monte-Carlo approach, which provides detailed information such as MWD and branching distribution. The simulated MWD was adjusted to the measured GPC curve using a single parameter simply related to the branching density λ (LCB/1000C). Relations between branching parameters and moments of the MWD were determined, which offer the possibility to calculate branching parameters directly from GPC results. The branching efficiency was estimated and correlations between engineering properties of polypropylenes and the structural information were obtained, which is of valuable industrial interest for polymer design.

A determination of the weight fractions of branches and segments between branch points from the relaxation spectrum is proposed. Due to the complexity of molecular relaxation mechanisms, only approximate correlations between molecular architecture and rheology were observed.

Resumé

Cette étude est consacrée au comportement linéaire en écoulement de polypropylènes linéaires synthétisés par polymérisation à l'aide de catalyseurs de type Ziegler-Natta et de leurs dérivés branchés obtenus par l'adjonction en proportions variées d'un agent réticulant.

Afin d'obtenir la signature complète du comportement viscoélastique de ces polypropylènes, on a employé une technique de superposition des mesures obtenues en fluage et en oscillation permettant de reconstituer le spectre de relaxation complet. On a pu observer que pour un ensemble de polypropylènes issus du même précurseur linéaire, le comportement viscoélastique à hautes fréquences est identique. En revanche le comportement à basses fréquences est très fortement modifié : une augmentation de la concentration en agents réticulants entraîne une nette croissance de la viscosité à cisaillement nul, une augmentation de la complaisance d'équilibre et un changement de forme du spectre de relaxation qui s'élargit et dont les pics sont décalés vers les temps longs.

En complément de l'étude expérimentale, on a testé plusieurs modèles moléculaires théoriques visant à prédire les propriétés viscoélastiques de polymères linéaires à partir de leur distribution de poids moléculaires (DPM). Les paramètres moléculaires obtenus à l'aide du modèle le plus performant ont été utilisés pour prédire un spectre de relaxation fictif pour les polymères branchés à partir de leur DPM, comme s'ils étaient linéaires. La comparaison avec le spectre déterminé expérimentalement montrent les effets respectifs de la polydispersité et du branchements sur le comportement rhéologique.

Pour obtenir de plus amples informations sur la structure moléculaire, on a simulé la réticulation des polypropylènes par extrusion réactive à l'aide d'une méthode de type Monte-Carlo qui permet d'obtenir des informations telle la DPM ou la distribution en masse de la densité de branchement. En ajustant un unique paramètre relié directement à la densité de branchement, on a pu reproduire par simulation la DPM mesurée par GPC.

Il a alors été possible de déduire la densité de branchement à partir des moments de la DPM uniquement. On a alors estimé l'efficacité de l'agent réticulant et on a obtenu des corrélations entre les informations structurales et les propriétés de mise en œuvre des polypropylènes qui revêtent un intérêt industriel pour la conception de polymères améliorés.

Enfin on propose un moyen d'obtenir les fractions massiques des branches longues et des segments entre points de branchement à partir du spectre de relaxation. Compte-tenu de la complexité des mécanismes de relaxation moléculaire, il est difficile de trouver des relations générales entre l'architecture moléculaire et le comportement rhéologique.

Acknowledgements

First, I would like to express my gratitude to my supervisor Paula Wood-Adams for her support, belief in me and friendship during this work.

My special thanks go to John Dealy, my advisor, for his mentorship and guidance. I am grateful for his active support throughout this project and the opportunities that he has afforded me.

I express my special appreciation to Stéphane Costeux, for his constant support, his many encouragements and for innumerable and valuable discussions which sometimes turned into animated debates.

I am indebted to The Dow Chemical Company who provided financial support, samples and characterization data, and especially to Teresa Karjala, Robert Sammler and Steve Chum who initiated this work and allowed me to make it public. I am also grateful to Willem Degroot, Marc Mangnus and Barbara Seliskar for sending me valuable information on rheology and chromatography procedures.

A sincere thank you to Cattaleeya Pattamaprom and Frédéric Léonardi, who shared with me their knowledge about molecular theory models.

I extend my thanks to Hee-Eon Park, Siripon Anantawaraskul, Kang Zhu and Junke Xu, my colleagues in the rheology research group, and to Hongmei Wei, Lijun Feng and Mohsen Sadeghi for their friendly support.

I gratefully acknowledge the staff of the Chemical Engineering Department, especially Alain Gagnon, Charles Dolan for always providing prompt technical service in the rheology lab.

I wish to recognize the strong part that my parents and siblings played in the completion of this work, for giving me, despite the distance which keeps us apart, their deep affection, their never-failing support and encouragement, and for always believing I could overcome so many difficulties.

Table of Contents

Abstract iii

Resumé v

Acknowledgements vii

Table of Contents viii

List of Figures xi

List of Tables xviii

Chapter 1. Introduction 1
- 1.1. Commercial Importance of Polypropylene 1
- 1.2. Linear Polypropylene 3
  - 1.2.1. Ziegler-Natta Polypropylene 3
  - 1.2.2. Metallocene Polypropylene 5
  - 1.2.3. Manufacture of Linear Polypropylene 8
  - 1.2.4. Engineering Properties of Linear Polypropylene 9
- 1.3. High Melt Strength Polypropylene 9
  - 1.3.1. Definition and Structure 9
  - 1.3.2. Manufacture of High Melt Strength Polypropylene 11
  - 1.3.3. Engineering Properties of High Melt Strength Polypropylene 13
- 1.4. Research Objectives 14
- Reference 15

Chapter 2. Methods for Determining the Branching Level in Polymers 17
- 2.1. Introduction 17
- 2.2. Methods for Determining Branching Level in Polymers 18
  - 2.2.1. Nuclear Magnetic Resonance 18
  - 2.2.2. Technique Based on the Reduced Radius of Gyration 21
  - 2.2.3. Rheological Property Based Methods 25
  - 2.2.4. Modeling of the Branching Process 26
- References 27

Chapter 3. Materials 29
- 3.1. Preparation 29
- 3.2. Properties 30
- 3.3. Sample Applications in This Study 32
- Reference 35

Chapter 4. Experimental Methods and Data 37
4.1. Relevant Linear Viscoelastic Functions 37
4.2. Effects of Long-Chain Branches on Linear Viscoelastic Properties 44
4.3. Experimental Methods and Data 51
4.3.1. Determination of Suitable Experimental Temperature 51
4.3.2. Small-Amplitude Oscillatory Shear 54
4.3.2.1. Thermal Stability of Samples 54
4.3.2.2. Limit of Linear Response 57
4.3.2.3. Oscillatory Shear Measurements 59
4.3.3. Creep and Creep Recovery 63
4.3.3.1. Linearity of The Response 63
4.3.3.2. Creep Compliance at Long Times 64
4.4. Results and Discussion 70
4.4.1. Discussion of Experimental Data 70
4.4.2. Conversion of Material Functions 72
4.4.2.1. Combination of Dynamic and Creep Recovery Results 72
4.4.2.2. Limitations of the Combined Method 82
4.4.2.3. Time-Weighted Relaxation Spectrum 83
References 87

Chapter 5. Modeling of Linear Viscoelastic Behavior of Polypropylenes 90
5.1. Introduction 90
5.2. Summary of the Two Models 95
5.2.1. The Dual Constraint Model 95
5.2.2. A Modified Double Reptation Model 100
5.3. Comparison of Predictions for 35L Using The Two Models 102
5.4. Predictions for The MFR 35 Set 106
5.4.1. Predicted Complex Moduli and Discussion 106
5.4.2. Transformation of Moduli to Time-Weighted Relaxation Spectrum 109
5.5. Predictions for the MFR 2 Set 113
5.5.1. Predicted Complex Moduli and Discussion 113
5.5.2. Transformation of Moduli to Time-Weighted Relaxation Spectrum 116
5.6. Conclusions 121
References 121

Chapter 6. Modeling of Polypropylene Branching Process 125
6.1. Introduction 125
6.2. Review of Modeling of Structure in Branched Polymers 126
6.3. The Monte Carlo Simulation used in This Study 134
6.4. Numerical Procedures of the Monte Carlo Simulation 135
6.4.1. Creation of Linear Precursor Chains 135
6.4.2. Creation of Branched Chains 137
6.4.3. Triple Detector Gel Permeation Chromatography 140
6.5. Results and Discussion 141
6.5.1. The Molecular Weight Distributions 141

6.5.2. Branching Information 154
6.5.3. Relationship between Molecular Weights and Branching Parameters ... 162
6.5.4. Branching Efficiency 169
6.5.5. Segment Compositions of Branched Systems 170
6.5.6. Relating Engineering Properties to Structural Information 173
6.5.7. Cyclization 175
6.6. Conclusions 176
References 178

Chapter 7. Structure Determination from Rheology 180
7.1. Introduction 180
7.2. Rheological Method to Determine the Branching Level 180
7.3. Inferring Branching Information from Rheological Data 186
7.3.1. Assignment of the relaxation spectrum peaks 186
7.3.2. Results and Discussion 190
7.3.3. Requirements of the Technique 194
7.4. Conclusions 195
Reference 195

Chapter 8. Conclusions 197

Chapter 9. Contributions to Knowledge 199

Bibliography 200

Appendix A. Differential Scanning Calorimetry Results 207

Appendix B: Determine Molecular Weight Corresponding to A Random Number From Cumulative Molecular Weight Distribution Curve 208

Nomenclature 210

List of Figures

Figure 1-1. U.S. PP production, 1960-1993. (U.S. International Trade Commission)........2
Figure 1-2: World PP consumption from 1998 to 2005 (from Gobi international)............3
Figure 1-3: Atom coordinating of titanium on the surface and interior of an α-crystal......4
Figure 1-4: Structure of the activated catalyst...4
Figure 1-5: (a) Isotactic and (b) syndiotactic configuration of a PP chain[1].........................5
Figure 1-6: Single-site catalyst for isotactic PP...6
Figure 1-7: bis(2-phenylindenyl)zirconium dichloride in *rac* and *meso* form.....................6
Figure 1-8: Solid-state structure of impact improved metallocene polypropylene.............7
Figure 1-9: Sketch of the tensile behavior of a polymer having high melt strength..........10
Figure 1-10: Sketch of some possible branching structures...11
Figure 1-11: β scission and branching in polypropylene..12
Figure 2-1: Microstructure of long and short chain branched mPE.................................19
Figure 2-2: Dependence of λ, as determined by the Zimm-Stockmayer method, on the intrinsic viscosity ratio, at two different molecular weights and for essentially linear PE...25
Figure 4-1: Sketch of a typical creep compliance curve for a polymer melt.....................40
Figure 4-2: The Maxwell element...41
Figure 4-3: The Voigt element..43
Figure 4-4: Schematic of some branched structures..44
Figure 4-5: Ratio of zero-shear viscosities of branched and linear fractions having the same molecular weight M_w vs. branching index g'..46
Figure 4-6: Dependency of $|\eta^*|$ on ω for high-density, branched mPEs at 150 °C..........48
Figure 4-7: Comparison of the creep and recoverable compliances of the two mLLDPE 49
Figure 4-8: Shear thinning behavior of the two mLLDPEs...50
Figure 4-9: Dependency of $|\eta^*|$ on frequency ω for the set of 12 MFR samples, 175 °C .52
Figure 4-10: Dependency of $|\eta^*|$ on time t for 12B1 at various molding and experimental temperatures, and $\omega = 1\mathrm{s}^{-1}$, $\gamma_0 = 5\%$...53
Figure 4-11: Dependency of $|\eta^*|$ on time t for linear isotactic polypropylene 20L and 20L-extruded at T = 180 °C, and $\omega = 1\mathrm{s}^{-1}$, $\gamma_0 = 5\%$..55
Figure 4-12: Dependency of $|\eta^*|$ on time t for linear isotactic polypropylene 35L at T = 180 °C, and $\omega = 1\mathrm{s}^{-1}$, $\gamma_0 = 5\%$...56
Figure 4-13: Dependency of $|\eta^*|$ on time t for branched isotactic polypropylene 35B3 at T = 180 °C, and $\omega = 1\mathrm{s}^{-1}$, $\gamma_0 = 5\%$...56
Figure 4-14: Dependency of complex moduli on stress amplitude for branched polypropylene 2B1 at 180 °C and 1 rad/s...58
Figure 4-15: Dependency of complex moduli on stress amplitude for branched polypropylene 2B1 at 180 °C and 100 rad/s...58

Figure 4-16: Dependency of |η*| and moduli on angular frequency ω for linear polypropylene 20L and 20L-extruded at 180 °C......59
Figure 4-17: Dependency of storage modulus G' on angular frequency ω for the set of 35 MFR polypropylene samples at 180 °C......60
Figure 4-18: Dependency of loss modulus G'' on angular frequency ω for the set of 35 MFR polypropylene samples at 180 °C......60
Figure 4-19: Dependency of |η*| on angular frequency ω for linear polypropylene 35L and three branched polypropylene 35B1, 35B2 and 35B3 at 180 °C......61
Figure 4-20: Dependency of storage modulus G' on angular frequency ω for linear PP 2L and four branched PP 2B1, 2B2, 2B3 and 2B4 at 180 °C......61
Figure 4-21: Dependency of loss modulus G'' on angular frequency ω for linear PP 2L and four branched PP 2B1, 2B2, 2B3 and 2B4 at 180 °C......62
Figure 4-22: Dependency of |η*| on angular frequency ω for linear PP 2L and four branched PP 2B1, 2B2, 2B3 and 2B4 at 180 °C......62
Figure 4-23: Creep compliance of 35B2 at different stresses and creep time (180 °C).....64
Figure 4-24: Dependency of strain on time in a creep and recovery test of branched polypropylene 35B2 at 10Pa, 180 °C......65
Figure 4-25: Dependency of creep compliance on time for branched polypropylene sample 35B2 in an extended time window obtained from the results in Fig. 4.24 at 180 °C......67
Figure 4-26: Dependency of strain and creep compliance on time for branched polypropylene sample 35B3 at 20 Pa, 180 °C......67
Figure 4-27: Dependency of strain and creep compliance on time for linear polypropylene sample 2L at 10 Pa, 180 °C......68
Figure 4-28: Dependency of strain and creep compliance on time for branched polypropylene sample 2B1 at 30 Pa, 180 °C......68
Figure 4-29: Dependency of strain and creep compliance on time for branched polypropylene sample 2B2 at 30 Pa, 180 °C......69
Figure 4-30: Dependency of strain and creep compliance on time for branched polypropylene sample 2B3 at 30 Pa, 180 °C......69
Figure 4-31: Dependency of strain and creep compliance on time for branched polypropylene sample 2B4 at 30 Pa, 180 °C......70
Figure 4-32: Retardation spectra for 35B2 obtained from dynamic moduli and creep compliance (180 °C)......75
Figure 4-33: Retardation spectra for 35B3 obtained from dynamic moduli and creep compliance (180 °C)......76
Figure 4-34: Retardation spectra for 2L obtained from dynamic moduli and creep compliance (180 °C)......76
Figure 4-35: Retardation spectra for 2B1 obtained from dynamic moduli and creep compliance (180 °C)......77
Figure 4-36: Retardation spectra for 2B2 obtained from dynamic moduli and creep compliance (180 °C)......77
Figure 4-37: Retardation spectra for 2B3 obtained from dynamic moduli and creep compliance (180 °C)......78

Figure 4-38: Retardation spectra for 2B4 obtained from dynamic moduli and creep compliance (180 °C) 78
Figure 4-39: Combined retardation spectrum for 35B2 and 35B3 at 180 °C 79
Figure 4-40: Combined retardation spectrum for linear sample 2L and four branched samples 2B1, 2B2, 2B3, 2B4 at 180 °C 80
Figure 4-41: Complex viscosities of the four samples shown in Fig.4.19 Solid lines are combined results in the extended window 81
Figure 4-42: Complex viscosities of the five samples shown in Fig.4.22. Solid lines are combined results in the extended window 81
Figure 4-43: Time-weighted relaxation spectrum of 2B4 at 180 °C. Dashed line is the results calculated from only dynamic data. Solid line is the results from the combined data of dynamic and creep/recovery 83
Figure 4-44: Relaxation spectrum of 35B2. The solid line is from the combined results of dynamic and interrupted creep; the open circles are oscillatory shear data. The dashed vertical line is the limit of the dynamic experiment, and the solid vertical lines are the limits of the creep experiment 84
Figure 4-45: Relaxation spectrum of 20L before and after extrusion 84
Figure 4-46: Normalized time-weighted relaxation spectra of MFR 35 polypropylenes .. 85
Figure 4-47: Normalized time-weighted relaxation spectra of MFR 2 polypropylenes 85
Figure 5-1: The chains A and B are entangled and there is a stress point at P 93
Figure 5-2: The crossover function (solid line) from $\tau_{early,i}$ (dotted line) to $\tau_{late,i}$ (dashed line). The crossover points are indicated by C_1 and C_2 (ref. 15) 97
Figure 5-3: Comparison of the dual constraint model predictions of storage and loss moduli (solid line) with experimental data (symbols) for 35L at 180 °C 103
Figure 5-4: Comparison of the double reptation model predictions of relaxation modulus (solid line) with experimental data (symbols) for 35L at 180 °C 104
Figure 5-5: Time weighted relaxation spectrum for 35L at 180 °C from experimental data (symbols) and from predicted data using the dual constraint model (solid line) 105
Figure 5-6: Time weighted relaxation spectrum for 35L at 180 °C from experimental data (symbols) and from predicted data using the double reptation model (solid line) .. 105
Figure 5-7: Comparison of the dual constraint model predictions of storage and loss moduli (solid line) of $(35B1)_{LE}$ with the experimental data for 35B1 (symbols) at 180 °C 107
Figure 5-8: Comparison of the dual constraint model predictions of storage and loss moduli (solid line) of $(35B2)_{LE}$ with the experimental data for 35B2 (symbols) at 180 °C 108
Figure 5-9: Comparison of the dual constraint model predictions of storage and loss moduli (solid line) of $(35B3)_{LE}$ with the experimental data (symbols) for 35B3 at 180 °C 108
Figure 5-10: Time weighted relaxation spectrum of 35B1 at 180 °C from experimental data (symbols) and of $(35B1)_{LE}$ from predicted data (solid line) 110
Figure 5-11: Time weighted relaxation spectrum of 35B2 at 180 °C from experimental data (symbols) and of $(35B2)_{LE}$ from predicted data (solid line) 110

Figure 5-12: Time weighted relaxation spectrum of 35B3 at 180 °C from experimental data (symbols) and of $(35B3)_{LE}$ from predicted data (solid line) 111
Figure 5-13: Molecular weight distribution of the MFR 35 based series 112
Figure 5-14: Relaxation spectra from predictions for 35L and three linear equivalents. The linear equivalents have the MWD of the corresponding branched sample shown in Fig. 5.13 112
Figure 5-15: Comparison of the dual constraint model predictions of storage and loss moduli (solid line) with experimental data (symbols) of 2L at 180 °C 113
Figure 5-16: Comparison of the dual constraint model predictions of $(2B1)_{LE}$ (solid line) with experimental data of 2B1 (symbols) at 180 °C 114
Figure 5-17: Comparison of the dual constraint model predictions of $(2B2)_{LE}$ (solid line) with experimental data of 2B2 (symbols) at 180 °C 114
Figure 5-18: Comparison of the dual constraint model predictions of $(2B3)_{LE}$ (solid line) with experimental data of 2B3(symbols) at 180 °C 115
Figure 5-19: Comparison of the dual constraint model predictions of $(2B4)_{LE}$ (solid line) with experimental data of 2B4 (symbols) at 180 °C 115
Figure 5-20: Time weighted relaxation spectrum of 2L at 180 °C from experimental data (symbols) and from predicted data using the dual constraint model (solid line)..... 117
Figure 5-21: Time weighted relaxation spectrum of 2B1 at 180 °C from experimental data (symbols) and of $(2B1)_{LE}$ from predicted data (solid line) 117
Figure 5-22: Time weighted relaxation spectrum of 2B2 at 180 °C from experimental data (symbols) and of $(2B2)_{LE}$ from predicted data (solid line) 118
Figure 5-23: Time weighted relaxation spectrum of 2B3 at 180 °C from experimental data (symbols) and of $(2B3)_{LE}$ from predicted data (solid line) 118
Figure 5-24: Time weighted relaxation spectrum of 2B4 at 180 °C from experimental data (symbols) and of $(2B4)_{LE}$ from predicted data (solid line) 119
Figure 5-25: Molecular weight distribution of the MFR 2 based series. The linear equivalents have the same MWD as the respective branched samples 120
Figure 5-26: Relaxation spectra from predictions for 2L and four linear equivalents..... 120
Figure 6-1: Ternary diagram representation of topology of LCB mPE.......................... 129
Figure 6-2: Sketch of structure of a crosslinked molecule 130
Figure 6-3: Weight fraction distribution development during random crosslinking of primary chains that conform to the most probable distribution with $P_n = 200$. [from ref] 132
Figure 6-4: Representation of the crosslinking rate coefficient as a function of the number of primary chains (*g* and *h*) of polymer molecules that participate in the crosslinking reaction (from ref) 133
Figure 6-5: Simulated weight distributions of chain length with $\theta = 0.2$ (from ref.) 134
Figure 6-6: Cumulative number distribution of 35L. Arrows indicate that for a random number between 0 and 1, there is a corresponding *M*.. 136
Figure 6-7: Molecular weight distributions of linear precursor chains and a branched system with $\alpha = 0.2$ and number-based random sampling 137
Figure 6-8: Molecular weight distributions of linear primary chains and a branched system with $\alpha = 0.1$ and weight-based random sampling....................................... 138

Figure 6-9: Molecular weight distribution of linear precursor 35L and three branched samples, 35B1, 35B2, 35B3, based on the same linear precursor as determined by GPC 139
Figure 6-10: Algorithm of the Monte Carlo simulation (a) creation of linear chains; (b) creation of branched chains 140
Figure 6-11: Molecular weight distribution of 35L from Monte Carlo simulation (thin line) and from GPC measurements (thick line) 142
Figure 6-12: Molecular weight distribution of 12L from Monte Carlo simulation (thin line) and from GPC measurements (thick line) 142
Figure 6-13: Molecular weight distribution of 2L from Monte Carlo simulation (thin line) and from GPC measurements (thick line) 143
Figure 6-14: Molecular weight distribution of 35B1 from Monte Carlo simulation (thin line) and from GPC measurements (thick line) 144
Figure 6-15: Molecular weight distribution of 35B2 from Monte Carlo simulation (thin line) and from GPC measurements (thick line) 145
Figure 6-16: Molecular weight distribution of 35B3 from Monte Carlo simulation (thin line) and from GPC measurements (thick line) 145
Figure 6-17: Molecular weight distribution of 12B1 from Monte Carlo simulation (thin line) and from GPC measurements (thick line) 146
Figure 6-18: Molecular weight distribution of 12B2 from Monte Carlo simulation (thin line) and from GPC measurements (thick line) 146
Figure 6-19: Molecular weight distribution of 12B3 from Monte Carlo simulation (thin line) and from GPC measurements (thick line) 147
Figure 6-20: Molecular weight distribution of 2B1 from Monte Carlo simulation (thin line) and from GPC measurements (thick line) 147
Figure 6-21: Molecular weight distribution of 2B2 from Monte Carlo simulation (thin line) and from GPC measurements (thick line) 148
Figure 6-22: Molecular weight distribution of 2B3 from Monte Carlo simulation (thin line) and from GPC measurements (thick line) 148
Figure 6-23: Molecular weight distribution of 2B4 from Monte Carlo simulation (thin line) and from GPC measurements (thick line) 149
Figure 6-24: Simulated molecular weight distribution of linear sample 35L and three branched samples 35B1, 35B2 and 35B3 149
Figure 6-25: Fractional molecular weight distributions of chains containing k_b branch points ($k_b = 0,1,2,3,4$) and the overall molecular weight distribution of 35B3 150
Figure 6-26: Fractional molecular weight distributions of chains containing k_b branch points ($k_b = 0,1,2,3,4$) and the overall molecular weight distribution of 12B3 151
Figure 6-27: Fractional molecular weight distributions of chains containing k_b branch points ($k_b = 0,1,2,3,4$) and the total molecular weight distribution of 2B4 151
Figure 6-28: Polydispersity index of chains containing k_b branch points in branched samples 35B1, 35B2 and 35B3 152
Figure 6-29: Polydispersity index of chains containing k_b branch points in branched samples 12B1, 12B2 and 12B3 153
Figure 6-30: Polydispersity index of chains containing k_b branch points in branched samples 2B1, 2B2, 2B3 and 2B4 153

Figure 6-31: Weight branch point distributions for the branched samples based on the linear precursor 35L 156

Figure 6-32: Weight branch point distributions for the branched samples based on the linear precursor 12L 156

Figure 6-33: Weight branch point distributions for the branched samples based on the linear precursor 2L 157

Figure 6-34: Weight branch point distributions for sample 35B3 and an mPE having the same β value 158

Figure 6-35: Branching $\beta(M)$ and molecular weight distributions of 35B3 159

Figure 6-36: Branching $\beta(M)$ and molecular weight distributions of 12B3 159

Figure 6-37: Branching $\beta(M)$ and molecular weight distributions of 2B4 160

Figure 6-38: Branching $\lambda(M)$ and molecular weight distributions of 35B3 160

Figure 6-39: Branching $\lambda(M)$ and molecular weight distributions of 12B3 161

Figure 6-40: Branching $\lambda(M)$ and molecular weight distributions of 2B4 161

Figure 6-41: Branching parameter β and reduced number average molecular weight M_n/M_n^0 for polypropylene series based on three different linear precursors 163

Figure 6-42: Branching parameter α and reduced weight average molecular weight M_w^0/M_w for polypropylene series based on three different linear precursors 164

Figure 6-43: Branching parameter α and reduced weight average molecular weight M_w/M_w^0 for branched systems based on two linear precursors, 35L and F-35L, which have the same number average molecular weight but different types of MWD 165

Figure 6-44: Branching parameter α and reduced weight average molecular weight M_w/M_w^0 for branched systems based on two linear precursors, 2L and F-2L, which have the same number average molecular weight but different types of MWD 166

Figure 6-45: Branching parameter α and reduced weight average molecular weight M_w/M_w^0 for branched systems based on two linear precursors, F-35L and F-2L 167

Figure 6-46: Branching information, (PDI^0 α), and reduced weight average molecular weight, M_w/M_w^0, for branched systems based on different linear precursors 168

Figure 6-47: Comparing α (branch points per precursor chain) and α_{nom} (nominal branch points per precursor chain) for all branched samples 169

Figure 6-48: Segment type composition in number fraction of branched systems based on five precursors compared with that of mPE 172

Figure 6-49: Segment type composition in weight fraction of branched systems based on five precursors compared with that of mPE 173

Figure 6-50: Melt flow rate (2.16 kg weight at 230 °C) and weight average molecular weight of the branched polypropylenes 174

Figure 6-51: Melt strength (190 °C) correlates with (f_{iw} M_w^0 PDI^0) 175

Figure 6-52: Number fractions of ring molecules in branched systems up to gel point .. 176

Figure 7-1: Prediction of zero-shear viscosity by Eq. 7.7 for randomly branched polyesters at M_w = 200000 g/mol and various levels of branching λ at 60 °C 185

Figure 7-2: Normalized time-weighted relaxation spectra of 35 MFR polypropylenes .. 187

Figure 7-3: Normalized time-weighted relaxation spectra of MFR 2 polypropylenes.... 189
Figure 7-4: The first peak location of the relaxation spectrum versus the weight fraction of free arms of branched polypropylenes (the straight line is an exponential fit of the data)........ 192
Figure 7-5: The second peak location of the relaxation spectrum versus the weight fraction of inner backbone of branched polypropylenes (the straight line is an exponential fit of the data)........ 192
Figure Appendix B-0-1: Cumulative number molecular weight distribution *CNM* along chain length *X* for linear polypropylene sample 35L........209

List of Tables

Table 3-1: Characteristics of the set of samples of 12 MFR and sample 20L 33
Table 3-2: Characteristics of the set of samples of 35 MFR...34
Table 3-3: Characteristics of the set of samples of 2 MFR...35
Table 4-1: Characteristics of metallocene polyethylenes 48
Table 4-2: Characteristics of the polypropylenes studied by Hingmann and Marczinke..50
Table 4-3: Samples and their optimum stresses for creep at 180 °C 63
Table 4-4: The time to reach steady state t_s and the steady-state compliance J_s^0 for samples at 180 °C..72
Table 6-1: The values of β and λ calculated from parameter α for all of the branched samples...155
Table 7-1: The weight average molecular weight of the linear portion in branched polymers and of their linear precursor 35L from modeling described in Chapter 6 188
Table 7-2: The weight average molecular weight of the linear portion in branched polymers and of their linear precursor 2L from modeling described in Chapter 6..189
Table 7-3: Peak locations of the relaxation spectrum (τ_a corresponds to the relaxation of free arms, and τ_i corresponds to the relaxation of inner backbones) and weight fractions of free arms (f_{aw}) and inner backbones (f_{iw}) of each branched polypropylene 191

Chapter 1. Introduction

1.1. Commercial Importance of Polypropylene

Polypropylene (PP) is a long chain polymer made by polymerizing propylene monomers as shown below.

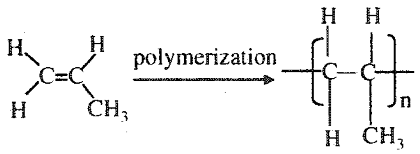

Polypropylene was only available as a low molecular weight oil that had no commercial interest until 1954 when Ziegler and Natta developed a new type of chemistry, latter known as Ziegler-Natta catalysis, to synthesize propylene into a polymer with high levels of crystallinity. Now, polypropylene is a very important industrial polymer because of its versatility, and it is of growing importance because of the development of new catalysts and polymerization processes.

Polypropylene has many applications due to its excellent properties and low price compared with other thermoplastics. Polypropylene is used both in molding and as a fiber. As a molding compound, it is used to make items such as dishwashers and coffee machines that can withstand heat; light, durable luggage and low-cost, rust resistant and attractive outdoor furniture. Its nontoxic nature and stiffness make it ideal for food containers and medical applications such as disposable syringes. The largest application for PP in molding is interior and exterior parts for automobiles, due to its high modulus and excellent heat and chemical resistance. Also, polypropylene film is widely used in food packaging.

As a fiber, polypropylene is used to make indoor and outdoor carpeting that is found around swimming pools and on golf courses. It is appropriate for outdoor carpeting, because it is easy to dye and does not absorb water. It is also used in apparel, and the cordage used in many water sport activities, for example in swimming pools to separate the lanes.

Sales of this versatile material have been growing vigorously since 1960 as shown in Fig. 1.1. Following its explosive early growth due to the emergence of Ziegler-Natta catalysts, the growth rate of PP production in U.S. was above 7% from the 1970s to the 1990s.

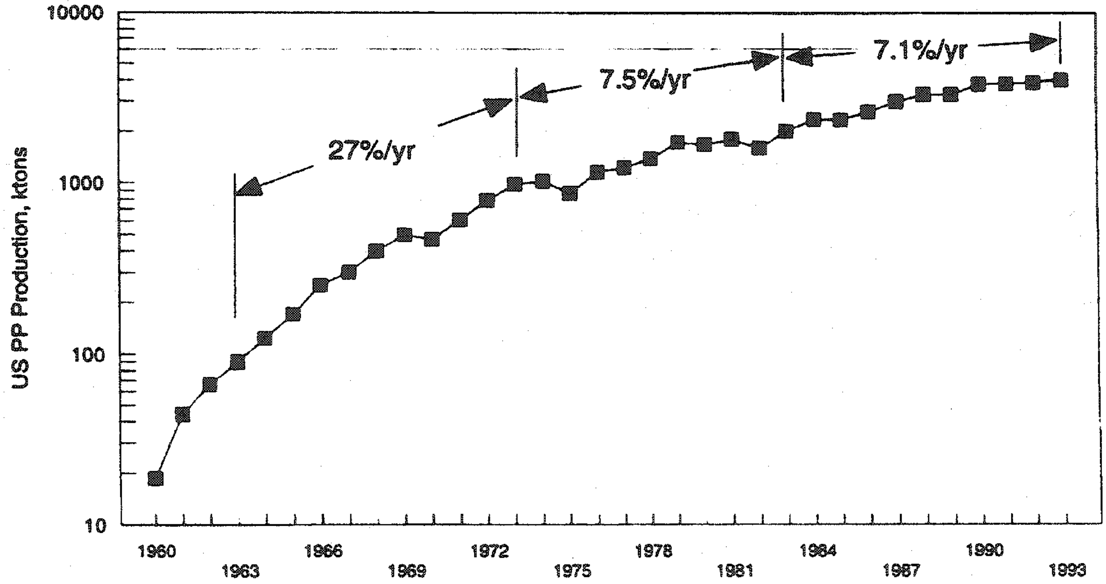

Figure 1-1. U.S. PP production, 1960-1993. (U.S. International Trade Commission)

It is estimated that from 1998 to 2005, the world market growth will average 3% a year, with world consumption rising to almost 33 million tones by 2005 as shown in Fig.1.2. The global polypropylene market is expected to be worth almost US $23 billion by 2005.

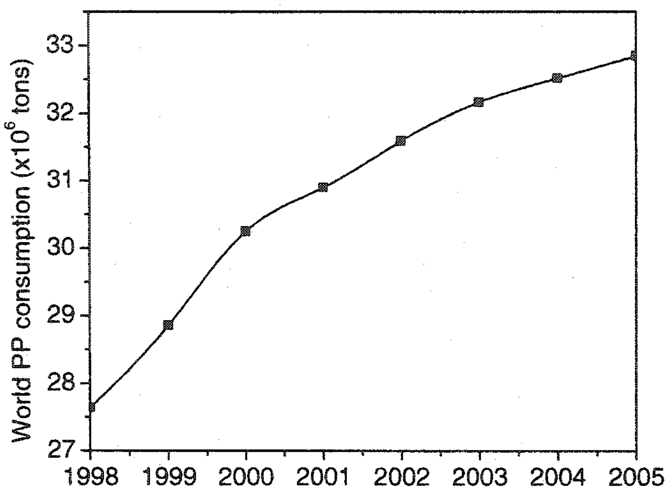

Figure 1-2: World PP consumption from 1998 to 2005 (from Gobi international)

Due to the cost and performance advantages of PP over other plastics, the relationship between structure and shear flow behavior of this material is of great importance in the design of polymers with improved processability.

1.2. Linear Polypropylene

1.2.1. Ziegler-Natta Polypropylene

Traditional linear polypropylene is made using Ziegler-Natta catalysts[1]. A Ziegler-Natta catalyst is a metal complex having a metal-carbon bond that allows the repeated insertion of olefin monomers. It usually consists of two components, a transition metal salt and a main-group metal alkyl (co-catalyst). The co-catalyst is used to generate the active metal-carbon bond. The most common Ziegler-Natta catalysts for olefin polymerization are: $TiCl_3$ with Al $(C_2H_5)_2Cl$ as co-catalyst and $TiCl_4$ with $Al(C_2H_5)_3$ as co-catalyst. The catalyst can arrange itself into a number of crystal structures. For example, in the $TiCl_3/Al(C2H5)_2Cl$ system, $TiCl_3$ forms a number of crystal structures, among which an α-crystal structure is interesting for polymerization. In the interior of the α-crystal structure each titanium atom coordinates to six chlorine atoms. However, on the surface of the crystal, a titanium atom is surrounded by five chlorine atoms and leaves one orbital empty as shown in Fig. 1.3. The co-catalyst Al $(C_2H_5)_2Cl$ activates $TiCl_3$ by donating the titanium one of its methyl groups and replacing one of the chlorines on the titanium atom. The activated catalyst system has the structure shown in Fig. 1.4, which still has an empty orbital.

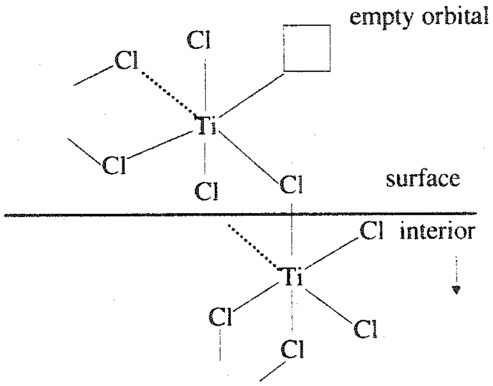

Figure 1-3: Atom coordinating of titanium on the surface and interior of an α-crystal

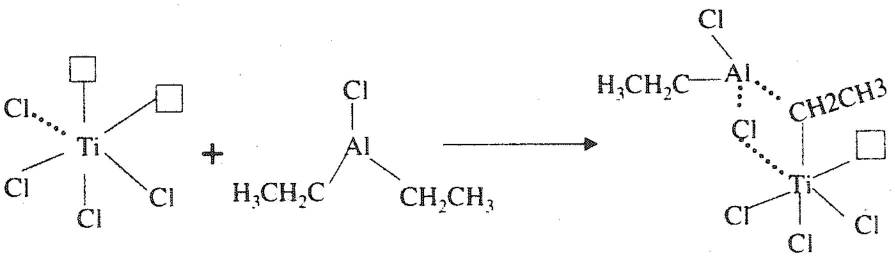

Figure 1-4: Structure of the activated catalyst

Because of the empty orbital on the titanium atom, the propylene monomer is always added from this location resulting in a product with high stereoregularity. A molecule is said to have high stereoregularity if the monomer unit always adds to the main chain in the same stereo configuration. By changing the components of the Ziegler-Natta catalyst, one can make polymers with specific stereoregularity. According to the degree of stereoregularity, there are three kinds of linear polypropylene[1]: isotactic, syndiotactic and atactic. Isotactic chains result from the head-to-tail addition of propylene monomer units, where the methyl groups always have the same configuration with respect to the polymer backbone. Syndiotactic chains also form by head-to-tail addition of monomer units, but the methyl groups have an alternating configuration with respect to the polymer backbone. Atactic chains do not have any consistent placement of the methyl groups. The molecular structures of isotactic and syndiotactic polypropylene are shown in Fig. 1.5. Most commercial polypropylenes are isotactic.

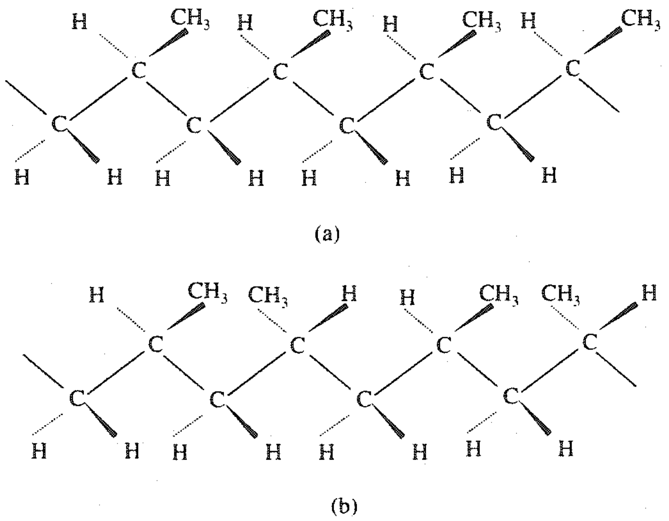

Figure 1-5: (a) Isotactic and (b) syndiotactic configuration of a PP chain[1]

Because each active site of a Ziegler-Natta catalyst has a different activity and lifetime, polypropylene produced using this type of catalyst has a fairly broad molecular weight distribution. The polydispersity index (*PDI*), M_w/M_n, ranges from 3.5 to 8.0[1].

1.2.2. Metallocene Polypropylene

Metallocene catalysts are different from Ziegler-Natta catalysts because of their single-site catalyst nature, *i.e.*, every catalytic site is the same and plays the same role in catalyzing the polymerization from monomer to polymer[2]. Figure 1.6 shows the general structure of such a catalyst for isotactic PP. Usually metallocene catalyst consists of two components, a transition metal complex compound and a main group metal alkyl (co-catalyst). The short bridge between the two rings has the effect of sterically opening up one side of the complex, producing a stable but highly open and active site upon activation by the co-catalyst.

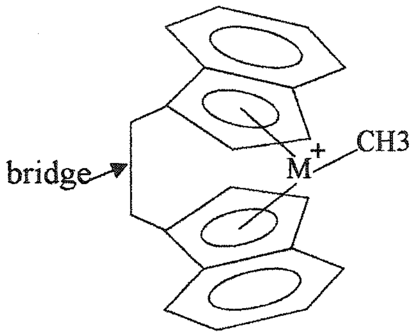

Figure 1-6: Single-site catalyst for isotactic PP[2]

Metallocene PP has a narrow molecular weight distribution, with a *PDI* in the range of 2.0 to 2.5, compared with 3.5-8.0 for polymers made using Ziegler-Natta catalysts[1]. The stereoregularity of polypropylenes can also be controlled using metallocene catalysts[1]. For example, by using the metallocene catalysts shown in Fig. 1.7, one can make polypropylenes having improved impact properties using only propylene monomer while traditionally impact properties are improved by using ethylene comonomer.

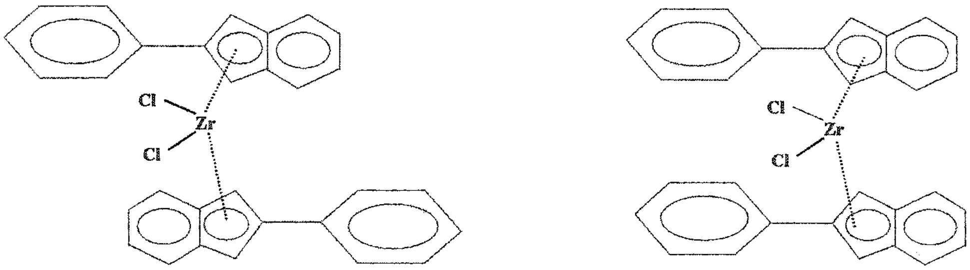

the *rac* form the *meso* form

Figure 1-7: bis(2-phenylindenyl)zirconium dichloride in *rac* and *meso* form

In Fig. 1.7 we see that there is no bridge between the two indenyl rings, which means that the two rings can spin freely, sometimes pointing in opposite directions (*rac* form), and sometimes pointing in the same direction (*meso* form). When the zirconocene is in the *rac* form, the propylene monomer can only approach in one orientation, thus giving isotactic polypropylene. When the zirconocene is in the *meso* form, the propylene monomer can approach in any orientation, producing atactic polypropylene. The zirconocene changes its form, *rac* or *meso*, even during the polymerization, producing chains having blocks of isotactic polypropylene and blocks of atactic polypropylene. The solid-state structure of the resulting polymer is shown in Fig. 1.8.

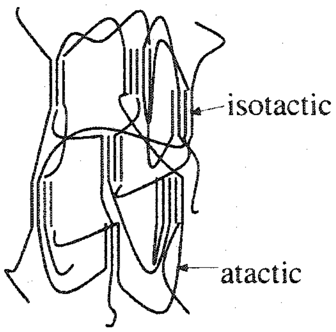

Figure 1-8: Solid-state structure of impact improved metallocene polypropylene

From Fig. 1.8 we can see that the isotactic blocks can form crystals giving improved strength. The hard crystalline regions are tied together by soft rubbery atactic polypropylene giving the resulting product improved impact resistance. This product is a thermoplastic elastomer, which is recyclable and environmentally friendly, while many elastomers are crosslinked polymers that cannot be recycled. Compared to traditional polypropylene/polyethylene (PP/PE) impact improved PP, impact improved metallocene PP is a one-monomer system, and there is a strong force tying the crystal and amorphous phases together. By changing slightly the structure of the rings in the catalyst, such as adding a group to sterically hinder the spin of the rings[3], one can control the proportion of isotactic/atactic blocks in the same chain and thus the end-use properties of the polymer. The development of new catalysts expands the usage of polypropylene and encourages the growth of the polypropylene market.

1.2.3. Manufacture of Linear Polypropylene

The development of polypropylene manufacturing processes is mainly focused on catalyst improvement. According to the catalyst used, manufacturing processes for PP can be classified into three main types[1]: slurry, solution or liquid, and gas phase.

The process first used was the slurry process[1], which was designed to accommodate early Ziegler-Natta catalysts that had low activity and stereo-specificity. In this process, the propylene monomer is dispersed in a hydrocarbon diluent such as kerosene, hexane or heptane, and the polymerization takes place at a temperature in the range of 60 °C to 80 °C. Catalyst residuals are deactivated by alcohol, and the crystalline polypropylene is separated from the diluent and the amorphous by-product atactic polypropylene. This process is energy and capital intensive due to the purification and recycling of the diluent and the alcohol, and the separation of the crystalline polymer from the amorphous polymer. In general, the product from the slurry process is less isotactic and has a broader molecular weight distribution than the products of other processes.

Two second-generation processes were developed for catalysts having higher activity: solution polymerization and liquid (or bulk) polymerization. In solution polymerization, the catalysts, monomers and hydrocarbon solvent are continuously fed into the reactor where the reaction takes place at a temperature above 140 °C, where crystalline PP is also soluble in the solvent. It is no longer necessary to deactivate the catalyst, which avoids the use of alcohol. This greatly reduces the production cost and lessens the load placed on the environment. However, the separation of crystalline PP from atactic PP is still required. The liquid polymerization process uses liquefied monomer, which results in a high polymerization rate. There is no solvent and no need to deactivate the catalyst. This significantly simplifies the process and reduces costs.

The newest process is the gas-phase polymerization process. This process uses high-yield and highly stereo-specific catalysts in which the removal of catalyst and amorphous polypropylene is not necessary. There is no reaction medium involved in the process, and this process is therefore considered to be the simplest of all PP processes.

The development of the liquid and gas-phase polymerization processes greatly reduced production costs, simplified the production line, and led to high yield products that are preferred by industry. Judging from the developments in the 1990's, the use of the liquid and gas phase processes is increasing, while the use of the slurry process is decreasing and will be phased out as economics dictate.

1.2.4. Engineering Properties of Linear Polypropylene

The major structural characteristics of linear polypropylene are high stereoregularity and broad molecular weight distribution. Both these characteristics favor high crystallinity. Because of its high crystallinity, linear polypropylene has high modulus, tensile strength and rigidity. Polypropylene also has a high melting temperature (165-170 °C), and thus has excellent heat resistance. Its moisture barrier property is excellent, and polypropylene is nontoxic and has very good chemical resistance. It has a low density of 0.9 g/cm^3, which makes it the lightest of all commodity plastics. It is 5% lighter than high-density polyethylene (HDPE), 14% lighter than polystyrene (PS) and ABS and 33% lighter than PVC. These excellent end-use properties of polypropylene make it a versatile material that can be used as both fibers and plastics.

While the exceptional end-use properties of polypropylene make it useful in many applications, its linear structure leads to poor processability in many industrial fabrications such as extrusion coating, fiber spinning, thermoforming, film blowing and foam extrusion. The processability can be improved by enhancing the melt strength of the polymer.

1.3. High Melt Strength Polypropylene

1.3.1. Definition and Structure

High melt strength refers to a polymer having sufficient strength in the melt state to maintain a desired geometry while being subjected to the forces and deformations that arise in melt processing. Depending on the process, high melt strength can be important at either very high deformation rates or very low deformation rates.

High melt strength at high deformation rates refers to a melt becoming stiffer instead of breaking upon stretching. This behavior is illustrated in the sketch below, which is also known as "strain-hardening".

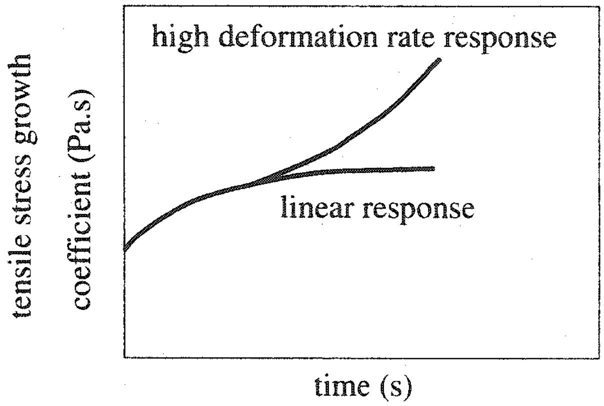

Figure 1-9: Sketch of the tensile behavior of a polymer having high melt strength

High melt strength at high deformation rates is favored in many processes where elongational flows are dominant, such as fiber spinning, extrusion coating, and film blowing. High melt strength allows high production speeds and prevents defects in processes. A high production rate and a high quality product are both important to the economics of the process. High melt strength at high deformation rates can be obtained by introducing branches into the polymer.

In some processes, high melt strength is required at very low deformation rates. In the foaming process, melt strength is necessary to avoid foam collapse before quench. In blow molding, the parison needs melt strength to resist sagging. In profile extrusion, the product needs to maintain its shape until reaching the quench bath. In all these process, high melt strength is required at nearly zero deformation rate. Branches or a broad molecular weight distribution give the polymer high melt strength at low deformation rates.

Long chain branches are introduced into polypropylene to improve its melt strength at both high and low deformation rates and thus improve its processability. Side chains whose lengths are longer than the critical entanglement molecular weight M_c, which is about twice the molecular weight between entanglement points M_e[4], are an example of branch structures of interest for improving melt strength. Some branched structures are sketched in Fig. 1.10.

Figure 1-10: Sketch of some possible branching structures

1.3.2. Manufacture of High Melt Strength Polypropylene

Two types of technique have been developed to make long-chain-branched polypropylenes: post-reactor treatment, and *in-situ* polymerization. Post-reactor treatment, which includes peroxide curing, electron beam irradiation and macromonomer grafting, is the more popular way to introduce branches into polypropylenes.

Polypropylene macroradicals are produced by the attack of electronic beam irradiation or by peroxide decomposition of the polypropylene backbone. The PP macroradical is not stable; either it undergoes β-scission leading to chain cleavage or it recombines with other macroradicals to make a branched structure as shown in Fig. 1.11. Based on this principle, techniques have been developed to stabilize PP macroradicals, favor branching processes, and hinder β-scission by adding reagents or controlling the reaction conditions.

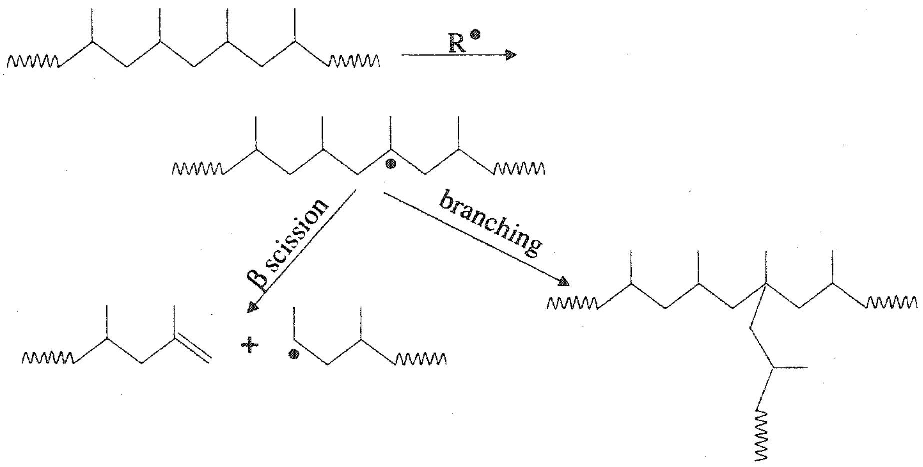

Figure 1-11: β scission and branching in polypropylene

Chodák and Zimányonvá[5] studied the effect of temperature on the branching of PP in the presence of peroxide. In the temperature range from 10 to 220 °C they found that the branching efficiency was highest between 65 and 80 °C. The branching of isotactic and syndiotactic PP with peroxide was investigated by Yu and Zhu[6] at 160 °C. They discovered that isotactic PP has a higher branching efficiency than syndiotactic PP. Lagendijk *et al.*[7] made long chain branched PP using reactive extrusion in the presence of selected peroxydicarbonates. The branching level was controlled by the type of peroxydicarbonate used. In all these techniques, branched PP is achieved by controlling the temperature and type of peroxide to promote branching.

The branching process can be accelerated by including a polyfunctional monomer. Wang *et al.*[8] prepared branched PP at 200 °C by a reactive extrusion process using 2,5-dimethyl-2, 5-di(tert-butyl peroxy) hexane as an initiator and the polyfunctional monomer, pentaerythritol triacrylate, as a coupling agent.

The β-scission process in Fig. 1.11 can be controlled by adding a co-agent that reacts with macroradicals to reduce their concentration. The reaction between co-agent and macroradicals is reversible and thus helps the branching process. In the work of Borsig *et al.*[9] on the branching of PP by peroxides and co-agents (thiourea and its derivatives), thiourea was found to be an efficient co-agent in the temperature range 170-200 °C.

Graebling[10] reported on the synthesis of branched polypropylene by a reactive extrusion process in the presence of a peroxide, a polyfunctional monomer and a co-agent. The combination of polyfunctional monomer and co-agent suppressed the β-scission process and favored the branching process, thus increasing the branching efficiency.

In all the examples mentioned above, the radicals come from the decomposition of peroxide. Macroradicals can also be generated by irradiation. De Nicola *et al.*[11] patented a PP branching technique involving high-energy irradiation of high molecular weight linear polypropylene in the solid state. The radiation abstracted a hydrogen from the PP backbone and generated PP macroradicals. The reaction was performed in a reduced active oxygen environment to limit the β-scission process and favor the branching process. In the patent of Saito and coauthors[12], branched PP was achieved by irradiation with an electron beam in a nitrogen atmosphere in the presence of 1,6-hexanediol diacrylate as co-agent.

Macromonomer grafting is a new approach of post-reactor treatment to make branched PP and can make relatively well-defined branched PP. Lu and Chung[13] prepared such a polymer by grafting polymer chains onto linear PP macromolecules.

Recently, Weng *et al.*[14] reported long chain branched isotactic polypropylene synthesized *in-situ* using a metallocene catalyst, *rac*-dimethylsilybis(2-methyl-4phenylindnyl) zirconium dichloride with methylaluminoxane as co-catalyst, in a diluent such as hexane or toluene. The metallocene catalyst is able to generate vinyl-terminated polypropylene macromolecules and incorporates them into the isotactic polypropylene backbones to make branched structures.

1.3.3. Engineering Properties of High Melt Strength Polypropylene

Branched PP has enhanced melt strength at high or near zero deformation rates, which expands its use in many industrial applications where melt strength is important. Branched polypropylene is also expected to be strongly shear thinning, making it easier to process at high shear rates.

To summarize, linear PP has many excellent end-use properties such as high modulus, high melting temperature, excellent chemical resistance and moisture barrier properties. Introducing branches improves the flow properties with little effect on end-use properties. Knowing the relationship between branching structure and flow behavior will make it possible to develop polymers having improved processability as well as good end-use properties.

1.4. Research Objectives

The research objectives are to:

1. Examine the effects of molecular structure of branched polypropylenes on shear flow behavior;
2. Obtain detailed structural information of branched polypropylenes by simulating the branching process using a Monte Carlo technique;
3. Evaluate the performances of molecular theory models for predicting linear viscoelastic properties of linear polypropylenes made using Ziegler-Natta catalysts;
4. Correlate rheological properties with branching information, making it possible to obtain branching information through rheological measurements.

The thesis is organized in the following way:

1. Various methods to obtain branching information in polymers are reviewed in Chapter 2;
2. The materials studied in this project are described in Chapter 3;
3. The experimental measurements and linear viscoelastic data are reported in Chapter 4;
4. Linear viscoelastic behavior of linear polypropylenes are predicted using molecular theory models in Chapter 5;
5. The modeling of the branching process using a Monte Carlo technique is described in Chapter 6 and detailed structural information of branched polymers is presented;
6. In Chapter 7, rheological properties are correlated with the branching information;
7. Finally the conclusions of the study and contributions to knowledge are listed in Chapters 8 and 9.

Reference

---

[1] Moore E. P., Jr., Polypropylene Handbook, Hanser/Gardner Publications, 1996

[2] Stevens J.C. "Constrained Geometry and Other Single Site Metallocene Polyolefin Catalysts: A Revolution in Olefin Polymerization", 11th international congress on catalysis – 40th anniversary studies in surface science and catalysis, vol. 101, 11-20, 1990

[3] Wilmes G. M., L. Shirley, R. M. Waymouth, "Propylene Polymerization with Sterically Hindered Unbridged 2-Arylindene Metallocenes", Macromolecules, 35, 5382-5387, 2002

[4] Bersted B.H., Encyclopedia of Fluid Mechanics, Vol.7, Chapter 22, Gulf Publishing Company, Houston, 1988

[5] Chodák I., E. Zimányová, "The Effect of Temperature on Peroxide Initiated Crosslinking of Polypropylene", European Polymer Journal, 20, 81-84, 1984

[6] Yu Q., S. Zhu, "Peroxide Crosslinking of Isotactic and Syndiotactic Polypropylene", Polymer, 40, 2961-2968, 1999

[7] Lagendijk, R.P., A.H. Hogt, A. Buijtenhuijs, A.D. Gotsis, "Peroxydicarbonate Modification of Polypropylene and Extensional Flow Properties", Polymer, 42, 10035-10043, 2001

[8] Wang X., C. Tzoganakis, G.L. Rempel, "Chemical Modification of Polypropylene with Peroxide/Pentaerythritol Triacrylate by Reactive Extrusion", J. Appl. Polym. Sci., 61, 1395-1404, 1996

[9] Borsig E., M. Capla, A. Fiedlerova, M. Lazár, "Crosslinking of Polypropylene using a System Consisting of Peroxide and Thiourea or its Derivatives", Polymer Communications, 31, 293-296, 1990

---

[10] Graebling D., "Synthesis of Branched Polypropylene by a Reactive Extrusion Process", Macromolecules, 35, 4602-4610, 2002

[11] DeNicola A. J. Jr., J. A. Smith, M. Felloni, "High Melt Strength, Propylene Polymer, Process for Making it, and Use Thereof", US Patent 5414027, 1995

[12] Saito J., S. Kikukawa, K. Makuuchi, F. Yoshii, "Process for Producing a Modified Polypropylene and a Molded Product" US Patent 5560886, 1996

[13] Lu B., T.C. Chung, "Synthesis of Maleic Anhydride Grafted Polyethylene and Polypropylene, with Controlled Molecular Structures", J. Polym. Sci., Part A: Polymer Chemistry, 38, 1337-1343, 2000

[14] Weng W., W. Hu, A.H. Dekmezian, C.J. Ruff, "Long Chain Branched Isotactic Polypropylene", Macromolecules, 35, 3838-3843, 2002

Chapter 2. Methods for Determining the Branching Level in Polymers

2.1. Introduction

Long-chain branches (LCB) are introduced into linear polymers to improve their processability, and it is crucial to control the level of branching in order to obtain polymers with the desired properties. The level of branching should be low enough to avoid gelation or significantly reduced molecule size that would degrade the end-use properties, but high enough to improve the processability. Therefore, techniques for determining branching levels in polymers are essential for material design.

Many techniques have been developed to determine the level of branching. They can be classified into four categories: 1) analytical measurements using nuclear magnetic resonance (NMR); 2) estimation of the level of branching from the reduced radius of gyration using the Zimm-Stockmayer[1] equation; 3) inferring the level of branching from rheological properties; 4) obtaining detailed structural information by simulating the reaction mechanisms of the branching process.

In this chapter, these techniques are described, and the ones selected for use in this study are noted.

2.2. Methods for Determining Branching Level in Polymers

2.2.1. Nuclear Magnetic Resonance

Nuclear magnetic resonance is an analytical characterization technique where a sample solution is immersed in a homogenous magnetic field and interacts with radio waves. Each atom of a polymer chain has a nucleus, which is positively charged and spinning. The charged spinning nuclei create magnetic moments, and when the spinning nuclei are placed in a homogenous magnetic field, these moments line up with the applied field. When the spinning nuclei interact with radio waves, the magnetic moments tilt (resonate), and the resonating moments can be detected. Different nuclei resonate at different radio frequencies, which means that one must stimulate a hydrogen atom with a different frequency from that for a carbon atom to make it resonate. Also, the same atoms in different environments will resonate at different radio frequencies. In the case of polymer chains, the carbon atom at a branch point, called a methane carbon, resonates at a different frequency than other carbon atoms. By performing NMR measurements, the total number of carbons at branch points and the total number of carbons in the sample can be determined. Therefore, λ, the number of branch points per 1000 carbons, can be calculated.

Randall[2] provided an extensive review of characterizations of ethylene-based polymers such as ethylene-butene, ethylene-propylene and ethylene-octene copolymers, long-chain branched polyethylene and low-density polyethylene using ^{13}C NMR.

In the work of Yan *et al.*[3] branching levels in metallocene polyethylenes (mPE) were measured using a Bruker AC 300 pulsed ^{13}C NMR spetrometer for samples with λ up to 0.044 branch points per 1000 carbons. The branching level was calculated from the ratio of integral area of the carbon resonance of interest to the total integral area of carbon resonance.

Shroff and Mavridis[4] reported LCB levels in polyethylenes determined using the same ^{13}C NMR procedure as was used in ref. 2. The ^{13}C NMR technique was able to quantify long chain branching levels successfully for a series of metallocene polyethylenes in the λ range of 0.02-0.3 branch points per 1000 carbons, but it failed to detect the long chain branching level in polyethylenes where branches were introduced by peroxide modification. By comparing the measurements of a sample undergoing multiple-pass extrusion with that of the base sample, they found no difference in the NMR results, while zero-shear viscosity increased from 1.3×10^6 to 2.3×10^8 Pa s. Therefore, they concluded that the ^{13}C NMR technique is not sensitive to structural modifications resulting from the thermal and shear histories.

Wood-Adams *et. al.*[5] reported the ^{13}C NMR data for mPEs with short- and long-chain branches. The microstructure of the polymers and the nomenclature used to describe the various carbons of the chain are shown in Fig. 2.1, where the short chains have a length of 4 carbons.

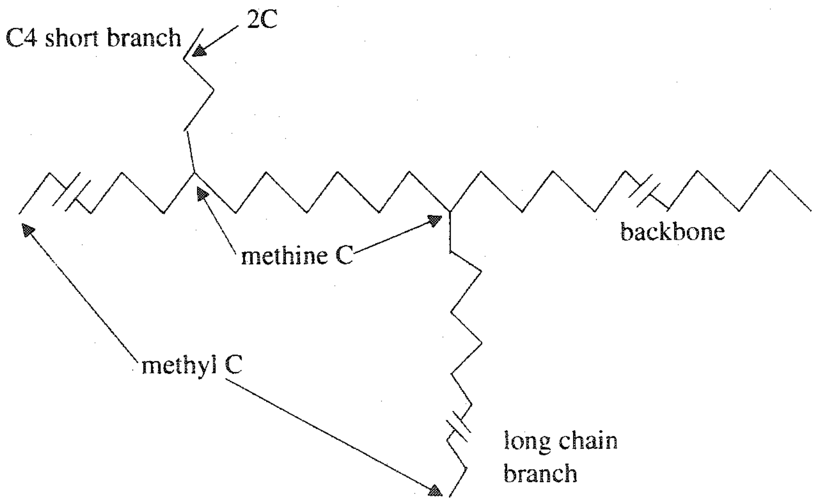

Figure 2-1: Microstructure of long and short chain branched mPE[5]

The branching level λ was obtained by comparing the long-chain branching methine carbon resonance with the methylene resonance in the NMR spectrum. The long-chain branching methine carbon intensity was corrected using the integrated intensity of carbon-2 of the short chain branch. The relative standard deviation of ^{13}C NMR measurements for low levels of long chain branching was studied, and it was found that it was 10-20% at a confidence level of 95%, which indicates that the signal-to-noise ratio was about 10 or greater. Higher precision could be obtained by significantly extending the data acquisition time. They found that a reasonable balance between experimental time and accuracy could be achieved with accuracy in the range of 95-98% for samples with low branching levels.

Striegel and Krejsa[6] reported branching levels for commercial polyethylenes containing both long and short chain branches using a Varian Unity Inova 500 NMR spectrometer at 150 °C. The spectrometer and procedure used was able to detect the levels of branches having lengths of 10 carbon atoms and above.

Weng *et al.*[7] synthesized long-chain branched polypropylenes using metallocene catalysts and determined branching levels using ^{13}C NMR. The assignments of the NMR resonances were based on a comparison of the resonances with those of the model polymer (propylene/4 methyl-1-pentene compolymer), stereo structure analysis at the branch point, and chemical shift calculations of the carbons around the branch point. Once the resonance peaks were assigned, the branching level could be determined. Their analysis of the NMR peaks also revealed a unique stereo structure at the branch point, which confirmed that the branches were formed by the incorporation of vinyl-terminated macromonomers.

While the ^{13}C NMR technique gives a direct measurement of branching level, it has some disadvantages. It cannot distinguish between branches containing 6 carbon atoms or more. Therefore, for polymers containing both short and long chain branches, the ^{13}C NMR technique overestimates the LCB level. However, only long-chain branches having lengths of $2M_e$ or longer affect rheological behavior[8] and thus processability. Thus corrections[3,5] are necessary to extract the rheologically effective long-chain branching level from NMR results.

Furthermore, it is challenging using NMR to detect branching levels below 0.01 branches per 1000 carbons because of the limited solubility of polymers and the low ^{13}C nuclei concentration. However, many industrial polymers have long-chain branching levels well below 0.01 branches per 1000 carbons. Finally, the NMR technique is not applicable to polymers in which branches are introduced by peroxide modification or a post-reactor process, which is a common method for introducing long-chain branches into polypropylenes.

2.2.2. Technique Based on the Reduced Radius of Gyration

Zimm and Stockmayer[1] derived formulae for the structural parameter, g, the ratio of the mean-square radius of gyration $\left\langle R_g^2 \right\rangle$ of the branched molecule to that of a linear molecule having the same molecular weight, for various branched systems based on the following assumptions:

1. the distance between any two points on a flexible polymer chain is proportional to the number of segments between the two points;
2. the "excluded volume effect" can be neglected, *i. e.*, configurations in which two segments occupy the same position do not exist;
3. the probability of occupancy of a region of each segment is independent;

According to Zimm and Stockmeyer, for polydisperse randomly branched polymers, the weight average values of g are as follows:

$$\left\langle g_3 \right\rangle_w = \frac{\left\langle R_g^2 \right\rangle_{branch}}{\left\langle R_g^2 \right\rangle_{linear}} = \frac{6}{n_w}\left[\frac{1}{2}\left(\frac{2+n_w}{n_w}\right)^{\frac{1}{2}} \ln\left(\frac{\left(2+n_w\right)^{\frac{1}{2}}+\left(n_w\right)^{\frac{1}{2}}}{\left(2+n_w\right)^{\frac{1}{2}}-\left(n_w\right)^{\frac{1}{2}}}\right)-1\right] \tag{2.1}$$

$$\left\langle g_4 \right\rangle_w = \frac{\left\langle R^2 \right\rangle_{branch}}{\left\langle R^2 \right\rangle_{linear}} = \left(1/n_w\right) \ln\left(1+n_w\right) \tag{2.2}$$

where n_w is the weight average number of branch points per molecule, and $\left\langle g_3 \right\rangle_w$ and $\left\langle g_4 \right\rangle_w$ are the weight average g ratios for branch functionalities of 3 and 4 respectively. The branch functionality is the number of segments attached to a branch point.

The above equations are used to determine n_w, which is then related to the branching level. For branched metallocene polyethylenes, the functionality of the branch point is 3 and Eq. 2.1 is used. In the case of the branched polypropylenes used in this study, the functionality of the branch point is 4 and Eq. 2.2 is applicable.

In order to use Eq. 2.1 or 2.2 to calculate n_w one needs a g value. There are two main approaches. First, for a polydisperse system, the mean-square radius of gyration $\left\langle R_g^2 \right\rangle$ as a function of molecular weight can be determined using multiangle laser light scattering (MALLS) coupled with gel permeation chromatography (GPC), and the weight average g ratio can then be calculated.

The other popular approach is to obtain a g value from the intrinsic viscosity $[\eta]$. The intrinsic viscosity is a characteristic property of a polymer in a very dilute solution, and can be expressed as:

$$[\eta] = \lim_{c \to 0} \frac{\eta_{1,2} - \eta_1}{\eta_1 c} \tag{2.3}$$

where η_1 and $\eta_{1,2}$ are the viscosities of the pure solvent and the solution respectively, c is the concentration of the solution. The intrinsic viscosity is related to the size of an isolated polymer molecule, and the structural parameter g' is defined as:

$$g' = \frac{[\eta]_{branch}}{[\eta]_{linear}} \tag{2.4}$$

where $[\eta]_{branch}$ and $[\eta]_{linear}$ are the intrinsic viscosities of the branched species and the linear species having the same weight average molecular weight. The two structural parameters g and g' are related by the Debye-Bueche[9] theory:

$$g' = g^{\varepsilon} \tag{2.5}$$

where ε is the Debye-Bueche viscosity shielding constant, which depends on the polymer, solvent and temperature, and has a value between 0.5 and 1.5[10]. Therefore, if ε is known, the value of g can be obtained from the intrinsic viscosity.

Weng *et al.*[7] characterized the level of long-chain branching in metallocene catalyzed branched isotactic polypropylenes using MALLS coupled with GPC. The absolute molecular weight and mean-square radius of gyration were measured by light scattering at each retention volume. The weight average value of g was calculated using Eq. 2.6.

$$\langle g \rangle_w = \frac{\sum w_i \langle R_g^2 \rangle_i}{\sum w_i \left(K M_i^{\alpha_1} \right)^2} \tag{2.6}$$

where w_i is the weight fraction of each species, and K and α_1 are constants determined experimentally. When comparing the λ values determined by ^{13}C NMR to the $\langle g \rangle_w$ values determined by GPC-MALLS for three branched polypropylenes, Weng *et. al.* saw a clear correlation.

Striegel and Krejsa[6] evaluated the levels of branching in a series of polyethylenes containing both short chain and long chain branches using size exclusion chromatography (SEC) equipped with a differential refractive index detector and a differential viscometry detector. The structure parameter g' was obtained from intrinsic viscosities by using Eq. 2.4. They assumed ε=0.75, a value reported earlier[11] for the same conditions. Values of n_w were then calculated using Eq. 2.1. Because of the very small influence of short chain braches (SCB) on hydrodynamic volume, and therefore on the intrinsic viscosity, this technique cannot detect SCB. Striegel and Krejsa demonstrated that SEC and ^{13}C NMR measurements complement each other in determining the branching levels of polyethylenes containing both short and long chain branches. They also demonstrated the importance of choosing an appropriate linear standard and an appropriate value of ε when analyzing SEC data to obtain branching information.

Wood-Adams *et al.*[5] presented the long-chain branching characterization in metallocene polyethylenes using high temperature gel permeation chromatography equipped with a differential refractive index detector, a viscometer and a light scattering detector. For each fraction, the g' value was calculated from the measured intrinsic viscosity. They used an experimentally determined ε value of 0.5 to calculate g from g' using Eq. 2.5. Zimm and Stockmayer[1] have shown that the g ratio can be approximately related to the average number of branch points per molecule, β, for a fractionated species with a maximum error of less than two percent:

$$\langle g_3 \rangle = \left[(1+\beta/7)^{1/2} + 4\beta/9\pi\right]^{-1/2} \tag{2.7}$$

For each fraction the average number of branch points per molecule was converted into the average number of branches per 1000 carbons λ_{M_i} using Eq. 2.8, and the overall average value of λ was calculated using Eq. 2.9

$$\lambda_{M_i} = \frac{14000\beta}{M_i} \tag{2.8}$$

$$\lambda = \sum w_i \lambda_{M_i} \tag{2.9}$$

Comparing long-chain branching levels determined using the triple detector GPC with those from NMR measurements, they found a reasonable agreement. Also they discovered that with the triple detector GPC they were able to detect λ values well below 0.1 branch points per 1000 carbons.

Tackx and Tacx[12] studied the dependency of ε on molecular weight at constant temperature and a given solvent and polymer for low-density polyethylenes (LDPE). The value of g_i' was obtained from SEC measurements, and g_i was obtained from the MALLS measurements of the mean-square radius of gyration of each fraction. They found that ε was a function of molecular weight and also depended on the type of reactor. For LDPE,

ε decreased continuously with increasing molecular weight from 1.8 to 1.2 for a tubular product and from 1.5 to 1 for an autoclave product.

Detecting low levels of branching using the Zimm-Stockmayer equations and the intrinsic viscosity is a challenging task, because at such low levels of branching, g' is very close to 1. Moreover, the accurate estimation of LCB when g' is close to 1 requires very precise measurements, because small variations in g' cause large differences in the LCB value as shown in Fig. 2.2[4]. The other challenge is to choose the right ε value, because ε depends on many factors, including temperature, solvent, type of reactor, the polymer itself, and the molecular weight. The wide range of possible ε values (0.5-1.5) makes this choice difficult.

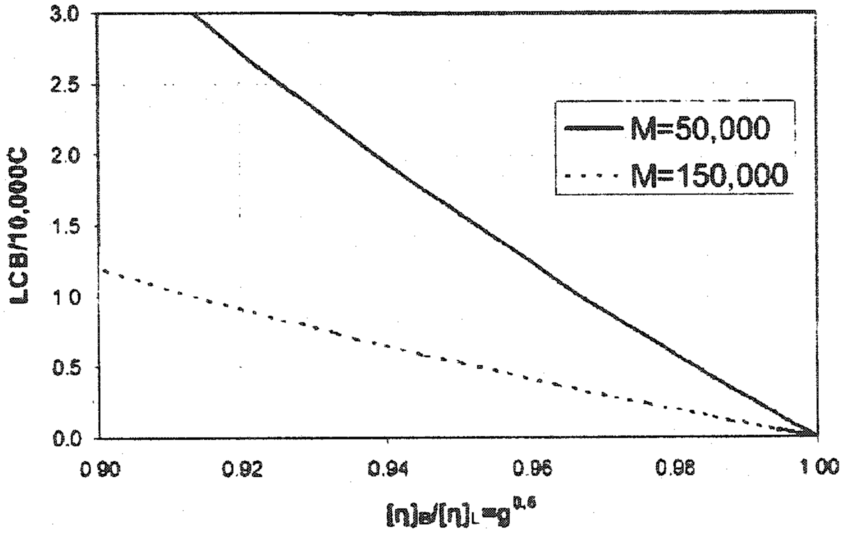

Figure 2-2: Dependence of λ, as determined by the Zimm-Stockmayer method, on the intrinsic viscosity ratio, at two different molecular weights and for essentially linear PE[4]

2.2.3. Rheological Property Based Methods

Linear viscoelastic properties can be used to characterize polymers in their equilibrium state. Long-chain branches have a significant influence on the linear viscoelastic properties of a polymer, and there has been considerable effort to infer long-chain branching information from linear viscoelastic properties. Commonly used properties are zero-shear viscosity, complex viscosity, and flow activation energy. However, the extraction of structural information from LVE data is an ill-posed problem because of the limited experimental frequency (or time) range and precision of the data. As a result, accurate data over a broad data range are required. One of the inherent difficulties in the rheological method lies in separating the effects of LCB from those of molecular weight and molecular weight distribution. Empirical relationships between rheological properties and the long-chain branching information are usually employed, so that the branching information obtained from LVE is only approximate. A more detailed review of previous work in this area is presented in Chapter 7.

2.2.4. Modeling of the Branching Process

Detailed structural information can be obtained by modeling the polymerization process of a branched polymer. A popular modeling technique is the Monte Carlo method, which is a stochastic technique based on the use of random numbers and probability statistics. By making certain assumptions to simplify the simulation of a complex polymerization process, the Monte Carlo technique can predict the molecular weight distribution as well as the detailed branching structure. For simple cases such as random branching with a Flory distributed linear precursor, an analytical solution for the molecular weight distribution and branching statistics can be obtained. A more detailed review of the modeling of branching processes is presented in Chapter 6.

In this study, detailed structural information for branched polypropylenes is obtained by simulating the branching process using the Monte Carlo technique. The results are presented in Chapter 6. The relaxation spectrum inferred from experimental linear viscoelastic data is correlated with the branching information. This makes it possible to obtain branching information using rheological measurements. This technique and its results are presented in Chapter 7.

References

---

[1] Zimm, B.H, W.H. Stockmayer, "The Dimensions of Chain Molecules Containing Branches and Rings", J. Chem. Phys., 17, 1301-1314, 1949

[2] Randall, J.C., "A Review of High Resolution Liquid ^{13}Carbon Nuclear Magnetic Resonance Characterizations of Ethylene-Based Polymers", Rev. Macromol. Chem. Phys., C29(2 & 3), 201-317, 1989

[3] Yan, D., W.J. Wang, S. Zhu, "Effect of Long Chain Branching on Rheological Properties of Metallocene Polyethylene", Polymer, 40, 1737-1744, 1999

[4] Shroff, R.N., H. Mavridis, "Assessment of NMR and Rheology for the Characterization of LCB in Essentially Linear Polyethylenes", Macromolecules, 34, 7362-7367, 2001

[5] Wood-Adams, P.M., J.M. Dealy, A.W. deGroot, O.D. Redwine, " Effect of Molecular Structure on the Linear Viscoelastic Behavior of Polyethylene", Macromolecules, 33, 7489-7499, 2000

[6] Striegel, A.M., M.R. Krejsa, "Complementarity of Universal Calibration SEC and 13C NMR in Determining the Branching State of Polyethylene", J. of Poly. Sci. Part B: Poly. Phys., 38, 3120-3125, 2000

[7] Weng, W., W. Hu, A.H. Dekmezian, C.J. Ruff, "Long Chain Branched Isotactic Polypropylene", Macromolecules, 35, 3838-3843, 2002

[8] Bersted B.H., Encyclopedia of Fluid Mechanics, Vol.7, Chapter 22, Gulf Publishing Company, Houston, 1988

[9] Debye, P., A.M. Bueche, "Intrinsic Viscosity, Diffusion, and Sedimentation Rate of Polymers in Solution", J. Chem. Phys. 16, 573-579, 1948

[10] Zimm, B.H., R.W. Kilb, "Dynamics of Branched Polymer Molecules in Dilute Solution", J. Polymer Sci. 37, 19-42, 1959

[11] Roovers, J., "Encyclopedia of Polymer Science and Engineering", Klingsber, A., J. Muldoon, A. Salvatore, Eds.; Wiley: New York, 2, 478-499, 1985

[12] Tackx, P., J.C.J.F. Tacx, "Chain Architecture of LDPE as a Function of Molar Mass Using Size Exclusion Chromatography and Multi-Angle Laser Light Scattering (SEC-MALLS)", Polymer, 39, 3109-3113, 1998

Chapter 3. Materials

Four sets of materials were selected to achieve the objectives of the project. A set is a group of samples, which consists of a linear precursor and several branched samples having various levels of branching based on the same linear precursor. A sample's name consists of two parts: the first part is a number that indicates the melt flow rate (MFR) of the precursor, and the second part is the letter "L" or "B", where "L" indicates that the sample is linear and "B" indicates that the sample is branched. The number following letter "B" indicates the level of branching, the larger the number the higher the level of long chain branching. For example, one set has four samples: 12L, 12B1, 12B2 and 12B3. The number 12 indicates that all the samples have the same linear precursor having MFR of 12. Sample 12L is linear while sample 12B1 is branched. Transitioning from B1 to B3, the level of branching increases. Key properties of these polymers are listed in Tables 3.1 to 3.3. Table 3.1 contains the set of 12 MFR based samples and sample 20L. Tables 3.2 and 3.3 contain the sample sets of 35 MFR and 2 MFR respectively. In the following sections, information about how these materials made, how their properties measured, and what their applications in this project is given.

3.1. Preparation

The linear polypropylenes are traditional homopolymer polypropylenes made using Ziegler-Natta catalysts. The most common Ziegler-Natta catalysts for olefin polymerization are: $TiCl_3$ with $Al(C2H5)_2Cl$ as co-catalyst, or $TiCl_4$ with $Al(C2H5)_3$ as co-catalyst. As mentioned in Chapter 1, due to the crystalline structure of the catalyst and the electron coordinating nature of titanium, the polypropylenes produced using Ziegler-Natta catalysts have high stereoregularity.

On the other hand, due to the multi-reactive site nature of Ziegler-Natta catalysts, polypropylenes produced using these catalysts have fairly broad molecular weight distributions. The polydispersity indices (M_w/M_n) of linear samples used in this study ranged from 3.6 to 6.1. All samples were stabilized with the types and levels of antioxidant commonly found in commercial polypropylenes.

The high melt strength polypropylenes with various levels of branching are the "B" samples in Tables 3.1-3.3. While introducing some branching improves the processability of the polymer, too high a branching level reduces mechanical properties such as stiffness and tensile strength. To achieve a balance between end-use mechanical properties and processability, the level of branching must be controlled so that it increases the melt strength without sacrificing the solid-state properties.

All the materials were received from The Dow Chemical Company in pellet form.

3.2. Properties

Melt flow rate (MFR) is a widely used standard test to describe in a general way the fluidity of commercial thermoplastics. The values shown in Tables 3.1 to 3.3 were determined by ASTM Standard Test Method D-1238. The material is loaded into the barrel of the extrusion plastometer, which has been heated to 230 °C. A weight of 2.16 kg is applied to a plunger and the molten material is forced through a standard die. A timed extrudate is collected and weighed. Melt flow rate values are reported in dg/min. From Tables 3.1-3.3 we can see that for a given linear precursor, MFR decreases with the increasing level of branching, which indicates that the polymers flow more slowly. The MFR data were supplied by The Dow Chemical Company.

Melt strength is another test result, which is critical to polymer processes such as fiber spinning, extrusion coating, thermoforming and blow molding. It is measured by a Goettfert Rheotens pulling the extrudate with increasing speed as it emerges from a die, while measuring the force on the melt. The result of this test is a graph of force against haul-off speed. The force at failure is referred to melt strength. The values shown in Tables 3.1 to 3.3 were measured at 190 °C using the method described by Hoenig *et al.*[1] The melt strength of sample 35L was too low to be measured reliably. For a given linear precursor, with the increasing level of branching, the melt strength increases.

A second property that is determined using a melt strength tester is drawability, which is of great importance in processes such as fiber spinning, film blowing, and blow molding. The speed at failure in the graph of force against haul-off speed is defined as drawability. With increasing the level of branching, the drawability decreases. The melt strength and drawability data were supplied by The Dow Chemical Company.

The molecular weight distributions, weight average molecular weight, M_w, number average molecular weight, M_n , and z-average molecular weight, M_z , were determined by high temperature gel permeation chromatography (GPC) on a Polymer Laboratories PL-GPC210 chromatographic unit equipped with a differential refractive index detector, a Viscotek model 210R viscometer and a Precision Detectors PD2040 light scattering instrument (15° angle)[2]. The unit contained three linear Polymer Laboratories mixed 10 μm columns. The oven temperature was 160 °C, which implies that the auto-sampler hot zone was at 160 °C and the warm zone was at 145 °C. The solvent was nitrogen purged 1,2,4-trichlorobenzene containing 200 ppm 2,6-di-t-butyl-4-methylphenol. The flow rate was 1.0 ml/min and the injection size was 100 μl. About 0.2% (by weight) solution of the sample was prepared for injection by dissolving the sample in the solvent for 2.5 hrs at 160 °C with gentle mixing. The system was calibrated using a standard material (NBS 1475) with a weight-average molecular weight of 52 000 g/mol and an intrinsic viscosity of 1.01 dL/g. Detector offsets were determined using the systematic approach of Mourey and Balke[3]. The GPC data were supplied by The Dow Chemical Company.

The zero-shear viscosities, η_0, of samples 35L and 20L were determined by melt state dynamic mechanical experiments. The zero-shear viscosities of the other samples in Tables 3.2 and 3.3 were determined by combining two types of measurement, dynamic frequency sweep and creep/recovery, as demonstrated by Kraft *et al.*[4]. The combination technique is described in detail in Chapter 4 Section 4.3.

3.3. Sample Applications in This Study

The materials in Table 3.1 based on the linear precursor of 12 MFR and with three levels of branching were used to study the thermal stability of the samples at the temperatures used to mold and gather experimental rheology data. The results were used to determine the optimum temperature for the rheological measurements. If the temperature is too close to the melting point of the sample, the sample has minimal degradation, but the preparation time is long due to the very slow relaxation of the sample after trimming and compression (loading of sample into the rheometer). In the extreme situation, the sample cannot relax to its equilibrium state, and it is impossible to measure the linear viscoelastic properties. If the temperature is too high, degradation occurs, and there is insufficient time to complete the measurements. At a suitable experimental temperature, samples should have minimal degradation for a period of at least 25 hours and the time for complete relaxation after sample loading should be within 3 hours.

Once optimal conditions were established, measurements were carried out over the broadest possible range of frequencies. Due to the limited amount of samples, only dynamic measurements were carried out on samples at 175 °C. Zero-shear viscosities of the branched samples were not determined.

Linear samples of 20 MFR before and after extrusion were selected. The sample before extrusion was labeled as "20L", and the sample after extrusion was named "20L-extruded". The flow mechanical properties and molecular weight characteristics of 20L are listed in Table 3.1. The flow characteristics of 20L-extruded were not available. These two samples were used to detect, in rheological point of view, the significance of chain scission of the linear chains during the extrusion.

Complete linear viscoelastic characterizations were carried out on the two sets of samples that are listed in Tables 3.2 and 3.3. The two linear precursors, 35L and 2L, have different weight average molecular weights and polydispersity indices. By studying these two sets of samples, the effects of branching on linear viscoelastic behavior were investigated and a quantitative technique determining the branching information is established based on the differences in rheological behavior.

Table 3-1: Characteristics of the set of samples of 12 MFR and sample 20L

Sample	12L	12B1	12B2	12B3	20L
M_n (kg/mol)	41.3	38	40.1	47.9	35.9
M_w (kg/mol)	248	328	391	488	210
M_z (kg/mol)	744	1229	1578	2051	640
PDI (M_w/M_n)	6.00	8.63	9.75	10.19	5.85
η_0(×10^3) (Pa.s)	5.3 (175 °C)	----	----	----	2.63 (180 °C)
MFR(dg/min) (230 °C)	12.0	4.7	1.1	0.8	20
Melt strength (cN) (190 °C)	1.14	51.4	100.1	131.8	0.76
Drawability (mm/s) (190 °C)	100	19.7	31.8	27.6	107

Table 3-2: Characteristics of the set of samples of 35 MFR

Sample	35L	35B1	35B2	35B3
M_n (kg/mol)	49.4	53.5	52.5	55.4
M_w (kg/mol)	179	195	246	307
M_z (kg/mol)	428	489	776	1136
PDI (M_w/M_n)	3.62	3.65	4.68	5.53
$\eta_0(\times 10^3)$ (Pa.s) (180 °C)	1.13	2.44	11	60
MFR(dg/min) (230 °C)	35.0	24.4	13.3	3.9
Melt strength (cN) (190 °C)	----	1.69	8.52	53.7
Drawability (mm/s) (190 °C)	----	177.4	178.3	42.1

Table 3-3: Characteristics of the set of samples of 2 MFR

Sample	2L	2B1	2B2	2B3	2B4
M_n (kg/mol)	61.4	63.6	62.5	65.8	59.1
M_w (kg/mol)	375	384	379	402	429
M_z (kg/mol)	1267	1274	1260	1394	1591
PDI (M_w/M_n)	6.11	6.04	6.06	6.11	7.26
η_0 ($\times 10^3$) (Pa.s) (180 °C)	27.25	39.32	85	263	900
MFR(dg/min) (230 °C)	2.04	2.04	1.82	1.22	1.08
Melt strength(cN) (190 °C)	5.6	6.2	8.0	18.8	43.7
Drawability (mm/s) (190 °C)	250.1	239.6	272.8	24.3	19.2

Reference

---

[1] Hoenig, W. D., C. P. Bosnyak, K. Sehanobish, W. Van Volkenburgh, C. Ruiz, L. M. Tau, "New polypropylene for differentiated blown films," SPE ANTEC Proceedings 2, 1843-1846, 2000

[2] Wood-Adams, P.M., J.M. Dealy, A.M. deGroot, O.D. Redwine, "Effect of Molecular Structure on the Linear Viscoelastic Behavior of Polytheylene", Macromolecules, 33, 7489-7499, 2000

[3] Mourey, T. H., S. T. Balke, ACS Symp. Ser. 521, 231, 1993

---

[4] Kraft, M., J. Meissner, J. Kaschta, "Linear Viscoelastic Characterization of Polymer Melts With Long Relaxation Times," Macromolecules, 32, 751-757, 1999

Chapter 4. Experimental Methods and Data

4.1. Relevant Linear Viscoelastic Functions

Polymers exhibit linear viscoelastic behavior when subjected to very small or very slow deformations, in which the deviation of the polymer chain from its equilibrium state is negligible. Material functions measured under such conditions are termed as linear viscoelastic properties. In a stress relaxation experiment, a small step strain, γ_0, is applied at $t = 0$, and the resulting stress, σ, is measured as a function of time. The results can be represented in terms of the relaxation modulus, $G(t)$,

$$\sigma(t) = G(t)\gamma_0 \tag{4.1}$$

If the response is linear, $G(t)$ is independent of the magnitude of the step strain. For more complex strain history, we can use the Boltzmann superposition principle (Eq. 4.2) to describe the stress response:

$$\sigma(t) = \int_{-\infty}^{t} G(t - t')d\gamma(t') \tag{4.2}$$

The linear viscoelastic response is also independent of the kinematics of the deformation, so we can replace the shear strain by the infinitesimal strain tensor and shear stress by the stress tensor to get the tensorial form of the Boltzmann superposition principle:

$$\tau_{ij}(t) = \int_{-\infty}^{t} G(t - t')d\gamma_{ij}(t') \tag{4.3}$$

Although it is convenient to use the shear relaxation modulus, $G(t)$, to describe the linear viscoelastic response, it is difficult to impose a step strain instantaneously. Therefore, we usually use small-amplitude oscillatory shear experiments to determine the linear viscoelastic properties of polymer melts. Instead of a step strain, the shear strain given by Eq. 4.4 is applied to the sample.

$$\gamma(t) = \gamma_o \sin(\omega t) \tag{4.4}$$

The stress response can be expressed as:

$$\sigma(t) = \sigma_o \sin(\omega t + \delta) \tag{4.5}$$

where σ_o and δ are functions of frequency ω. If we introduce the storage modulus $G'(t)$ and loss modulus $G''(t)$, we also can write the stress as:

$$\sigma(t) = \gamma_o[G'(\omega)\sin(\omega t) + G''(\omega)\cos(\omega t)] \tag{4.6}$$

From G' and G'' we can define the complex modulus as follows:

$$G^*(\omega) = G'(\omega) + iG''(\omega) \tag{4.7}$$

An alternative representation of Eq. (4.6) is:

$$\sigma(t) = \dot{\gamma}_o[\eta'(\omega)\cos(\omega t) + \eta''(\omega)\sin(\omega t)] \tag{4.8}$$

The viscosity functions η' and η'' are defined by:

$$\eta' = G''/\omega \text{ and } \eta'' = G'/\omega \tag{4.9}$$

and the complex viscosity is:

$$\eta^* = \eta'(\omega) - i\eta''(\omega) \tag{4.10}$$

A material function often used to describe linear behavior is the absolute value of the complex viscosity, which is given by Eq. 4.11.

$$\left|\eta^*\right| = \sqrt{(\eta')^2 + (\eta'')^2} \tag{4.11}$$

Creep is another useful linear viscoelastic characterization technique, which is employed to study polymers having long relaxation times. In a creep test, instead of a small step strain, a small step stress σ_0 is applied at $t = 0$, and the resulting strain $\gamma(t)$ is measured as a function of time. The shear creep compliance, $J(t)$, is the resulting material function:

$$J(t) = \frac{\gamma(t)}{\sigma_0} \tag{4.12}$$

The creep compliance is independent of σ_0 in the case of linear behavior.

The deformation of the polymer under constant stress is related to the relaxation of the corresponding structure species. For a polymer melt at a sufficiently long time, the shear rate becomes constant, and the creep compliance increases linearly with time as sketched in Fig. 4.1. This is considered steady state.

After the experiment has reached steady state, the linear portion of the creep compliance curve can be extrapolated to $t = 0$ to determine the steady-state compliance J_s^0, and the slope of the straight line is the reciprocal of the zero-shear viscosity η_0.

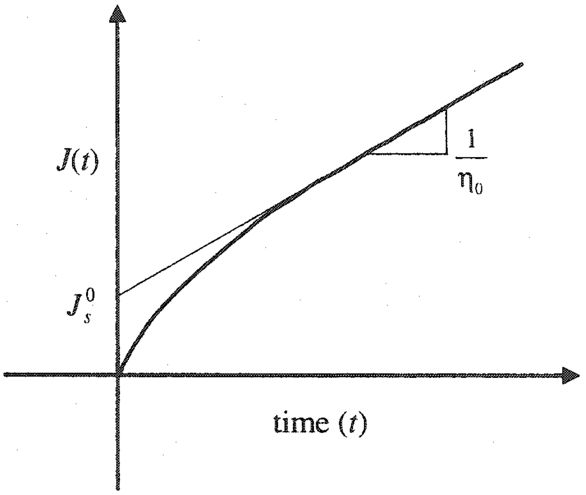

Figure 4-1: Sketch of a typical creep compliance curve for a polymer melt

The complex compliance is an alternative function used to describe the response of a polymer to a sinusoidal stress. The complex compliance is defined as:

$$J^*(\omega) = J'(\omega) - iJ''(\omega) \tag{4.13}$$

where $J^*(\omega)$ is the complex compliance, $J'(\omega)$ is the storage compliance and $J''(\omega)$ is the loss compliance, and the storage and loss compliances are calculated as follows:

$$J' = \left(\gamma_0 / \sigma_0 \right) \cos\delta \tag{4.14}$$

$$J'' = \left(\gamma_0 / \sigma_0 \right) \sin\delta \tag{4.15}$$

For linear viscoelastic behavior, the applied stress in the creep experiment must be small enough so that the polymer chain deviates from its equilibrium state to a negligible extent. However, it is not always possible to use such a small stress due to limitations of the instrument. For some polymers, when they are subjected to a constant stress, the deformation will go beyond the linear region before the shear rate reaches a steady state. In this case, the " creep and recovery" technique described by Kraft *et al.*[1]

can be used. In this experiment, first a constant stress σ_0 is applied at $t = 0$ to start a standard creep test, and then, at a time t_1, while the strain is still within the linear region, the stress is reduced to zero. The part of the experiment after the stress is removed is called "recovery", and the material recoils in the direction opposite to that of the original stress. In this way, the linearity of the deformation is preserved. The recoil strain γ_r is a function of the creep time t_1 and the recoil time $(t-t_1)$,

$$\gamma_r(t-t_1, t_1) = \gamma(t_1) - \gamma(t) \tag{4.16}$$

By use of the Boltzmann superposition principle and the results of creep and recovery experiments, the creep compliance can be obtained in a broad time window while maintaining the deformation within the linear region. The detailed procedure is given in Section 4.3.2.4.

All these linear shear material functions, $G(t)$, $G'(\omega)$, $G''(\omega)$, $\eta^*(\omega)$, $J(t)$, $J'(\omega)$, $J''(\omega)$ can be interrelated[2] by two additional material functions, the relaxation spectrum and the retardation spectrum.

The basic features of a stress relaxation experiment can be represented by a simple mechanical model, the Maxwell element, which is a spring with modulus G_i and a dashpot with viscosity η_i connected in series. The Maxwell element is shown in Fig. 4.2. The spring represents the elastic behavior, while the dashpot represents the viscous behavior. The relaxation time of the element is $\tau_i = {}^{\eta_i}/_{G_i}$.

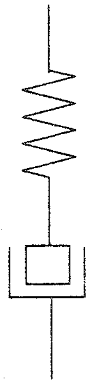

Figure 4-2: The Maxwell element[2]

However, for a polymer melt, the stress relaxation is not described quantitatively by this simple model. To completely describe the viscoelastic behavior of the stress relaxation of a polymer melt, many Maxwell elements in parallel are necessary. In the case of an infinite number of elements, this leads to a continuous relaxation spectrum $Hd\,ln\,\tau$, which is the contribution to the modulus in the time interval between $ln\,\tau$ and $(ln\,\tau + d\,ln\,\tau)$. This contribution includes all the possible relaxation mechanisms during this time period. The relaxation modulus can be expressed in terms of a continuous relaxation spectrum as shown by Eq. 4.17:

$$G(t) = \int_{-\infty}^{+\infty} He^{-t/\tau} d\ln\tau \tag{4.17}$$

Similarly, the storage and loss moduli can be related to the continuous relaxation spectrum as in the following:

$$G' = \int_{-\infty}^{+\infty} H \frac{\omega^2\tau^2}{1+\omega^2\tau^2} d\ln\tau \tag{4.18}$$

$$G'' = \int_{-\infty}^{+\infty} H \frac{\omega\tau}{1+\omega^2\tau^2} d\ln\tau \tag{4.19}$$

Another mechanical model, the Voigt element, represents the basic features of the response of a crosslinked elastomer to a creep experiment. In this model the spring and dashpot are connected in parallel as shown in Fig. 4.3

The characteristic time $\tau_i = {}^{\eta_i}\!/_{G_i}$ of the element is the time for the element to reach its equilibrium length when subjected to a constant stress. This process is retarded by the dashpot, so τ_i is called the retardation time.

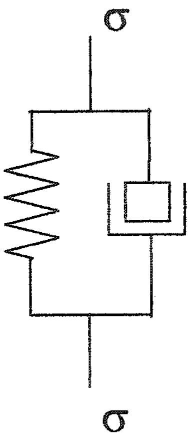

Figure 4-3: The Voigt element[2]

As in the stress relaxation experiment, we need to introduce many Voigt elements in series and therefore a continuous retardation spectrum $Ld\ln\tau$ to represent the continuous response of a polymer to a creep experiment. Also, for a melt, we must include one element that consists of only a dashpot to account that one of the springs has zero rigidity. The creep compliance can then be expressed in terms of the continuous retardation spectrum as in Eq. 4.20:

$$J(t) = J_g + \int_{-\infty}^{+\infty} L\left(1 - e^{-t/\tau}\right) d\ln\tau + t/\eta_0 \qquad (4.20)$$

where J_g is the instantaneous compliance, which is often negligible in magnitude for thermoplastic melts.

The storage and loss compliances can now be expressed as follows:

$$J' = J_g + \int_{-\infty}^{+\infty} \frac{L}{1+\omega^2\tau^2} d\ln\tau \qquad (4.21)$$

$$J'' = \int_{-\infty}^{+\infty} \frac{L\omega\tau}{1+\omega^2\tau^2} d\ln\tau + 1/\omega\eta_0 \qquad (4.22)$$

If we could measure material functions such as $G(t)$, $G'(\omega)$, $G''(\omega)$, $\eta^*(\omega)$, $J(t)$, $J'(\omega)$, $J''(\omega)$ over the entire time or frequency range from 0 to $+\infty$, we could calculate the continuous spectra from Eqs 4.17-22. However, the long-time part of the experimental time window is limited by factors such as the physical limitations of the instrument and the thermal stability of the sample. Therefore, we can only make measurements in a limited time window, and as a result the calculation of the continuous spectra by using Eqs 4.17-22 is an ill-posed problem, because there is no unique solution. As a result, special techniques are required to obtain a continuous spectrum approximating the actual spectrum. This issue is discussed in detail in Section 4.4.2.1.

4.2. Effects of Long-Chain Branches on Linear Viscoelastic Properties

Long-chain branched polymers are materials having side chains longer than the critical entanglement molecular weight M_c, which is about twice the molecular weight between two consecutive entanglement points M_e[3]. Some branched structures are sketched in Fig. 4.4.

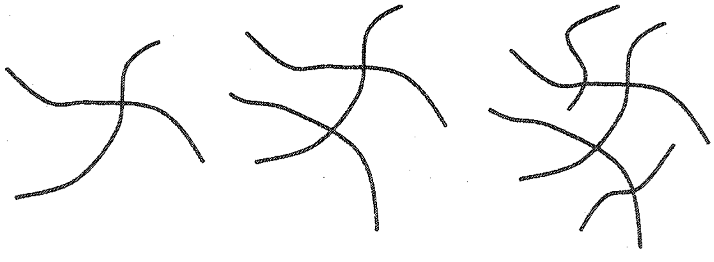

Figure 4-4: Schematic of some branched structures.

The study of the effects of long-chain branches on rheological behavior is of great interest in both the academic and industrial sectors. In the plastics industry, long-chain branches are often introduced to improve processability without sacrificing solid-state properties. Polymer scientists have invested a great deal of effort in studying the effects of long-chain branching on rheological behavior and using rheological data to detect the level of branching.

Many factors, including branch points per chain, branch length and the branch structure affect the linear viscoelastic behavior of polymer melts. Bersted[4] has reviewed the general effects of branching structure and branching level on melt rheology. For a randomly branched material, he predicted that the low shear rate viscosity increases with branching level, reaches a maximum, and then decreases with a further increase of the branching level. The tendency is resulted from the competitive effect of branching and molecular size on rheology. This tendency was observed by Constantin[4] in the behavior of fractionated polyethylenes as shown in Fig. 4.5, where the y-axis is $\frac{\eta_0(\mathrm{br})}{\eta_0(\mathrm{lin})}$, the ratio of zero-shear viscosities of branched and linear fractions having the same weight average molecular weight M_w at 190 °C, and the x-axis is the branching index g', which is defined as $g' = \left(\frac{[\eta]}{[\eta]^*}\right)^{1+\alpha_2}$ in which α_2 is the Mark-Houwink exponent of linear polyethylene ($\alpha_2 = 0.69$). $[\eta]$ is the intrinsic viscosity of the sample, and $[\eta]^*$ is the intrinsic viscosity of a linear polyethylene having the same molecular weight.

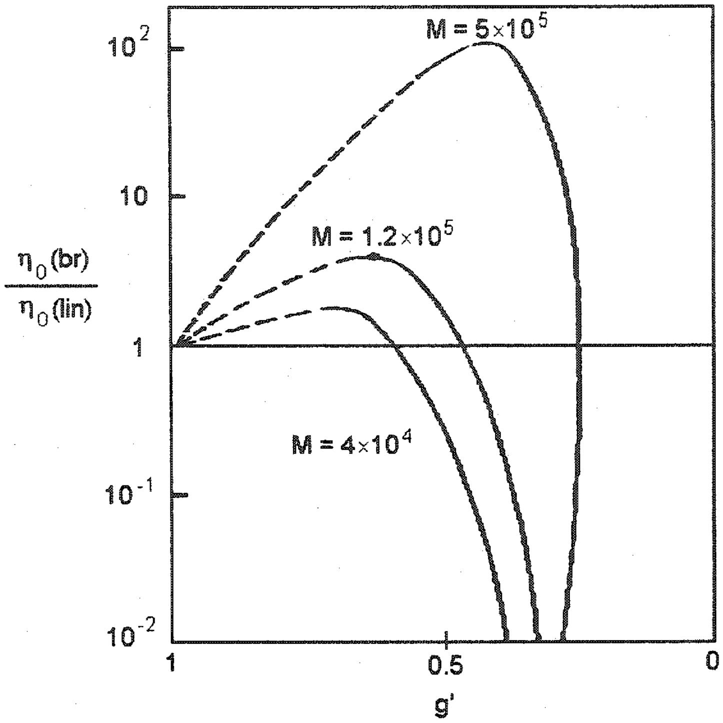

Figure 4-5: Ratio of zero-shear viscosities of branched and linear fractions[4] having the same molecular weight M_w vs. branching index g'

In Fig. 4.5 we see that for the same branching index g', the higher the molecular weight the broader the zone in which the zero-shear viscosity increases with increasing of branching level. In another words, for a low molecular weight polymer, introducing branches will not affect the zero-shear viscosity or may even decrease it. This phenomenon was found by Roovers[5] in his study of H-shaped polystyrenes. For low molecular weight H-polystyrenes, the zero-shear viscosities are the same as those of linear polymers of the same size. However, high molecular weight H-polystyrenes exhibit enhanced viscosities in comparison with three-arm or four-arm stars having the same number of entanglements per branch. The work of Fetters *et al.*[6] on symmetric star polyisoprene and Gell *et al.*[7] on asymmetric poly(ethylene-alt-propylene) also revealed the increase of the zero-shear viscosity by branches. For star polymers, arm length has a significant effect on the low-frequency behavior, whereas the number of arms has no detectable effect. Kasehagen *et al.*[8] reached the same conclusion regarding the enhancement of zero-shear viscosity in their study of randomly branched polybutadienes.

Robertson *et al.*[9] observed a decrease of zero-shear viscosity due to the high level of long-chain branching in the study of randomly hyperbranched polyisobutylenes. Long-chain branches also extend the plateau zone due to the slow, hierarchical relaxation of branched chains[8,9].

The authors in ref. 9 found that long-chain branches introduced an intermediate relaxation regime between the plateau and terminal zones and increased the steady-state compliance J_s^0. Gabriel *et al.*[10] investigated a long-chain branched, low-density polyethylene (LDPE) with a broad MWD and a low-density linear polyethylene (LLDPE) with narrower MWD using creep recovery in shear. The two samples had different weight average molecular weight and polydispersity. They found that the steady-state compliance of LLDPE is more than two times that of LDPE, whereas in the short-time region up to 1000 s, the time dependent recoverable compliance of LDPE is greater than that of LLDPE. However, both polydispersity and long-chain branching affect the creep compliance, so it is hard to draw a conclusion about the effect of long-chain branching on creep compliance from this study.

A new class of polyethylene, long-chain branched metallocene polyethylene (mPE), has attracted a great deal of attention because of its unique and well-controlled structure. It is possible to make metallocene polyethylenes with almost the same polydispersity and weight average molecular weight but various levels of long-chain branching. Therefore, it is possible to separate the effects of long-chain branching from those of polydispersity and weight average molecular weight by studying these materials. Wood-Adams *et al.*[11] studied a set of mPEs including one linear polymer and three having various levels of branching. The characteristics of these polymers are given in Table. 4.1.

Table 4-1: Characteristics of metallocene polyethylenes[11]

Resin	M_w*	M_w/M_n	λ (LCB/10^3C*)
HDL1	100900	2.08	0
HDB1	88400	1.98	0.026
HDB3	101500	1.99	0.042
HDB4	90200	2.14	0.121

*Molecular weight was measured by differential refractive index detector gel permeation chromatography; LCB was measured by nuclear magnetic resonance.

These materials have approximately the same weight average molecular weight and polydispersity index but varying levels of long-chain branching. Therefore, the differences in rheological behavior are due to long-chain branching.

The complex viscosity data are shown in Fig. 4.6. With increasing level of LCB, the low frequency viscosity increases, and the transition zone between the power law region and terminal zone is extended. This is in agreement with the findings of other researchers.

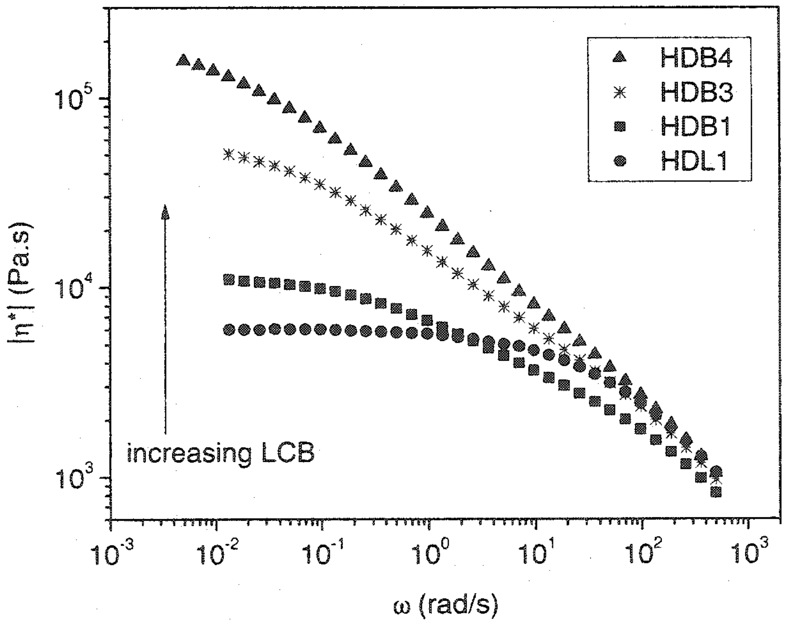

Figure 4-6: Dependency of |η*| on ω for high-density, branched mPEs[11] at 150 °C

Gabriel and Münstedt[12] studied two metallocene, linear low-density polyethylenes (mLLDPE) that had homogeneous comonomer distributions and similar molecular weight distributions but different levels of long-chain branching. mLLDPE3 contained a few long-chain branches, while mLLDPE4 was linear. Thus, the differences in rheological behavior are due mainly to long-chain branching. Long-chain branches increased the elasticity of the sample, as shown in Fig. 4.7. The steady-state compliance of the branched mLLDPE3 is about 8 times that of linear mLLDPE4.

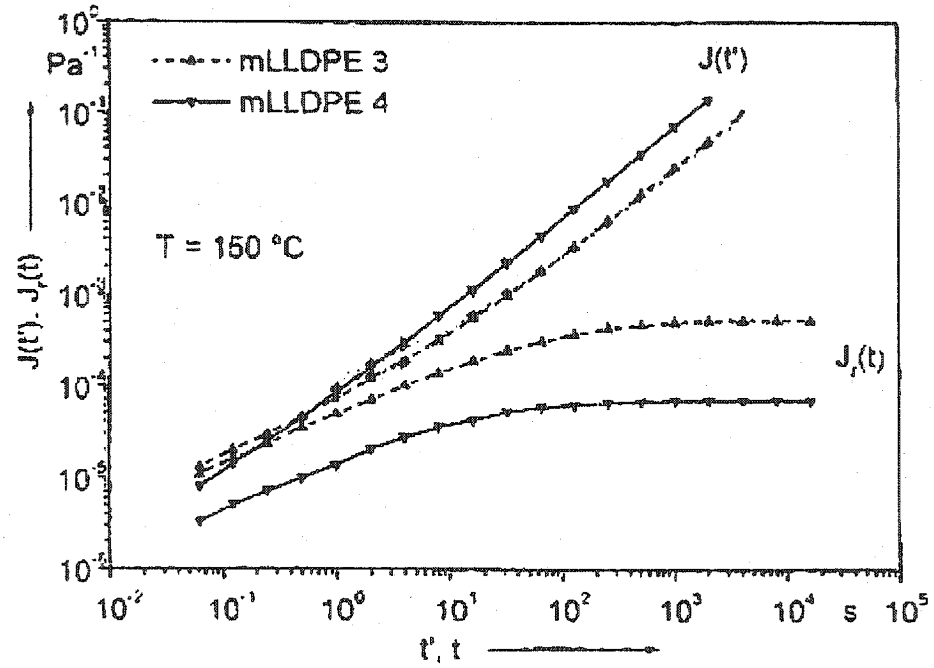

Figure 4-7: Comparison of the creep and recoverable compliances of the two mLLDPE[12]

Gabriel and Münstedt[12] also found that long-chain branching causes increased shear thinning. The results were presented as plots of $|\eta^*|/\eta_0$ versus $\omega\eta_0$, as shown in Fig. 4.8. The shear thinning of mLLDPE3 starts at a lower frequency than that of mLLDPE4, and at high frequencies the viscosity of the branched mLLDPE3 is below that of mLLDPE4. Similar reports of the effects of long-chain branches on zero-shear viscosity, elasticity and shear thinning were reported by Yan *et al.*[13] and by Gabriel and Münstedt[14] in other studies of metallocene polyethylenes.

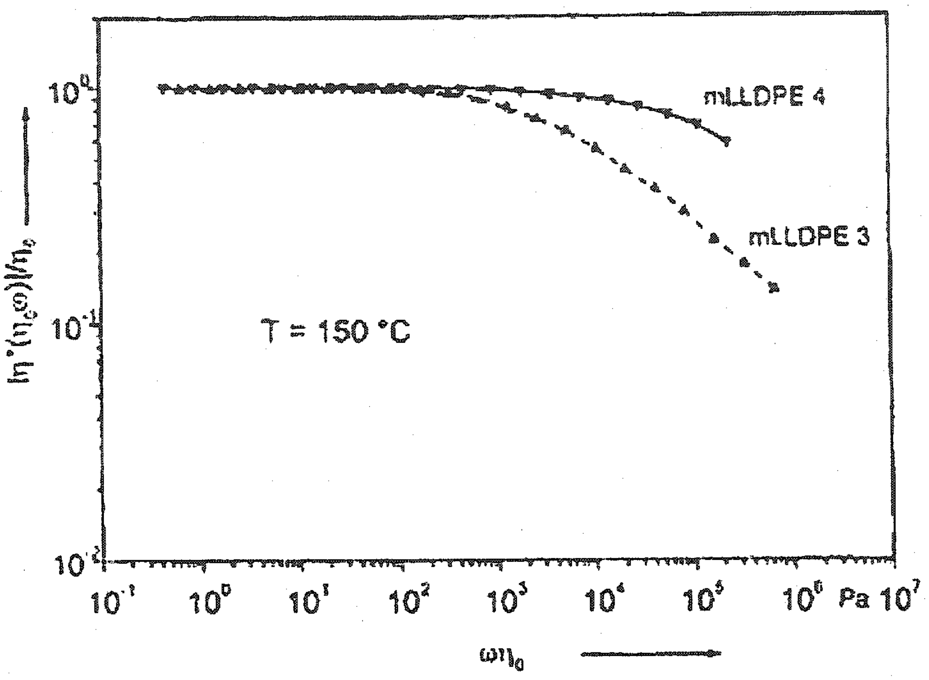

Figure 4-8: Shear thinning behavior of the two mLLDPEs[12]

While metallocene polyethylenes offered a great opportunity to study the effects of long-chain branching on rheological behavior, few studies of the rheology of long-chain branched polypropylenes have been reported. Hingmann and Marczinke[15] studied one linear, isotactic polypropylene and two chemically branched polypropylenes. The characteristics of these samples are shown in Table 4.2.

Table 4-2: Characteristics of the polypropylenes studied by Hingmann and Marczinke[15]

Sample	M_w(g/mol)	M_w/M_n	LCB*
PP-1	9.1×10^5	4.2	0
PP-2	3.4×10^5	2.5	1.5
PP-3	4.5×10^5	3.0	3.0

*statistically estimated number of long-chain branches per molecule

They presented dynamic LVE data over the frequency range from 10^{-3} to 10^{2} rad/s and found that the branched samples did not reach their terminal zones at the lowest accessible frequency. The effects of long-chain branching on the zero-shear viscosity, shear thinning and extended transition zone could not be learned from this study, because the samples had different M_w, M_w/M_n and branching levels as shown in Table 4.2. The differences in the behavior of these samples were the combined effects of changes in M_w, M_w/M_n and long-chain branching.

Kurzbeck *et al.*[16] subjected a linear ethylene-propylene copolymer and a long-chain-branched polypropylene to oscillatory shear and low shear stress creep tests. By use of the Cox-Merz rule, the complex viscosity was extended into the Newtonian region. However, the storage and loss moduli could not be determined in the low frequency region using this approach.

In this work, linear characterizations were performed on Ziegler-Natta polypropylenes based on a single linear precursor with various levels of branching. These samples have different values of M_w and M_w/M_n as was mentioned in Chapter 3. To have a complete picture of the linear viscoelastic behavior, the characterization was carried over a broad frequency range by using the creep and recovery technique demonstrated by Kraft *et al.*[1] The zero-shear viscosity, the complex moduli, and the creep compliance expose different aspects of the linear behavior. The effects of branching on the rheological behavior complicate the comparison of the materials studied. Therefore, the measured material functions were transformed into relaxation spectra. From the time-weighted relaxation spectrum $\tau H(\tau)$, it is possible to see the role of each relaxation mechanism.

4.3. Experimental Methods and Data

4.3.1. Determination of Suitable Experimental Temperature

Experiments were first carried out at 175 °C because extensional data were available at that temperature from The Dow Chemical Company. The set of samples based on the linear precursor of 12 MFR was studied. The thermal stability of the samples and the linearity at various strains of each sample were determined. The small-amplitude oscillatory tests were performed on an ARES (Advanced Rheometric Expansion System) rheometer made by Rheometric Scientific. The results shown in Fig. 4.9 are the averages of four runs.

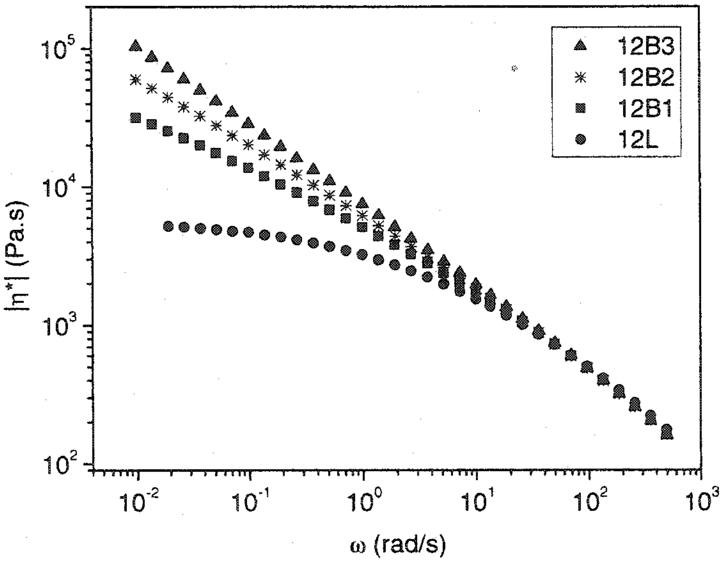

Figure 4-9: Dependency of $|\eta^*|$ on frequency ω for the set of 12 MFR samples, 175 °C

In Fig. 4.9 we see that for branched samples the long time (low frequency) relaxation behavior, which is activated in the low frequency plateau region, is not accessible in the experimental window of the dynamic measurement. However, it is the branched species that have the longest relaxation times and manifest themselves at the missed low frequencies. Therefore, in order to extract branching information from rheological measurements, we need to extend the experimental window into the lower frequency region, *i.e.*, into the terminal zone. Creep and recovery experiments are useful for characterizing the viscoelastic properties of samples having long relaxation times. Therefore, in addition to the dynamic measurements, creep and recovery experiments were used to obtain the zero-shear viscosity and to extend the dynamic measurements to lower frequencies.

During the dynamic experiments on the set of 12 MFR samples, it was found that the relaxation of the normal force for samples 12B1, 12B2 and 12B3 after pressing and trimming the sample was extremely slow. A differential scanning calorimetry (DSC) measurement was carried out on sample 12B3, and the peak location of the second melting curve showed that the melting temperature was 163 °C. The data are in Appendix A. The slow relaxation was thought to be due to the proximity of the experimental temperature to the melting temperature. In order to carry out measurements in an equilibrium state (zero normal force), a higher experimental temperature was thus deemed necessary.

In order to choose an appropriate temperature for the experiments, thermal stability tests were carried out at several temperatures. The results of these tests are shown in Fig. 4.10.

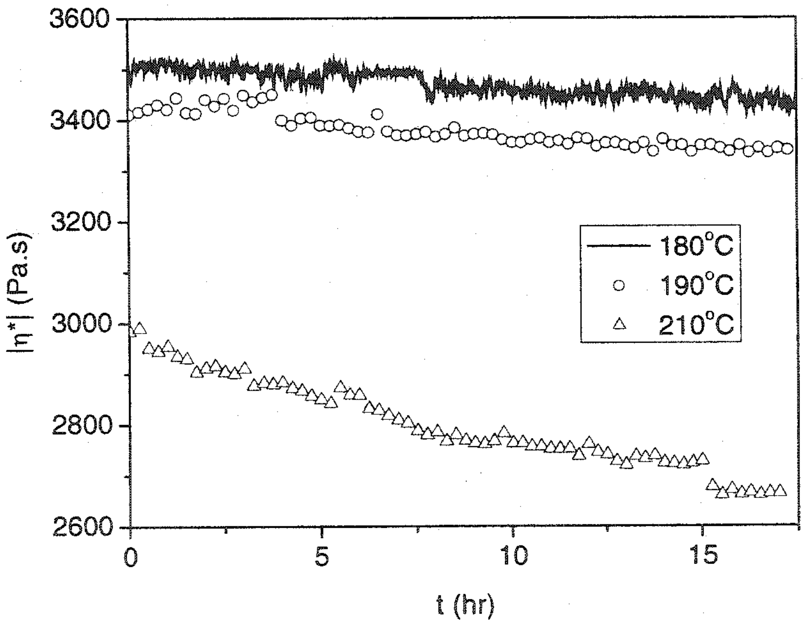

Figure 4-10: Dependency of |η*| on time *t* for 12B1 at various molding and experimental temperatures, and $\omega = 1 s^{-1}$, $\gamma_0 = 5\%$

We see in Fig. 4.10 that 180 °C is an appropriate molding and experimental temperature at which degradation is minimal. All samples were molded at 180 °C using a

Carver Laboratory Press, and all measurements were carried out at 180°C in a nitrogen atmosphere. As mentioned before, two kinds of measurement, small-amplitude oscillatory shear, and creep/recovery, are necessary for samples having long relaxation times. The experimental methods for these two types of test are described in the following sections.

4.3.2. Small-Amplitude Oscillatory Shear

4.3.2.1. Thermal Stability of Samples

Before making measurements, the thermal stability and effective lifetime of the samples were established using time sweep experiments. In such an experiment, the sample is subjected to oscillating strain or stress at fixed amplitude, frequency and temperature during a period of time and the material responses are recorded. The frequency selected should not be too low, where the measurements take a long time and degradation is probable, but should not be too high, where the instrument compliance can introduce errors. Usually, we chose a frequency of either 1 rad/s or 0.1 rad/s. The strain (stress) should be within the linear deformation limit for the sample at the chosen frequency but should not be so small that the transducer output has poor precision.

The time sweep results for samples 20L and 20L-extruded are shown in Fig. 4.11. The samples have very similar behavior and are stable for more than 6 hours. A sample is considered to be stable if the change of $|\eta^*|$ compared to the initial value (in the case of linear samples) or the level off value (in the case of branched samples) is less than 3%. The results for sample 35L are shown in Fig. 4.12, and the results for the branched sample, 35B3 are shown in Fig. 4.13. The linear sample was stable for the entire ten hours under the stated conditions. As was typical of the branched samples, the complex viscosity of 35B3 decreased for the first four hours and then leveled off for the next six hours. We attribute the initial transient to the very slow relaxation of the orientation and normal force induced during sample loading. Therefore, for the branched samples we waited four hours after sample loading to ensure that the sample was in its equilibrium state before starting measurements. Time sweep experiments were performed for all the materials, and all the measurements were carried out within the period of thermal stability. The time sweep data of the other samples are included on the CD attached to this thesis.

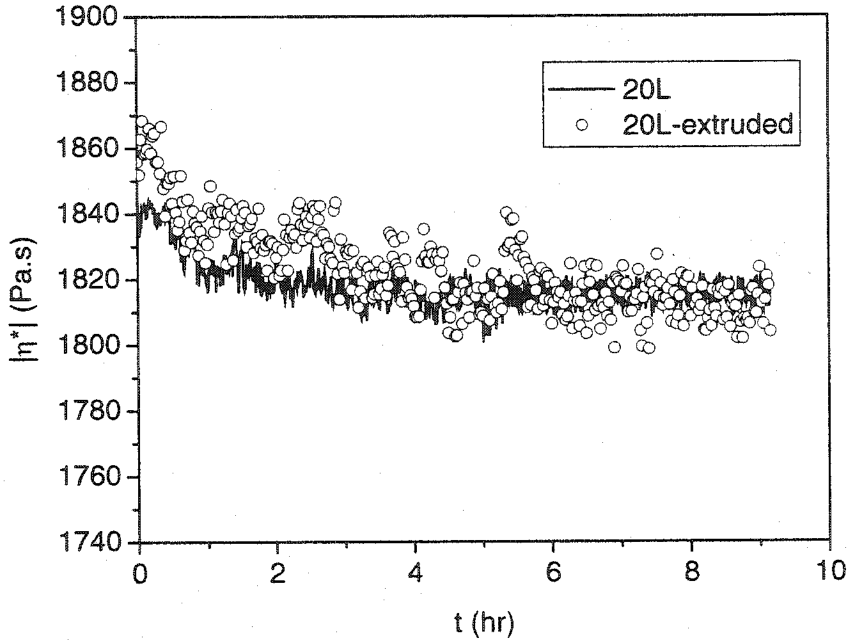

Figure 4-11: Dependency of |η*| on time *t* for linear isotactic polypropylene 20L and 20L-extruded at T = 180 °C, and $\omega = 1 s^{-1}$, $\gamma_0 = 5\%$

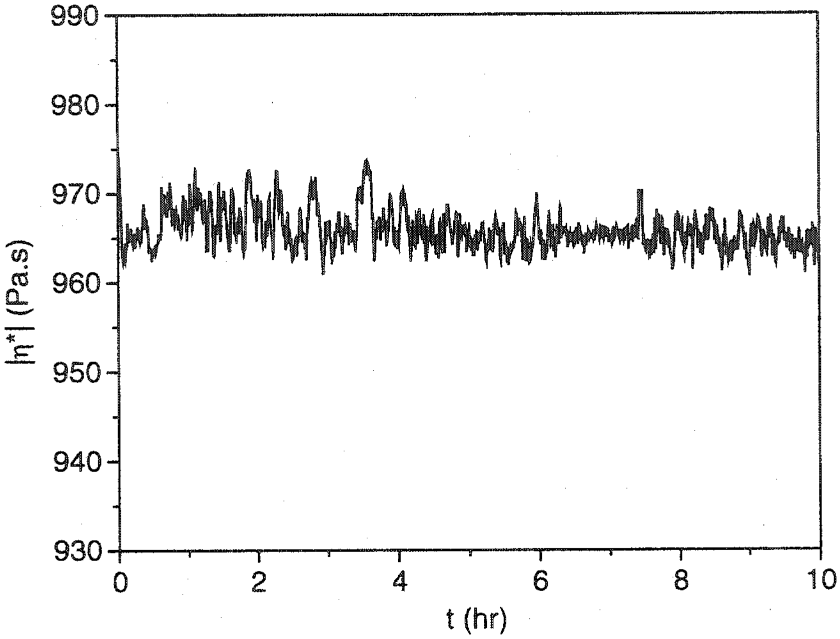

Figure 4-12: Dependency of |η*| on time *t* for linear isotactic polypropylene 35L at T = 180 °C, and $\omega = 1s^{-1}$, $\gamma_0 = 5\%$

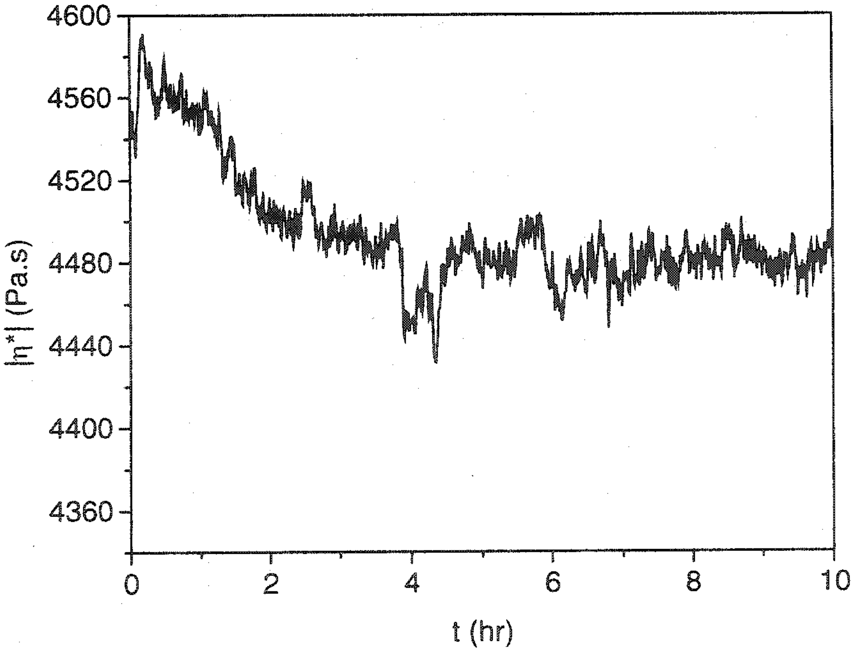

Figure 4-13: Dependency of |η*| on time *t* for branched isotactic polypropylene 35B3 at T = 180 °C, and $\omega = 1s^{-1}$, $\gamma_0 = 5\%$

4.3.2.2. Limit of Linear Response

In order to ensure that the experiments were carried out in the linear region, stress sweep experiments were performed using a Rheometric Scientific dynamic stress rheometer SR5000 with parallel plates of 25 mm diameter. Theoretically, the stress limit at high frequency should also be good at low frequency. However, sometimes, this value is so small in the low frequency range that it limits the precision of the data. Therefore, for the same sample, stress sweeps were usually performed at several frequencies. In this way, both the linearity and precision of the measurement were taken into account. In the stress sweep experiment, the response of the sample at a fixed frequency and temperature is measured as a function of increasing stress amplitude. If the applied stress amplitude is within the linear limit, the response will not depend on the stress amplitude. The response is non-linear if it depends on the stress amplitude level.

As an example, the results for sample 2B1 are shown in Figs. 4.14-15. From Fig. 4-14, we can see that the response at 1 rad/s was within the linear region in the stress amplitude range from 5-30 Pa. In Fig. 4-15 we see that at the stress amplitude lower than 15 Pa, the resulting strain amplitude was smaller than the minimum strain amplitude, and the measured complex moduli results were therefore not reliable. In the stress amplitude range of 15-30Pa, the complex moduli level off and are independent of stress amplitude. Therefore, for sample 2B1, we chose 25Pa as the applied stress amplitude over the whole frequency range. When a single stress amplitude appropriate for both low and high frequencies could not be found, it was necessary to split the frequency sweep into several zones to guarantee both linearity and precision. Stress sweep experiments were performed on each sample to determine its linear stress limit. The results are included on the attached CD.

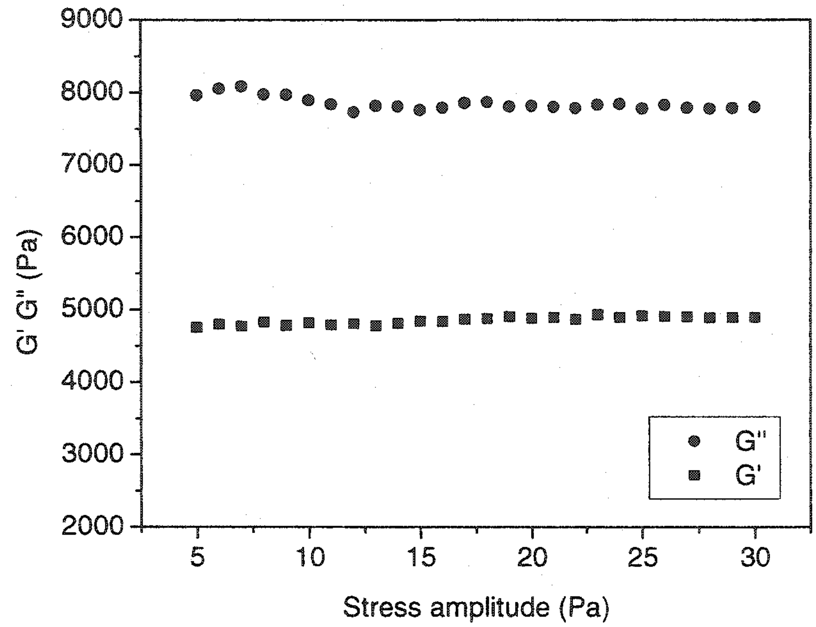

Figure 4-14: Dependency of complex moduli on stress amplitude for branched polypropylene 2B1 at 180 °C and 1 rad/s

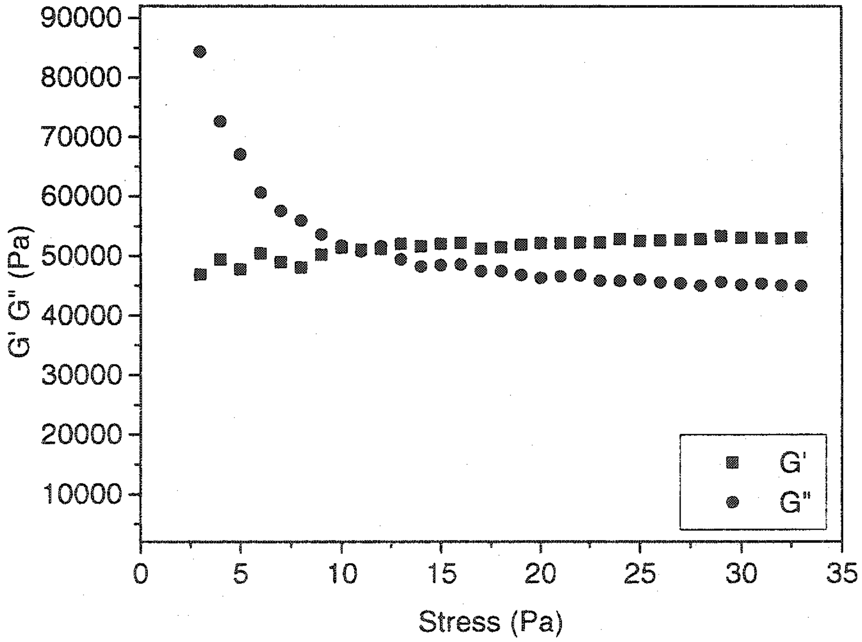

Figure 4-15: Dependency of complex moduli on stress amplitude for branched polypropylene 2B1 at 180 °C and 100 rad/s

4.3.2.3. Oscillatory Shear Measurements

Dynamic measurements were performed using a Rheometric Scientific dynamic stress rheometer SR5000 with parallel plates of 25 mm diameter. Measurements were performed at 180 °C at the predetermined linear stress limit and within the thermally stable period. For each material, at least three experiments with different samples were carried out under exactly the same conditions. The run-to-run variation, which is the deviation from the two-run average, was less than 1.2%. The run-to-run variation examines the reproducibility of the experimental data. We consider that 1.2% is an acceptable experimental deviation value. The standard deviation from the average, which measures how widely the experimental data are dispersed from the average value, was less than 1.5% for all the samples. The averaged results are shown in Figs. 4.16-22.

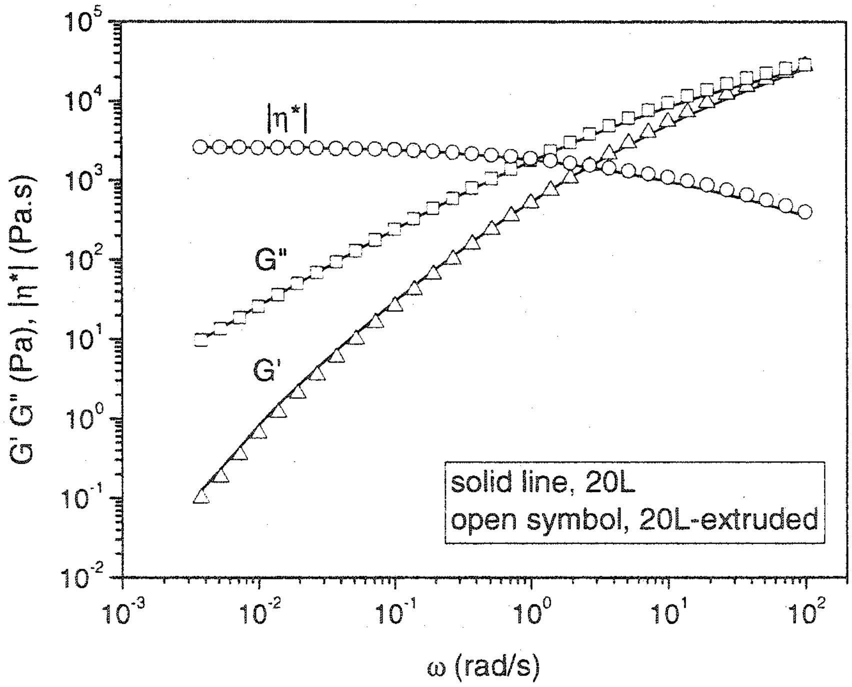

Figure 4-16: Dependency of |η*| and moduli on angular frequency ω for linear polypropylene 20L and 20L-extruded at 180 °C

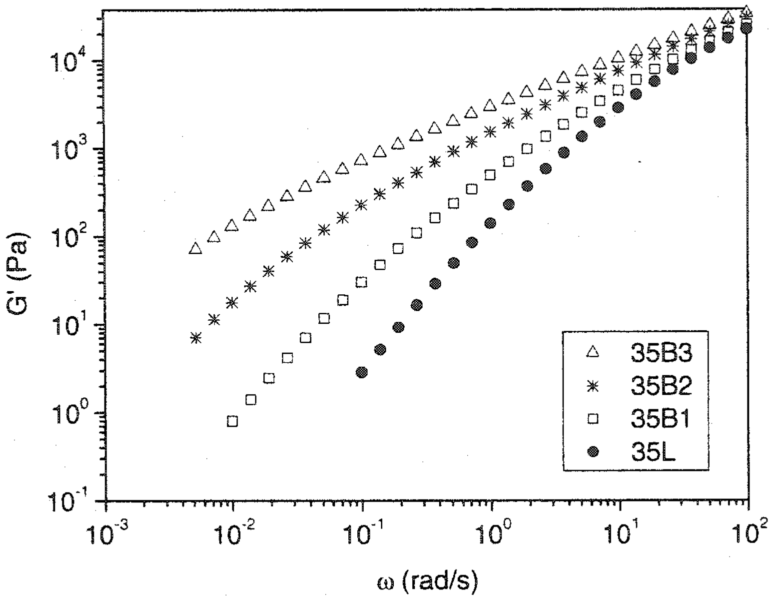

Figure 4-17: Dependency of storage modulus G' on angular frequency ω for the set of 35 MFR polypropylene samples at 180 °C

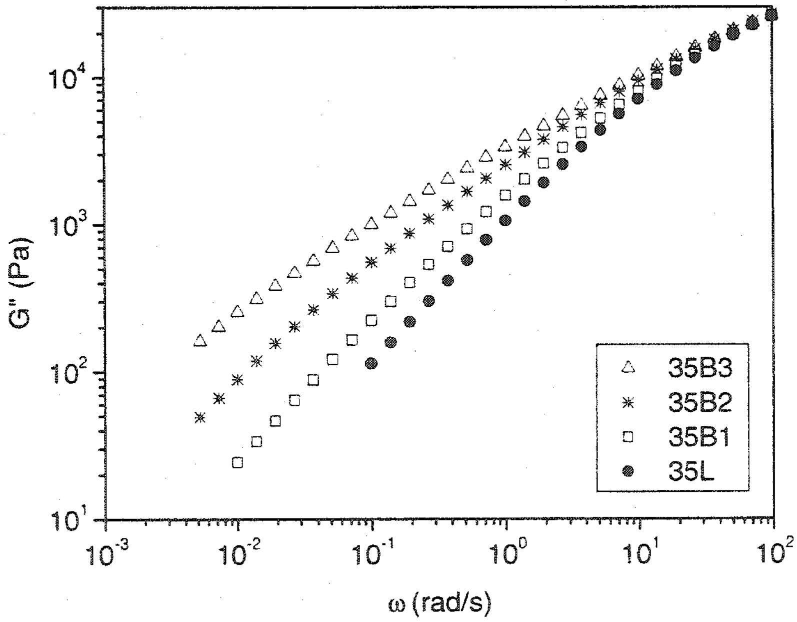

Figure 4-18: Dependency of loss modulus G'' on angular frequency ω for the set of 35 MFR polypropylene samples at 180 °C

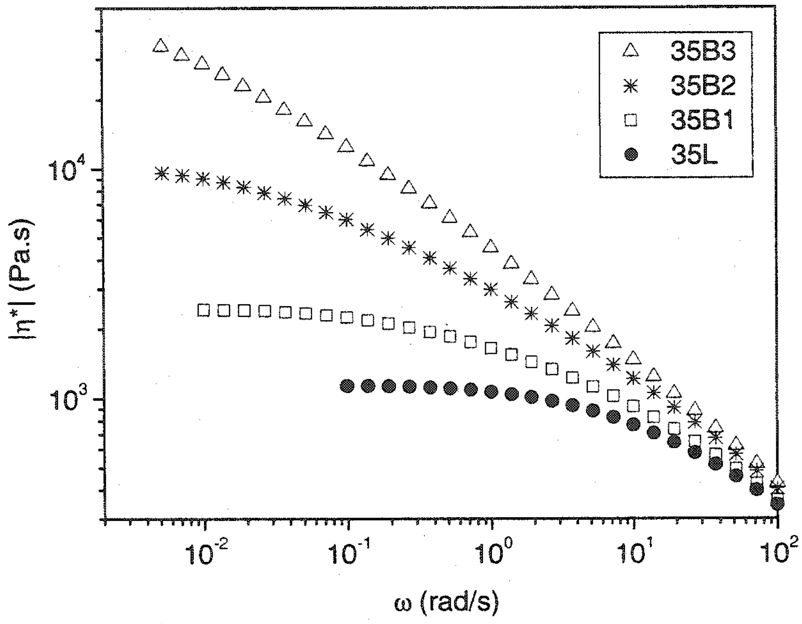

Figure 4-19: Dependency of $|\eta^*|$ on angular frequency ω for linear polypropylene 35L and three branched polypropylene 35B1, 35B2 and 35B3 at 180 °C

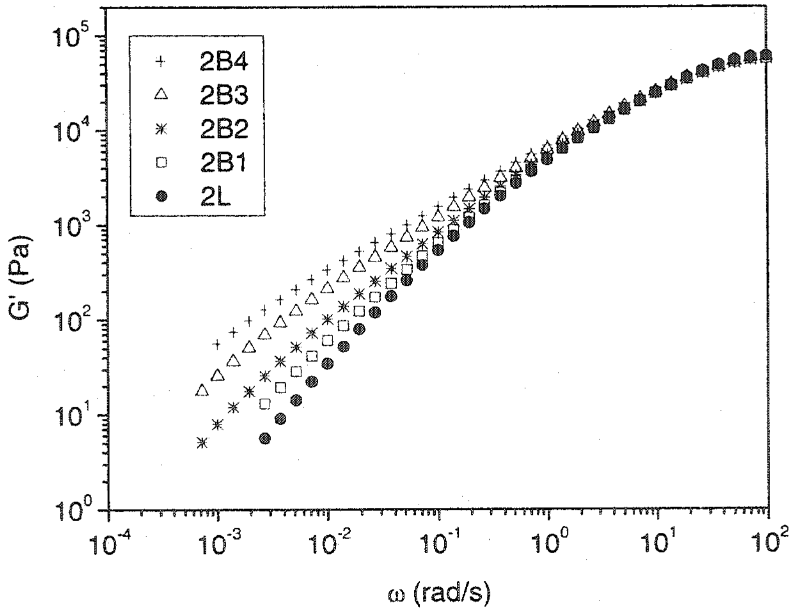

Figure 4-20: Dependency of storage modulus G' on angular frequency ω for linear PP 2L and four branched PP 2B1, 2B2, 2B3 and 2B4 at 180 °C

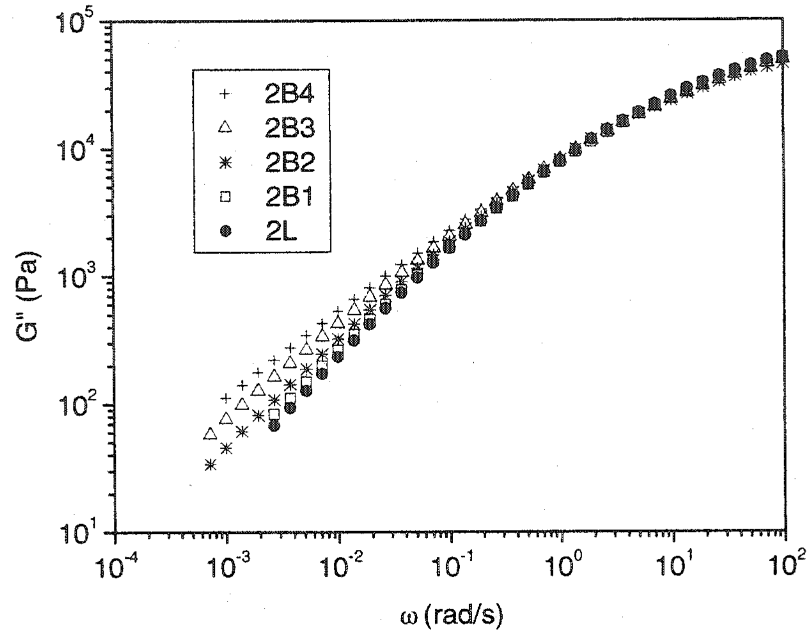

Figure 4-21: Dependency of loss modulus G'' on angular frequency ω for linear PP 2L and four branched PP 2B1, 2B2, 2B3 and 2B4 at 180 °C

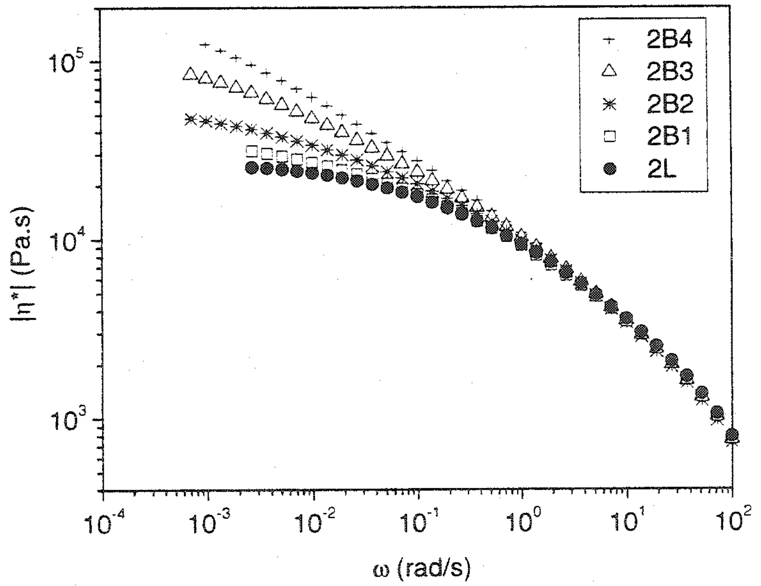

Figure 4-22: Dependency of |η*| on angular frequency ω for linear PP 2L and four branched PP 2B1, 2B2, 2B3 and 2B4 at 180 °C

4.3.3. Creep and Creep Recovery

4.3.3.1. Linearity of The Response

Creep and creep recovery experiments were also performed using the Rheometric Scientific SR5000 stress-controlled rheometer with parallel plates of 25 mm diameter. To ensure that the measurements were performed within the linear region, preliminary tests were carried out at several stresses. If the deformation is within the linear region, the creep compliance is independent of stress. For example, Figure 4.23 shows the creep compliance, $J(t)$, of sample 35B2 at stresses ranging from 5 to 25Pa and various creep times. The results superpose perfectly. Therefore, we conclude that the maximum strain reached at these stresses and creep times is within the linear region, and we can choose an optimal stress to perform the creep recovery test. The optimal stress for measurements should be small enough to avoid entering the non-linear region, but large enough to provide satisfactory resolution. For this material, 35B2, a shear stress of 10Pa is well within the linear range and provides good resolution. Similar tests for the linearity of the rheological response were performed for the other materials and the optimal stress for each sample was found. The results are listed in Table 4.3.

Table 4-3: Samples and their optimum stresses for creep at 180 °C

Sample	35B2	35B3	2L	2B1	2B2	2B3	2B4
Stress (Pa)	10	20	10	30	30	30	30

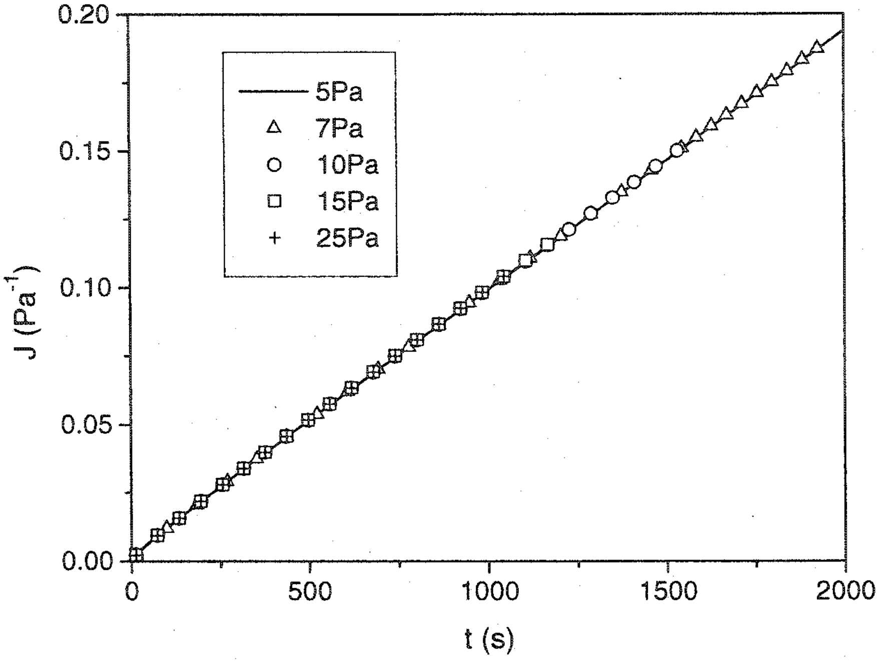

Figure 4-23: Creep compliance of 35B2 at different stresses and creep time (180 °C)

4.3.3.2. Creep Compliance at Long Times

Creep and recovery tests were carried out at the optimal stress. Typical strain data for sample 35B2 are shown in Fig.4.24, where the stress was applied during the first 700 s and then removed to allow recovery.

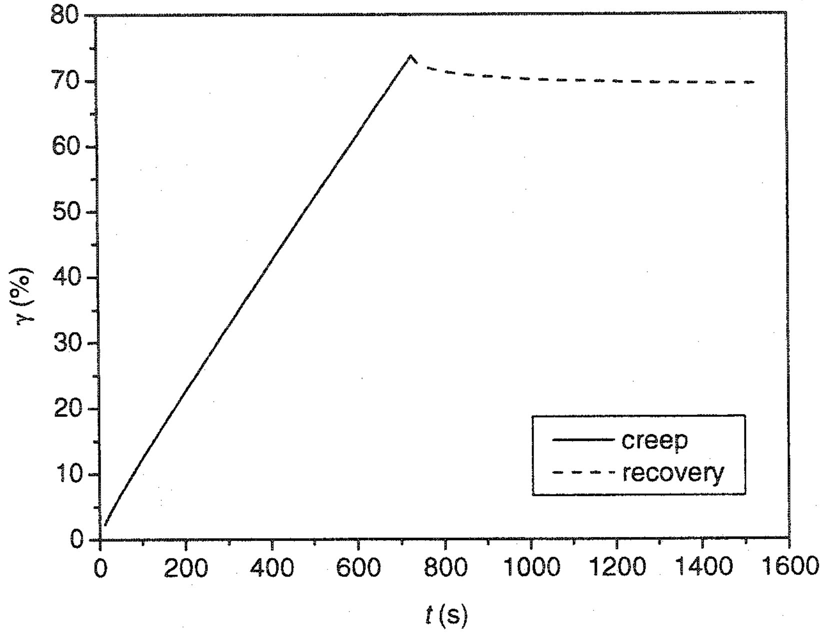

Figure 4-24: Dependency of strain on time in a creep and recovery test of branched polypropylene 35B2 at 10Pa, 180 °C

With the creep and recovery data shown in Fig. 4.24, the Boltzmann superposition principle was used to extend the creep curve to longer times to obtain the creep compliance up to very long times. This is the technique described by Kraft *et al.*[1] During a standard creep experiment at a stress of σ_0, the stress is reduced to zero at a time, t_1, while the deformation is still within the range of linear behavior, and the resulting recoil is recorded.

This experiment can be analyzed by use of the Boltzmann superposition principle in the form of Eq. 4.23, where stress, rather than strain, is the independent variable.

$$\gamma(t) = \int_{-\infty}^{t} J(t-t')d\sigma(t') \qquad (4.23)$$

The unloading at t_1 can be represented by a second creep experiment commencing at this time and driven by a stress of $-\sigma_0$. From Eq. 4.23, the resulting shear deformation, $\gamma(t)$, is:

$$\gamma(t) = J(t)\sigma_0 + J(t-t_1)(-\sigma_0) = \sigma_0[J(t) - J(t-t_1)] \qquad (4.24)$$

Thus, the creep compliance can be extended up to $t = 2t_1$as follows:

$$J(t) = \gamma(t)/\sigma_0 + J(t-t_1) \quad (t_1 < t < 2t_1) \qquad (4.25)$$

Now that $J(t)$ has been determined up to $t = 2t_1$, this information can be used in combination with the next portion of the recoil curve to determine the compliance at times longer than $2t_1$:

$$J(t) = \gamma(t)/\sigma_0 + J(t-t_1) \quad (2t_1 < t < 3t_1) \qquad (4.26)$$

This procedure is repeated until the terminal zone is reached, *i.e.*, until $J(t)$ becomes linear with time. The zero-shear viscosity is the reciprocal of the slope of the linear portion of $J(t)$. Figure 4.25 shows the extended creep compliance for sample 35B2 created by using the Boltzmann superposition principle and the information in Fig. 4.24.

The same procedure was used for each sample. The strain behaviour in the creep/recovery tests and the creep compliances at long times for the other samples are shown in Figs. 4.26-31.

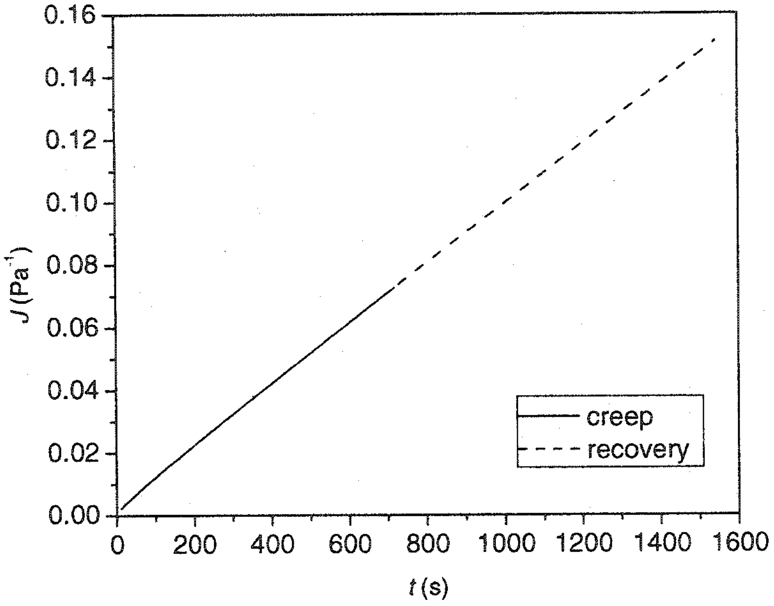

Figure 4-25: Dependency of creep compliance on time for branched polypropylene sample 35B2 in an extended time window obtained from the results in Fig. 4.24 at 180 °C

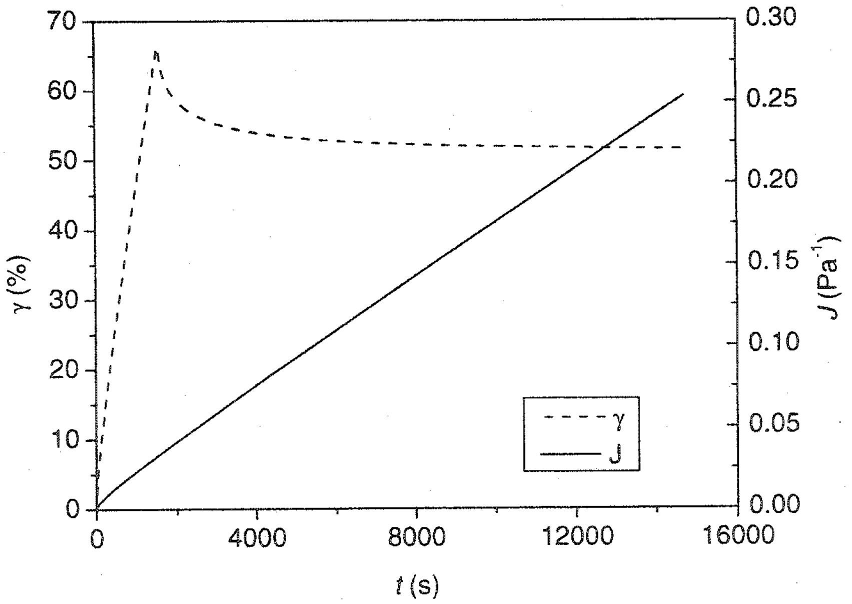

Figure 4-26: Dependency of strain and creep compliance on time for branched polypropylene sample 35B3 at 20 Pa, 180 °C

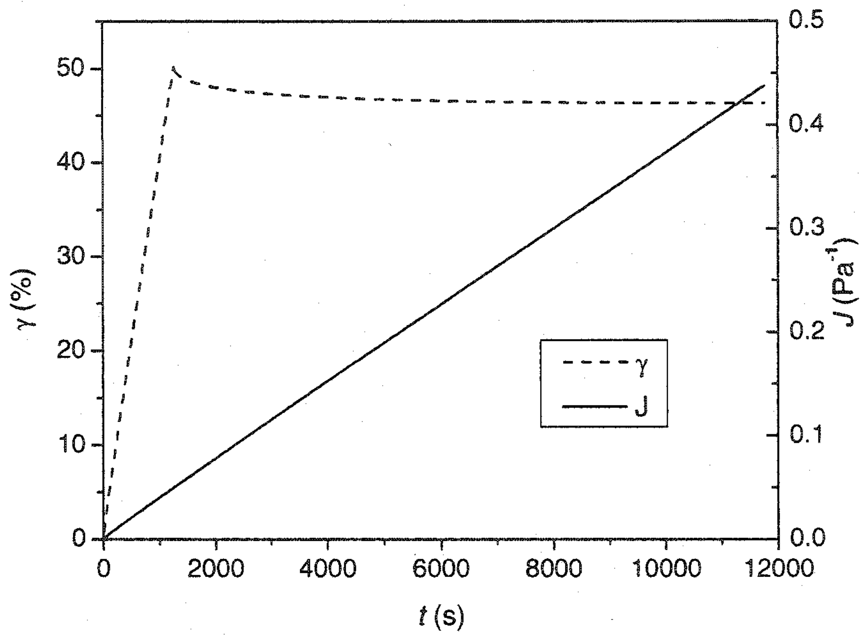

Figure 4-27: Dependency of strain and creep compliance on time for linear polypropylene sample 2L at 10 Pa, 180 °C

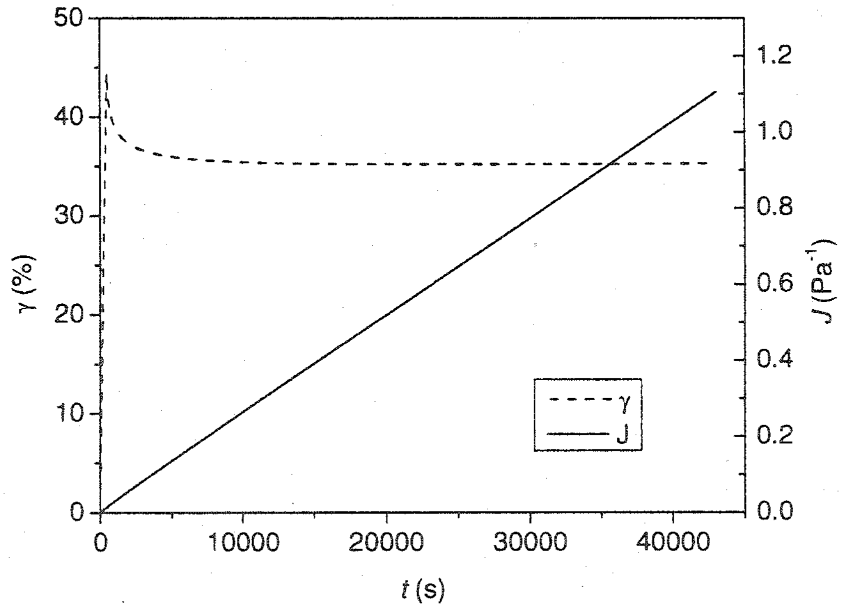

Figure 4-28: Dependency of strain and creep compliance on time for branched polypropylene sample 2B1 at 30 Pa, 180 °C

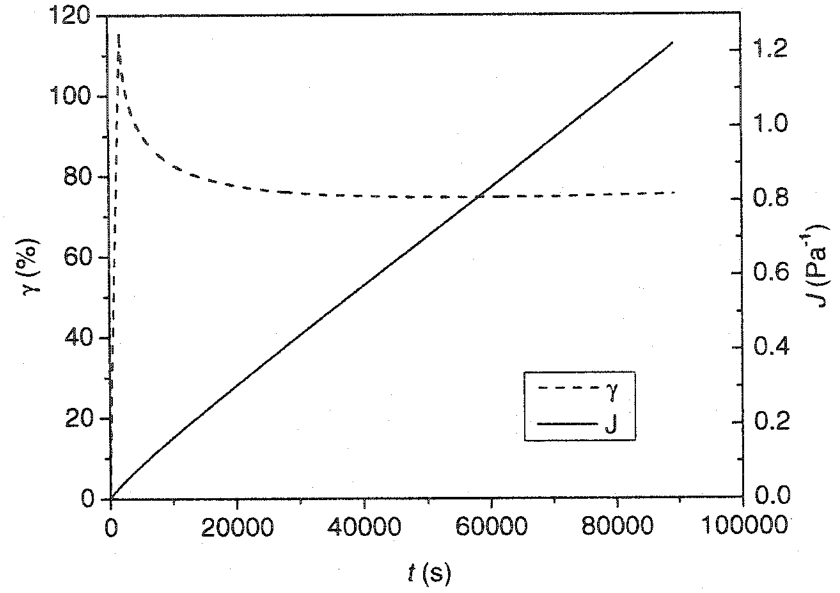

Figure 4-29: Dependency of strain and creep compliance on time for branched polypropylene sample 2B2 at 30 Pa, 180 °C

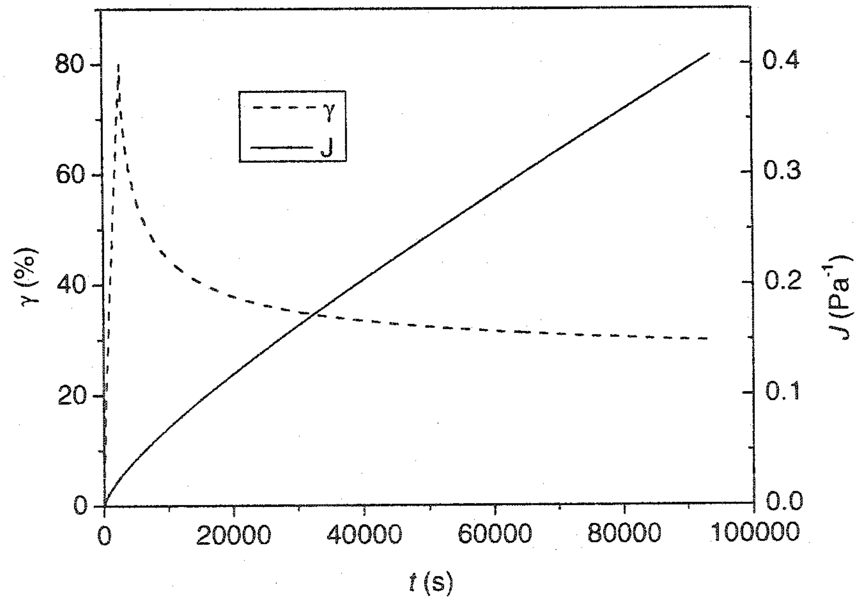

Figure 4-30: Dependency of strain and creep compliance on time for branched polypropylene sample 2B3 at 30 Pa, 180 °C

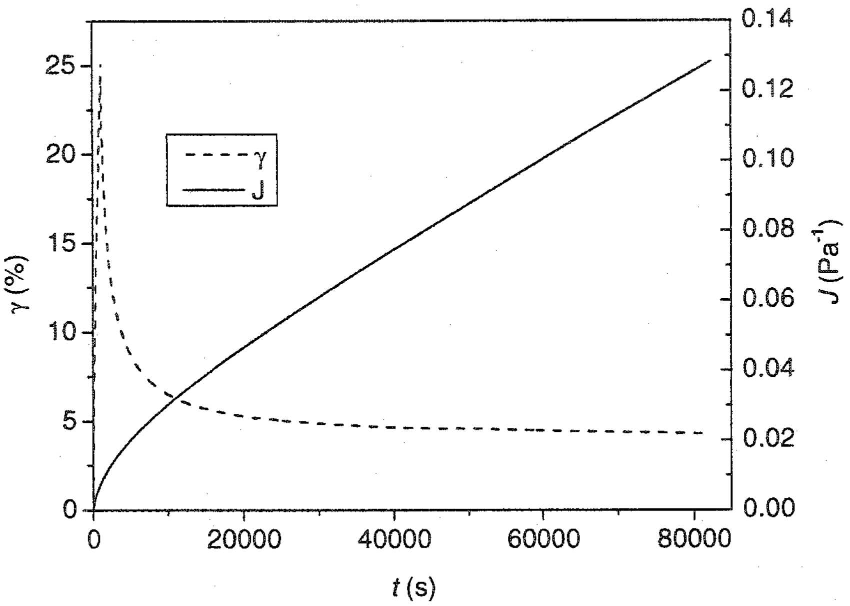

Figure 4-31: Dependency of strain and creep compliance on time for branched polypropylene sample 2B4 at 30 Pa, 180 °C

4.4. Results and Discussion

4.4.1. Discussion of Experimental Data

From Fig. 4.16 we can see that for the same linear polymer before and after passing through the extruder, the complex moduli and viscosity superpose reasonably well over the whole experimental window except for the slight differences at low and high frequencies. Therefore, it was concluded that the extrusion process caused β-chain scission of the linear samples to such a small extent that there is no significant change in the rheological behavior.

Figures 4.17-19 show the storage and loss moduli and the complex viscosity of the set of samples that includes the linear precursor 35L together with materials having three levels of branching, 35B1, 35B2 and 35B3. At high frequencies all the samples have very similar behavior. This is what we expect since at high frequencies only very short portions of chains far from the entanglements and very small unentangled chains can relax this quickly. On this time scale, all the samples have the same structure and thus the same viscoelastic behavior. As the frequency decreases, differences between the samples become more and more obvious due to the increasing influence of entanglements and branching. The viscosity of the linear precursor reaches its zero-shear plateau at about 0.1 rad/s, whereas for the relatively weakly branched sample, 35B1, the plateau is not quite reached at 10^{-2} rad/s. For samples 35B2 and 35B3, terminal zone behavior was inaccessible in oscillatory shear. Moving from 35L to 35B3, the low frequency viscosity increases and the transition zone is extended. These trends are the same as those observed by Wood-Adams *et al.*[11] in their study of branched metallocene polyethylenes. However, going from 35L to 35B3, the weight averaged molecular weight and polydispersity also increase. As mentioned before, these two factors affect the rheological behavior in similar ways as long-chain branching. Therefore, the differences in rheological behavior between these four samples are the combined effects of three factors: M_w, polydispersity and branching level. To examine the effect of branching, the relaxation spectrum was used. The method of transforming the experimental material functions into relaxation spectra is described in the next section.

Figures 4.20-22 show the dynamic data for the set of 2 MFR samples having a different linear precursor than 35L. The same trends as those observed for the set of 35 MFR samples can be seen in this set. However, in this set, the level of branching is much lower than in the 35 MFR samples. Thus, the differences in G', G'' and complex viscosity are not as large as for the 35 MFR samples in the detectable frequency range. All five samples: 2L and 2B1-4, have similar behavior in the frequency range from 0.1-100 rad/s. Only at the frequencies below 0.1 rad/s, do differences between the samples become obvious. Due to the much higher M_w and broader polydispersity than for the 35 MFR samples, the 2 MFR samples have much higher viscosities and broader transition zones. By examining the differences between the two sets, a clear picture of the effects of M_w and long-chain branching on rheological behavior can be obtained.

Figures 4.25-31 show the creep compliance over a long time period that reaches into the steady state for samples whose Newtonian plateau zone is not accessible by dynamic measurement. In advancing from 2L to 2B4, the time to reach state steady increases, and the slope of $J(t)$ at steady state decreases, which again indicates an increase of the zero-shear viscosity. The steady-state compliance, J_s^0 increases from 2L to 2B4, which indicates increasing elasticity. Again these are the combined effects of M_w, polydispersity and long-chain branching. The time to reach the steady state and the steady-state compliance for samples are listed in Table 4.4.

Table 4-4: The time to reach steady state t_s and the steady-state compliance J_s^0 for samples at 180 °C

Sample	35B2	35B3	2L	2B1	2B2	2B3
t_s (s)	850	9,000	7,500	10,000	47,500	74,000
J_s^0 (Pa^{-1})	0.004	0.012	0.006	0.009	0.054	0.064

4.4.2. Conversion of Material Functions

In this section, first the method to combine the results of dynamic and creep/recovery experiments to extend the experimental window is described. Then, the weighted relaxation spectra $\tau H(\tau)$ of various samples are compared and the effect of long-chain branching on these spectra is discussed.

4.4.2.1. Combination of Dynamic and Creep Recovery Results

From the dynamic experiments the storage and loss moduli are obtained, and in creep and recovery experiments the creep compliance, $J(t)$, is determined. The dynamic data are more reliable at short times (high frequencies), while the creep and recovery data are more trustworthy at long times. In order to obtain the most complete picture of a material's linear rheological behavior it is necessary to combine the information contained in these two types of data. In this work, we convert both sets of experimental data to continuous retardation spectra and then compare them. The comparison of these two spectra provides a reliable indication of the success of the technique by showing whether the two spectra agree over some range of times and yields a composite spectrum that can be used to calculate other material functions.

From the dynamic experiments we calculate the storage and loss moduli, $G'(\omega)$ and $G''(\omega)$, which can be expressed in terms of the relaxation spectrum function[2] $H(\tau)$ as shown by Eqs. 4.18-19. If we could obtain precise experimental data over the entire range of frequencies from 0 to ∞, the exact function $H(\tau)$ could be determined using Eqs. 4.18-19. However, it is not possible to obtain such data. Because of the limited precision and range of actual data, a unique spectrum cannot be inferred, and special computational techniques are required to determine a spectrum close to the "real" one, *i.e.*, the one characterizing the polymer. A method proposed by Honerkamp and Weese[17] was used to compute the relaxation spectrum from experimental data. In this method, the relaxation spectrum $h(\tau)$ is estimated by minimizing the function $V(\lambda_{reg})$

$$V(\lambda_{reg}) = \text{least square term (1)+regularization term (2)} \qquad (4.27)$$

where λ_{reg} is a regularization parameter. In order to avoid calculation difficulties caused by the considerably different contributions of various portions of the relaxation spectrum (at short times, there is a large contribution and for long times there is a very small contribution) the logarithm of the spectrum function $\tilde{h}(\tau) = \log h(\tau)$ is used instead of the spectrum function $h(\tau)$. Term (1) in Eq. 4.27 is designed to force the calculated storage and loss modulus results from relaxation spectrum close to the experimental data.

$$\begin{aligned} \text{term}(1) = {} & \sum_{i=1}^{n} \frac{1}{\sigma_i'^2} \left[G_i' - \left(\int_{-\infty}^{+\infty} \frac{\omega_i^2 \tau^2}{1+\omega_i^2 \tau^2} 10^{\tilde{h}(\tau)} \, d\ln\tau \right) \right]^2 \\ & + \sum_{i=1}^{n} \frac{1}{\sigma_i''^2} \left[G_i'' - \left(\int_{-\infty}^{+\infty} \frac{\omega_i \tau}{1+\omega_i^2 \tau^2} 10^{\tilde{h}(\tau)} \, d\ln\tau \right) \right]^2 \end{aligned} \qquad (4.28)$$

where G_i' and G_i'' are the experimental data, and σ_i' and σ_i'' are the corresponding relative errors. In the calculation, the initial input value of the relative error is usually set as 0.01.

Term (2), the sum of the squares of the second derivative of the logarithm spectrum curve, prevents the rapid change in the relaxation spectrum and leads to a smooth spectrum.

$$\mathrm{term}(2) = \lambda_{\mathrm{reg}} \int_{-\infty}^{+\infty} \left(\frac{\mathrm{d}^2}{\mathrm{d}\tau^2} \tilde{\mathrm{h}}(\tau) \right)^2 \mathrm{d} \ln \tau \tag{4.29}$$

Because the logarithmic spectrum $\tilde{h}(\tau)$ is used, the regularization is nonlinear. Therefore, the method proposed by Honerkamp and Weese[17] is a nonlinear regularization method (NLREG).

By minimizing $V(\lambda_{reg})$, the method yields a smooth relaxation spectrum curve while taking into account noise in the data. The resulting relaxation spectrum is reliable in the region narrower than the corresponding experimental time window as pointed out by Davies and Anderssen[18]. They have shown that the range of validity for the spectrum is: $\frac{e^{\pi/2}}{\omega_{max}} < t < \frac{e^{-\pi/2}}{\omega_{min}}$, where ω_{min} and ω_{max} correspond to the low and high experimental frequency limits. From the relaxation spectrum obtained from the dynamic moduli, a retardation spectrum is obtained using Eq. 4.30:

$$L(\tau) = \frac{H(\tau)}{\left[\int_{-\infty}^{\infty} \frac{H(\tau)}{\tau / t - 1} d \ln t \right]^2 + \pi^2 H(\tau)^2} \tag{4.30}$$

The creep compliance can be expressed in terms of the retardation spectrum, $L(\tau)$, as shown by Eq. 4.20. Using the same computational technique (NLREG), we can infer a second retardation spectrum from the creep compliance. The retardation spectrum calculated from the experimental G' and G'', and creep compliance $J(t)$ data are shown in Figs. 4.32-38. The dashed line shows the retardation spectrum derived from the oscillatory shear data, and the solid line shows the spectrum derived from the extended creep compliance curve. The vertical lines show the time limits for the two techniques, outside of which the spectra are not meaningful. The limits of the dynamic range were calculated using the criterion of Davies and Anderssen[18]. The retardation spectra from the two types of experiment are different because each type of experiment misses a certain portion of the time scale.

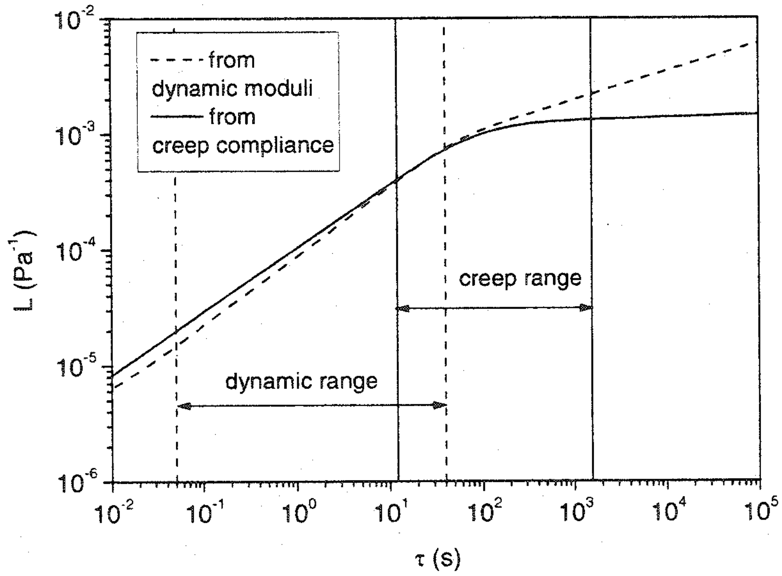

Figure 4-32: Retardation spectra for 35B2 obtained from dynamic moduli and creep compliance (180 °C)

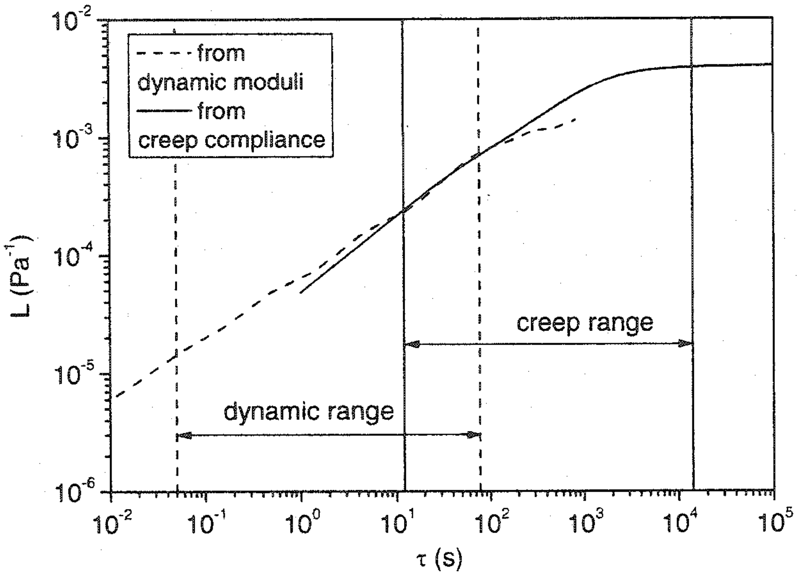

Figure 4-33: Retardation spectra for 35B3 obtained from dynamic moduli and creep compliance (180 °C)

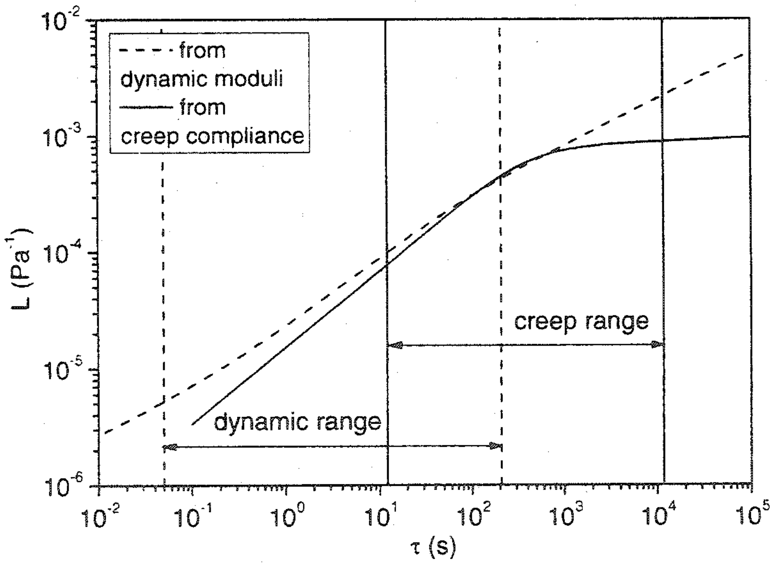

Figure 4-34: Retardation spectra for 2L obtained from dynamic moduli and creep compliance (180 °C)

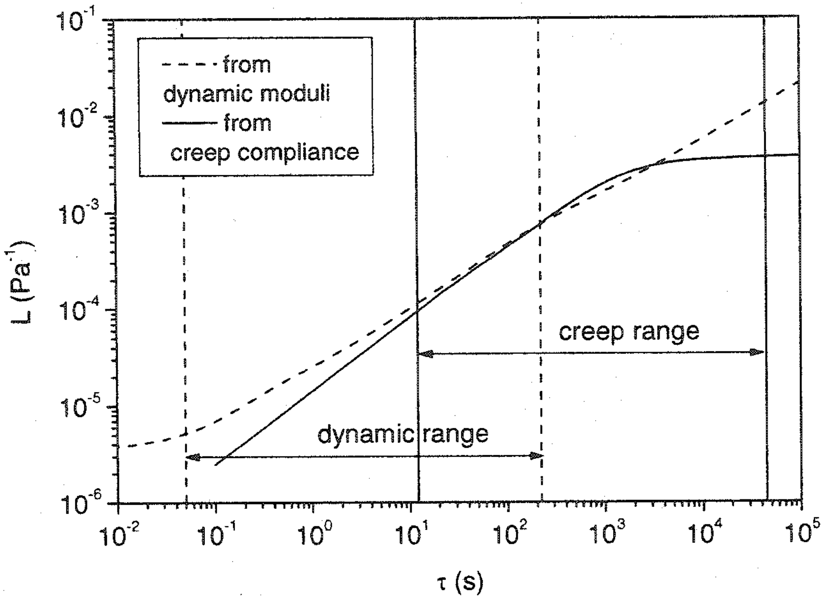

Figure 4-35: Retardation spectra for 2B1 obtained from dynamic moduli and creep compliance (180 °C)

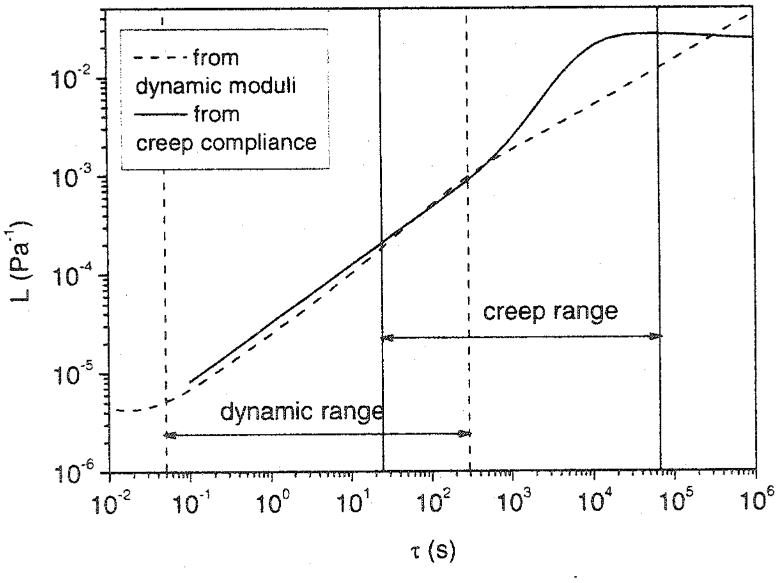

Figure 4-36: Retardation spectra for 2B2 obtained from dynamic moduli and creep compliance (180 °C)

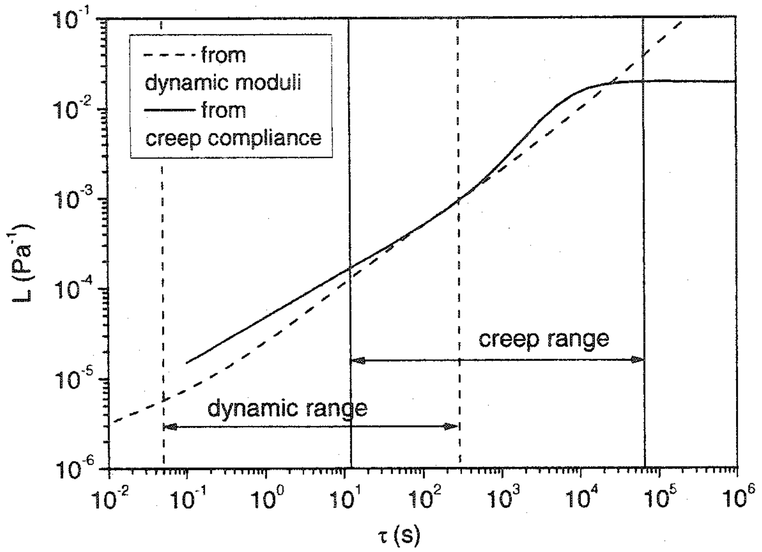

Figure 4-37: Retardation spectra for 2B3 obtained from dynamic moduli and creep compliance (180 °C)

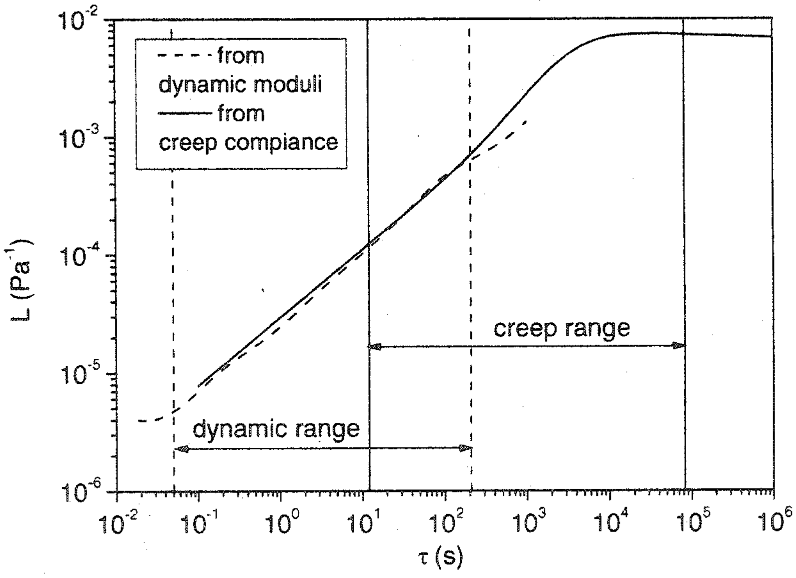

Figure 4-38: Retardation spectra for 2B4 obtained from dynamic moduli and creep compliance (180 °C)

The retardation spectrum, $L(\tau)$, is then used as an intermediate tool to combine the data from dynamic and creep/recovery experiments. There was an excellent superposition of the spectra within the region of overlapping experimental windows (10 s to 1000 s). Therefore, we can obtain a combined retardation spectrum by taking the short time part of *L(τ)* from the complex modulus and the long time part from the creep compliance. In the superposition zone, the two spectra crossed at a very small angle, and the precise point of switching from one to the other was chosen as the crossing point. The combined retardation spectra are shown in Figs.4.39 and 4.40.

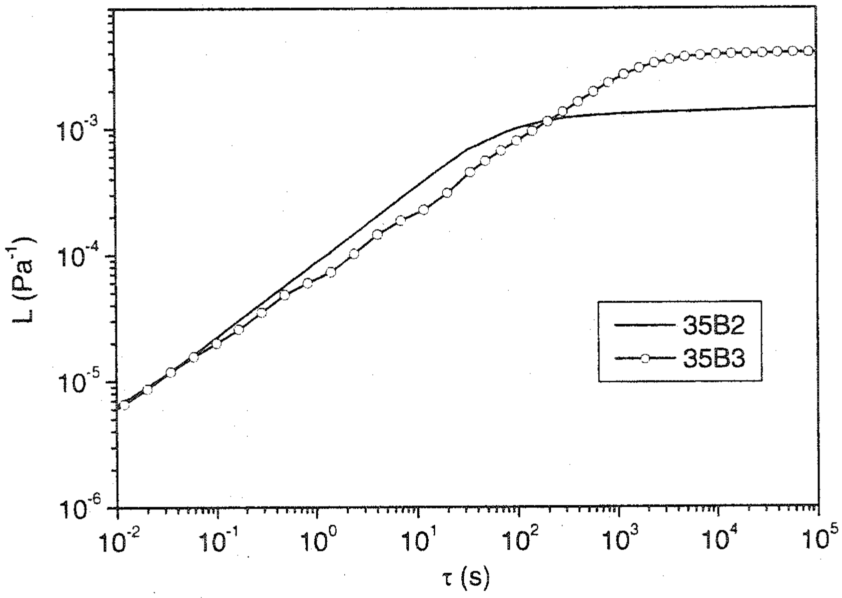

Figure 4-39: Combined retardation spectrum for 35B2 and 35B3 at 180 °C

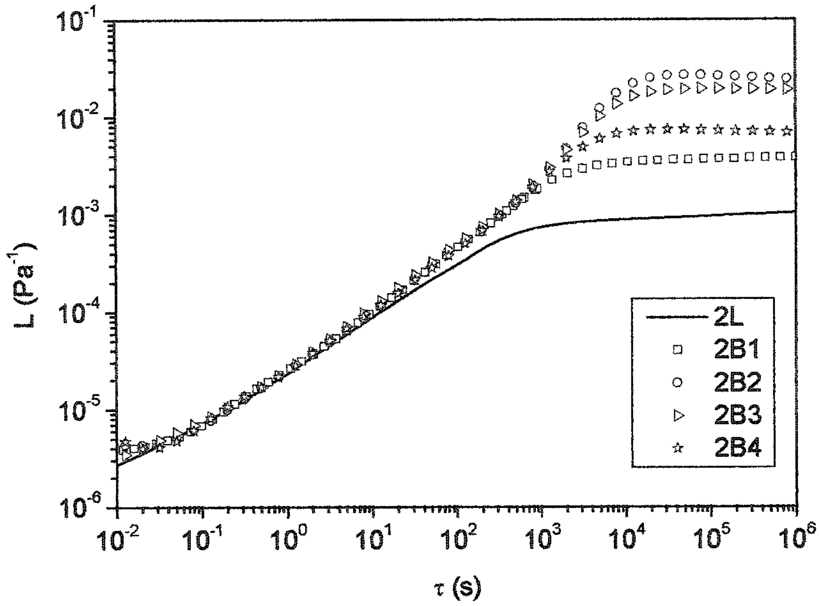

Figure 4-40: Combined retardation spectrum for linear sample 2L and four branched samples 2B1, 2B2, 2B3, 2B4 at 180 °C

Now we have the retardation spectrum over an extended time range, and with this information we can calculate other material functions such as the complex compliance and the storage and loss moduli. The complex compliance is expressed in terms of the retardation spectrum by Eqs 4.21-22. From the storage and loss compliances, the storage and loss moduli can be calculated using Eq. 4.31:

$$\begin{aligned} G'(\omega) &= \frac{J'(\omega)}{J'(\omega)^2 + J''(\omega)^2} \\ G''(\omega) &= \frac{J''}{J'(\omega)^2 + J''(\omega)^2} \end{aligned} \tag{4.31}$$

In Figs. 4.41 and 4.42 the complex viscosity generated from the combined retardation spectra are compared with experimental data. By combining dynamic and creep data, the experimental window has been extended into the terminal zone, where the complex viscosity reaches its Newtonian plateau.

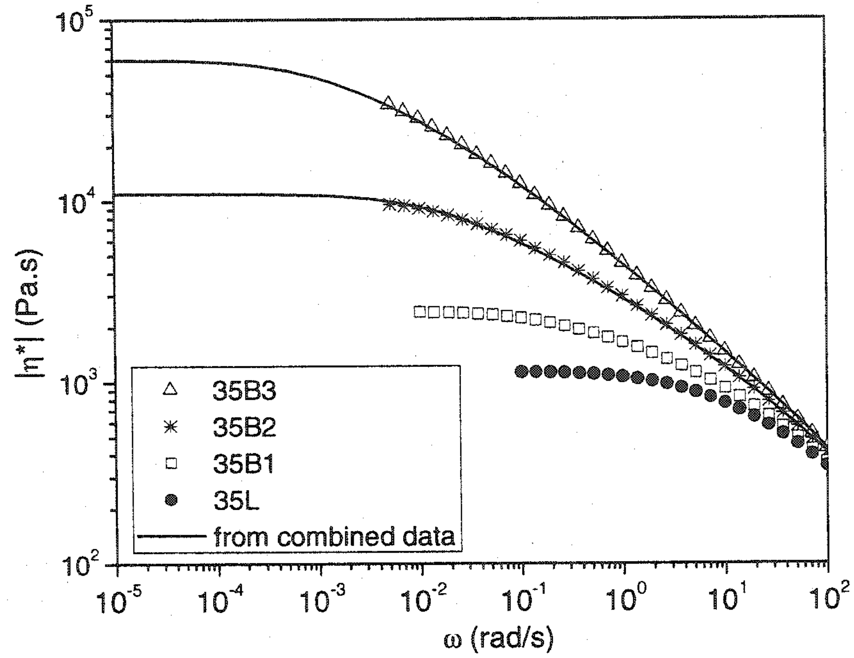

Figure 4-41: Complex viscosities of the four samples shown in Fig.4.19 Solid lines are combined results in the extended window

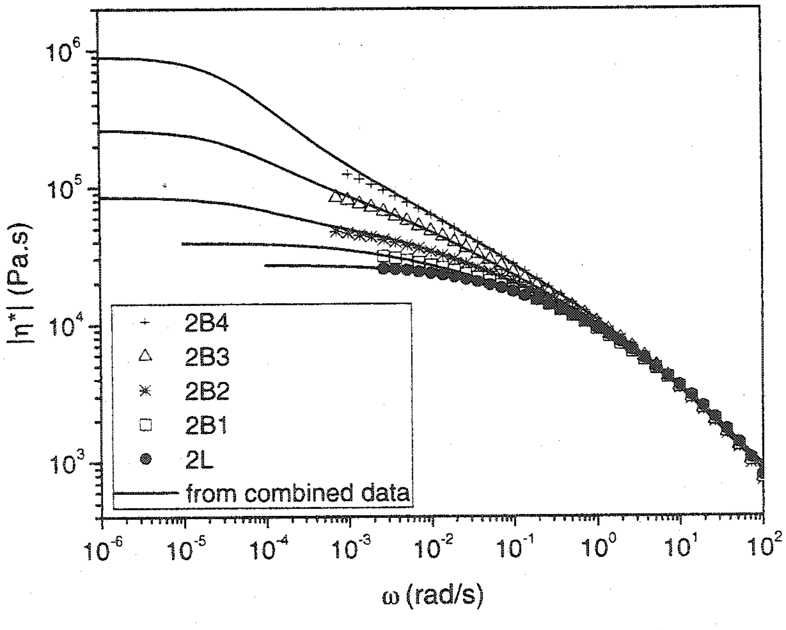

Figure 4-42: Complex viscosities of the five samples shown in Fig.4.22. Solid lines are combined results in the extended window

4.4.2.2. Limitations of the Combined Method

While we see the power of using the creep/recovery experiment to extend the dynamic experimental window into low frequencies, it is also important to note the limitations of the method. Due to the ultimate thermal instability of the polymer and the duration of the experiment, for polymers with extremely long relaxation times, it is not always possible to continue the creep/recovery measurement to a long enough time to reach the terminal zone. Fig. 4.43 shows the time-weighted relaxation spectrum of sample 2B4 at 180 °C. The dashed line represents the results calculated from only dynamic experimental data. This spectrum is only reliable in the experimental window as illustrated by the vertical dashed line in the plot. Because of the lack of information at long times, the spectrum function increases without limit at long time and is therefore not reliable. By combining the creep/recovery experiment, the experimental window is extended to 82300 s, or 23 hours. This range is indicated in the plot as the creep region. By using the combined data, we are able to obtain a relaxation spectrum that falls mainly in the experimental window except when $t > 10^5$ s. To make a 23-hour creep/recovery measurement, the residence time of the sample in the rheometer is well beyond 27 hours, if the preparation time is taken into account. For such a long residence time degradation becomes important, especially in the recovery period as the shear rate is very small, on the order of 10^{-8} s^{-1}. In this case, it is very hard to see the plateau zone of the recovery strain. Therefore, for polymers with higher levels of branching than sample 2B4, even the combination method cannot reveal the terminal zone behavior.

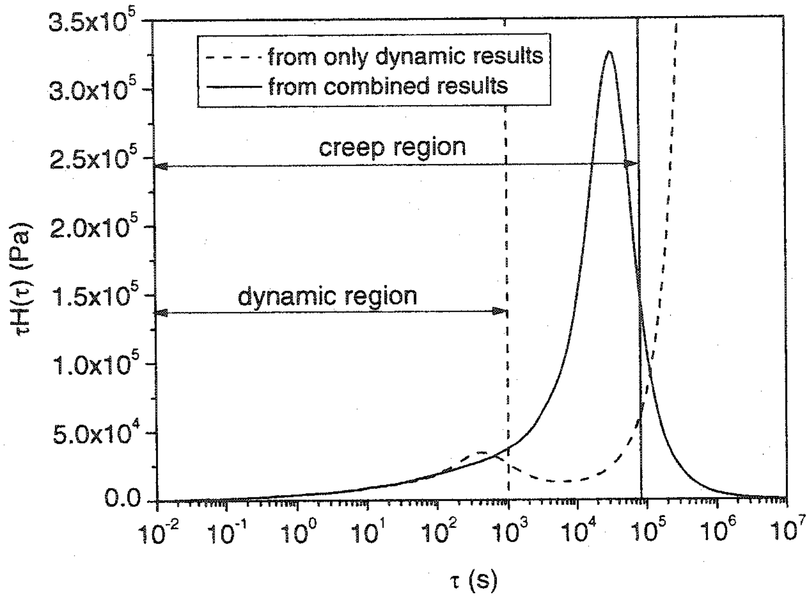

Figure 4-43: Time-weighted relaxation spectrum of 2B4 at 180 °C. Dashed line is the results calculated from only dynamic data. Solid line is the results from the combined data of dynamic and creep/recovery

4.4.2.3. Time-Weighted Relaxation Spectrum

Rheological behavior related to entanglement coupling, *i.e.*, that in the plateau and terminal zones, is very sensitive to molecular structure. As a result, the long-time (low frequency) behavior is of the greatest interest in polymer characterization. Thus, for the complete characterization of a molten polymer, it is essential to have data in the terminal zone. If a relaxation spectrum function is inferred from data that do not include the terminal zone, it will not reflect the true, long-time behavior of the material. Figure 4.44 shows the time-weighted spectrum for 35B2 based solely on oscillatory shear data along with a spectrum based on both dynamic and creep/recovery data. At short times, the two curves superpose, but at longer times they diverge. The spectrum based on the combined data is almost entirely within the experimental window and is therefore considered to be close to the true relaxation spectrum of the material. For all samples except 2B4, the experimental window includes the terminal zone, either from oscillatory shear data alone or by combining these with creep data. The final spectra for all materials are shown in Figs. 4.45-47.

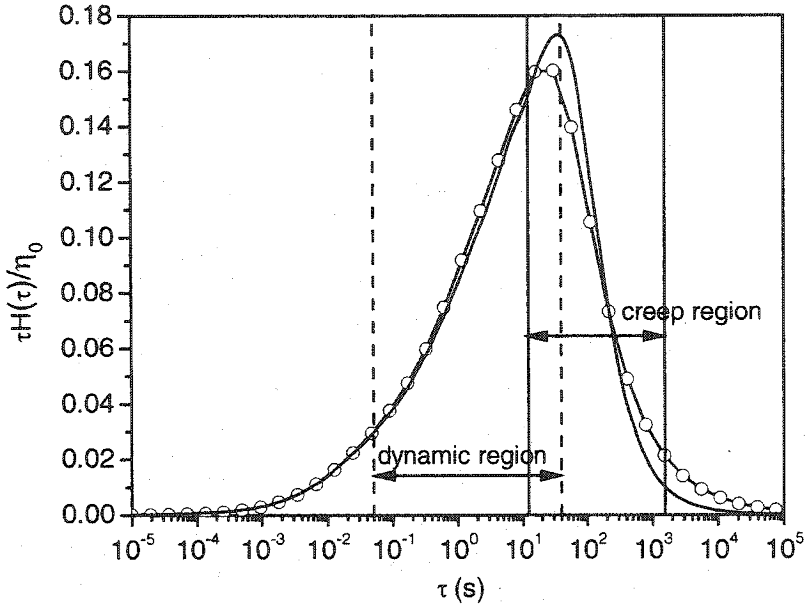

Figure 4-44: Relaxation spectrum of 35B2. The solid line is from the combined results of dynamic and interrupted creep; the open circles are oscillatory shear data. The dashed vertical line is the limit of the dynamic experiment, and the solid vertical lines are the limits of the creep experiment

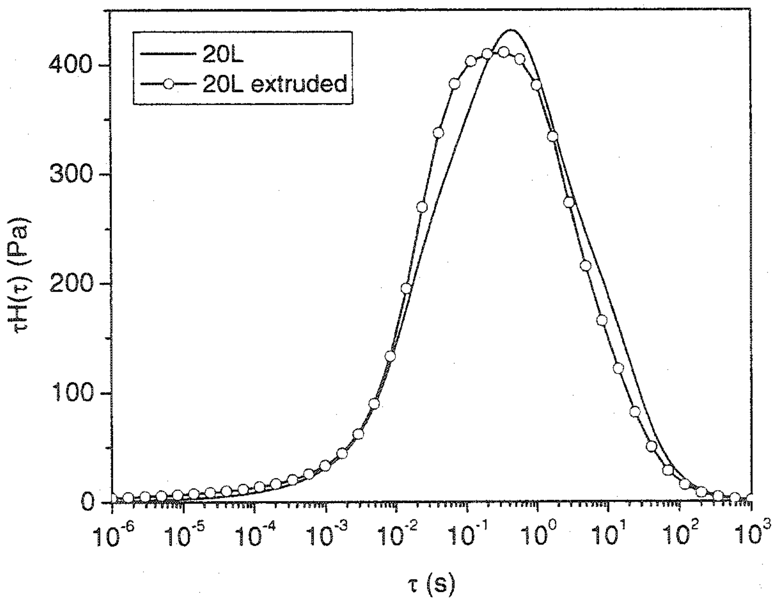

Figure 4-45: Relaxation spectrum of 20L before and after extrusion

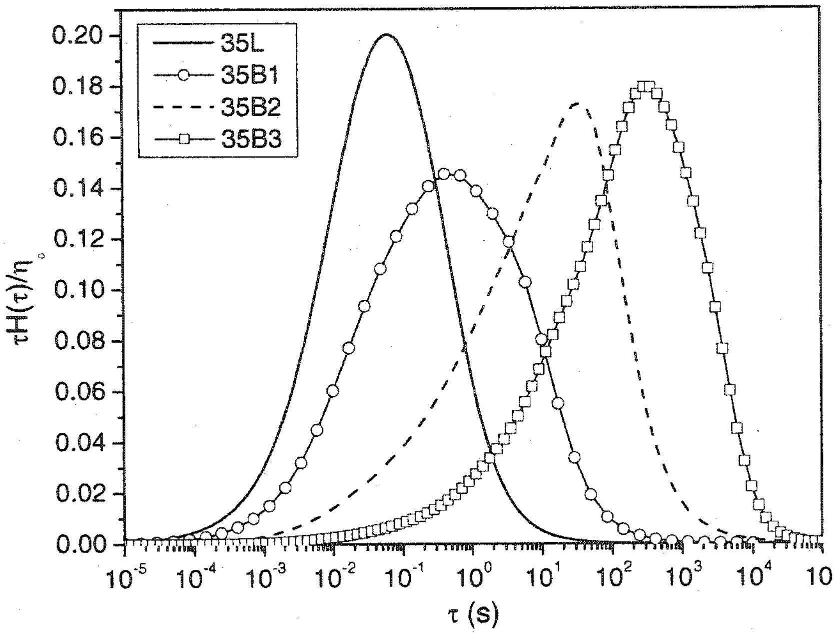

Figure 4-46: Normalized time-weighted relaxation spectra of MFR 35 polypropylenes

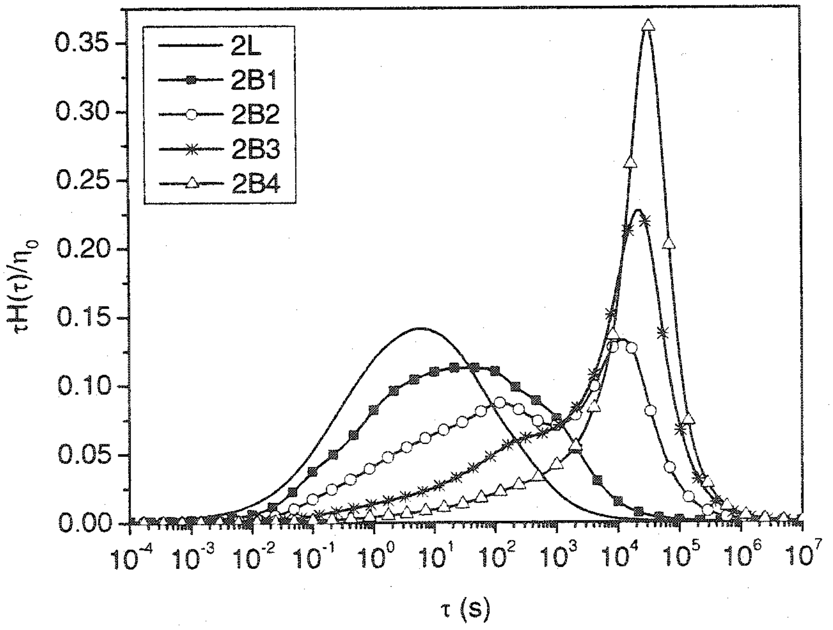

Figure 4-47: Normalized time-weighted relaxation spectra of MFR 2 polypropylenes

Figure 4.16 shows oscillatory shear data for the samples of 20L before and after extrusion, and we saw that the two materials appeared to be nearly the same over the whole experimental window. However, if we look at the behavior of the samples in terms of time-weighted relaxation spectra shown in Fig. 4.45, the difference is more detectable. The long chains underwent β-chain scission during extrusion. Therefore, the fraction of the chains with long relaxation times decreased, whereas the fraction of medium chains increased. From this comparison it can be concluded that the time-weighted relaxation spectrum is a more sensitive function to examine the effect of molecular structure on rheological behavior. However, because the degree of chain scission is small, the relaxation time range was not changed, and at the short and long time ends, the two relaxation spectra are nearly identical. Therefore, we conclude that chain scission during the extrusion process is negligible, which is the conclusion reached on the basis of the dynamic data.

From Figs. 4.46 and 4.47 we can see clearly that with increased level of branching, the shape and peak location of the relaxation spectra change dramatically. These changes can be explained qualitatively by molecular theories, in which the mechanisms for relaxation of branched molecules are quite different from those available to linear molecules[19]. Reptation is not possible for branched molecules, and instead they relax hierarchically from the free ends to the interior of the molecule. The initial step in this relaxation process is arm length fluctuation. This gives rise to a very broad range of relaxation times, and the terminal relaxation time increases exponentially with the length of the arms. The interior portions of branched molecules can relax their stress only after this initial process is completed, resulting in a very broad relaxation spectrum. As the level of branching increases, the fraction of the molecules that are branched and the complexity of the branching structure increase. This results in the extension of the relaxation spectrum to very long times.

It is important to remember that it is not only the level of branching that influences stress relaxation but also, and more importantly, the topology of the molecules. The polypropylene samples considered here have broad molecular weight distributions and complex branching architectures. These differences in structure cause the differences in rheological behavior observed in Figs. 4.46 and 47. By examining the relaxation spectrum of the samples using molecular theory, and with the information of branching obtained by simulation of the branching process, it is possible to learn something about the topology of the samples studied.

References

[1] Kraft, M., J. Meissner, J. Kaschta, "Linear Viscoelastic Characterization of Polymer Melts with Long Relaxation Times," Macromolecules, 32, 751-757, 1999

[2] Ferry J. D., "Viscoelastic Properties of Polymers", New York, Wiley, 1980

[3] Bersted B.H., Encyclopedia of Fluid Mechanics, Vol.7, Chapter 22, Gulf Publishing Company, Houston, 1988

[4] Constantin, D., "Linear-Low-Density Polyethylene Melt Rheology: Extensibility and Extrusion Defects", Polym. Eng. & Sci., 24, 268-274, 1984

[5] Roovers, J., "Melt Rheology of H-Shaped Polystyrenes", Macromolecules, 17, 1196-1200, 1984

[6] Fetters, L. J., A. D. Kiss, D. S. Pearson, G. F. Quack, F. J. Vitus, "Rheological Behavior of Star-Shaped Polymers", Macromolecules, 26, 647-654, 1993

[7] Gell, C. B., W. W. Graessly, V. Efstratiadis, M. Pittsikalis, N. Hadjichristidis, "Viscoelasticity and Self-Diffusion in Melts of Entangled Asymmetric Star Polymers", J. Poly. Sci. Part B: Polymer Physics, 35, 1943–1954, 1997

[8] Kasehagen, L. J., C. W. Macosko, D. Trowbridge, and F. Magnus, "Rheology of Long-Chain Randomly Branched Polybutadiene", J. Rheol., 40, 689-709,1996

[9] Robertson C. G., C. M. Roland, C. Paulo and J. E. Puskas, "Linear Viscoelastic Properties of Hyperbranched Polyisobutylene", J. Rheol. 45, 759–772, 2001

[10] Gabriel, C., J. Kaschta, H. Munstedt, "Influence of Molecular Structure on Rheological Properties of Polyethylenes I. Creep Recovery Measurements in Shear", Rheol. Acta, 37, 7-20, 1998

[11] Wood-Adams, P. M., J. M. Dealy, A. W. deGroot, O. D. Redwine, "Effect of Molecular Structure on the Linear Viscoelastic Behavior of Polyethylene", Macromolecules, 33, 7489-7499, 2000

[12] Gabriel, C., H. Munstedt, "Creep Recovery Behavior of Metallocene Linear Low-Density Polyethylene", Rheol. Acta, 38, 393-403, 1999

[13] Yan, D., W. J. Wang, S. Zhu, "Effect of Long-Chain Branching on Rheological Properties of Metallocene Polyethylene", Polymer, 40, 1737-1744, 1999

[14] Gabriel, C., H. Munstedt, "Influence of Long-Chain Branches in Polyethylenes on Linear Viscoelastic Properties in Shear", Rheol. Acta, 41, 232-244, 2002

[15] Hingmann, R., B. L. Marczinke, "Shear and Elongational Flow Properties of Polypropylene Melts", J. Rheol., 38, 573-587, 1994

[16] Kurzbeck, S., F. Oster, H. Munstedt, T. Q. Nguyen, R. Gensler, "Rheological Properties of Two Polypropylenes with Different Molecular Structure", J. Rheol., 43, 359-374, 1999

[17] Honerkamp, J., J. Weese, "A Nonlinear Regularization Method for the Calculation of Relaxation Spectra", Rheol. Acta, 32, 65-73, 1993

[18] Davies, A.R. and R.S. Anderssen, "Sampling Localization in Determining the Relaxation Spectrum", J. Non-Newt. F. Mech., 73, 163-179, 1997

[19] McLeish, T. C. B., Chapter 6 "Topology of Polymers: Entangled Dynamics and Melt Flow", of "Chemical Topology Introduction and Fundamentals" Edited by D. Bonchev and D.H. Rouvray, Gordon and Breach Science Publishers, 1999

Chapter 5. Modeling of Linear Viscoelastic Behavior of Polypropylenes

5.1. Introduction

The theoretical prediction of the rheological properties of polymer melts based on molecular theory complements experimental measurements. Usually polyolefins are highly entangled because of the low entanglement molecular weight. Predicting rheological properties of well-entangled linear polymers was not possible until the reptation model was first proposed by de Gennes[1] in 1971. The fundamental assumptions of the tube model are that the topological constraints imposed on an entangled chain can be modeled as a tube having its own contour. Motions perpendicular to the contour are prevented, and the only long-range motions that are possible are those in which the chain moves along its own length. This motion is called reptation and is a simultaneous motion of all elementary units. This model was further developed into a polymer dynamics theory by Doi and Edwards[2] in 1986. The tube model is able to explain the strong dependence of viscosity and diffusivity on molecular weight. Experimental results, however, showed that viscosity has an even stronger dependency on molecular weight than was predicted by the model. The tube model also fails to predict the linear viscoelastic properties at high frequencies. Non-reptative relaxation mechanisms such as contour-length fluctuations and Rouse relaxations are responsible for these differences.

Two decades of continuous efforts were made to improve the tube model. The first improvement was to include the constraint release relaxation mechanism. The tube of the test chain, which is made up of the surrounding chains, is not stationary because the surrounding chains are themselves relaxing. This phenomenon was called "tube renewal". De Gennes[3] proposed that the tube motion should be Rouse-like with the temperature replaced by the frequency of constraint release. Montfort *et al.*[4] studied the effect of constraint release on the reptation of entangled chains by using binary blends of monodisperse linear polystyrenes with very different molecular weights. They concluded that the tube could be considered as a Rouse chain. A detailed, self-consistent theory of constraint release was developed by Rubinstein and Colby[5] and refined by Likhtman and McLeish[6].

The second improvement was to include contour length fluctuation as proposed by Doi[7]. Milner and McLeish[8] and others[6] used Doi's assumptions to incorporate both reptation and contour-length fluctuation in a stress relaxation theory for monodisperse, linear polymers.

The third addition to the reptation theory was the longitudinal Rouse-like relaxation of the entire chain in its tube. This relaxation mode was modeled by Viovy[9]. Milner and Mcleish[8] proposed to divide this contribution by three, because only one of the three vector components of the Rouse mode is free in the tube. However, in the recent work of Likhtman and McLeish[6], this contribution is claimed to be 1/5, rather than 1/3, of the low frequency Rouse-like relaxation, because this process is only active at times up to the Rouse time.

While improvements were being made in the tube theory for monodisperse polymers by including contour length fluctuations and different modes of Rouse relaxation of the chain or Rouse-like relaxation of the tube, efforts were also made to extend the use of the improved tube theory to a linear, polydisperse system. In a polydisperse system, the stress relaxation after a step strain is governed by both the survival probability of chains and that of constraints surrounding the chains. The tube diameter of the test chain, which is governed by the constraints imposed by the surrounding chains, is not fixed as in a monodisperse system; instead it changes its size and shape due to the relaxation of the surrounding chains. Marrucci[10] calculated the tube diameter of a test chain as a function of time after a step strain in a linear, polydisperse system and the resulting relaxation modulus as a function of time by taking into account the enlargement of the tube. Montfort *et al.*[11] considered the tube-renewal effect coupled with reptation in linear, polydisperse systems. Doi *et al.*[12] studied the dynamics of a mixture of two narrow molecular weight distribution homopolymers on the basis of reptation and constraint release due to reptation. They found that the constraint release due to reptation of surrounding chains was responsible for both tube renewal and tube dilation. A more recent "dual constraint" model (Mead *et al.* [13]) considers the binary topological interaction of the test chain with a surrounding chain while taking into account contour-length fluctuations and constraint release. Pattamaprom *et al.*[14] enhanced the model of Mead *et al.*[13] by using a more accurate function to separate the early and late time contour length fluctuations and including a constraint release, Rouse-like motion. By applying the improved "dual constraint" model to several polymer systems, they found that the model was able to predict the linear viscoelastic properties of monodisperse, bidisperse, and polydisperse systems without adjustable parameters. When comparing the predicted results with the experimental data in the literature, a good agreement was found.

Another very popular method to deal with binary topological interactions of polymer chains in a polydisperse system is the "double reptation" model. The double reptation concept is illustrated in Fig. 5.1. In a polymer melt, two chains, A and B, are entangled at point P. The stress at P disappears if either A or B reptates through P. Then the survival probability of the entanglement point P at time t is $\phi'(t)$:

$$\phi'(t)=\sum_{A} w_A(t)\phi_A(t)\sum_{B} w_B(t)\phi_B(t)=\left[\sum_{i} w_i(t)\phi_i(t)\right]^2 \qquad (5.1)$$

where w_i is the fraction of chain i, and $\phi_i(t)$ is the survival probability of chain i at time t.

The relaxation modulus is proportional to $\phi'(t)$ multiplied by the plateau modulus G_N^0. Des Cloizeaux[15] derived a quadratic mixing rule by using the double reptation concept.

$$G(t)=G_N^0\left[\sum_{i} w_i(t)p_i(t)\right]^2 \qquad (5.2)$$

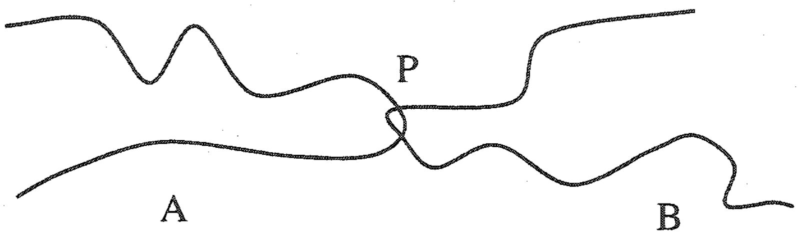

Figure 5-1: The chains A and B are entangled and there is a stress point at P

Tsenoglou[16] developed a generalized mixing rule of the same type for polydisperse systems as shown in Eq. 5.3:

$$G(t) = G_N^0 \left[\int_{\ln(2M_e)}^{+\infty} F^{1/\chi}(t, M) w(\ln M) d \ln M \right]^{\chi} \tag{5.3}$$

where *F(t,M)* is a kernel function describing the relaxation behavior of a monodisperse species of molecular weight *M*; χ is a mixing exponent, $\chi = 1$ gives the Doi-Edwards function and $\chi = 2$ is the case of double reptation; M_e is the molecular weight between two successive entanglement points; *w(ln M)dlnM* is the weight fraction of the molecules having molecular weight between *lnM* and *lnM+d(lnM)*. Because double reptation follows directly from the Doi-Edwards reptation model, the kernel function is usually the original Doi-Edwards function, which is given by Eq. 5.4.

$$F(t, M) = \sum_{p\ odd}^{\infty} \frac{8}{p^2 \pi^2} \exp\left(\frac{-tp^2}{\tau_d(M)} \right) \tag{5.4}$$

where $\tau_d(M)$ is the longest relaxation time of the chain having molecular weight *M*. Doi-Edwards assume the same scaling law as de Gennes[1].

$$\tau_d(M) = \tau_{mon} \frac{N^3}{N_e} \tag{5.5}$$

and τ_{mon} is an elementary monomer time scale that includes the effects of temperature and chain microstructure; N is the number of monomers per chain, and N_e is the number of monomers between two successive entanglement points.

Noticing that the above function is dominated by the first term for which $p = 1$, Tsenoglou[16], Carrot[17], and Wasserman and Graessley[18] used a kernel function in their models that contained only the dominant first term, which is a single exponential.

$$F(t,M) = \exp\left(\frac{-t}{\tau_d(M)}\right) \tag{5.6}$$

The double reptation model gives a good prediction of linear viscoelastic properties in the terminal zone for monodisperse systems. For polydisperse systems, the double reptation model is able to extend the prediction into the intermediate frequency zone, because in this regime the relaxation is dominated by the reptation of chains shorter than the longest ones.

Efforts were also made to account for Rouse relaxations in the double reptation model in order to extend the prediction to a wider range of frequency. Benallal *et al.*[19] proposed that the relaxation of a monodisperse polymer melt consists of the following mechanisms: reptation of polymer chains; longitudinal Rouse relaxation of the entire chain; Rouse relaxation between two successive entanglement points; and a high frequency relaxation process related to the glassy behavior of the chain. Léonardi[20] and coworkers modified the model of Benallal[19] by including contour length fluctuations, tube renewal effects, and Rouse relaxation of unentangled chains, and applied it to several polymers (polystyrene, polymethyl methacrylate, and high-density polyethylene) having a wide range of polydispersity index values (M_w/M_n = 1.06-4.6). They found that only the double reptation model that took into account the effects of polydispersity of surrounding chains through "tube renewal" was able to describe correctly the linear viscoelastic behavior of polydisperse systems.

The enhanced "dual constraint" model by Pattamaprom *et al.*[14] and the revised double reptation model by Léonardi *et al.*[20] most completely included the various relaxation mechanisms of a polydisperse system. Therefore, these two models are used in this work to predict the linear viscoelastic properties of linear polypropylenes.

A brief review of the main concepts of these two models is given in the next section. Following that, a comparison of LVE predictions for sample 35L using the two models is presented, and based on the comparison, a model giving the better prediction is chosen to predict the LVE of the other linear polypropylenes. Finally, the LVE predictions for linear polypropylenes using the chosen model are presented, and a discussion of the predictions is given.

5.2. Summary of the Two Models

5.2.1. The Dual Constraint Model

In the dual constraint release model, there are two types of constraint release[14]. The first is the reptative relaxation of constraints. The second type of constraint release, global loosening of the entanglement network, is called "dynamic dilution" or "tube dilution". The constraint release rate from both mechanisms is limited by the Rouse-like motions of the tube containing the test chain. This relaxation mechanism is called "Rouse constraint release".

In order to incorporate the two types of constraint release into the model, the model solves the diffusion equation for the reptation and fluctuation of linear polymers twice.

$$\frac{\partial p_i(s_i,t)}{\partial t}=\frac{D_i}{L_i^2}\frac{\partial^2 p_i(s_i,t)}{\partial s_i^2}-\frac{p_i(s_i,t)}{\tau_{\xi,i}(s_i)} \qquad (5.7)$$

The equation is first solved in a fixed tube, *i.e.*, in the absence of constraint release. The first term on the left side of Eq. 5.7 represents the diffusion of the test chain, and the second term corresponds to the contour length fluctuation; $p_i(s_i,t)$ is the survival probability of a tube segment occupied by a chain of type i as a function of time t and contour length s_i. s_i ranges from zero at the center to one-half at the end of a linear chain; D_i is the curvilinear diffusion coefficient; L_i is the averaged contour length of the tube; and $\tau_{\xi,i}$ is the time constant for contour length fluctuations. The contour length fluctuation process is split into two time regions: early time and late time:

$$\tau_{early,i}(s_i) = \frac{225}{256}\pi^3 \frac{\tau_{R,i}}{4}(1-2s_i)^4\left(\frac{N_{en,i}}{2}\right)^2 \tag{5.8}$$

$$\tau_{late,i}(s_i) = \frac{\tau_{R,i}}{4}\exp(U(s_i)) \tag{5.9}$$

where $N_{en,i}$ is the number of entanglements of chain i, and $\tau_{R,i}$ is the longest Rouse relaxation time of chain i and is related to the reptation time $\tau_{d,i}$ by $\tau_{R,i} = \dfrac{\tau_{d,i}}{6N_{en,i}}$.

Now we have:

$$\tau_{\xi,i} = \tau_{early,i} \text{ when } (1-2s_i) < C_1 \tag{5.10}$$

$$\tau_{\xi,i} = \sqrt{\tau_{early,i}\cdot\tau_{late,i}} \text{ when } C_1 < (1-2s_i) < C_2 \tag{5.11}$$

$$\tau_{\xi,i} = \tau_{late,i} \text{ when } (1-2s_i) > C_2 \tag{5.12}$$

where C_1 is the first crossover of $\tau_{early,i}$ and $\tau_{late,i}$ close to the chain end, and C_2 is the second crossover of $\tau_{early,i}$ and $\tau_{late,i}$ as shown in Fig. 5.2.

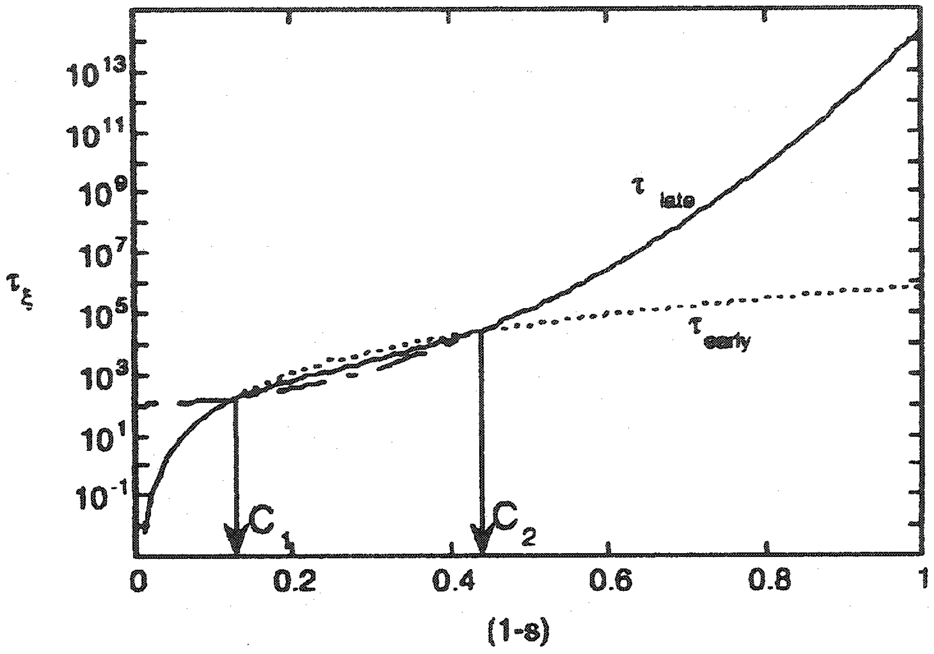

Figure 5-2: The crossover function (solid line) from $\tau_{early,i}$ (dotted line) to $\tau_{late,i}$ (dashed line). The crossover points are indicated by C_1 and C_2 (ref. 15)

The solution of Eq. 5.7 is the tube survival probability in the fixed matrix. The solution is corrected by the constraint-release Rouse relaxation mechanism and is donated as $\phi^*(t)$.

Contour-length fluctuations are incorporated into the model by using a reduced, effective activation energy when solving Eq. 5.7 for the second time. The effective activation energy is $U_{eff}(s,t)=U(s)\phi^*(t)$. In this way, the late time arm retraction is time dependent and accelerated.

$$\tau_{late}(s,t)\propto exp(U_{eff}(s,t)) \tag{5.13}$$

The local relaxation of entanglement constraints is caused by the reptation of chains. This constraint relaxation mode is taken into account in the model by using the double diffusion mechanism. This mechanism considers the survival probability of a binary topological interaction of the test chain with a surrounding chain. The double diffusion mechanism accounts for the effect of the surrounding chains on the overall relaxation process by multiplying the average survival probability of the test chain by that of the constraints surrounding the chain. By solving Eq. 5.7 a second time including constraint release via the effective activation energy for late time arm retraction, the average survival probability of the chains is obtained as $\phi(t)$. The average survival probability of the constraints surrounding a chain is $\phi'(t)$. Taking into account constraint release Rouse motion, $\phi'(t)$ can be expressed as follows:

$$\phi'(t) = max(\phi(t), \phi_R(t)) \tag{5.14}$$

where $\phi_R(t) = \phi(t_0)\left(\frac{t}{t_0}\right)^{-\frac{1}{2}}$ in which t_0 is the time when $\phi(t)$ begins to drop faster than $t^{(-1/2)}$, and $\phi(t_0)$ is the average chain survival probability at t_0.

Thus, the relaxation modulus with contributions from reptation, contour-length fluctuations, constraint release and constraint release Rouse can be expressed as:

$$G(t) = G_N^0\ \phi(t)\phi'(t) \tag{5.15}$$

The high frequency Rouse relaxation processes, the longitudinal Rouse motion of the entire chain and the Rouse motion of small chains are included in this model as $G_{R,i}(t)$ using the formula proposed by Milner and McLeish[8].

$$G_{R.i}(t) = \left[\frac{1}{5}G_N^0 \sum_{k=1}^{N_{en.i}} \exp\left(\frac{-k^2 t}{\tau_{R.i}}\right) + G_N^0 \sum_{k=N_{en.i}}^{N_i} \exp\left(\frac{-k^2 t}{\tau_{R.i}}\right)\right]\frac{1}{N_{en.i}} \tag{5.16}$$

where N_i is the number of monomers in a chain of type i. According to Likhtman and McLeish[6] the front factor in Eq. 5.16 is 1/5 rather than 1/3 as was used earlier[8]. Therefore, the total stress relaxation modulus G_{total} is:

$$G_{total}(t) = G(t) + \sum_i w_i G_{R.i}(t) \tag{5.17}$$

where w_i is the weight fraction of chains of type i.

The model can be used to calculate the storage and loss moduli from the stress relaxation modulus $G_{total}(t)$ using Eqs. 5.18(a) and (b).

$$G'(\omega) = \omega \int_0^\infty G_{total}(t) \sin(\omega t) dt \tag{5.18a}$$

$$G''(\omega) = \omega \int_0^\infty G_{total}(t) \cos(\omega t) dt \tag{5.18b}$$

For each species of molecular weight M, it is necessary to solve the diffusion equation 5.7 twice. Considering the complexity of the computation, it is not practical to enter MWD data from a GPC measurement; instead a discrete MWD with 20 components is used.

Another input parameter is the monomer molecular weight M_0, and for polypropylene this is 42. The last parameter requried is the entanglement molecular weight. Eckstein[21] and coworkers found that the entanglement molecular weight is 6900 g/mol for isotactic polypropylene and 7050 g/mol for atactic polypropylene. However, by fitting the predictions to the experimental data, it is found that M_e has the value of 6730 g/mol.

The results of the calculation are the reduced frequency and modulus: $(\omega\tau_e)$, (G'/G_N^0) and (G''/G_N^0), where τ_e is the characteristic Rouse relaxation time of an entanglement segment, which is determined by fitting the predictions to the experimental data. G_N^0 is calculated from M_e using Ferry's[22] relationship:

$$G_N^0 = \frac{\rho RT}{M_e} \tag{5.19}$$

5.2.2. A Modified Double Reptation Model[20]

Léonardi *et al.*[20] extended the rheological model of Benallal[19] to polydisperse systems by taking into account the effects of polydispersity on relaxation behavior. For a linear, polydisperse system, the relaxation of the molecules is due to the following mechanisms: Rouse relaxation of unentangled chains; Rouse relaxation between two successive entanglement points (called the A relaxation process); Rouse relaxation along the entire chain inside its tube (called the B relaxation process); and the slowest relaxation of the chain by reptation (called the C relaxation process). The A and B processes are different modes of the Rouse relaxation mechanism, which have the same physical significance and formula as those in the "dual constraint" model[14]. In this summary, only the longest relaxation process, the C relaxation process, will be addressed.

In the model of Léonardi *et al.*[20] the contribution of reptation to the relaxation modulus is expressed as:

$$G(t)=\left(\int_{\ln M_C}^{\infty} G_C^{1/2}(t,M)\,w(\ln M)\,d\ln M\right)^2 \qquad (5.20)$$

The above expression considers the binary topological interaction of the chains but does not take into account the constraint release Rouse motion process. Therefore, the survival probability of the test chain and that of the constraints surrounding the chain are the same and are given by:

$$\phi(t)=\phi'(t)=\int_{\ln M_C}^{\infty} G_C^{1/2}(t,M)\,w(\ln M)\,d\ln M \qquad (5.21)$$

the kernel function is $G_C(M,t)=G_N^0\int_0^1 \exp\left(-\frac{t}{\tau_\xi}\right)d\xi$ (5.22)

$$\text{with } \tau_\xi = \begin{Bmatrix} \tau_{\xi 1} = N_{en}\xi^4 \tau(M, w(\ln M))/16\upsilon^2, & for 0 < \xi < 2\upsilon/\sqrt{N_{en}}, \\ \tau_{\xi 2} = \left(\xi - \upsilon/\sqrt{N_{en}}\right)^2 \tau(M, w(\ln M)), & for 2\upsilon/\sqrt{N_{en}} < \xi < 1 \end{Bmatrix} \tag{5.23}$$

where N_{en} is the number of entanglements (M/M_e) and ν is an adjustable parameter that is equal to 0.5 in this model as proposed by Majeste[23]. If we ignore the plateau modulus, G_N^0, Eq. 5.22 is the survival probability of the chain that is calculated from the Doi and Edwards theory[24] with a single relaxation time taking into account tube length fluctuations. The tube length fluctuation constant, τ_ξ, is split into two time regions that are equivalent to early and late time arm retraction in the dual constraint release model. $\tau(M, w(\ln M))$ is the longest relaxation time of the chains of molecular weight M and fraction $w(\ln M)$. The model adopted the idea of Graessley[25] that $\tau(M, w(\ln M))$ is the harmonic average of the reptation time $\tau_d(M)$ in a fixed entanglement matrix and the "tube renewal time" $\tau_t(M, w(\ln M))$ as follows:

$$\frac{1}{\tau(M, w(\ln M))} = \frac{1}{\tau_d(M)} + \frac{1}{\tau_t(M, w(\ln M))} \tag{5.24}$$

Following Graessley[25] the tube renewal time $\tau_t(M, w(\ln M))$ is:

$$\tau_t(M, w(\ln M)) = N^2 \langle \tau_{obs}(w(\ln M)) \rangle \tag{5.25}$$

where $\langle \tau_{obs}(w(\ln M)) \rangle$ is the average lifetime of a constraint. He assumed that each segment of the test chain has on average, three contacts with the surrounding chains, and the average lifetime of one of these contacts is:

$$\langle \tau_{obs}(w(\ln M)) \rangle = \int_0^{+\infty} \left[\int_{\ln(2M_e)}^{+\infty} \exp\left(-\frac{t}{3\tau_{obs}(M)} \right) w(\ln M)\, d\ln M \right]^3 dt \tag{5.26}$$

where $\tau_{obs}(M)$ is the entanglement lifetime of a monodisperse species. Cassagnau *et al.*[26] proposed

$$\tau_{obs}(M)=\frac{4\tau_d(M)}{M^{1/2}} \tag{5.27}$$

Now the total relaxation modulus $G_{total}(t)$ is:

$$G_{total}(t)=G(t)+G_A(t)+G_B(t) \tag{5.28}$$

The input parameters, M_0 and M_e, have the same value as in the dual constraint model, which are 42 and 6730 g/mol, respectively. In this model, we can enter all the molecular weight distribution data from the GPC measurement. However, the plateau modulus G_N^0 and elementary relaxation time τ_0 are obtained by fitting the model to experimental data.

5.3. Comparison of Predictions for 35L Using The Two Models

The linear viscoelastic properties of sample 35L were predicted using the two models, and the predictions were compared with experimental data. The complex moduli predicted with the dual constraint model and the stress relaxation modulus predicted with the double reptation model are then transformed into time-weighted relaxation spectra, and these spectra are compared with those obtained from experimental data. Based on the comparisons the model giving better predictions was chosen to predict the LVE of the other linear polypropylenes.

The complex moduli for 35L simulated using the dual constraint model are shown in Fig. 5.3 as solid lines and compared with the experimental data (symbols). The model gives good predictions of the loss modulus over the entire experimental frequency range although there are small discrepancies in the storage modulus at low frequency (< 1 rad/s).

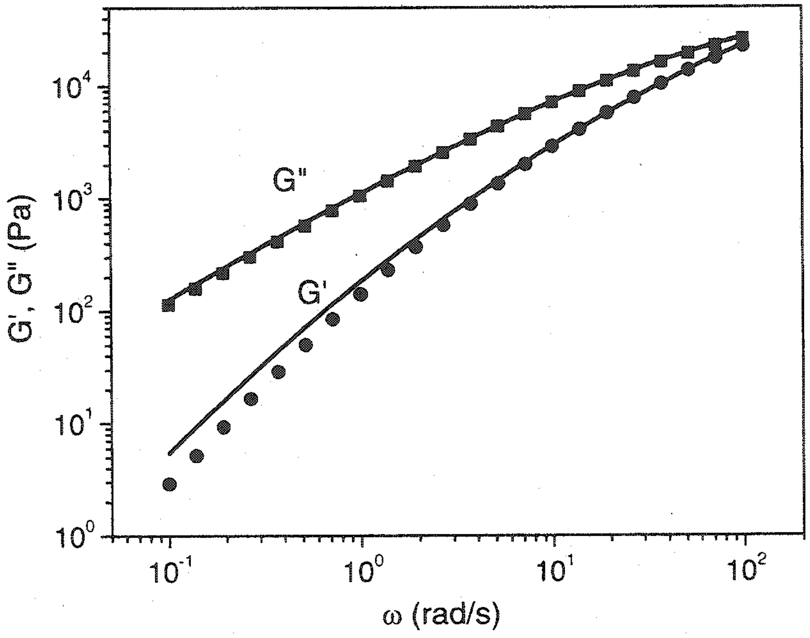

Figure 5-3: Comparison of the dual constraint model predictions of storage and loss moduli (solid line) with experimental data (symbols) for 35L at 180 °C

The fitting parameter for 35L is $\tau_e = 9.17\times10^{-7}$s. The plateau modulus, which is calculated from Eq. 5.19 with $\rho = 0.75$ g/cm^3, $M_e = 6730$ g/mol and $T = 453$K, is G_N^0 = 4.20×10^5Pa.

The predicted stress relaxation modulus for 35L using the modified double reptation model[20] is shown in Fig. 5.4 as the solid line and compared with the results calculated from experimental data, which are shown as symbols. At short times the predictions agree with the experimental data very well, but there is a discrepancy at times greater than 1s. The fitting parameters for sample 35L are $\tau_0 = 5.23\times10^{-11}$s and G_N^0 = 2.43×10^5 Pa. We note that G_N^0 is almost half of the value calculated from the entanglement molecular weight M_e. The modeling parameters τ_0 and τ_e should be related as:

$$\tau_e = \frac{1}{6} N_e^2 \tau_0 \tag{5.29}$$

However, the values of τ_0 and τ_e obtained by fitting two models to the 35L data are not related as indicated by Eq. 5.29. According to Eq. 5.29, with $\tau_e = 9.17\times10^{-7}$s (found by fitting the dual constraint model), τ_0 should be 1.98×10^{-10}s instead of 5.23×10^{-11}s.

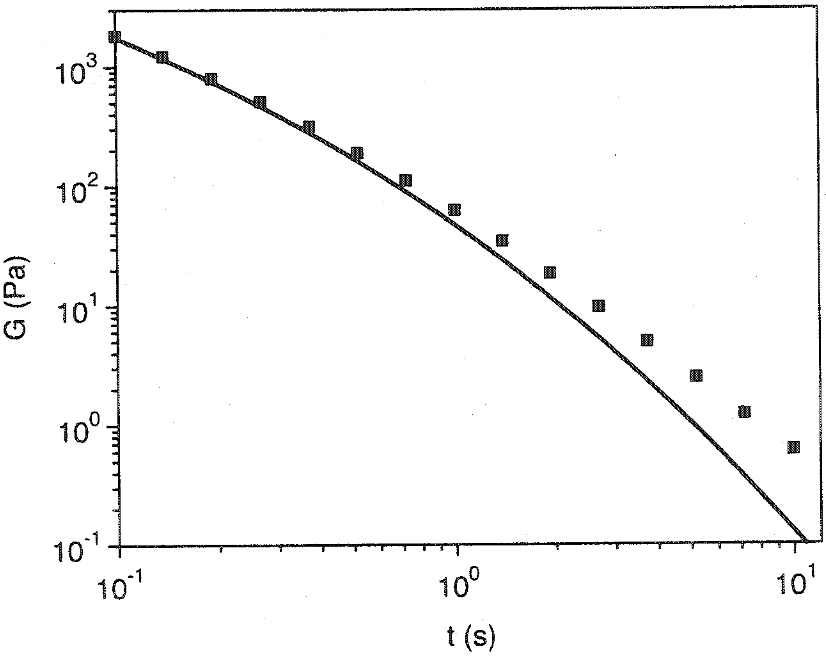

Figure 5-4: Comparison of the double reptation model predictions of relaxation modulus (solid line) with experimental data (symbols) for 35L at 180 °C

The predicted linear viscoelastic properties are transformed into time-weighted relaxation spectra using the nonlinear regularization method (NLREG) proposed by Honerkamp and Weese[27], which is described in Chapter 4, and the spectra are compared with those calculated from experimental data. These comparisons are shown in Figs. 5.5 and 5.6.

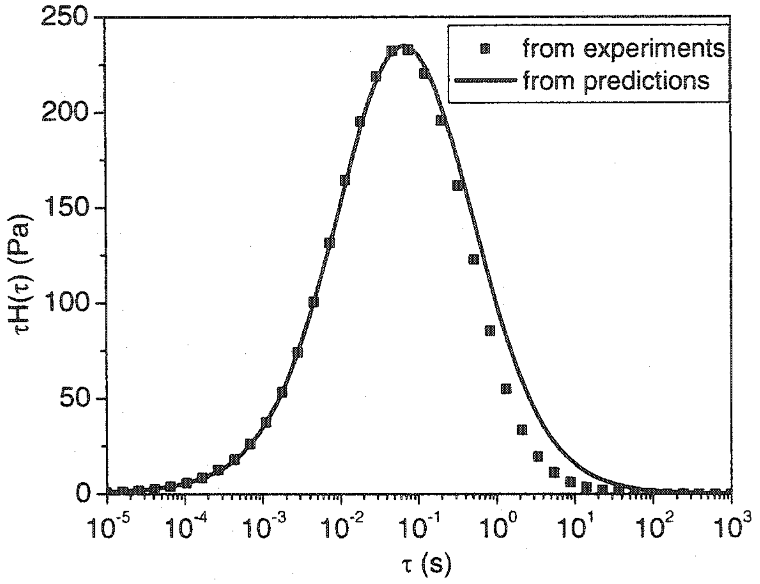

Figure 5-5: Time weighted relaxation spectrum for 35L at 180 °C from experimental data (symbols) and from predicted data using the dual constraint model (solid line)

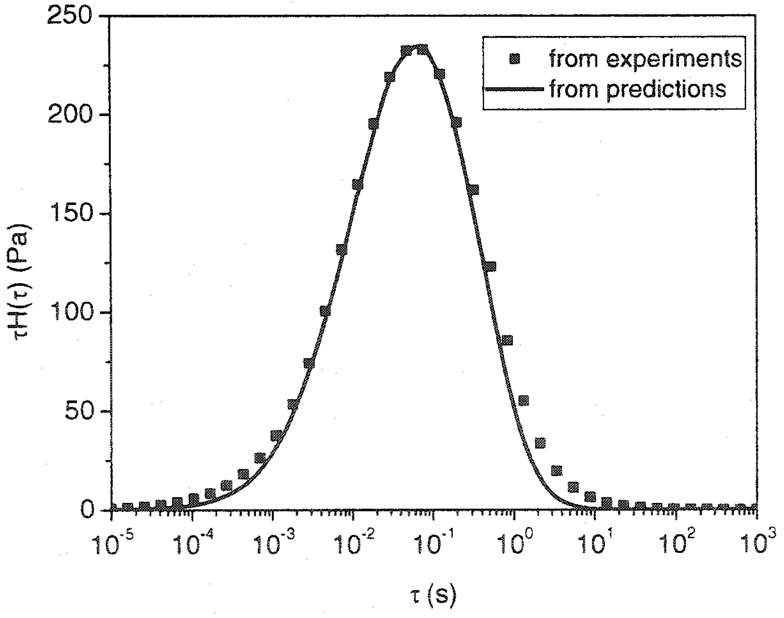

Figure 5-6: Time weighted relaxation spectrum for 35L at 180 °C from experimental data (symbols) and from predicted data using the double reptation model (solid line)

From Fig. 5.5 we see that at short time (< 0.1s) the predicted spectrum superposes with that from the experimental data; the predicted spectrum has the same shape as that from the experimental data and that the predicted peak is correct. However, a small discrepancy at long time is observed. For the present work, the peak, which represents the reptation of the weight average molecule, is of special importance. Therefore, we conclude that the model performs well for 35L.

In Fig. 5.6 it can be seen that the time-weighted relaxation spectrum from the predictions is smaller than that from the experimental data at long times. This may be due to the modification of the longest relaxation time by the "tube renewal time". This modification may over-estimate the effect of polydispersity on linear chain relaxation. The assumption that each segment of the test chain has three average contacts with the surrounding chains may not be correct for polypropylene, and this could cause the discrepancy at long times. Discrepancy between the two spectra at short times is also observed.

Based on the above comparisons, we conclude that the dual constraint model is able to capture the relaxation behavior of linear chains over most of the relaxation time window, and the modeling parameters have better literature support. Therefore, this model was used to predict the linear viscoelastic properties for the other linear polypropylenes.

5.4. Predictions for The MFR 35 Set

5.4.1. Predicted Complex Moduli and Discussion

The MFR 35 sample set includes: 35L, 35B1, 35B2 and 35B3. The polydispersity index (M_w/M_n) of 35L is 3.6. The predictions are made for hypothetical linear polypropylenes having exactly the same molecular weight distributions as those of the corresponding branched samples. Such a hypothetical linear polypropylene is a "linear equivalent" of the branched sample. Corresponding to three levels of long-chain branching, there are three linear equivalents, which are $(35B1)_{LE}$, $(35B2)_{LE}$, and $(35B3)_{LE}$. The same modeling parameters as for 35L are used for the predictions of the LVE properties of the three linear equivalents. The predicted complex moduli are shown in Figs. 5.7-5.9 and compared with those from experimental measurements on the branched samples.

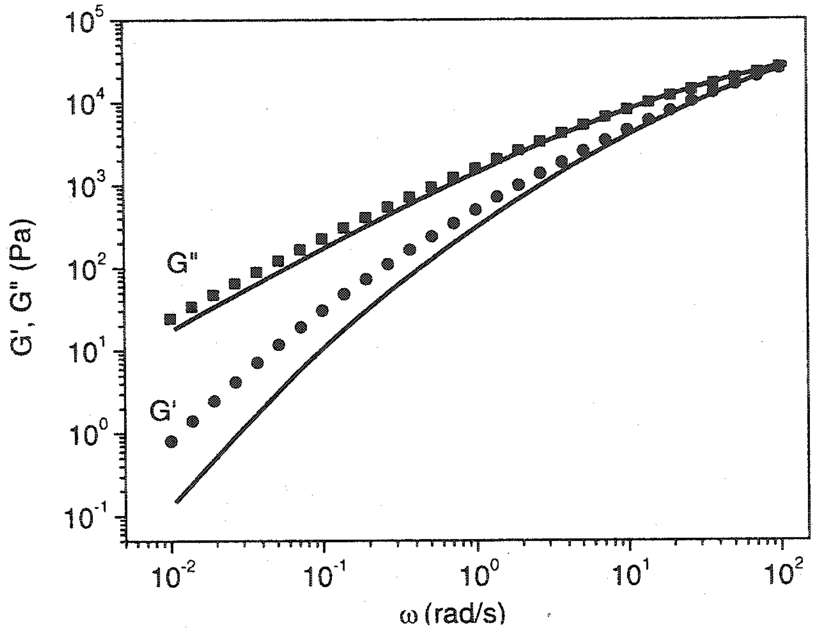

Figure 5-7: Comparison of the dual constraint model predictions of storage and loss moduli (solid line) of $(35B1)_{LE}$ with the experimental data for 35B1 (symbols) at 180 °C

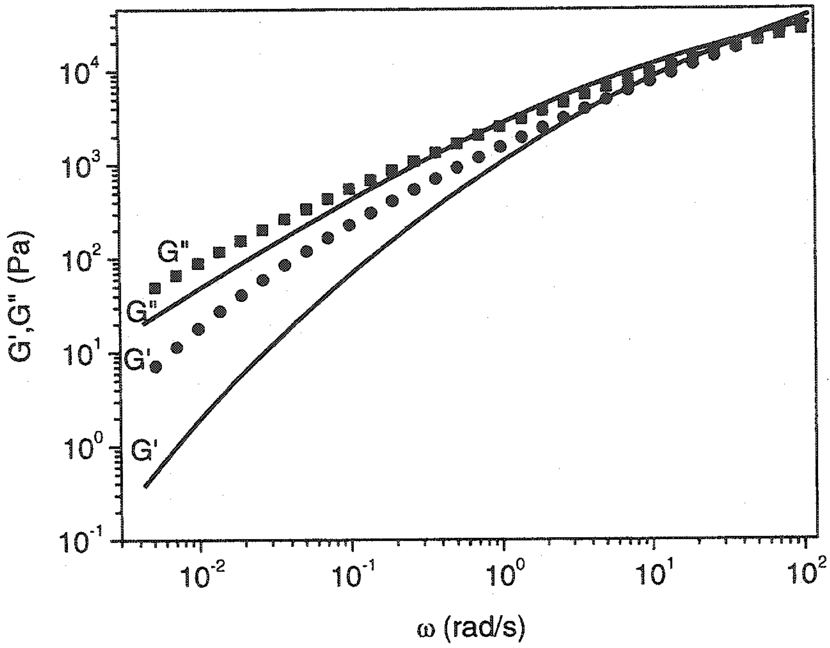

Figure 5-8: Comparison of the dual constraint model predictions of storage and loss moduli (solid line) of $(35B2)_{LE}$ with the experimental data for 35B2 (symbols) at 180 °C

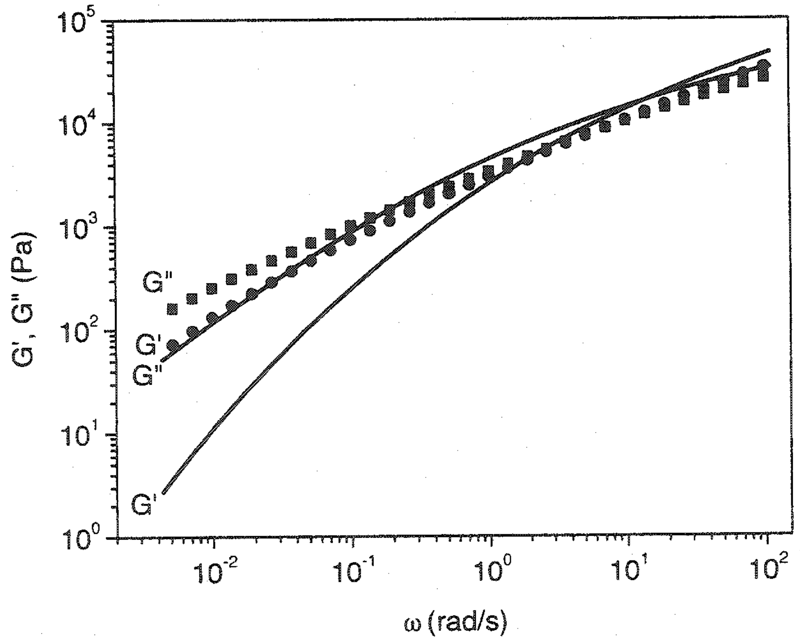

Figure 5-9: Comparison of the dual constraint model predictions of storage and loss moduli (solid line) of $(35B3)_{LE}$ with the experimental data (symbols) for 35B3 at 180 °C

From Figs 5.7 to 5.9 we can see that the storage and loss moduli of the branched samples and their linear equivalents are quite different, although they have exactly the same molecular weight distributions. In the high frequency region, the moduli of the branched samples are lower than those of their linear equivalents, because there are more chain ends in the branched system, and the relaxation due to the chain end retractions is therefore faster. However, with decreasing frequency the relaxation is slowed down in the branched systems because the relaxation mechanisms of branched molecules are different from those of the linear ones. For branched molecules, reptation is not possible, and they relax hierarchically from the chain ends to the interior of the chains. This leads to a broad transition to the terminal zone. The interior portions of the branched molecules can relax their stress only after the arms are relaxed. This leads to much higher moduli at low frequency than for the linear equivalents. With increasing level of branching, the differences between the moduli of a branched sample and its linear equivalent become more significant.

5.4.2. Transformation of Moduli to Time-Weighted Relaxation Spectrum

The predicted moduli were transformed into time-weighted relaxation spectra using the NLREG[27] technique, and the spectra were compared with those from experimental data. The comparisons are shown in Figs 5.10-5.12.

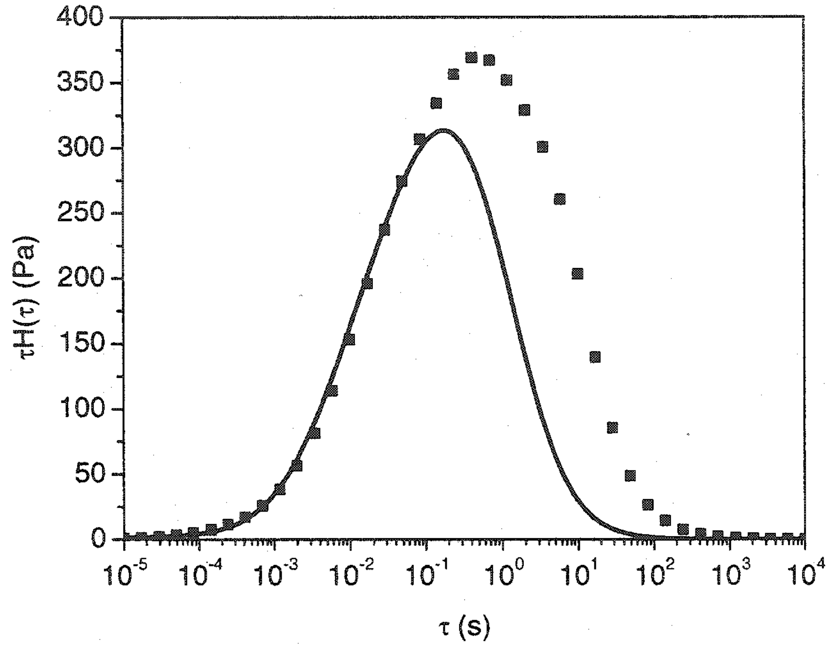

Figure 5-10: Time weighted relaxation spectrum of 35B1 at 180 °C from experimental data (symbols) and of $(35B1)_{LE}$ from predicted data (solid line)

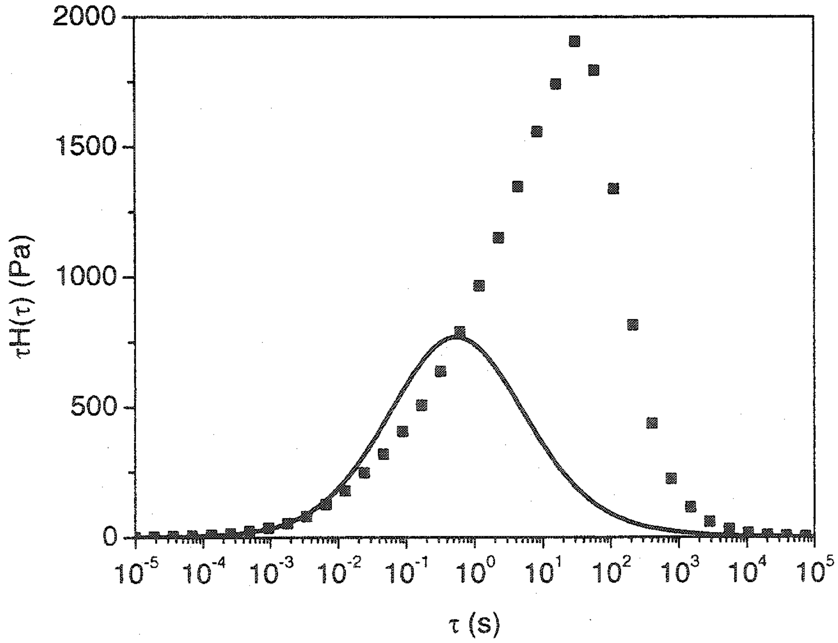

Figure 5-11: Time weighted relaxation spectrum of 35B2 at 180 °C from experimental data (symbols) and of $(35B2)_{LE}$ from predicted data (solid line)

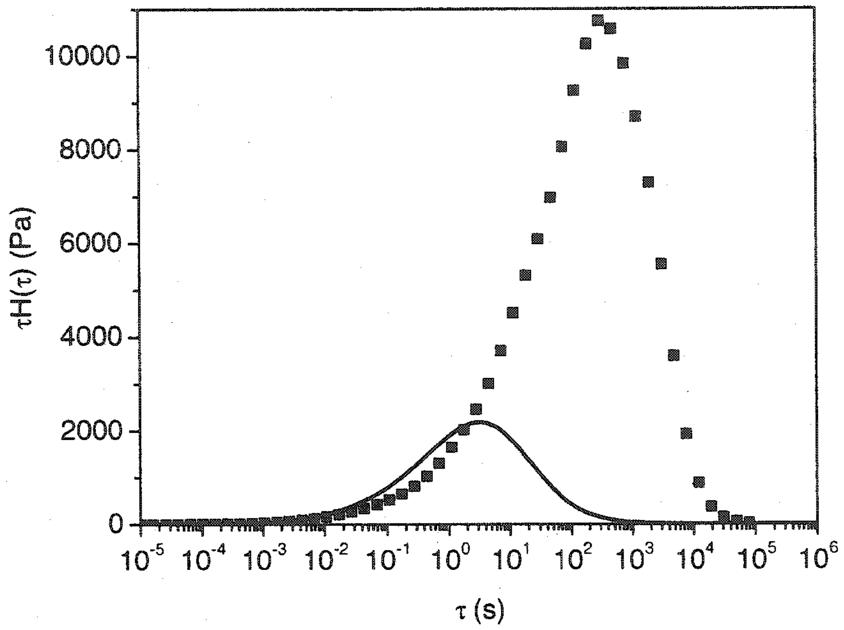

Figure 5-12: Time weighted relaxation spectrum of 35B3 at 180 °C from experimental data (symbols) and of $(35B3)_{LE}$ from predicted data (solid line)

Figures 5.10 to 5.12 show more clearly the differences in relaxation behavior between a branched sample and its linear equivalent. For low levels of branching, at short times, both the branched sample and its linear equivalent have similar behavior. However, at long times the relaxation is dominated by the long-chain branched chains, and the difference between two spectra becomes quite large. With increasing the level of branching, the contribution of the branched chains increases dramatically.

The molecular weight distributions of the MFR 35 series are shown in Fig. 5.13. With increasing level of long-chain branching, from 35L to 35B3, the fraction of high molecular weight species and the weight average molecular weight M_w increase.

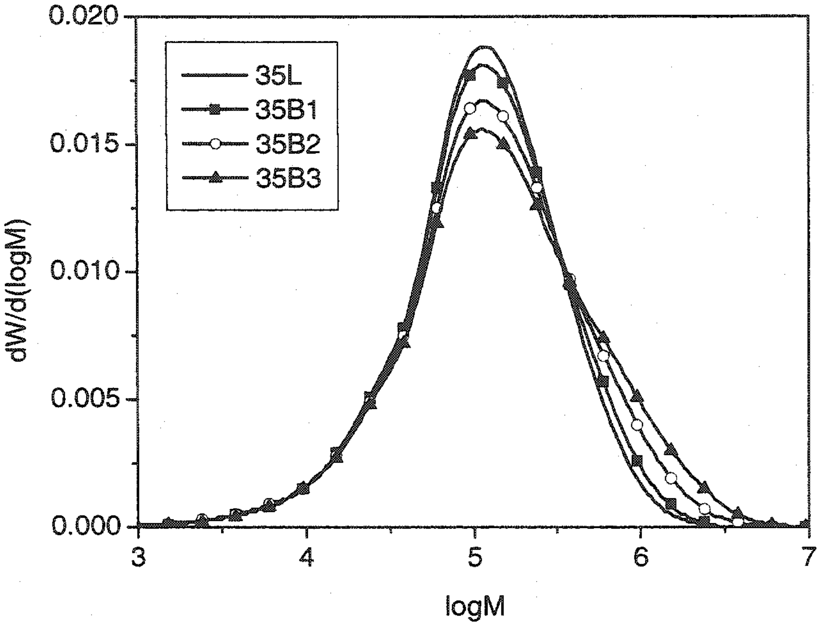

Figure 5-13: Molecular weight distribution of the MFR 35 based series

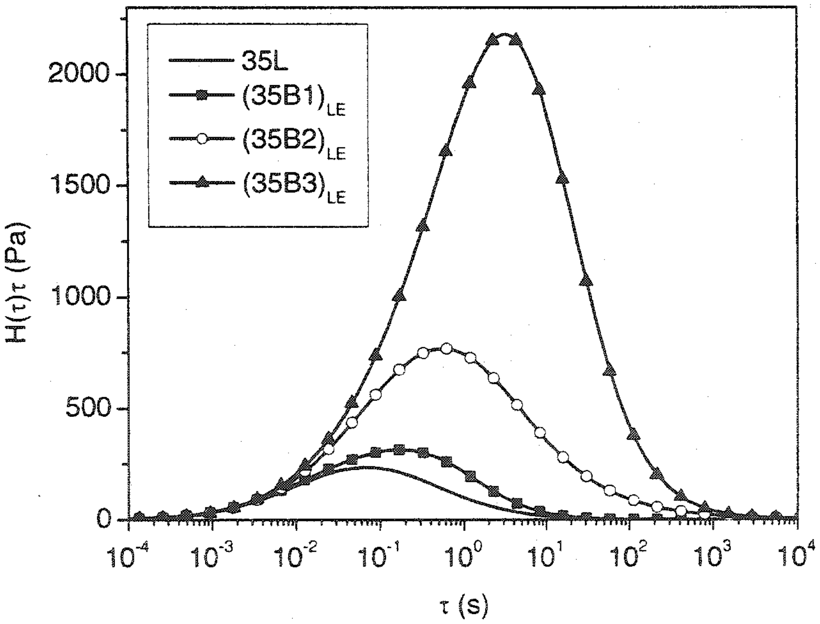

Figure 5-14: Relaxation spectra from predictions for 35L and three linear equivalents. The linear equivalents have the MWD of the corresponding branched sample shown in Fig. 5.13

The predicted relaxation spectrum of 35L is compared with data for the three linear equivalents in Fig. 5.14. In advancing from 35L to (35B3)$_{LE}$, the peak, which is related to M_w, shifts to longer times, and the area under the curve, which is the zero-shear viscosity, increases.

5.5. Predictions for the MFR 2 Set

5.5.1. Predicted Complex Moduli and Discussion

The MFR 2 set consists of one linear sample, 2L, and four branched ones. The linear sample has a polydispersity index of 6.2. Corresponding to the four branched samples are four linear equivalents, named (2B1)$_{LE}$, (2B2)$_{LE}$, (2B3)$_{LE}$, and (2B4)$_{LE}$. The simulations were performed for the linear sample 2L and the four linear equivalents with the determined parameters τ_e and G_N^0 from sample 35L. The predicted complex moduli are shown in Figs. 5.15 to 5.19.

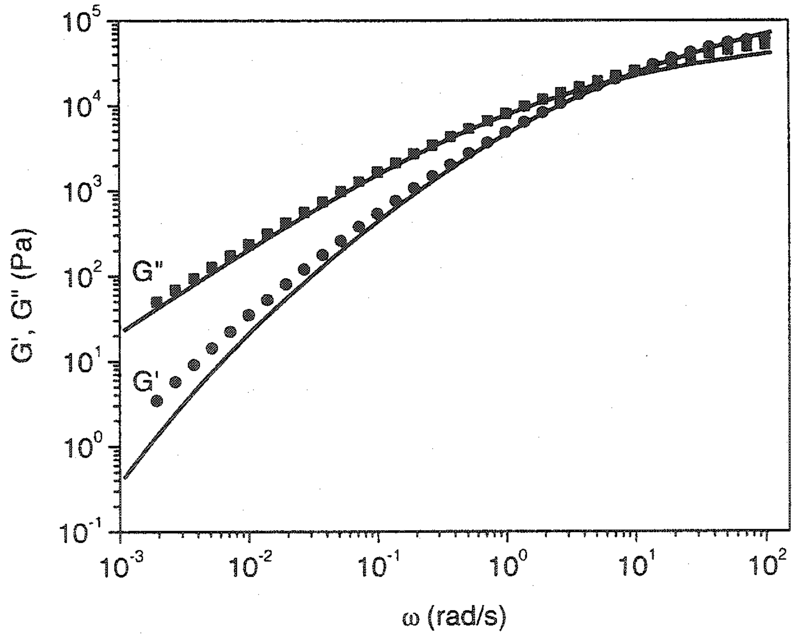

Figure 5-15: Comparison of the dual constraint model predictions of storage and loss moduli (solid line) with experimental data (symbols) of 2L at 180 °C

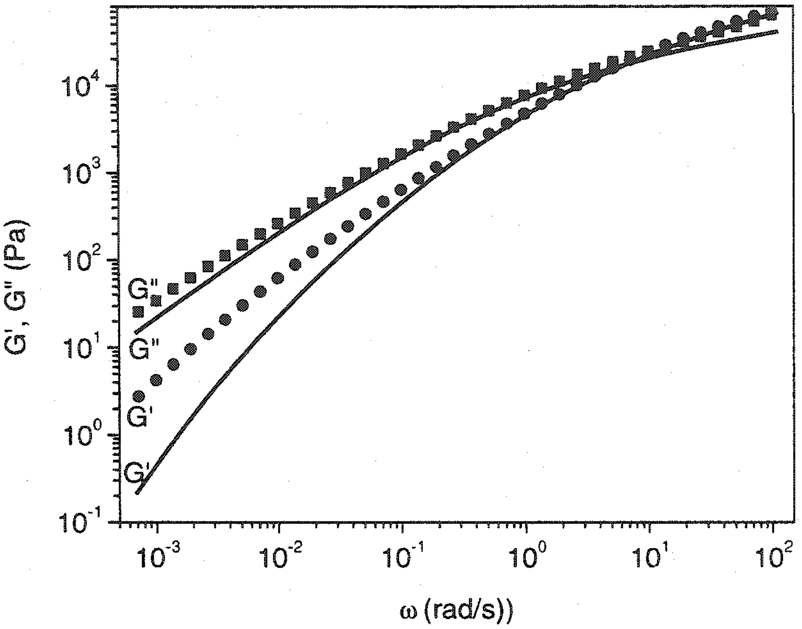

Figure 5-16: Comparison of the dual constraint model predictions of $(2B1)_{LE}$ (solid line) with experimental data of 2B1 (symbols) at 180 °C

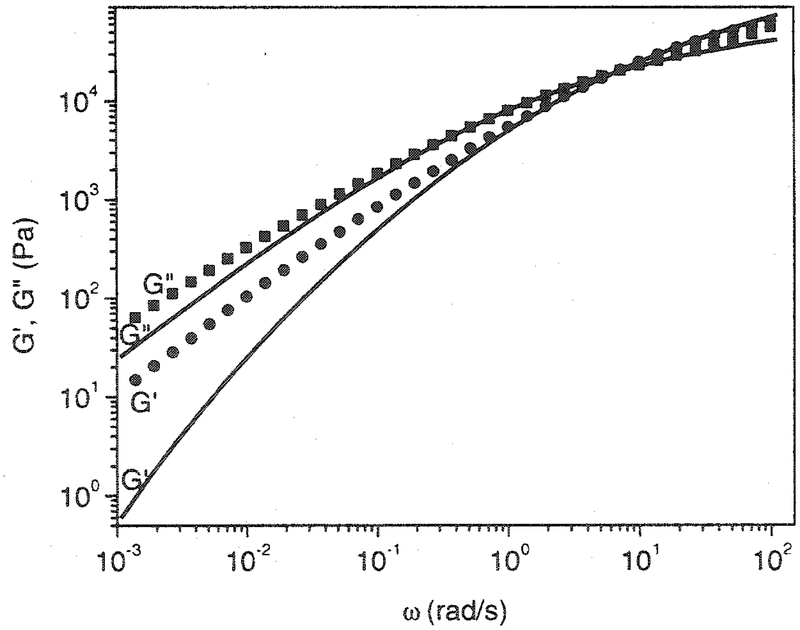

Figure 5-17: Comparison of the dual constraint model predictions of $(2B2)_{LE}$ (solid line) with experimental data of 2B2 (symbols) at 180 °C

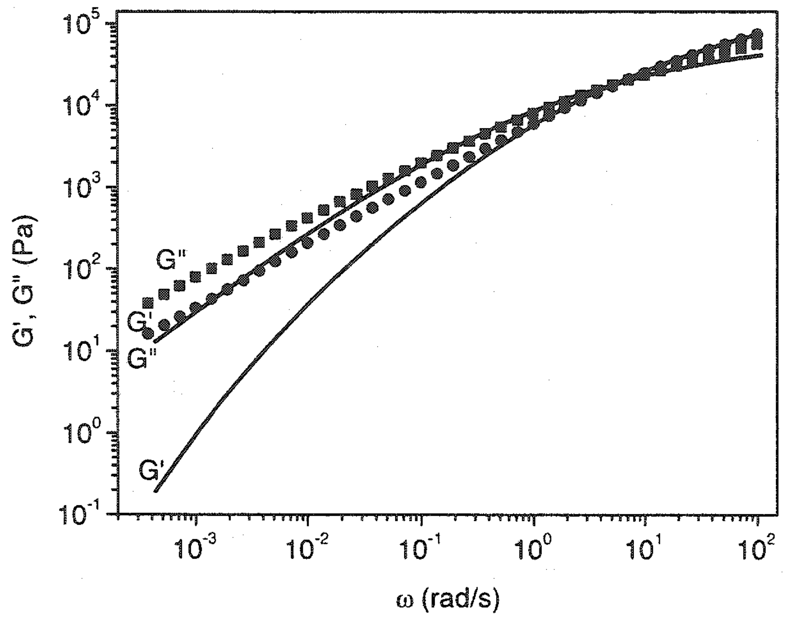

Figure 5-18: Comparison of the dual constraint model predictions of $(2B3)_{LE}$ (solid line) with experimental data of 2B3(symbols) at 180 °C

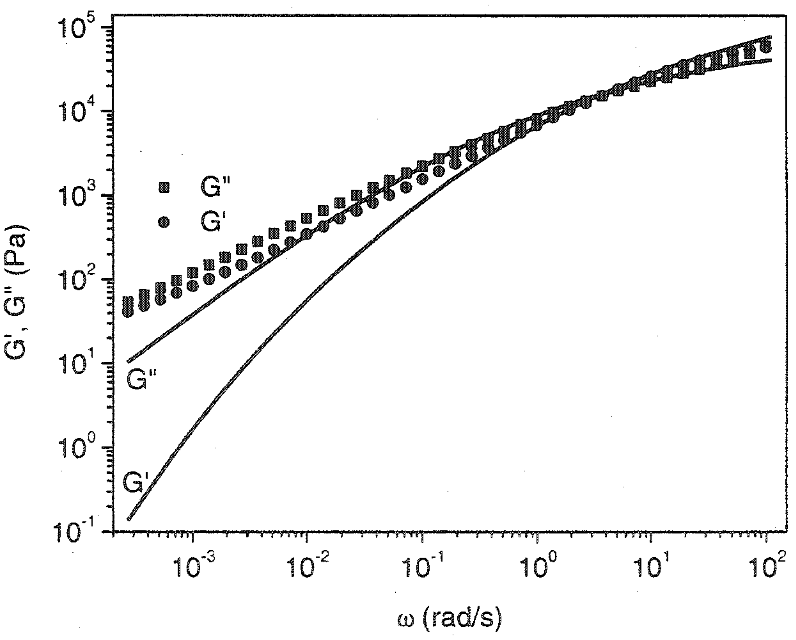

Figure 5-19: Comparison of the dual constraint model predictions of $(2B4)_{LE}$ (solid line) with experimental data of 2B4 (symbols) at 180 °C

The parameters τ_e and G_N^0 are the characteristic properties of a polymer at the same temperature. However, low performance of the prediction for linear sample 2L with the determined parameters τ_e and G_N^0 is observed. This may be because the model cannot predict the LVE of polymers having such broad molecular weight distributions.

From Fig. 5.15 we see that the model is able to predict both the storage and loss moduli at intermediate frequencies ($\omega = 0.1$-10 rad/s) quite well at the price of sacrificing the predictions at high and low frequencies. It can be seen in Figs. 5.16 to 5.19 that the branched sample has a much broader transition to the terminal zone and much slower relaxation than its linear equivalent. With increasing level of long-chain branching the differences in relaxation behavior at low frequencies between the branched sample and its linear equivalent become more pronounced.

5.5.2. Transformation of Moduli to Time-Weighted Relaxation Spectrum

The predicted complex moduli were transformed to time-weighted relaxation spectra using the NLREG[27] technique. The spectra are compared with those from the experimental data in Figs. 5.20 to 5.24. In Fig. 5.20 we see that for 2L the predicted spectrum agrees with the data at time region up to 10 s. However, there are large differences at long relaxation times. This model takes into account the dynamic dilution effect by using an effective energy for late time retraction. For a very polydisperse polymer such as 2L, which has $M_w/M_n = 6.2$, this may overestimate the dynamic dilution effect and be responsible for the differences in the two spectra.

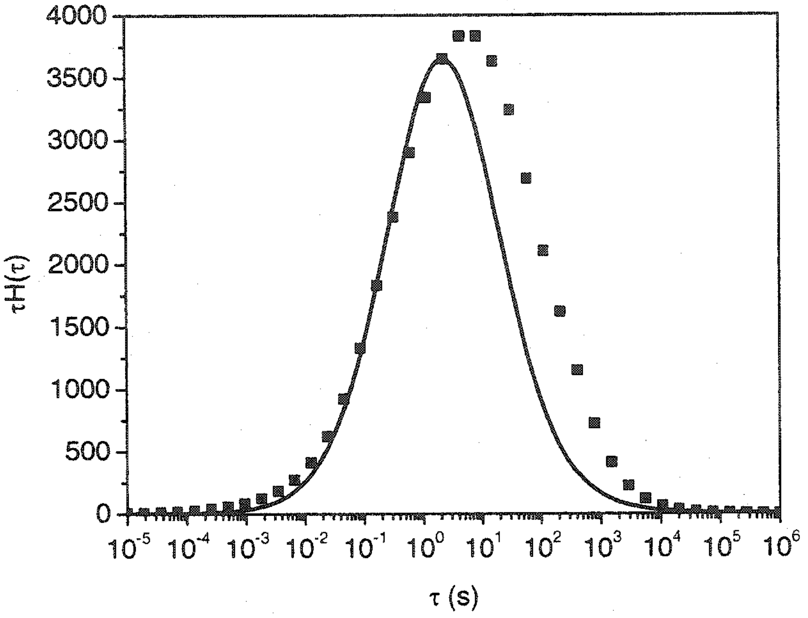

Figure 5-20: Time weighted relaxation spectrum of 2L at 180 °C from experimental data (symbols) and from predicted data using the dual constraint model (solid line)

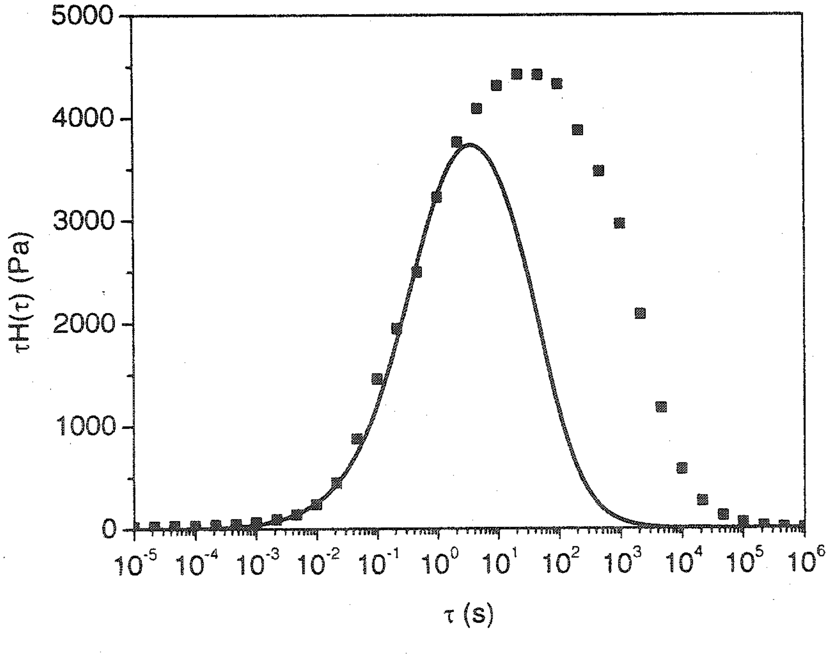

Figure 5-21: Time weighted relaxation spectrum of 2B1 at 180 °C from experimental data (symbols) and of $(2B1)_{LE}$ from predicted data (solid line)

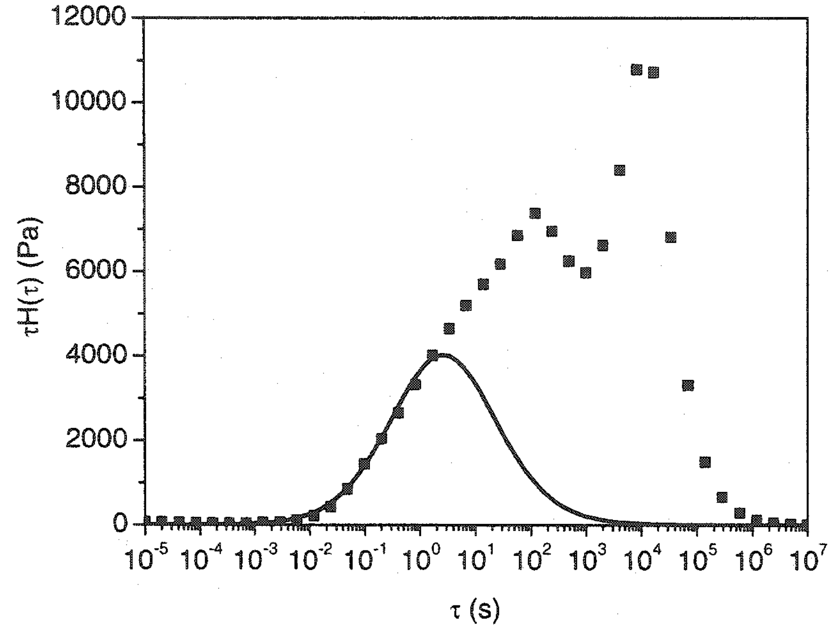

Figure 5-22: Time weighted relaxation spectrum of 2B2 at 180 °C from experimental data (symbols) and of $(2B2)_{LE}$ from predicted data (solid line)

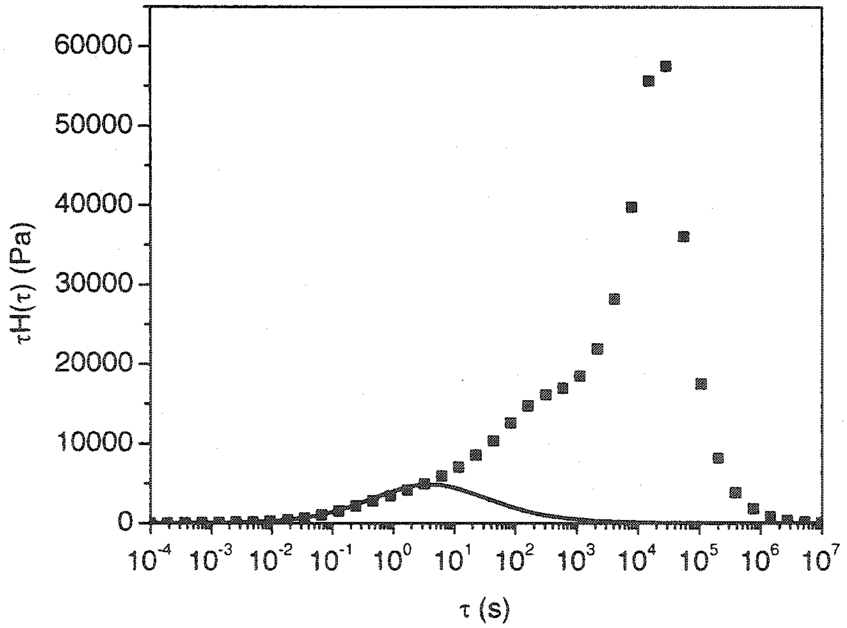

Figure 5-23: Time weighted relaxation spectrum of 2B3 at 180 °C from experimental data (symbols) and of $(2B3)_{LE}$ from predicted data (solid line)

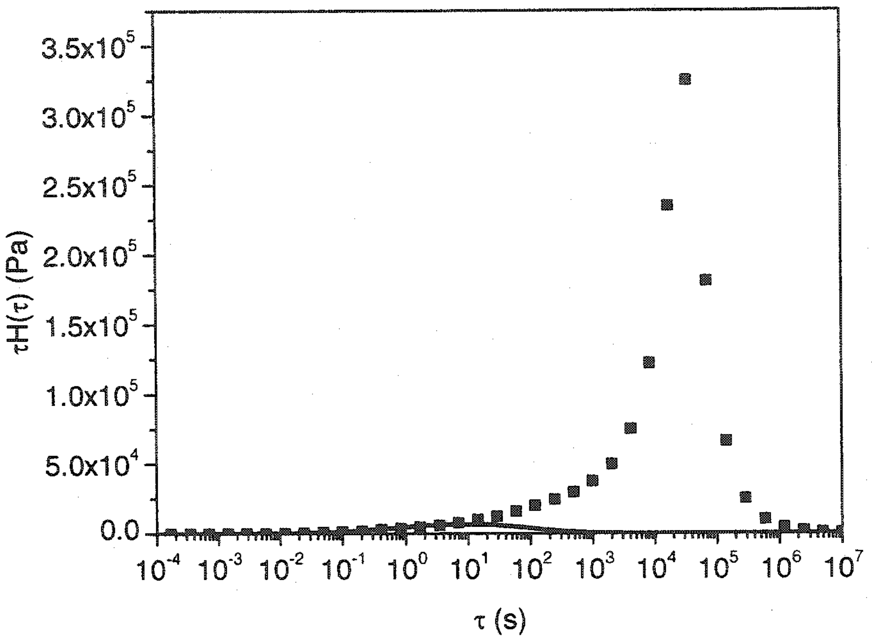

Figure 5-24: Time weighted relaxation spectrum of 2B4 at 180 °C from experimental data (symbols) and of $(2B4)_{LE}$ from predicted data (solid line)

Although 2B1 and $(2B1)_{LE}$ have exactly the same molecular weight distribution, even for this slightly branched sample, the differences in relaxation behavior at long time are very large, where the relaxation is dominated by the branched chains.

In Figs. 5.22 to 5.23 we see that the branched samples have multiple peaks, while their linear equivalents have only one peak. In Fig. 5.24, the first peak is smoothed out because of the very big magnitude of the second peak. The peak moves to a much longer time compared with that of its linear equivalent. The zero-shear viscosity, which is the area under the curve, is much higher for the branched samples. Particularly in the case of 2B4 and $(2B4)_{LE}$, the relaxation spectrum and the zero-shear viscosity of $(2B4)_{LE}$ are much smaller as shown in Fig. 5.24.

Molecular weight distributions for the MFR 2 series are shown in Fig. 5.25. Due to the small amount of long chain branching, the differences between the molecular weight distributions are very small. Samples 2L, 2B1 and 2B2 have almost the same molecular weight distributions. Slightly larger fractions are shown in the high molecular weight tail for 2B3 and 2B4.

The predicted relaxation spectra of 2L and the four linear equivalents are shown in Fig. 5.26. The small differences in the molecular weight distributions of $(2B3)_{LE}$ and $(2B4)_{LE}$ compared with that of 2L have a significant effect on the relaxation spectrum. The zero-shear viscosities of $(2B3)_{LE}$ and $(2B4)_{LE}$ are much higher than that of 2L.

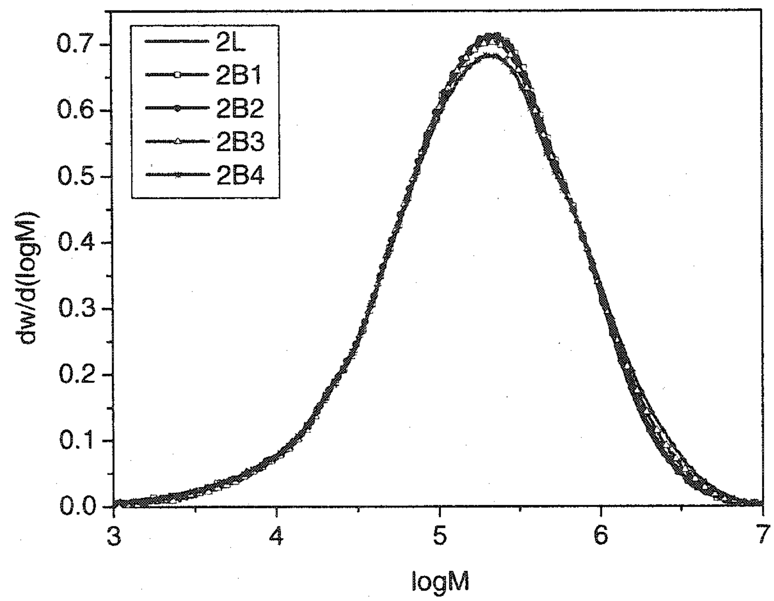

Figure 5-25: Molecular weight distribution of the MFR 2 based series. The linear equivalents have the same MWD as the respective branched samples

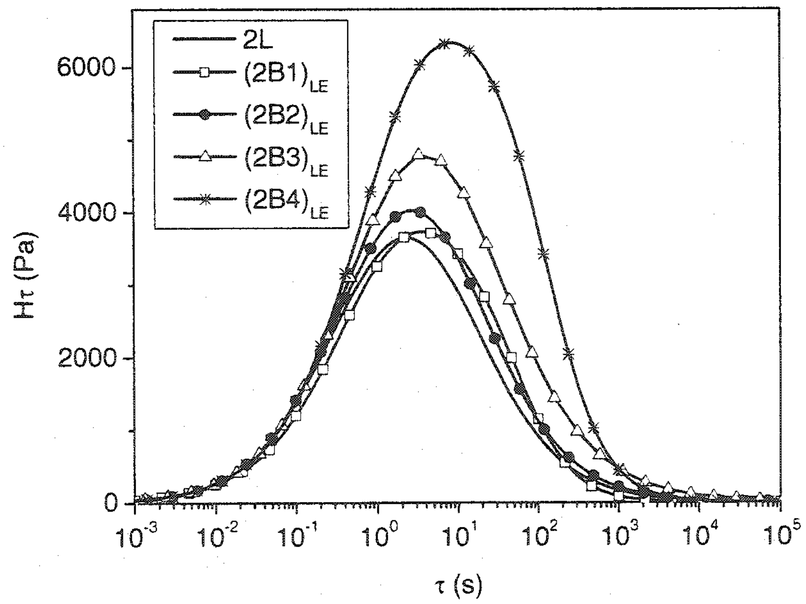

Figure 5-26: Relaxation spectra from predictions for 2L and four linear equivalents

5.6. Conclusions

The dual constraint model[14] gives good predictions of complex moduli for 35L with $M_w/M_n = 3.6$ using values of M_e and G_N^0 from the literature. For broader MWD polypropylene, 2L, with $M_w/M_n = 6.2$, the performance of the model is poor.

By modeling the complex moduli of the linear equivalents and comparing the relaxation spectrum of the branched sample to that of its linear equivalent, we see clearly differences due to the branched molecules. By comparing the predicted relaxation spectrum of 35L with data for the three linear equivalents, we see the role of molecular weight. In advancing from 35L to $(35B3)_{LE}$, the peak, which is related to M_w, shifts to longer times, and the area under the curve, which is the zero-shear viscosity, increases.

References

---

[1] De Gennes, P.G., "Reptation Of A Polymer Chain in The Presence of Fixed Obstacles", J. Chem. Phys. 55, 572-579, 1971

[2] Doi, M., S.F. Edwards, "The Theory of Polymer Dynamics", Oxford, 1986

[3] De Gennes, P. G., "Possible Moessbauer or Neutron Experiments on Fluid Interfaces and Smectics", Journal de Physique (Paris), 36, 603-606, 1975

[4] Montfort, J.P., G. Marin, P. Monge, "Effects of Constraint Release on the Dynamics of Entangled Linear Polymer Melts", Macromolecules, 17, 1551-1560, 1984

[5] Rubinstein, M., R. H. Colby, " Self-Consistent Theory of Polydisperse Entangled Polymers: Linear Viscoelasticity of Binary Blends", J. Chem. Phys., 89, 5291-5306, 1988

[6] Likhtman, A.E., T.C.B. McLeish, "Quantitative Theory for Linear Dynamics of Linear Entangled Polymers", Macromolecules, 35, 6332-6343, 2002

---

[7] Doi, M., "Explanation for the 3.4 Power Law of Viscosity of Polymeric Liquids on the Basis of the Tube Model", J. Polym. Sci., Polym. Lett. Ed., 19, 265-273, 1981

[8] Milner, S. T., T. C. B. McLeish, "Reptation and Contour-Length Fluctuations in Melts of Linear Polymers", Phys. Rev. Lett., 81, 725-728, 1998

[9] Viovy, J.L., "Tube Relaxation: A Quantitative Molecular Model for the Viscoelastic Plateau of Entangled Polymeric Media", J.Polym. Sci., Polym. Phys. Ed. 23, 2423-2442, 1985

[10] Marrucci, G., "Relaxation by Reptation and Tube Enlargement: A Model for Polydisperse Polymers", J. Polym. Sci., Polym. Phys. Ed. 23, 159-177, 1985

[11] Montfort, J.P., G. Marin, P. Monge, "Molecular Weight Distribution Dependence of the Viscoelastic Properties of Linear Polymers: The Coupling of Reptation and Tube-Renewal Effects", Macromolecules, 19, 1979, 1986

[12] Doi, M., W.W. Graessley, E. Helfand, D.S. Pearson, "Dynamics of Polymers in Polydisperse Melts", Macromolecules, 20, 1900-1906, 1987

[13] Mead, D.W., T.J. Van Dyke, R.G. Larson, M. Doi, Private communication, 1997

[14] Pattamaprom C., R.G. Larson, T.J. Van Dyke, "Quantitative Predictions of Linear Viscoelastic Rheological Properties of Entangled Polymers", Rheol. Acta, 39, 517-531, 2000

[15] Des Cloizeaux, J., "Double Reptation vs. Simple Reptation in Polymer Melts", Polym. Sci. Phys. Ed. 5, 437-442,1988

[16] Tsenoglou, C., "Molecular Weight Polydispersity Effects on the Viscoelasticity of Entangled Linear Polymers", Macromolecules, 24, 1761-1767, 1991

[17] Carrot, C., P. Revenu, J. Guillet, "Rheological Behavior of Degraded Polypropylene Melts: From MWD to Dynamic Moduli", J. Appl. Polym. Sci., 61, 1887-1897, 1996

---

[18] Wasserman, S.H., W.W. Graessley, "Effects of Polydispersity on Linear Viscoelasticity in Entangled Polymer Melts", J. Rheol., 36, 543-572, 1992

[19] Benallal, A., G. Marin, J. P. Montfort, C. Derail, "Linear Viscoelasticity Revisited: The Relaxation Function of Monodisperse Polymer Melts", Macromolecules, 26, 7229-7235,1993

[20] Léonardi, F., J.-C. Majeste, A. Allal, G. Marin, "Rheological Models Based on the Double Reptation Mixing Rule: The Effects of A Polydisperse Environment", J. Rheol., 44(4), 675-692, 2000

[21] Eckstein, A., J. Suhm, C. Friedrich, R.-D. Maier, J. Sassmannshausen, M. Bochmann, R. Mulhaupt, "Determination of Plateau Moduli and Entanglement Molecular Weights of Isotactic, Syndiotactic, and Atactic Polypropylenes Synthesized with Metallocene Catalysts", Macromolecules, 31, 1335-1340, 1998

[22] Ferry J. D., "Viscoelastic Properties of Polymers", New York, Wiley, 1980

[23] Majesté, J.C., "Propriétés Viscoélastiques de Polymers Linéaires à Très Large Distribution de Masses Molaires", Thèse de l'Université de Pau et des Pays de l'Adour, 1998

[24] Doi, M., S.F. Edwards, "Dynamics of Concentrated Polymer Systems", J. Chem. Soc., Farady Trans. II, 74, 1789-1832, 1978

[25] Graessley, W.W., "Entangled Linear, Branched and Network Polymer Systems-Molecular Theories", Adv. Polym. Sci., 47, 67-117,1982

[26] Cassagnau, Ph., J. P. Montfort, G. Marin, Ph. Monge, "Rheology of Polydisperse Polymers: Relationship Between Intermolecular Interactions and Molecular Weight Distribution", Rheol. Acta, 32, 156-167, 1993

[27] Honerkamp, J., J. Weese, " A Nonlinear Regularization Method for The Calculation of Relaxation Spectra", Rheol. Acta, 32, 65-73, 1993

Chapter 6. Modeling of Polypropylene Branching Process

6.1. Introduction

In the polymer industry, continuous efforts are made to design polymers having both good end-use properties and good processability, and molecular structure determines the melt flow behavior and final properties of a polymer. The objective of applied polymer science is to understand the relationships between structure and properties, so that the structure can be optimized to yield good processability without sacrificing solid-state properties. Therefore, the determination of polymer structure is of a great importance in both polymer science and industrial polymer development.

The structure of a linear homopolymer is described by its molecular weight distribution, which can be determined using gel permeation chromatography (GPC). From the molecular weight distribution, one can calculate the weight average molecular weight, M_w, which is related to the zero-shear viscosity, and the polydispersity index, M_w/M_n, which is related to the degree of shear thinning.

In order to fully describe the structure of a branched polymer, in addition to the overall molecular weight distribution one must have information about the branching, such as the branching density, architecture and several distributions. While the molecular weight distribution of a branched polymer can be measured using GPC with a light scattering detector, analytical techniques to measure branching characteristics are very limited.

For long-chain branched (LCB) metallocene polyethylenes (mPE), the average branch points per 1000 carbon (λ) can be measured by ^{13}C nuclear magnetic resonance (NMR). Costeux *et al.* [1] pointed out that for a long-chain branched mPE produced in a single reactor by a single-site catalyst , only two independent parameters are needed to describe all structural features. These two parameters can be calculated from λ and M_w.

Weng *et al.*[2] studied long-chain branched isotactic polypropylenes synthesized using a metallocene catalyst in dilute solutions of hexane or toluene. They proposed a way to measure λ using ^{13}C NMR for these polymers. Due to the small NMR signals of the carbons around the branch points, the assignments of NMR resonance were based on the comparison of the resonances with those of a model polymer (propylene/4 methyl-1-pentene copolymer); stereo structure analysis at the branch points, and chemical shift calculations of the carbons around the branch points. However, ^{13}C NMR is not applicable to polypropylenes crosslinked in a post-reactor process, because the NMR peaks corresponding to the branched structure are often very small or even missing in the spectrum, and if there are any, the assignment of the peaks is complicated by the different structures at the branching point for branched metallocene polypropylene and polypropylenes crosslinked in a post-reactor process.

In the polypropylene industry, branching is often introduced into linear polypropylene by a post-reactor process. Currently, there is no analytical technique to measure directly the branching level in these materials. It is the branching structure that has the greatest influence on the rheological behavior and thus the processability of polymer melts and is of most interest. Therefore, methods other than direct measurement are needed to determine the structure of branched polypropylenes. A popular approach is the numerical simulation of the branching reaction.

6.2. Review of Modeling of Structure in Branched Polymers

The Monte Carlo (MC) algorithm is a technique based on the use of random numbers and probability statistics to investigate stochastic processes. It is widely used in polymer science to predict molecular structure and is especially useful in the numerical solution of reaction kinetics equations when a direct solution is not possible. Many studies of the structure of long-chain branched metallocene polyethylenes using the MC technique have been reported in the literature. Soares and Hamielec[3] analyzed the branching of a mPE using four kinetics equations:

$$P_r + M_0 \xrightarrow{k_p} P_{r+1} \tag{6.1}$$

$$P_r + \overset{=}{D}_y \xrightarrow{k_{LCB}} P_{r+y} \tag{6.2}$$

$$P_r + CTA \xrightarrow{k_{CTA}} D_r^+ \tag{6.3}$$

$$P_r \xrightarrow{k_\beta} \overset{=}{D}_r + P_1 \tag{6.4}$$

where M_0 represents a monomer, P_r is a living chain of polymerization degree r with active catalyst attached at one end, D^+ is a saturated dead chain, and $\overset{=}{D}$ is a vinyl-terminated dead chain, which can be connected to a backbone as a branch. Equation 6.4 describes the β-hydride elimination process that produces unsaturated chains. *CTA* is a chain transfer agent. From the above kinetics equations we see that the propagation (Eq. 6.1) and the branching (Eq. 6.2) reactions are competitive, and long-chain branches are formed in the same reactor as the linear chains. The analysis of Soares and Hamielec gives the molecular weight distribution of the whole system, the average number of branches per molecule, and the fractions of molecules having various numbers of branch points. They found that all types of segment, linear chains (both ends free), free arms (one end free and the other attached to a branch point), and inner backbones (both ends attached to branch points), have identical Flory molecular weight distributions with a polydispersity index M_w/M_n of 2. They also used the Monte Carlo method to predict the molecular structure. In the simulation, molecules were built up monomer by monomer until there were a sufficient number of molecules to show the structural distributions. The results from MC simulations agreed very well with analytical solutions. Read and McLeish[4] used Eqs. 6.1-6.4 to classify segments according to seniority and priority. Seniority is related to the distance of a segment from a free end, and priority is related to the number of paths leading from a segment to a free end. They showed that the rheological properties of branched mPE are closely related to the distributions of seniority and priority of segments.

Regardless of its architecture, a branched chain can always be decomposed into three types of segment: linear, free arms and inner backbones. Recently Costeux *et al.* [1] used a modified MC method that significantly accelerates the computation of the structure of LCB mPE. Instead of building up chains monomer-by-monomer, they added segments according to the appropriate distribution to complete a chain. For example, if the number distribution of segments is assumed to follow the most probable distribution, one knows immediately that:

$$N_p(r) = \frac{1}{\overline{P}_{np}} \exp\left(\frac{r}{\overline{P}_{np}}\right) \tag{6.5}$$

where $\overline{P}_{np}$ is the number average length of segments. For a randomly generated number, a, which follows the number distribution of segments, $N_p(r)$, the corresponding segment length can be determined:

$$r = \mathrm{int}\left[\overline{P}_{np} \ln\left(a\overline{P}_{np}\right)\right] \tag{6.6}$$

They represented the structure of branched metallocene polyethylenes by means of a ternary diagram showing composition in terms of the fractions of the three types of segment. This diagram is shown in Fig. 6.1. Each type of segment makes its own contribution to rheological behavior. For example, the inner backbones are responsible for strain-hardening, and the free arms cause an increase in the zero-shear viscosity. By locating a polymer system on this ternary diagram, one can immediately determine the fraction of each type of segment in the polymer and thus has a general picture of its rheological behavior.

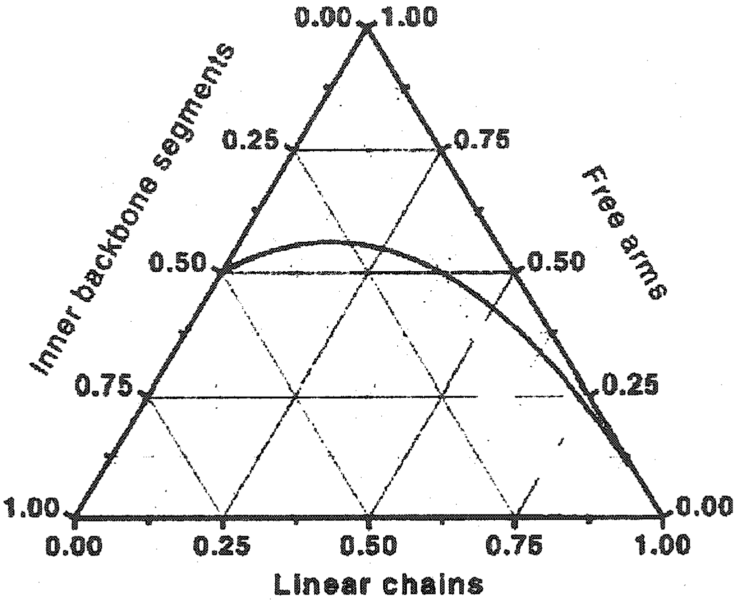

Figure 6-1: Ternary diagram representation of topology of LCB mPE[1]

In the studies mentioned above, Monte Carlo simulations were used to investigate structure by building up molecules to represent the polymer system. The random sampling technique proposed by Tobita[5] examines the problem from another point of view. Assuming there already exists a large number of polymer chains (a "sea" of chains), the technique randomly samples polymer chains selected from this sea. There are two fundamental approaches to random sampling: number-based sampling and weight-based sampling. In number-based sampling one selects a chain by randomly selecting a chain end from the sea of chains. In this sampling technique, all the chains have the same probability of being selected regardless of its size. In weight-based sampling one supposes that all the monomer units form a monomer sea. A monomer unit is selected at random from the sea, and the chain containing this particular monomer unit is identified. In weight-based sampling, all monomer units have the same probability of being selected. Therefore, the longer the molecule chain, the higher the probability of being selected. In the case of linear polymers, the number or weight chain length distribution can be obtained depending on whether number or weight-based sampling is used. In the case of nonlinear polymers, combining random sampling with the Monte Carlo method provides a powerful technique to simulate the branching process and predict the structure of a polymer.

Tobita[6] used the random sampling technique to obtain analytical solutions of molecular weight distributions for various types of nonlinear polymerization. In the case of random crosslinking, he obtained an analytical solution for the weight-average chain length ($\overline{P}_w$) for a gel-free system. In random crosslinking the branch point can be anywhere on the chain rather than at the chain end as in the case of LCB mPE. One example of the structure of the crosslinked molecule is shown in Fig. 6.2.

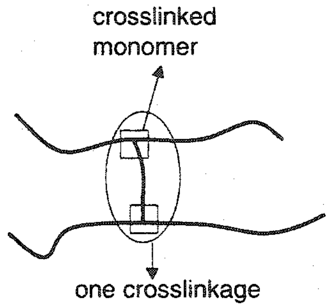

Figure 6-2: Sketch of structure of a crosslinked molecule

The weight average chain length $\overline{P}_w$ is given by the following expression:

$$\overline{P}_w = \frac{\overline{P}_{wp}(1+\rho)}{1-(\overline{P}_{wp}-1)\rho} \tag{6.7}$$

where $\overline{P}_{wp}$ is the weight average chain length of the linear precursor, and ρ is the crosslinking density, defined as:

$$\rho = \frac{\text{no. of crosslinked monomers}}{\text{no. of monomers}} \tag{6.8}$$

A crosslinked monomer is a monomer bearing a branch point, so one crosslinkage contains two crosslinked monomers, as shown in Fig. 6.2.

Macosko and Miller[7] derived a generalized formula for calculating M_w and M_n of nonlinear polymers by using the recursive nature of the branching process and probability law. They arrived at a formula for the weight-average chain length $\overline{P}_w$ that is identical to Eq. 6.7. The number-average chain length $\overline{P}_n$ is given by:

$$\overline{P}_n = \frac{\overline{P}_{np}}{1-\rho\overline{P}_{np}} \tag{6.9}$$

where, $\overline{P}_{np}$ is the number-average chain length of the linear precursor.

Tobita[8] calculated the molecular weight distribution of randomly crosslinked polymers using the MC technique. The crosslinking process is random in the sense that the probability of branching is the same for all monomer units, so the weight-based sampling technique was used. The MWD of the linear precursor had the Schulz-Zimm distribution, which is given by Eq. 6.10.

$$W(r) = \frac{\vartheta^{\vartheta}}{\overline{P}_{np}\Gamma(\vartheta)}\left(\frac{r}{\overline{P}_{np}}\right)^{\vartheta}\exp\left(\frac{-\vartheta r}{\overline{P}_{np}}\right) \tag{6.10}$$

where r is the chain length, and ϑ is a parameter governing the narrowness of the distribution,

$$\vartheta = \frac{\overline{P}_{np}}{\overline{P}_{np}-\overline{P}_{wp}} \tag{6.11}$$

Tobita found that the overall molecular weight distribution of the branched polymer had multiple peaks when the polydispersity index of the precursor chain was less than about 1.1.

In another study, Tobita[9] calculated molecular weight distributions of randomly crosslinked polymers in more detail again using the MC technique. The precursor chains again had the Schulz-Zimm distribution. This time he simulated branched systems based on linear precursors having ϑ values of 200, 0.11 and 1. While ϑ = 200 represents a sharp distribution with a polydispersity index of 1.005, ϑ = 0.11 represents a broad distribution with a polydispersity index of 10.1, and ϑ = 1 corresponds to a polydispersity index of 2; in this case Eq. 6.10 reduces to the most probable distribution. For each value of ϑ, various crosslinking levels were simulated. The simulation results included the MWDs of polymer molecules containing various crosslinkages and the MWD of the whole system, which is the sum of the MWDs of species having various crosslinkages.

For random crosslinking of primary chains with the most probable molecular weight distribution (ϑ = 1), the simulated MWDs for several crosslinking densities ρ are shown in Fig. 6.3. All curves are smooth, even at the high molecular weight end.

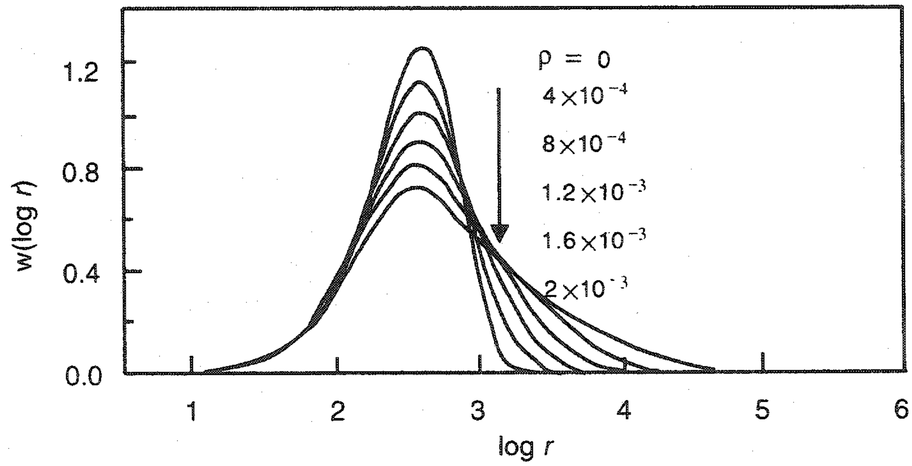

Figure 6-3: Weight fraction distribution development during random crosslinking of primary chains that conform to the most probable distribution with P_n = 200. [from ref 9]

In addition to the random crosslinking process, Tobita[10] investigated chain-length-dependent crosslinking reactions in which the number fraction distribution of the linear precursor had the most probable distribution. Chain-length-dependent crosslinking means that there is a distribution of probabilities of branching among the precursor molecules. He assumed that the rate coefficient, k_{ce}, for the crosslinking reaction was given by Eq. 6.12.

$$k_{ce} = (gh)^{-\theta} \tag{6.12}$$

where g and h are the lengths of two successive connected chains, θ is a constant that represents the degree of chain-length dependence, and $\theta = 0$ corresponds to the random crosslinking case. This relationship is shown in Fig. 6.4 where we see that the crosslinking rate coefficient for large molecules decreases with the increasing θ.

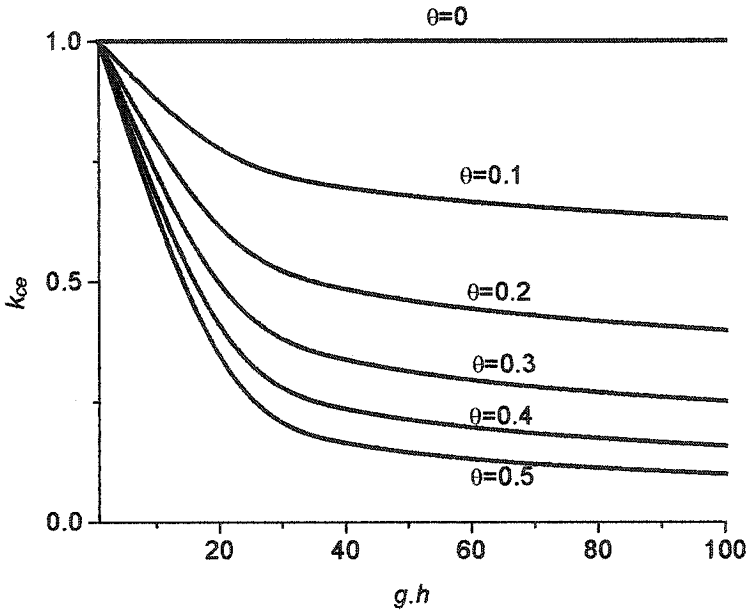

Figure 6-4: Representation of the crosslinking rate coefficient as a function of the number of primary chains (g and h) of polymer molecules that participate in the crosslinking reaction (from ref 10)

Typical simulated MWDs for a chain-length dependent crosslinking reaction with $\theta = 0.2$ at various conversions are shown in Fig. 6.5. When the crosslinking rates for large polymer molecules are reduced (compared with the random branching case) the high molecular weight tails were not smooth, but instead were distorted.

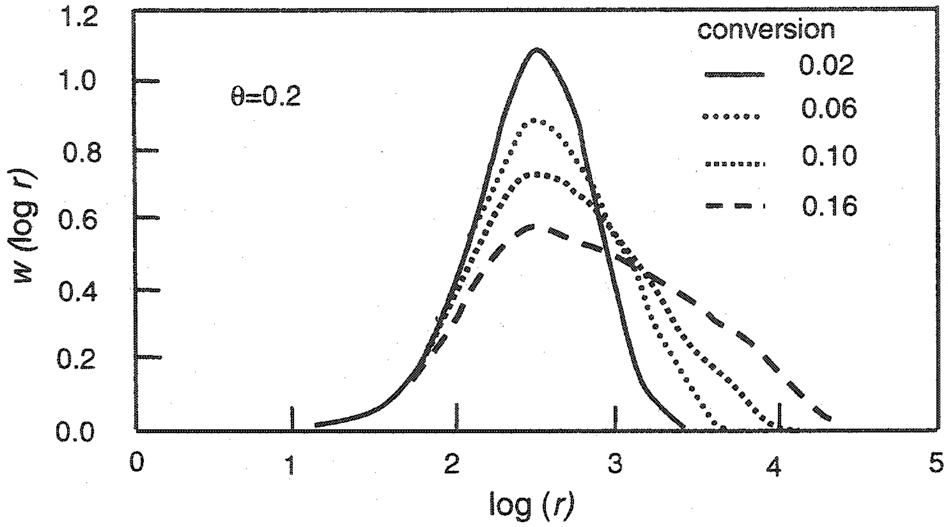

Figure 6-5: Simulated weight distributions of chain length with $\theta = 0.2$ (from ref.10)

6.3. The Monte Carlo Simulation used in This Study

To simulate the branching process of the polypropylenes considered here, we need to take into account two special aspects of the branching process. First, the primary chains were made using Ziegler-Natta catalysts, and there are no simple formulae to describe the molecular weight distributions of such polymers. This complicates the simulation, because for a given random number (corresponding to a weight/number fraction) we cannot calculate the corresponding molecular weight or chain length using a distribution formula.

Second, the branching process of the polypropylenes studied is different from that of metallocene polyethylenes. For mPE, the branching process competes with the linear chain propagation in a single reactor, so the branched and linear chains are formed in the same process. To simulate a branching process of polypropylenes with primary chains made using Ziegler-Natta catalysts, a modified MC technique was required.

In the following section, the MC technique for generating the linear precursor chains and the sampling technique for creating the branched polypropylenes are described. The MWDs of the simulated polypropylenes are presented and compared with those from GPC measurements. The number and weight fractions of molecules with various numbers of branch points are obtained from the simulation. Commonly used parameters indicating the branching level, such as β (the averaged branch points per chain) and λ (branch points per 1000 carbons) are calculated from the simulations for each branched polypropylene. Relationships between the average branching parameter and the number and weight average molecular weights are established. The branching efficiency is evaluated. Finally, the branched samples are represented in ternary diagrams in terms of segment fractions of three types to provide a general picture of their structures and rheological behavior. The probability of cyclization during the branching process is also predicted.

In addition to the two sets of samples based on linear precursors of 35 MFR and 2 MFR, there is another set of samples based on the linear precursor 12 MFR, which were insufficient in quantity for rheological characterization but for which GPC data were available. The 12 MFR set consists of one linear sample, 12L, and three samples having different levels of branching, 12B1, 12B2 and 12B3. Monte Carlo simulations were also performed to determine the structure of these samples. The characteristics of the 12 MFR samples are listed in Table 3.1.

6.4. Numerical Procedures of the Monte Carlo Simulation

6.4.1. Creation of Linear Precursor Chains

For linear chains made using Ziegler –Natta catalysts, there is no simple formula to describe the MWD; therefore, we cannot calculate directly the chain length corresponding to a random number. Instead, we determine the chain length numerically according to the GPC MWD as described below.

From the GPC measurements, we have the MWD in terms of weight fraction, *i. e.* $w(\log M)\mathrm{d}\log M$, as a function of molecular weight M. First we calculate the corresponding number fraction, $n(\log M)\mathrm{d}\log M$, using Eq. 6.13.

$$n(\log M)d\log M = \frac{[w(\log M)d\log M]\cdot M_n}{M} \qquad (6.13)$$

The cumulative number distribution, *CNM*, is then easily obtained by summing the number fractions from M_{min} to M_{max}, where M_{min} and M_{max} are the low and high limiting molecular weights respectively of the distribution. For example, for 35L, the cumulative number distribution calculated from the GPC data is shown in Fig. 6.6. By definition, the cumulative number distribution ranges from 0 to 1. Next we generate a random number in this range and determine the corresponding molecular weight according to the cumulative number fraction curve by an iterative procedure. The chain of this molecular weight is then stored in memory. A detailed explanation of this procedure is given in Appendix B. This procedure is continued until 10^6 chains have been created leading to a statistically consistent population. By creating chains in accordance with the cumulative number fraction curve, a set of linear chains having the same MWD as the GPC MWD of the linear precursor is created.

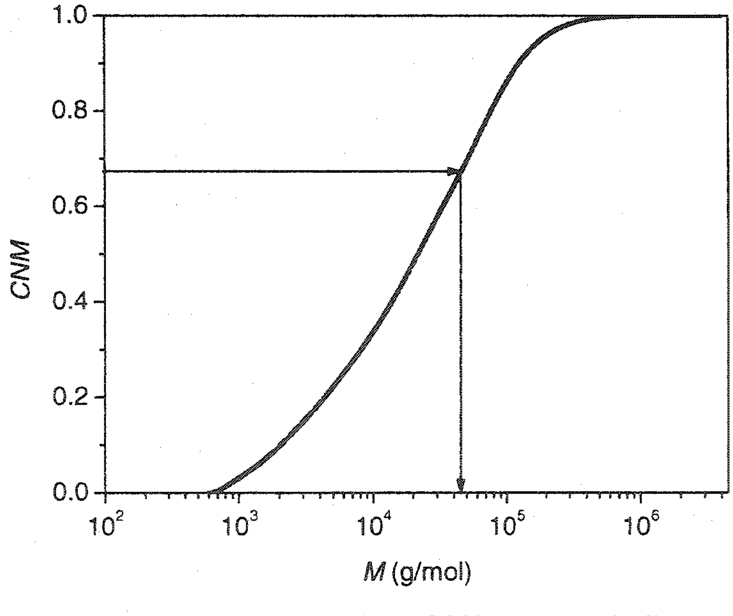

Figure 6-6: Cumulative number distribution of 35L. Arrows indicate that for a random number between 0 and 1, there is a corresponding M

6.4.2. Creation of Branched Chains

The branching of polypropylene is a very complex process. To capture the main features of the process we need to make some simplifying assumptions. First we assume, that the branching process is random. Second, we assume that some branching reactions are not complete. In the simulation, we only consider branching reactions result branch points. We use a simulation parameter α that is the branch points per precursor chain to describe the net result of the branching process. Finally, we assume the system to be perfectly mixed.

Based on these assumptions, the random sampling technique is employed to simulate the branching process. As mentioned previously there are two random sampling approaches[6], number-based random sampling, and weight-based random sampling. The molecular weight distributions of both a linear precursor and a branched system with $\alpha = 0.2$ from number-based sampling are shown in Fig. 6.7.

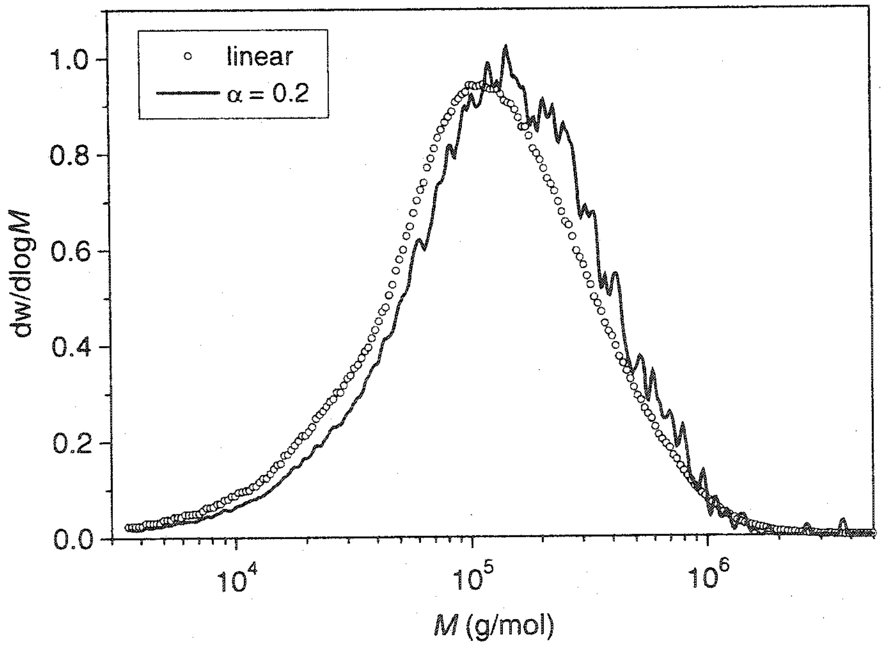

Figure 6-7: Molecular weight distributions of linear precursor chains and a branched system with $\alpha = 0.2$ and number-based random sampling

From Fig. 6.7 we see that compared to the molecular weight distribution of the linear precursor chains, the molecular weight distribution of the branched system is shifted to the right, because all of the precursor chains have the same probability of taking part in the branching reaction.

The molecular weight distributions of linear precursor chains and the branched system with $\alpha = 0.1$ from weight-based random sampling are shown in Fig. 6.8.

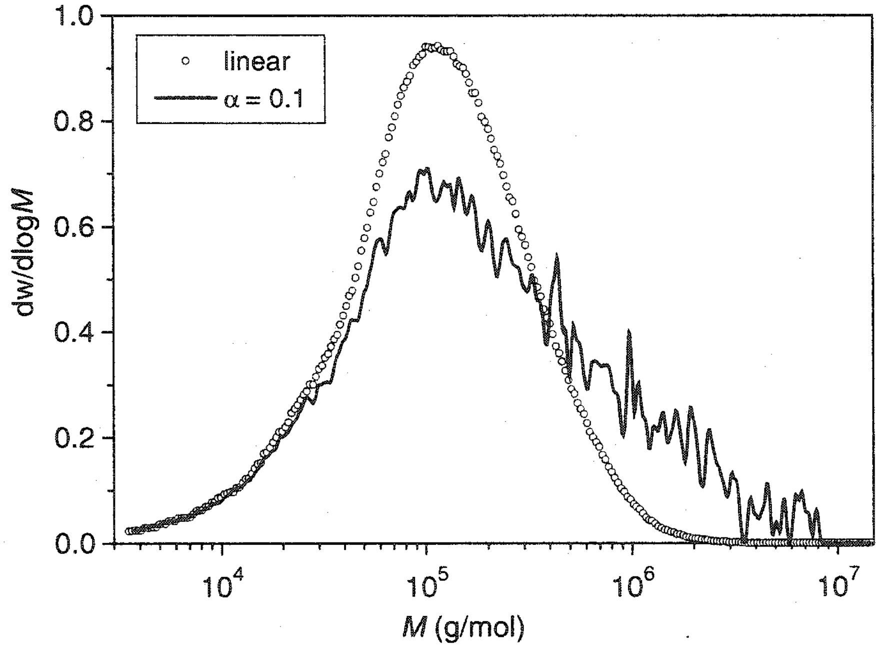

Figure 6-8: Molecular weight distributions of linear primary chains and a branched system with $\alpha = 0.1$ and weight-based random sampling

The weight fractions of small molecules are almost the same for both the linear and the branched systems, because small molecules contain few monomers, and the probability of their being selected is therefore small. Many molecules around the peak in the MWD of the linear polymer are consumed to make larger branched chains. Therefore, compared to the linear polymer, the peak is lower, and the weight fractions of chains with high molecular weights increase in the branched system.

Comparing the molecular weight distributions in Figs. 6.7-6.8 with the measured distributions shown in Fig. 6.9, we see that the actual MWD evolution with branching is similar to that predicted using weight-based random sampling. Weight –based random sampling implies the equal reactivity of all monomers, which makes sense from the point of view of the chemistry. Therefore, in this simulation, we use a weight-based random sampling technique to select the chains to form nonlinear chains for all the branched samples. The structure of the algorithms used in the MC simulation is shown in Fig. 6.10.

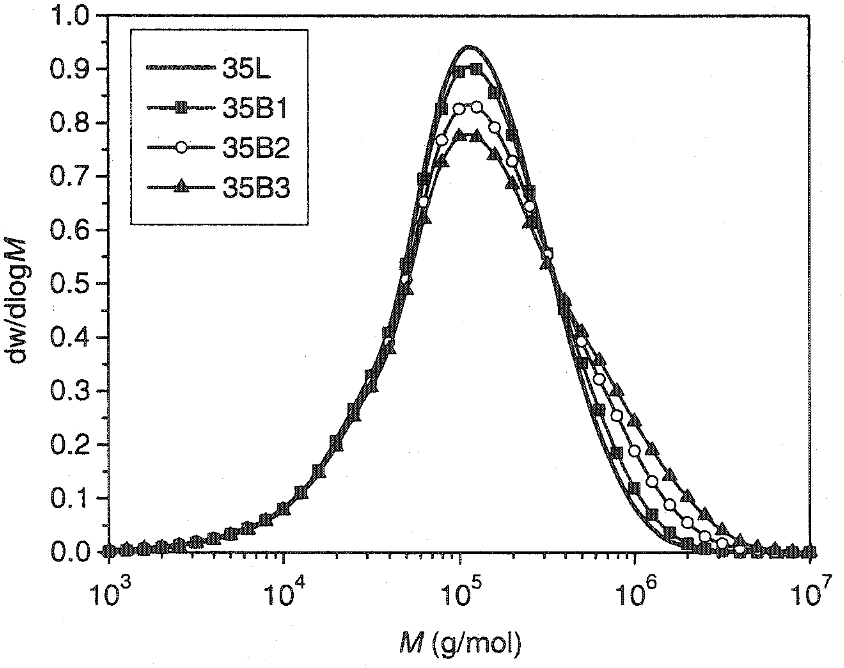

Figure 6-9: Molecular weight distribution of linear precursor 35L and three branched samples, 35B1, 35B2, 35B3, based on the same linear precursor as determined by GPC

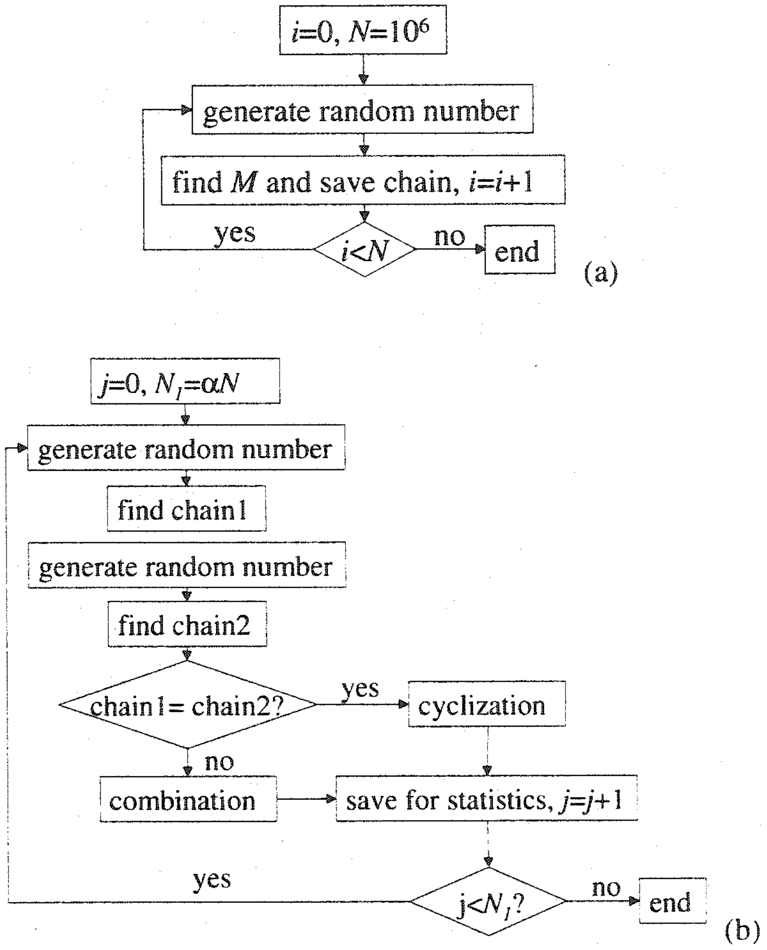

Figure 6-10: Algorithm of the Monte Carlo simulation (a) creation of linear chains; (b) creation of branched chains

6.4.3. Triple Detector Gel Permeation Chromatography

The molecular weight distributions were determined by high-temperature gel permeation chromatography (GPC) with three detectors: a refractive index detector, a viscometer, and a light scattering instrument. Detailed descriptions of the instrument and procedures are given in Section 2 of Chapter 3. Gel permeation chromatography columns separate molecules according to their size. After leaving the GPC columns, the molecules pass through the light scattering detector, which is able to measure the absolute molecular weight without the need for calibration standards. However, in the case of branched polymers, at a given size, branched molecules have higher molecular weights than linear ones, but leave the column at the same time. In spite of this uncertainty, the modeled molecular weight distributions are compared here with those determined using the light scattering detector.

6.5. Results and Discussion

6.5.1. The Molecular Weight Distributions

The simulated molecular weight distributions of the linear precursors 35L, 12L and 2L are shown in Figs. 6.11-6.13 and compared with the GPC results. The simulated molecular weight distributions fluctuate around the GPC MWDs to give very good agreement. Therefore, we conclude that the numerical technique does a good job of creating linear chains based on the GPC data. We note that this technique is able to create linear chains of any type of distribution; broad/narrow, unimodal/bimodal, as long as the GPC measurement is available. Also the distribution formula for the linear chains is not required.

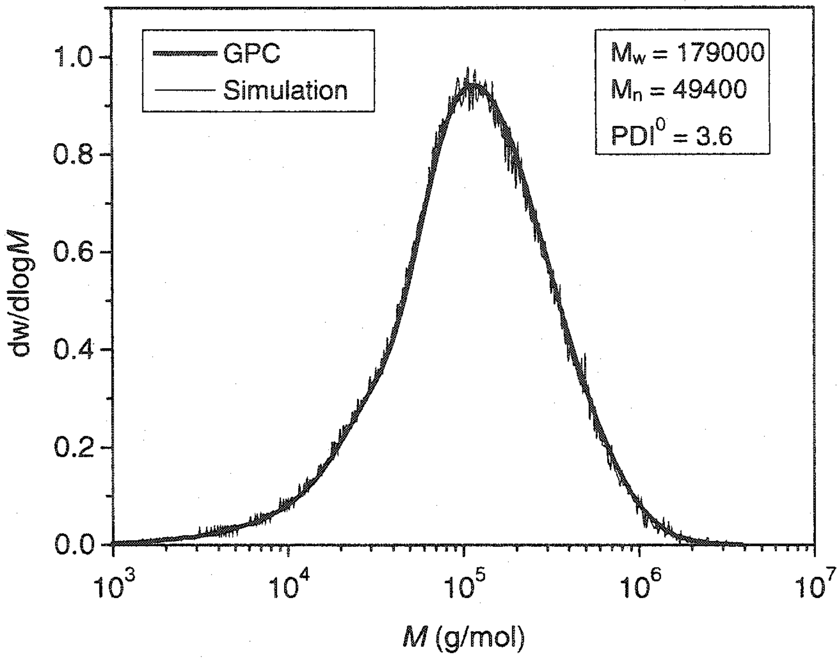

Figure 6-11: Molecular weight distribution of 35L from Monte Carlo simulation (thin line) and from GPC measurements (thick line)

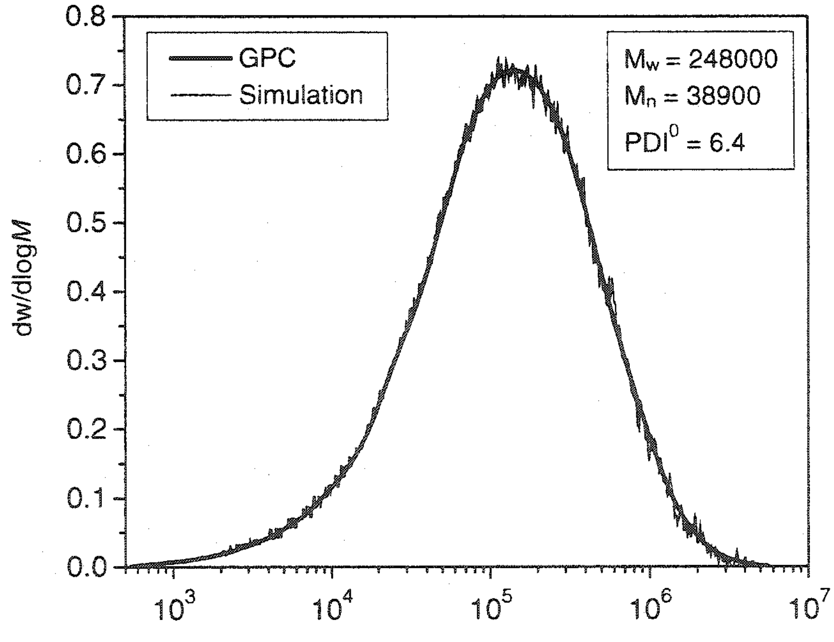

Figure 6-12: Molecular weight distribution of 12L from Monte Carlo simulation (thin line) and from GPC measurements (thick line)

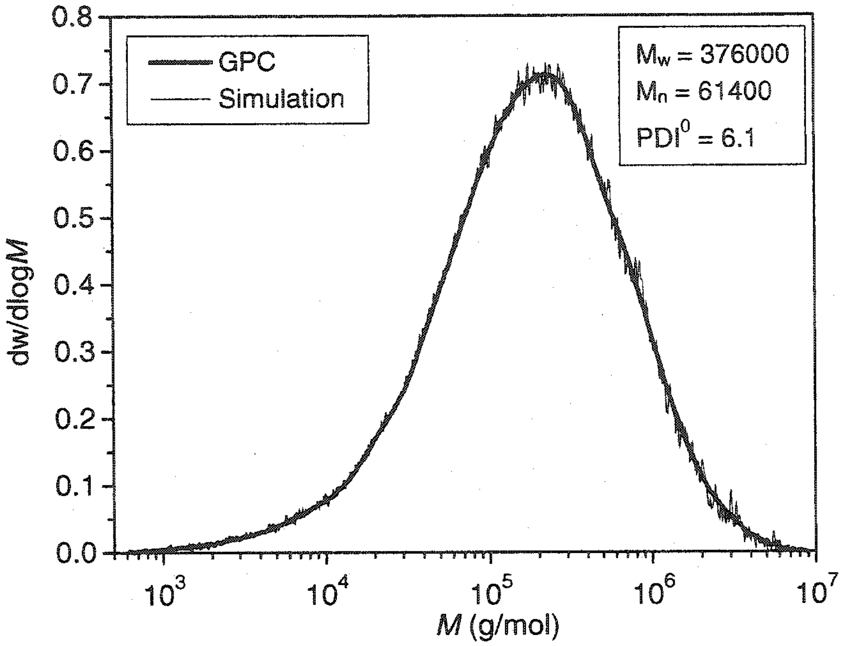

Figure 6-13: Molecular weight distribution of 2L from Monte Carlo simulation (thin line) and from GPC measurements (thick line)

Starting with the simulated linear chains, we can vary the parameter α to obtain molecular weight distributions for polypropylenes having various levels of branching. For each branched sample, we choose the α value that gave the best agreement between the simulated and actual MWD. The simulated molecular weight distributions of the branched polypropylenes are shown in Figs. 6.14-23 and compared with the corresponding GPC data. The simulated molecular weight distributions match the GPC results very well. This indicates that the assumption of random branching and the use of weight-based sampling technique are suitable for modeling the polypropylene branching process. With increasing levels of branching, α increases. Going from 35L to 35B3, the *PDI* increases from 3.6 to 5.9; from 12L to 12B3, the *PDI* ranges from 5.91 to 11.34, and from 2L to 2B4, the *PDI* ranges from 6.61 to 7.63. Therefore, for a set of branched samples based on the same linear precursor, the polydispersity index increases with the level of branching.

The simulated molecular weight distributions of linear sample 35L and the three branched samples 35B1 to B3 are shown in Fig. 6.24. By comparing with Fig. 6.9 we see that by varying only the one parameter, α, we can simulate the evolution of the molecular weight distributions of branched samples.

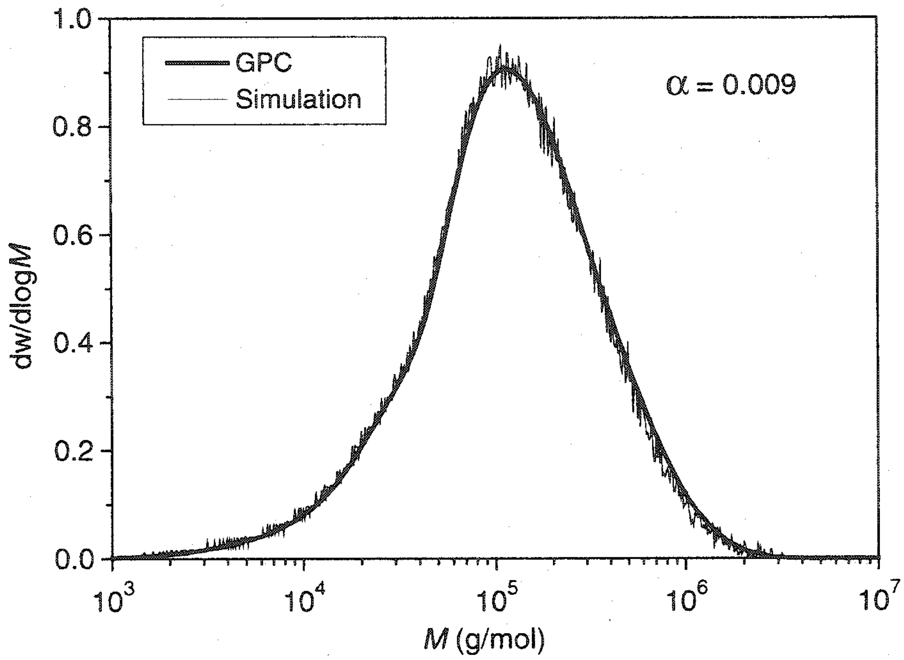

Figure 6-14: Molecular weight distribution of 35B1 from Monte Carlo simulation (thin line) and from GPC measurements (thick line)

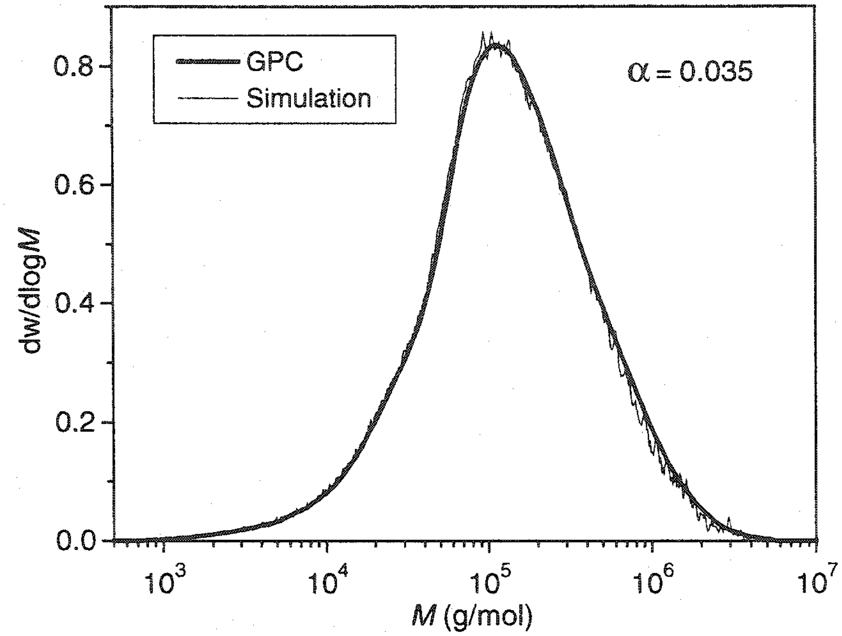

Figure 6-15: Molecular weight distribution of 35B2 from Monte Carlo simulation (thin line) and from GPC measurements (thick line)

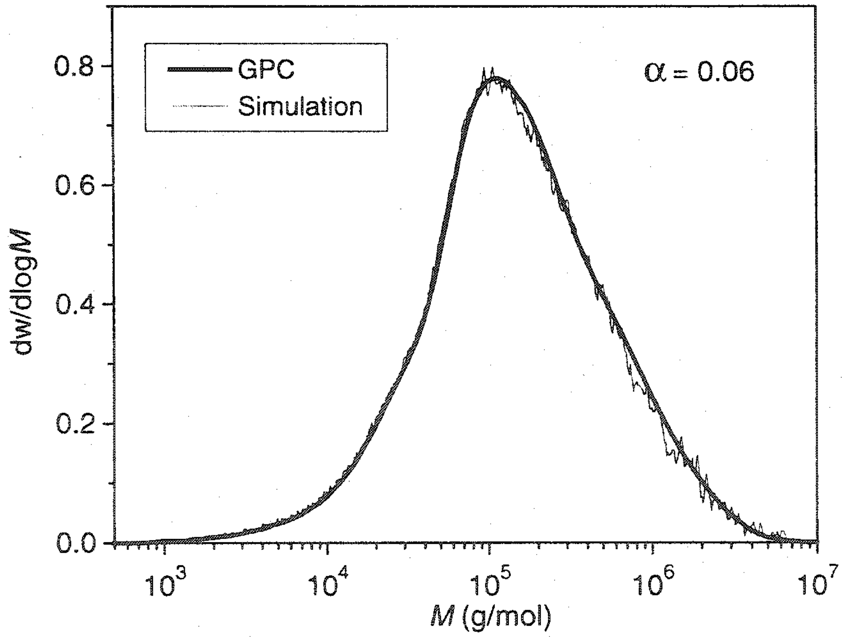

Figure 6-16: Molecular weight distribution of 35B3 from Monte Carlo simulation (thin line) and from GPC measurements (thick line)

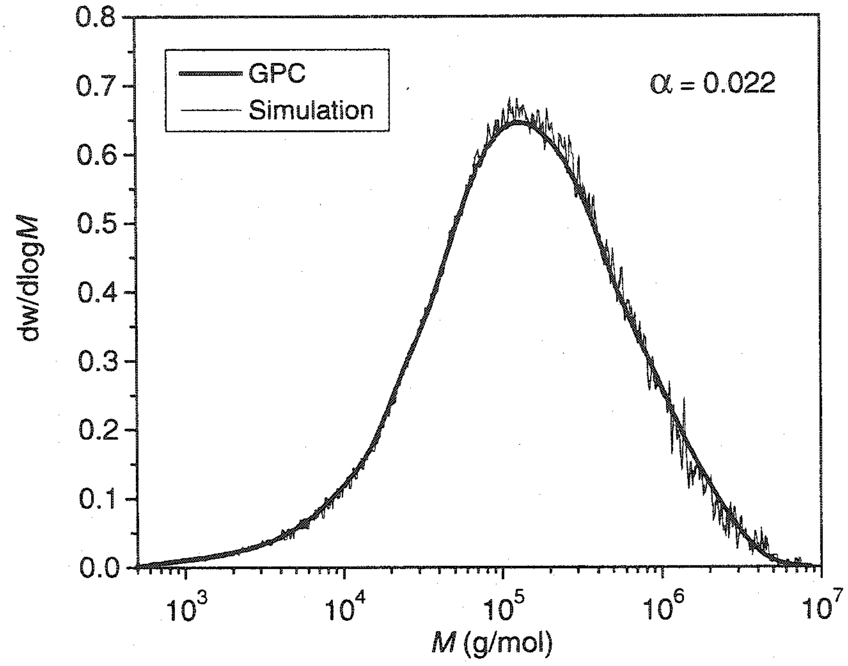

Figure 6-17: Molecular weight distribution of 12B1 from Monte Carlo simulation (thin line) and from GPC measurements (thick line)

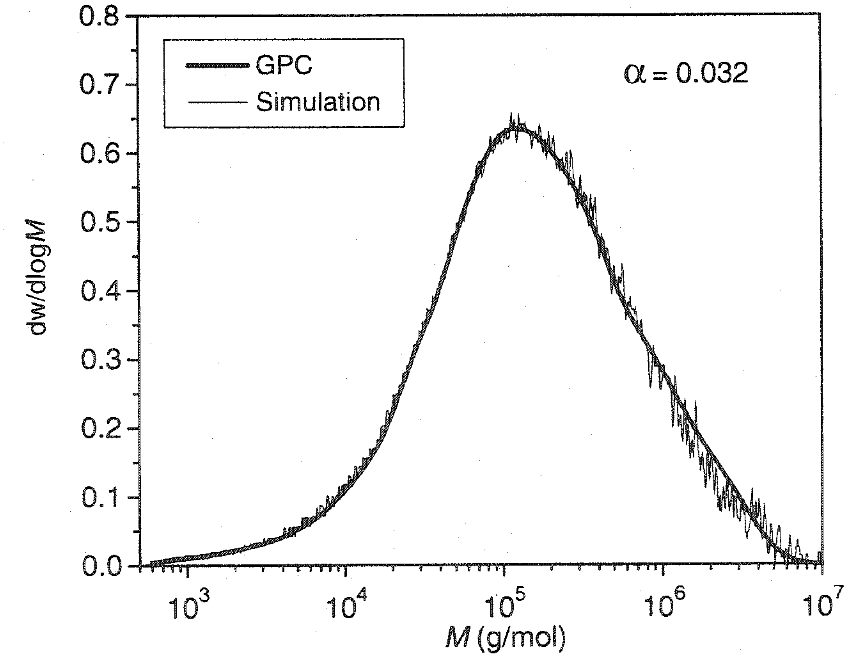

Figure 6-18: Molecular weight distribution of 12B2 from Monte Carlo simulation (thin line) and from GPC measurements (thick line)

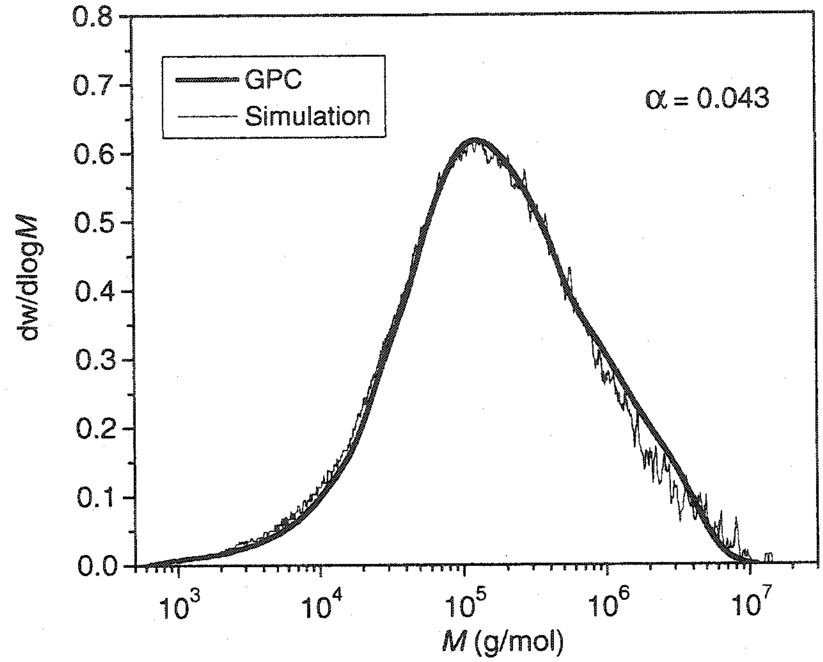

Figure 6-19: Molecular weight distribution of 12B3 from Monte Carlo simulation (thin line) and from GPC measurements (thick line)

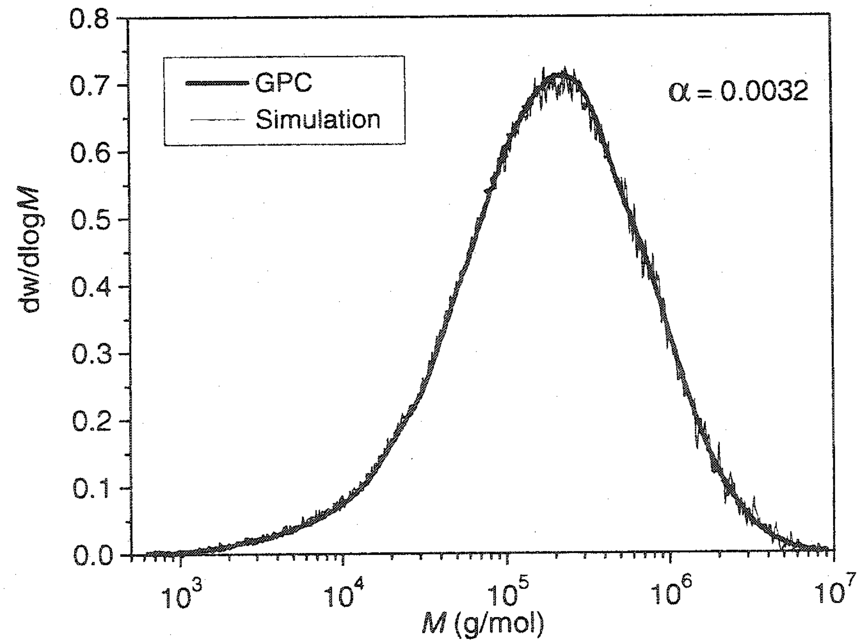

Figure 6-20: Molecular weight distribution of 2B1 from Monte Carlo simulation (thin line) and from GPC measurements (thick line)

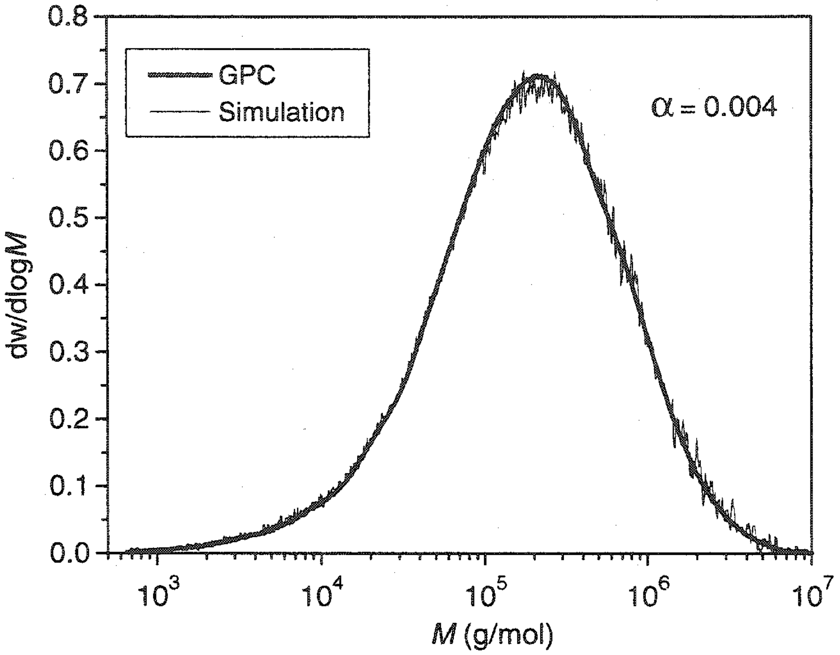

Figure 6-21: Molecular weight distribution of 2B2 from Monte Carlo simulation (thin line) and from GPC measurements (thick line)

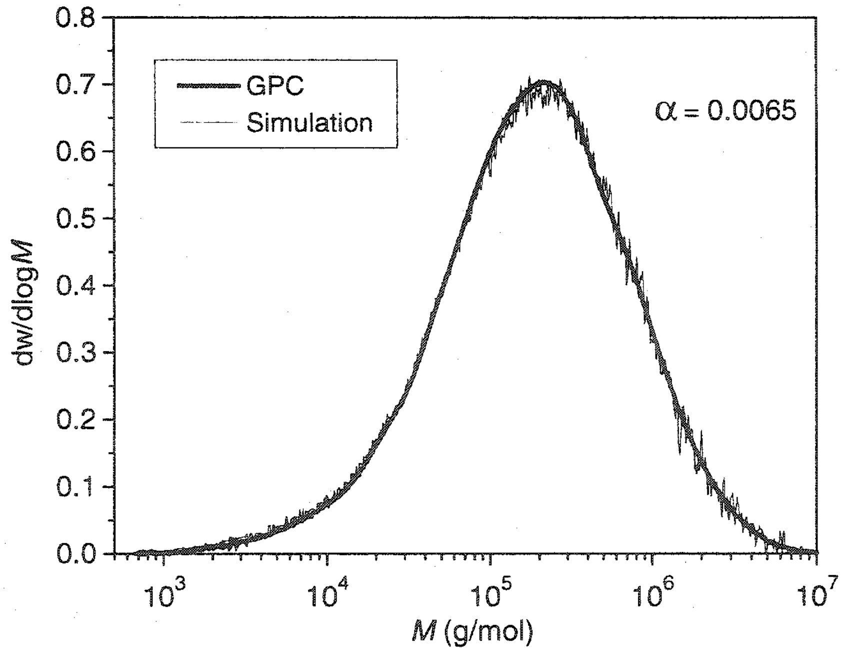

Figure 6-22: Molecular weight distribution of 2B3 from Monte Carlo simulation (thin line) and from GPC measurements (thick line)

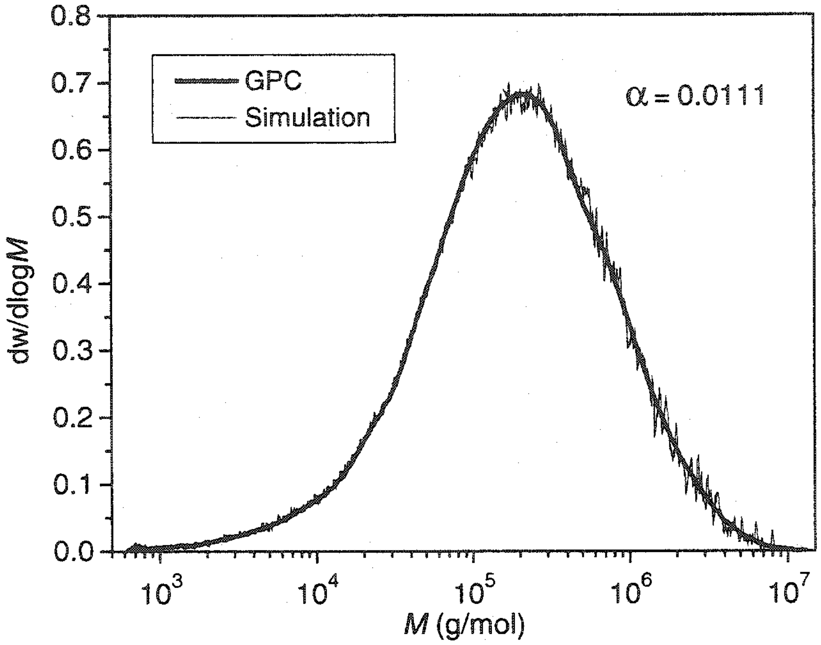

Figure 6-23: Molecular weight distribution of 2B4 from Monte Carlo simulation (thin line) and from GPC measurements (thick line)

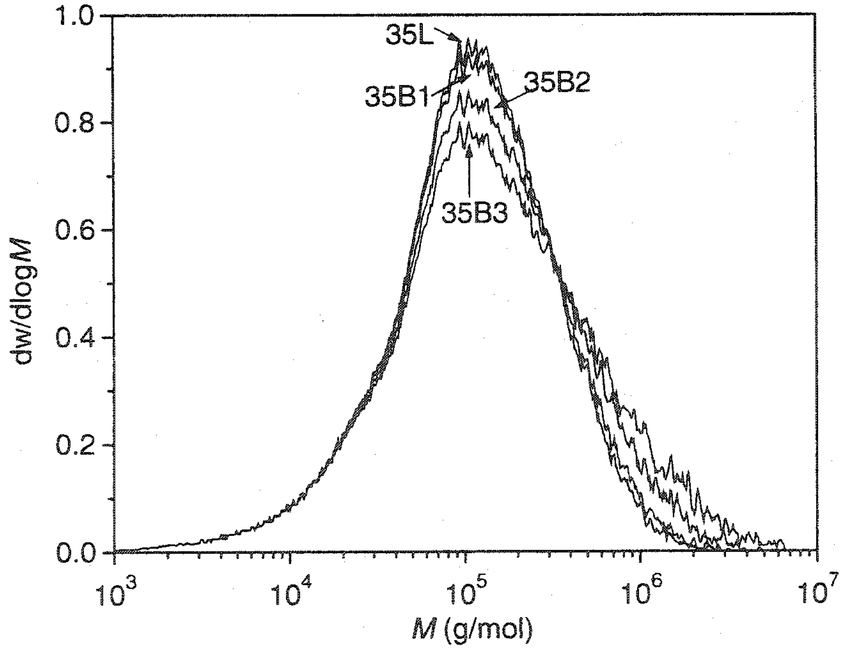

Figure 6-24: Simulated molecular weight distribution of linear sample 35L and three branched samples 35B1, 35B2 and 35B3

From the simulations, we also obtain the fractional molecular weight distributions of chains with k_b branch points. Typical fractional molecular weight distributions for samples 35B3, 12B3 and 2B4 are shown in Figs. 6.25-27 together with the overall molecular weight distributions. The overall molecular weight distribution is the sum of all the distributions for chains containing k_b branch points, where $k_b = 0$ represents the linear chains in the branched system. Samples 35B3, 12B3 and 2B4, which have the highest levels of branching in their sets, contain mainly linear chains. The fraction of chains containing k_b branch points decreases with increasing k_b. Sample 2B4 contains mostly linear chains with some star-shaped chains ($k_b = 1$). The fractions of chains having more than one branch point are very low for 2B4 and are not shown in Fig. 6.27. In Figs. 6.25-6.27, the fractional MWDs overlap each other significantly resulting in a smooth overall molecular weight distribution. The significant overlapping of fractional molecular weight distributions is due to the broad molecular weight distribution of the linear precursor.

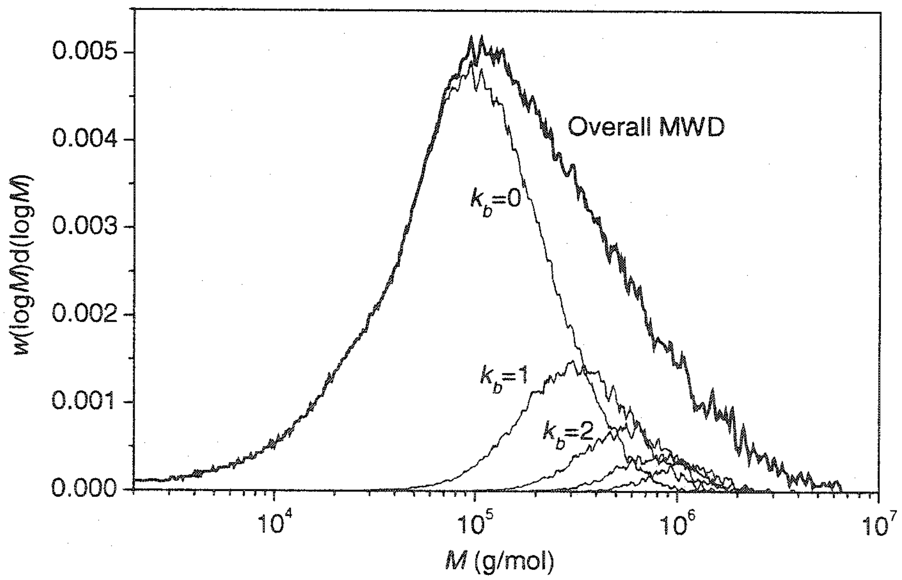

Figure 6-25: Fractional molecular weight distributions of chains containing k_b branch points (k_b = 0,1,2,3,4) and the overall molecular weight distribution of 35B3

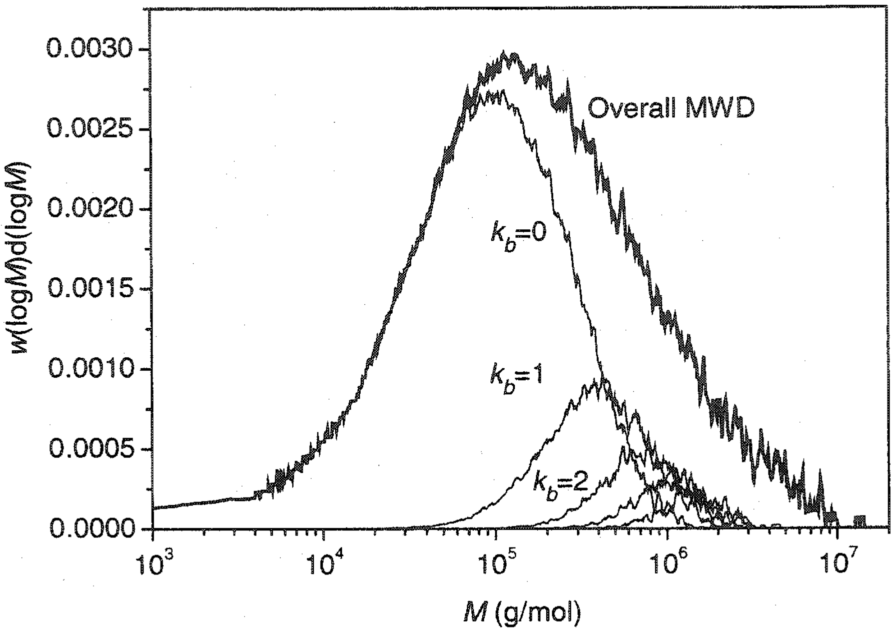

Figure 6-26: Fractional molecular weight distributions of chains containing k_b branch points ($k_b = 0,1,2,3,4$) and the overall molecular weight distribution of 12B3

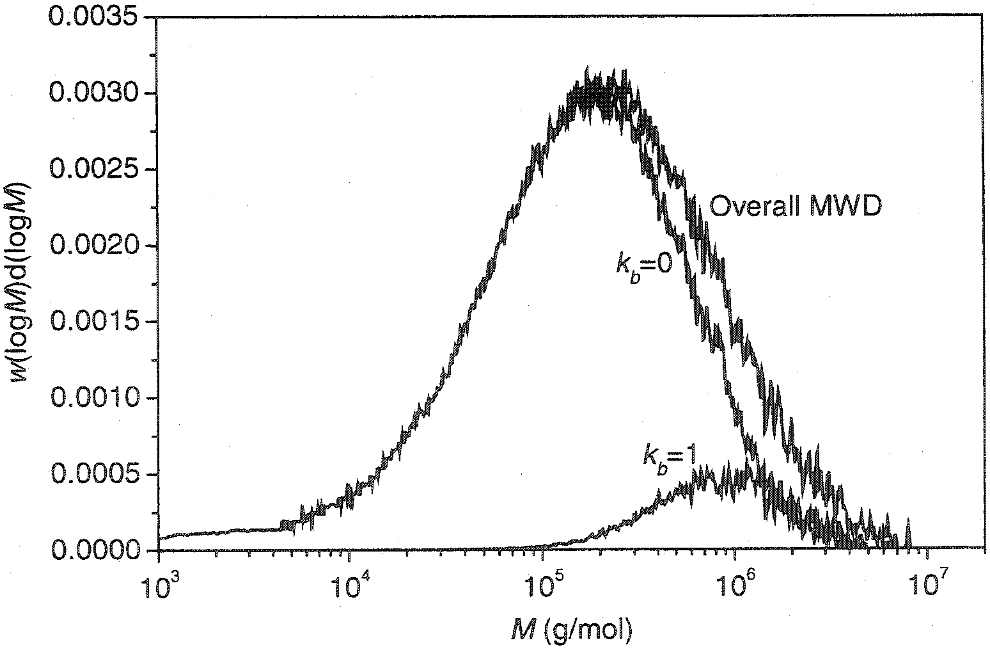

Figure 6-27: Fractional molecular weight distributions of chains containing k_b branch points ($k_b = 0,1,2,3,4$) and the total molecular weight distribution of 2B4

The number and weight average molecular weights, $M_n(k_b)$ and $M_w(k_b)$, of chains having k_b branch points, can be obtained from the fractional molecular weight distributions. The corresponding polydispersity indexes, $M_w(k_b)/M_n(k_b)$, can then be calculated and are shown in Figs 6.28-30. We can see that the branched chains ($k_b > 0$) have a much lower polydispersity index than the linear chains ($k_b = 0$). With increasing k_b, the polydispersity decreases and converges to 1, showing that chains with high k_b are monodisperse.

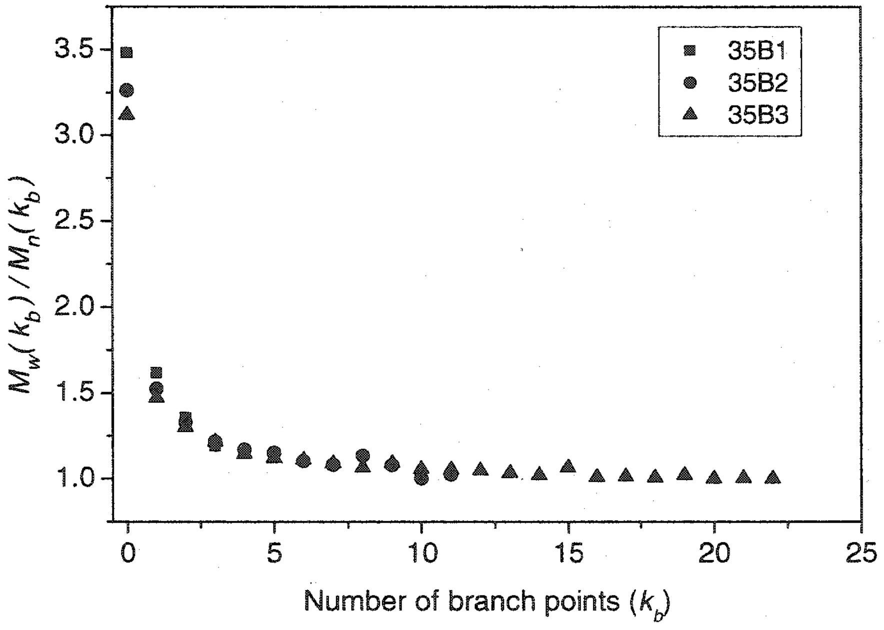

Figure 6-28: Polydispersity index of chains containing k_b branch points in branched samples 35B1, 35B2 and 35B3

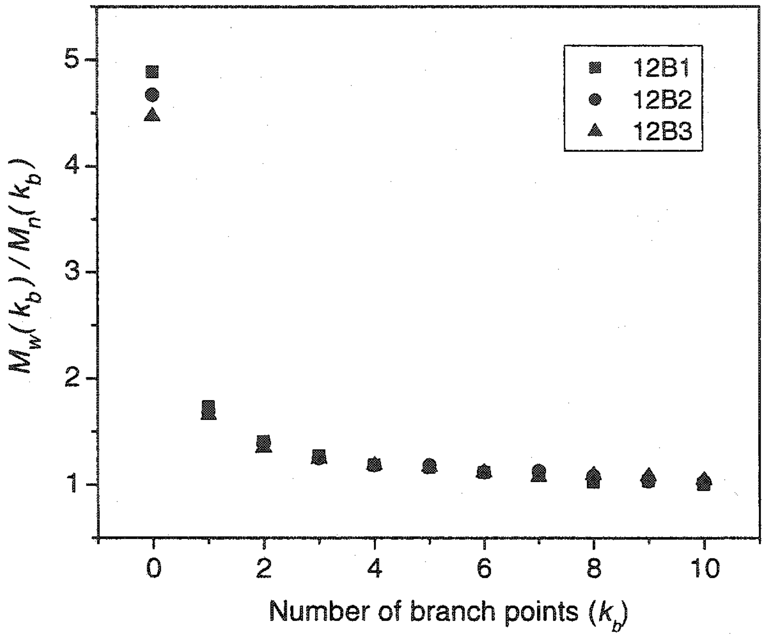

Figure 6-29: Polydispersity index of chains containing k_b branch points in branched samples 12B1, 12B2 and 12B3

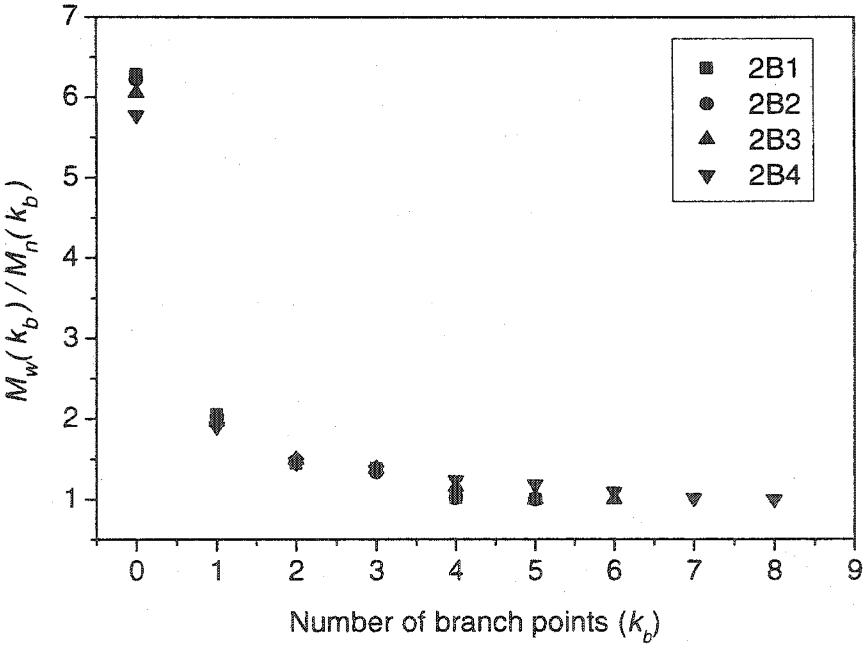

Figure 6-30: Polydispersity index of chains containing k_b branch points in branched samples 2B1, 2B2, 2B3 and 2B4

6.5.2. Branching Information

From the value of α we can calculate the branching parameter β as follows. The number of chains present after the branching reaction is (1-α). Therefore, the two parameters are related as shown by Eq. 6.14.

$$\beta = \frac{\alpha}{1-\alpha} \tag{6.14}$$

Another commonly used parameter to indicate the branching level is λ , which can be expressed in the term of α as shown by Eq. 6.15:

$$\lambda = \frac{14000\,\alpha}{M_n^0} \tag{6.15}$$

where M_n^0 is the number average molecular weight of the linear precursor.

The values of β and λ were calculated using Eqs. 6.14-15 for all the branched samples, and are listed in Table 6.1.

Table 6-1: The values of β and λ calculated from parameter α for all of the branched samples

Sample	$\alpha\left(\frac{\text{branches}}{\text{precursor chain}}\right)$	$\beta\left(\frac{\text{branches}}{\text{molecule}}\right)$	$\lambda\left(\frac{\text{branches}}{\text{1000 carbons}}\right)$
35B1	0.009	0.0091	0.0025
35B2	0.035	0.0363	0.0098
35B3	0.06	0.0638	0.0168
12B1	0.022	0.0225	0.0075
12B2	0.032	0.0331	0.011
12B3	0.043	0.0449	0.015
2B1	0.0032	0.0032	0.0008
2B2	0.004	0.004	0.001
2B3	0.0065	0.0065	0.0016
2B4	0.0111	0.0112	0.0028

From the simulation we can calculate not only the average branching parameters β, and λ, but also the number (or weight) branch point distributions that describe the number (or weight) fraction of molecules having k_b branch points. The weight branch point distributions ($w(k_b)$ versus k_b) are shown in Figs. 6.31-6.33. From Fig. 6.31 we can see that sample 35B1 has mainly linear chains and a few chains with one branch point with a very small portion (~0.1%) of more highly branched chains. However, for 35B2 and 35B3, the weight fractions of highly branched chains increases. The same tendency can be observed in Figs. 6.32-33 for the other two sets of samples. The number branch point distribution has a tendency similar to that of the weight branch point distribution except that the fractions of chains having high k_b values are lower than those in the weight distribution.

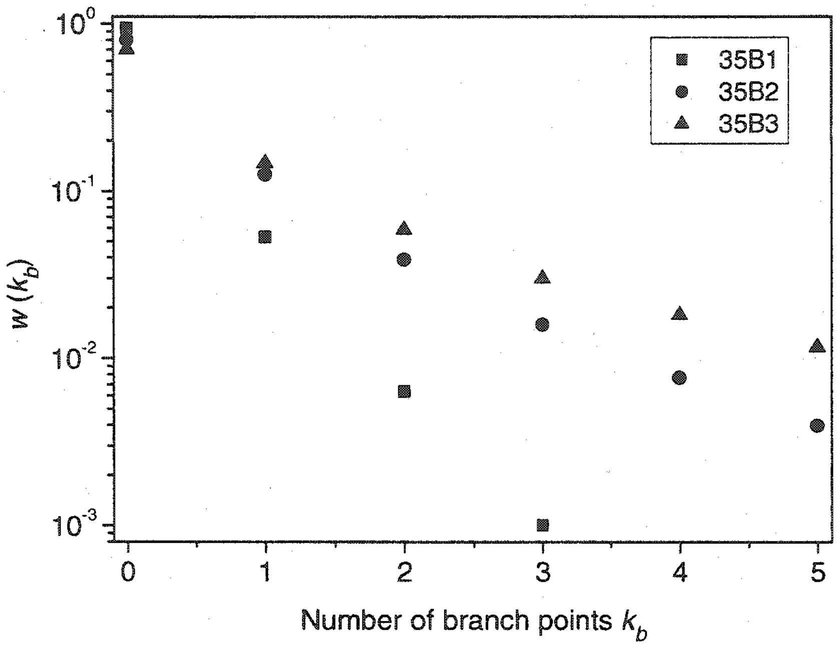

Figure 6-31: Weight branch point distributions for the branched samples based on the linear precursor 35L

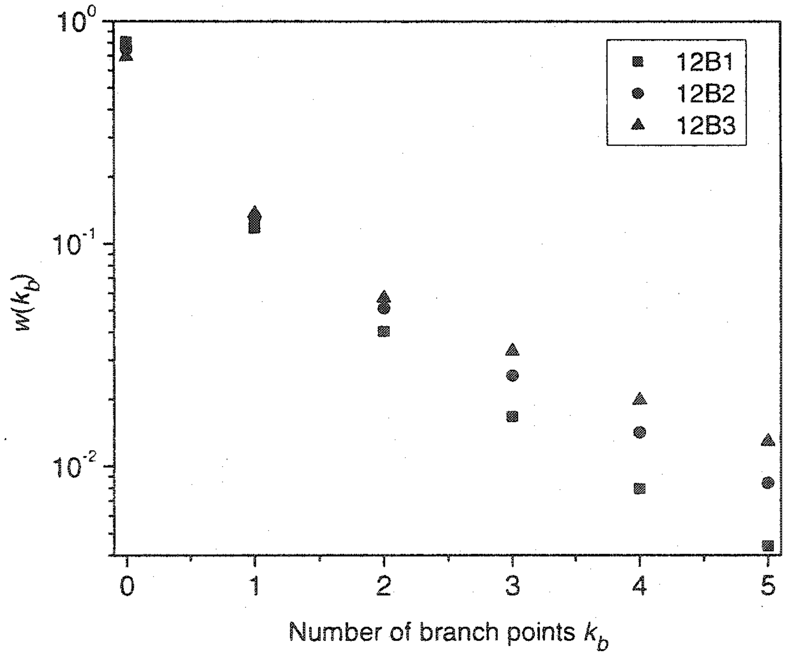

Figure 6-32: Weight branch point distributions for the branched samples based on the linear precursor 12L

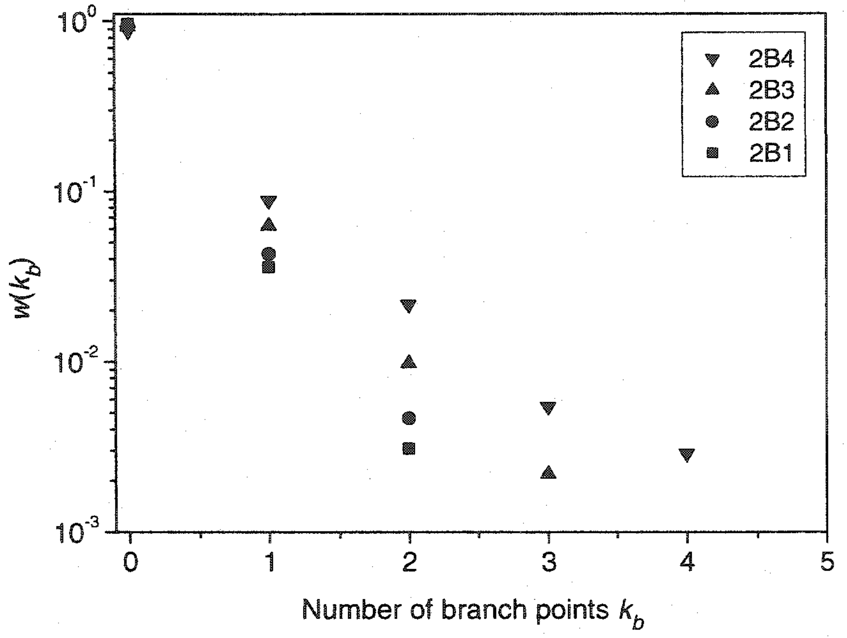

Figure 6-33: Weight branch point distributions for the branched samples based on the linear precursor 2L

Figure 6.34 compares the weight branch point distribution of 35B3 with that of a mPE having the same value of β. Although the two branched systems have the same average branching parameter, the weight branch point distributions are very different. Compared to the mPE, sample 35B3 has fewer linear chains, almost the same fraction of chains with one branch point, and a much higher fraction of highly branched chains ($k_b > 1$). As pointed out by Costeux *et al.*[1], the highly branched chains contain inner backbones and thus help to enhance the melt strength. Consequently, we expect 35B3 to have a higher melt strength than mPE.

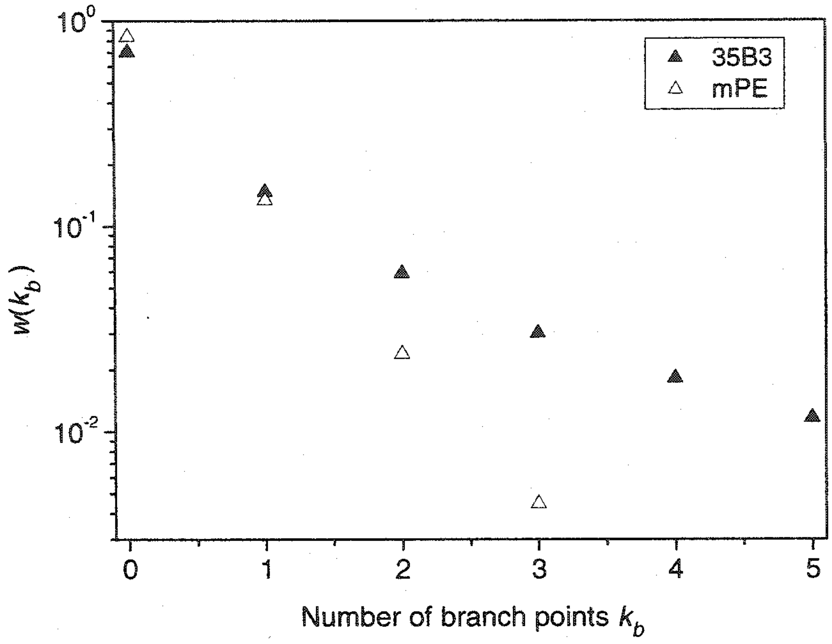

Figure 6-34: Weight branch point distributions for sample 35B3 and an mPE having the same β value

While the average branching parameters, β and λ, are important for classifying branching structure, for processability and solid-state properties, it is more important to know the distribution of branching levels. The branching distributions, β(*M*), for 35B3, 12B3 and 2B4 are shown in Figs. 6.35-37, where we see that β(*M*) increases with molecular weight. At low molecular weight ($M<10^5$ g/mol), the value of β(*M*) is very low (< 0.01), which indicates that small chains are mainly linear and that branch points are found mostly in the large molecules ($M>10^6$ g/mol). This type of branching distribution improves processability without sacrificing solid-state properties. If branch points are concentrated on small chains, strain-hardening does not occur due to the short branch segment, and the solid properties are degraded because of the significantly smaller chain size.

The branching distributions λ(*M*) of 35B3, 12B3 and 2B4 are shown in Figs. 6.38-40, where we see that λ increases with molecular weight and then levels off. Since β(*M*) does not level off, while λ(*M*) does and the highly branched chains are monodisperse, we conclude that the segment lengths are essentially equal at the high molecular weight end.

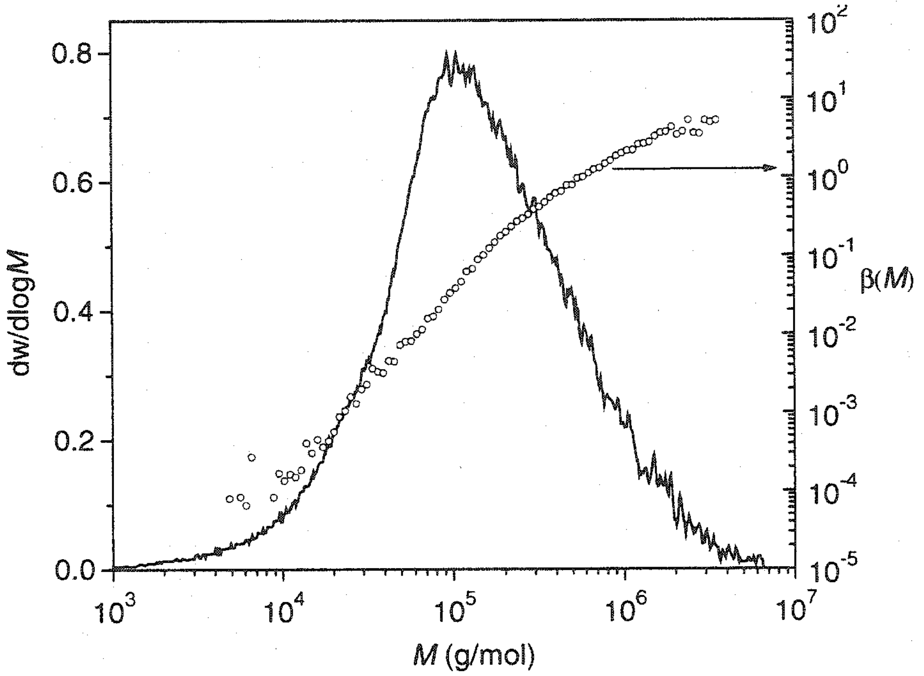

Figure 6-35: Branching $\beta(M)$ and molecular weight distributions of 35B3

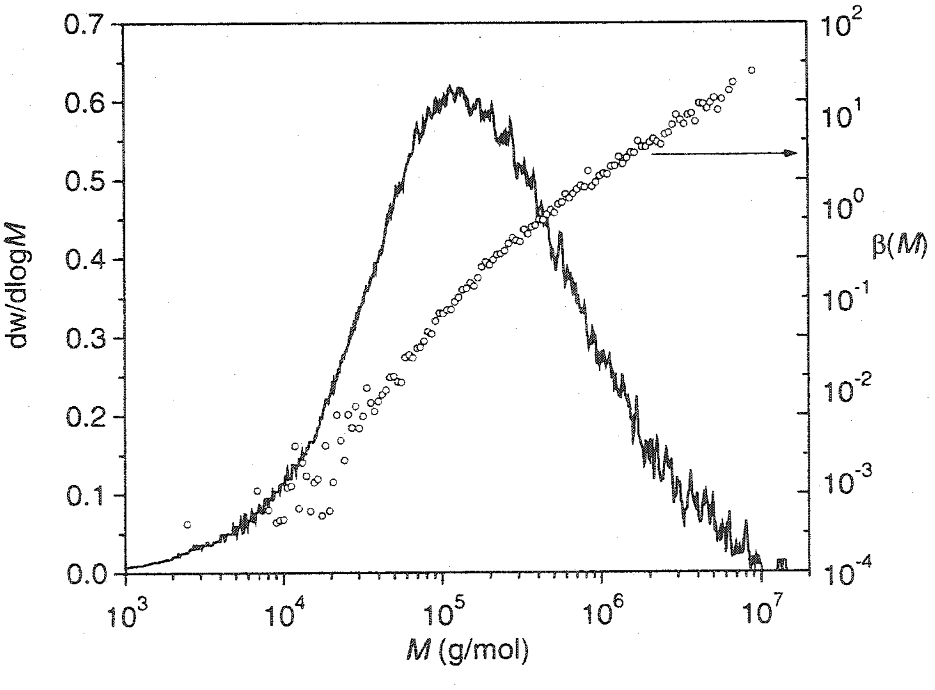

Figure 6-36: Branching $\beta(M)$ and molecular weight distributions of 12B3

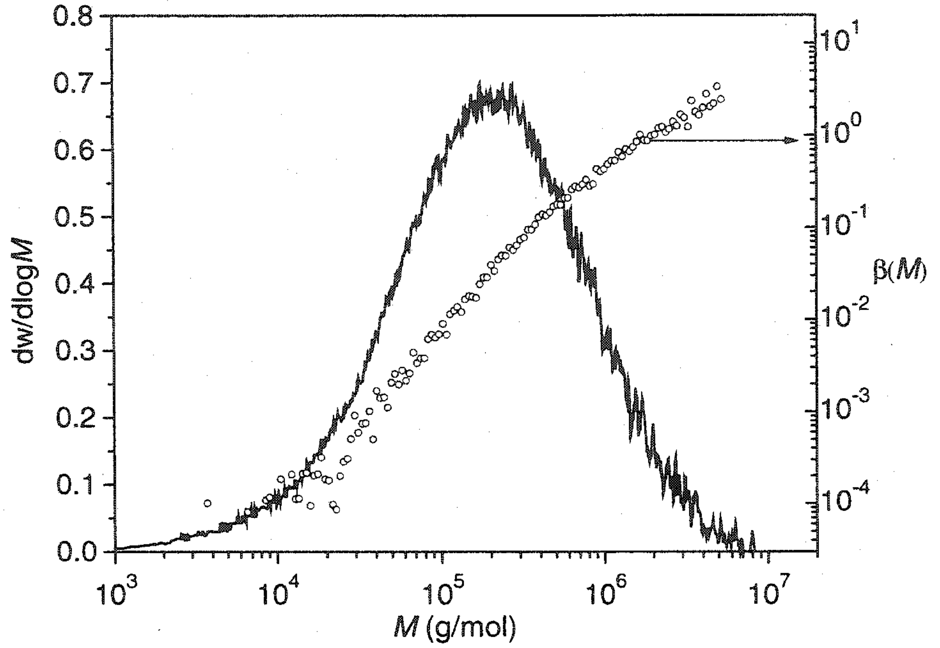

Figure 6-37: Branching $\beta(M)$ and molecular weight distributions of 2B4

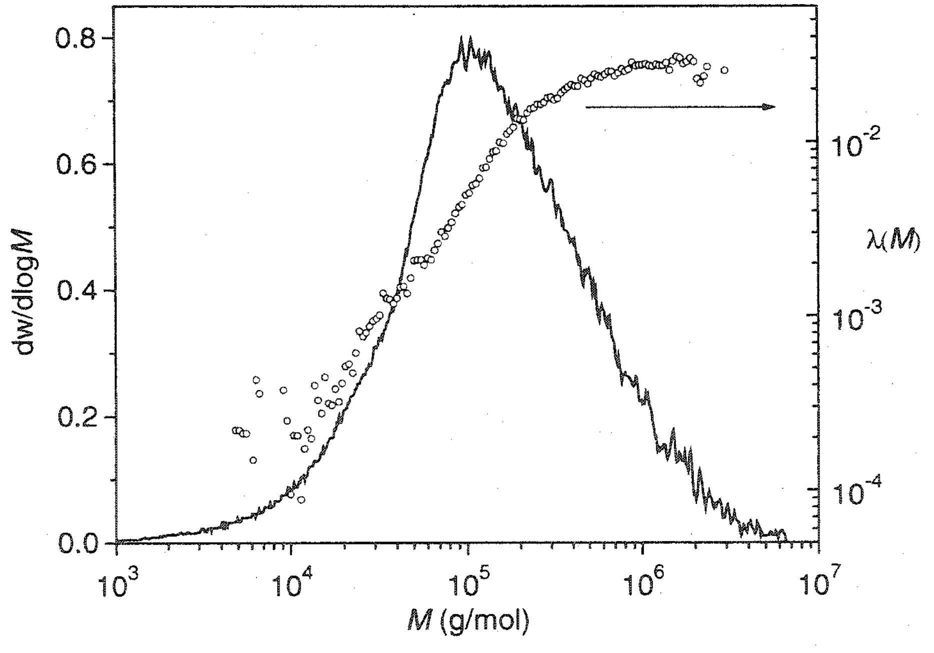

Figure 6-38: Branching $\lambda(M)$ and molecular weight distributions of 35B3

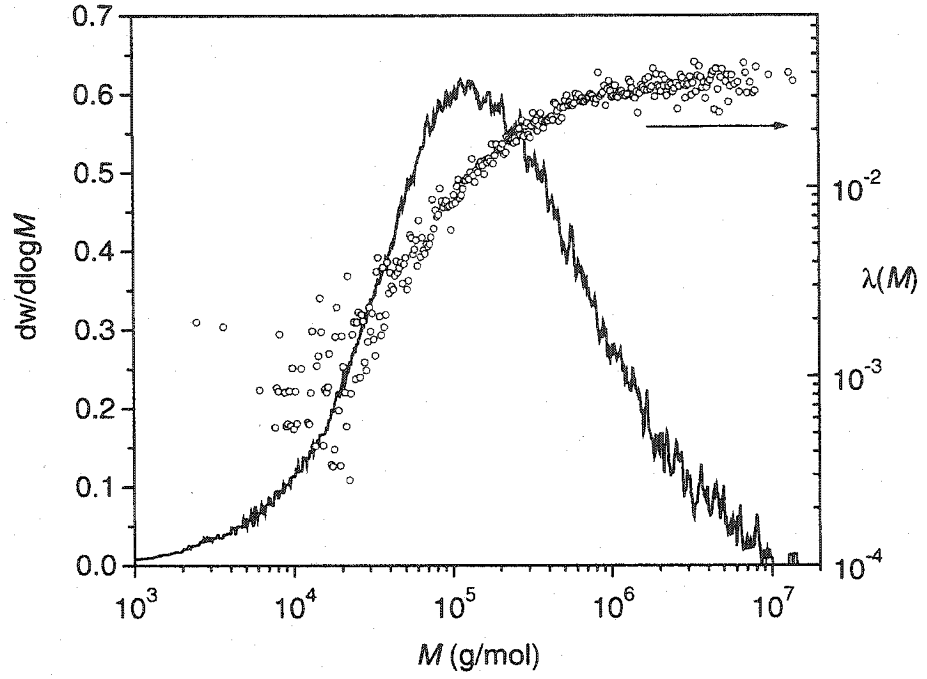

Figure 6-39: Branching λ(M) and molecular weight distributions of 12B3

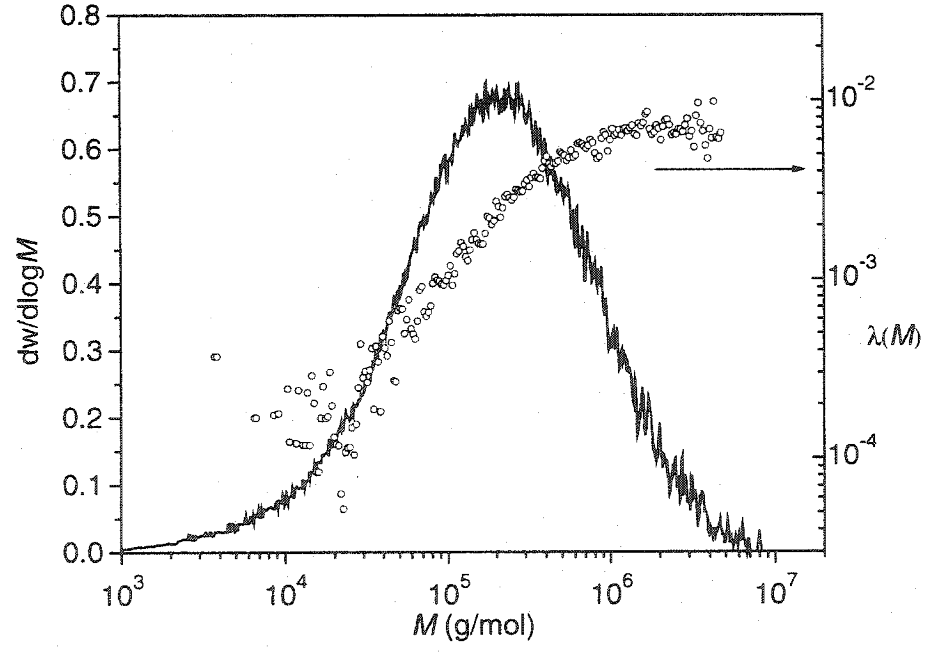

Figure 6-40: Branching λ(M) and molecular weight distributions of 2B4

6.5.3. Relationship between Molecular Weights and Branching Parameters

The relationship between β and the reduced number average molecular weight, M_n/M_n^0, is shown in Fig. 6.41, where M_n^0 is the number average molecular weight of the linear precursor. We find a perfect linear relationship that follows Eq. 6.16:

$$\beta+1=\frac{M_n}{M_n^0} \tag{6.16}$$

The weight-based random branching process is very similar to the iterative branching process considered by Macosko and Miller[7]. They found that the number average molecular weight could be expressed by Eq. 6.9. The crosslinking density ρ and simulation parameter α are related as follows:

$$\rho=\frac{2\alpha M_0}{M_n^0} \tag{6.17}$$

By substituting Eqs. 6.17 and 6.14 into Eq. 6.9, we obtain the following relationship:

$$\frac{1+\beta}{1-\beta}=\frac{M_n}{M_n^0} \tag{6.18}$$

When $\beta << 1$, $1-\beta \cong 1$ and Eq. 6.18 becomes identical to Eq. 6.16.

Using Eq. 6.16 the branching parameter β can be calculated from the two number average molecular weights, M_n and M_n^0, which can be determined using GPC. This relationship does not depend on the molecular weight distribution of the linear precursor.

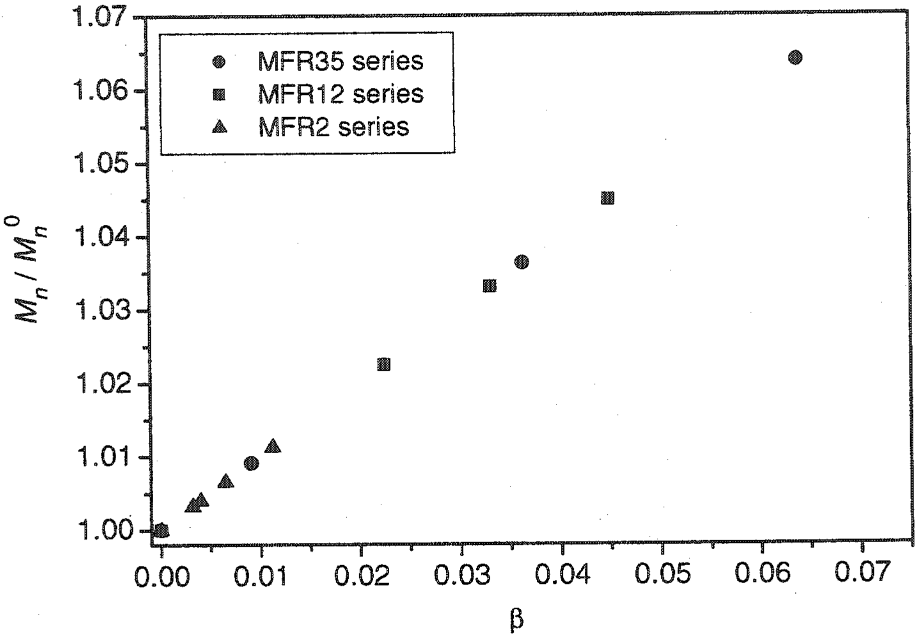

Figure 6-41: Branching parameter β and reduced number average molecular weight M_n/M_n^0 for polypropylene series based on three different linear precursors

While it is convenient to use Eq. 6.16 to calculate the branching parameter β from number average molecular weights, it is preferable to use the weight average molecular weights for this purpose, because for branched polymers, triple-detector GPC gives more accurate results for M_w than for M_n. The relationship between α and the reduced weight average molecular weight M_w^0/M_w is shown in Fig. 6.42, where M_w^0 is the weight average molecular weight of the linear precursor.

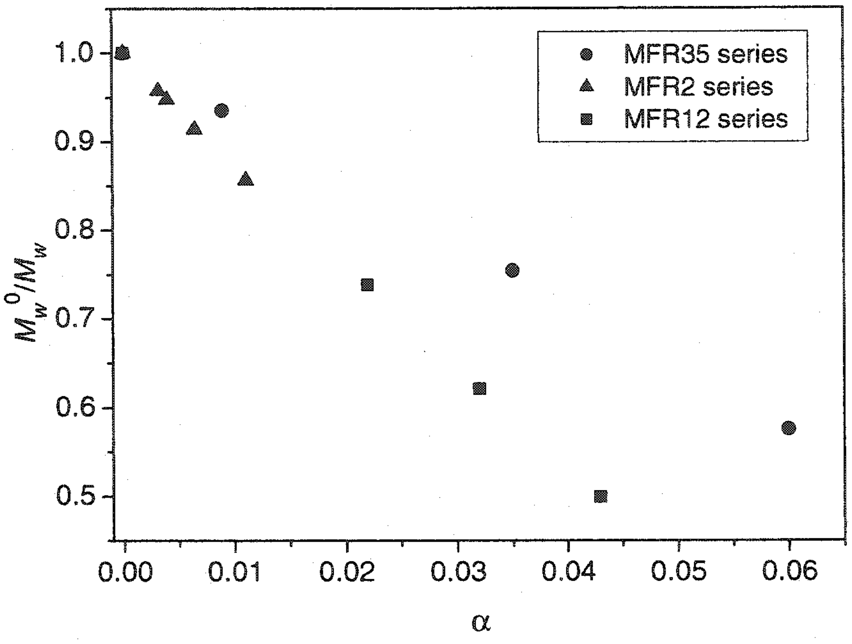

Figure 6-42: Branching parameter α and reduced weight average molecular weight M_w^0/M_w for polypropylene series based on three different linear precursors

From Fig. 6.42 we see that the points for the 2 MFR series and the 12 MFR series fall close to a single line at low alpha. However, symbols for the 35 MFR series fall on a line having a distinctly different slope, ξ. The slope may depend on the molecular weight or polydispersity of the precursor. The relationship can be expressed as follows:

$$\frac{M_w^0}{M_w} = 1 - \xi \alpha \qquad (6.19)$$

To examine the dependence of the slope on the polydispersity of the linear precursor, two hypothetical Flory molecular weight distributions, F-35L and F-2L, were created.

$$w(M) = \frac{M}{M_n^2} \exp\left(-\frac{M}{M_n} \right) \qquad (6.20)$$

where $w(M)$ is the weight molecular weight distribution function. F-35L has the same M_n as 35L, and F-2L has the same M_n as 2L.

Hypothetical branched systems having various values of β and based on linear precursor F-35L were simulated. The relationship between α and M_w^0 / M_w is compared with that for a series based on the linear precursor 35L in Fig. 6.43. Another comparison between the branched systems based on precursors 2L and F-2L is shown in Fig. 6.44. From Figs. 6.43 and 44 we can see that the polydispersity of the linear precursor affects the slope, ξ.

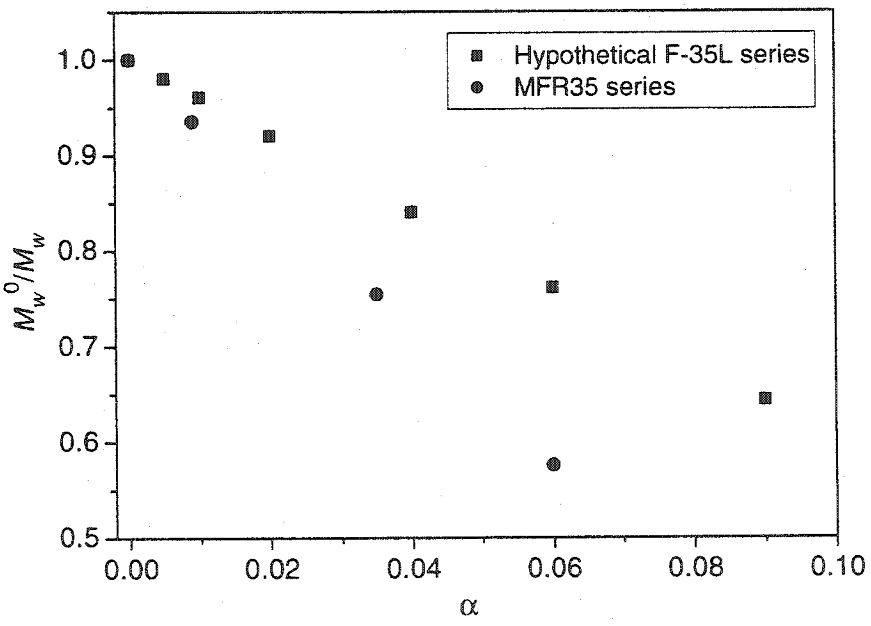

Figure 6-43: Branching parameter α and reduced weight average molecular weight M_w / M_w^0 for branched systems based on two linear precursors, 35L and F-35L, which have the same number average molecular weight but different types of MWD

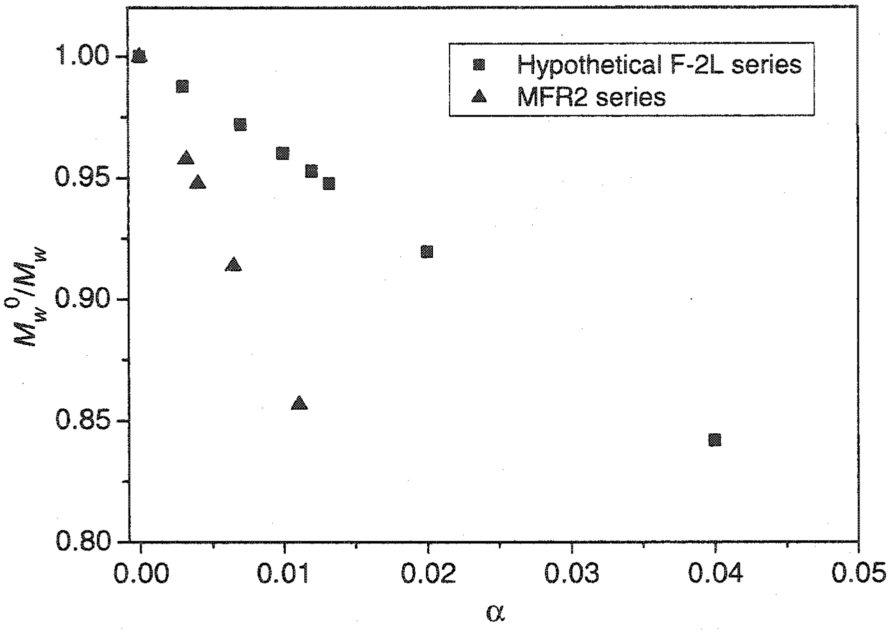

Figure 6-44: Branching parameter α and reduced weight average molecular weight M_w/M_w^0 for branched systems based on two linear precursors, 2L and F-2L, which have the same number average molecular weight but different types of MWD

To look at the influence of molecular weight on the slope ξ we compare the branched systems based on the two hypothetical linear precursors F-35L an F-2L, which have the same polydispersity but different molecular weights. The comparison is shown in Fig. 6.45, where all the symbols fall on the same line. Therefore, the molecular weight of the linear precursor has no effect on the slope ξ.

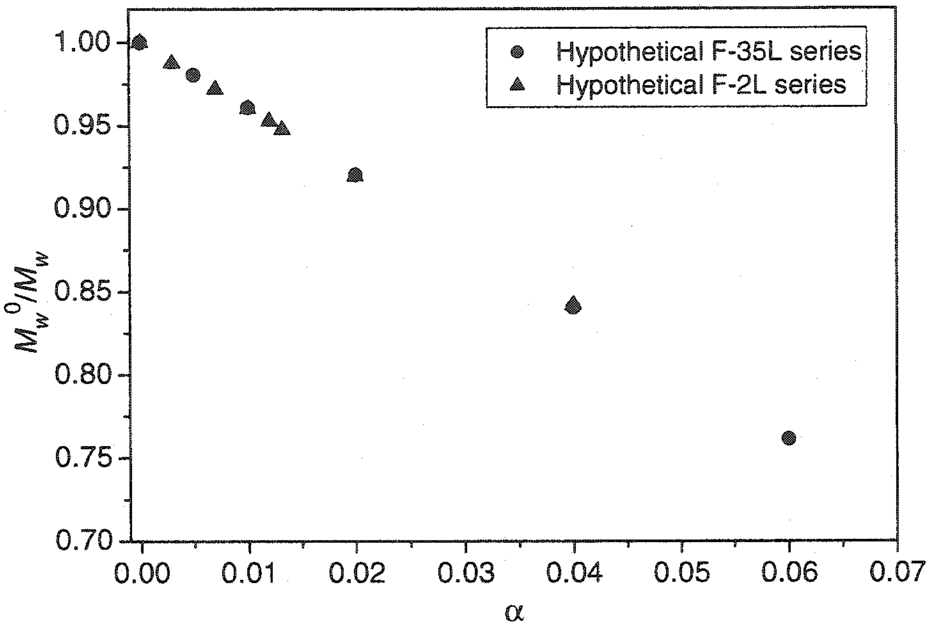

Figure 6-45: Branching parameter α and reduced weight average molecular weight M_w/M_w^0 for branched systems based on two linear precursors, F-35L and F-2L

Taking into account the effect of the polydispersity of the linear precursor on the relationship in Eq. 6.19, we can represent the relationship in terms of reduced molecular weight, M_w^0/M_w, and (PDI^0.α), where PDI^0 is the polydispersity index of the linear precursor. The relationship for branched systems based on five linear precursors is shown in Fig. 6.46, where all the symbols fall on the same line. Therefore, Eq. 6.19 can be revised to give:

$$\frac{M_w^0}{M_w} = 1 - 2\alpha\,(PDI^0) \tag{6.21}$$

The weight average molecular weight of a branched system, M_w, depends on the branching parameter α, the weight average molecular weight of the linear precursor, M_w^0, and the polydispersity, M_w^0/M_n^0, of the linear precursor.

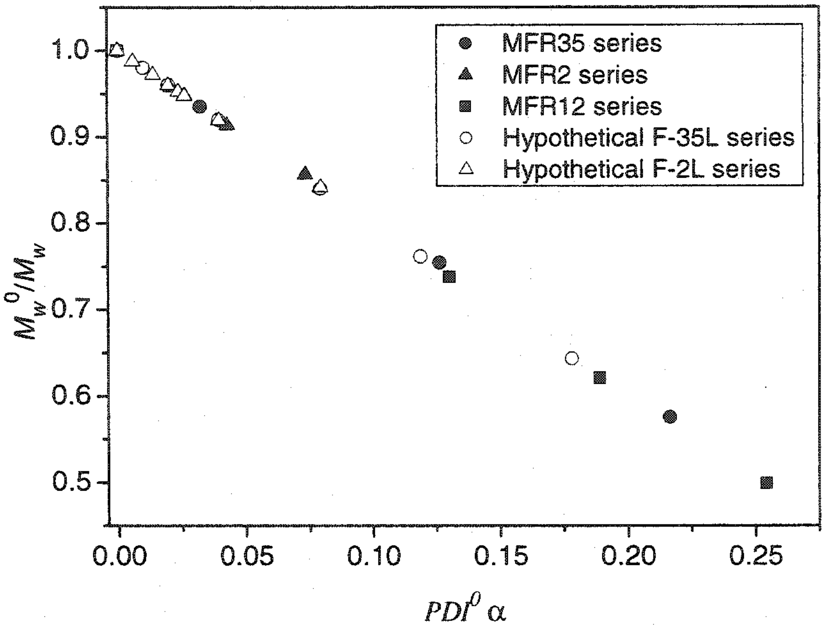

Figure 6-46: Branching information, (PDI^0 α), and reduced weight average molecular weight, M_w/M_w^0, for branched systems based on different linear precursors

The relationship of Tobita[6] for randomly crosslinked polymer chains given by Eq. 6.7 takes the form of Eq. 6.21 if $\overline{P}_{wp} >> 1$ and $\rho_x << 1$. Therefore, the relationship between the weight average molecular weight and the branching parameter α from the MC simulations agrees very well with the analytical formula derived by Tobita[6].

Using Eq. 6.21 the branching parameter α can be calculated from the weight average molecular weight of a branched system, which can be determined by triple-detector GPC, and the weight average molecular weight and the polydispersity of the linear precursor, which can also be obtained using GPC.

In Eq. 6.21, when ($1-2\alpha\, PDI^0$) equals zero, M_w goes to infinity, which indicates that the system reaches the gel point. In industrial applications, it is important to keep the branching level below the gel point, and the criterion for this is:

$$\alpha < \frac{1}{2\,PDI^0} \qquad (6.22)$$

6.5.4. Branching Efficiency

As mentioned before, there are several ways of not fully completing a branching reaction. The branch points per precursor chain, α, can be obtained for each branched sample from simulation. The nominal branch points per precursor chain, α_{nom}, can be determined.

A comparison of α with α_{nom} for all the branched samples is shown in Fig. 6.47.

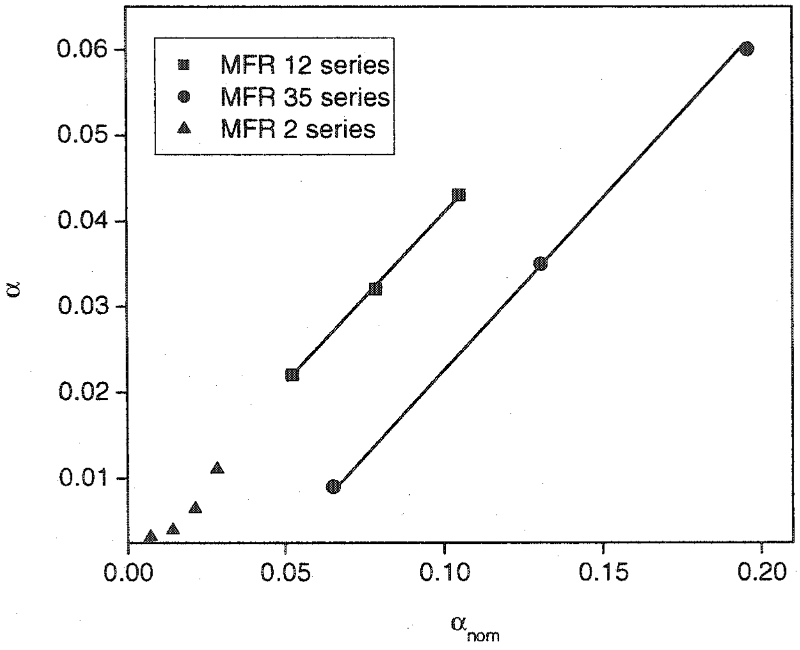

Figure 6-47: Comparing α (branch points per precursor chain) and α_{nom} (nominal branch points per precursor chain) for all branched samples

From Fig. 6.47 we see that the slopes of the linear fits for the 12 MFR and 35 MFR series data are the same. The slope, α divided by α_{nom}, is defined as the branching efficiency E_{bran}. Therefore, E_{bran} for these two sets of samples are the same, and has a value of 40%.

For the MFR 2 series, α_{nom} is very low. In Table 3.3 we see that the values of M_w and *PDI* of 2L and 2B1, 2B2, 2B3 are very close to each other, and M_w of the branched sample 2B2 is even lower than that of the linear precursor 2L. Therefore, uncertainty exists in these results, and α_{nom} calculated from the simulation, which is based on GPC measurements, has the same uncertainty.

The branching efficiency may be related to characteristics such as chemical composition and purity, and to the temperature of the reaction.

Knowing the branching efficiency E_{bran} and the α value at the gel point, the maximum α_{nom} for a gel-free branched system can be calculated. For example, for the MFR35 series, the α value at the gel point is:

$$\alpha = \frac{1}{2PDI^0} = \frac{1}{2\times 3.6} = 0.138 \tag{6.23}$$

The maximum α_{nom} equals α divided by E_{bran}, and has the value of 0.345. Therefore, for linear precursor 35L, the nominal branches per precursor chain α_{nom} should be less than 0.345 in order to ensure a gel-free branched system.

6.5.5. Segment Compositions of Branched Systems

Due to the two special aspects of the polypropylene branching process, there are no analytical solutions for the molecular weight distribution and segment distributions. The molecular weight distributions for the three types of segments, linear, arm and inner backbone, are not available from the simulation, and there is no reason why they should be identical.

It is the fractions of the types of segment that affect rheological behavior[1]. Therefore, it is more meaningful to look at a branched system at the segment level. To obtain a numerical solution for the number and weight fractions of the three types of segments, branched systems based on five precursors were simulated. The five precursors are 35L, 12L, 2L, F-35L and S-35L. Precursors 35L, 12L and 2L have polydispersities of 3.6, 5.9 and 6.6, respectively. Precursor F-35L has a polydispersity of 2.0 and the same M_n value as 35L. This precursor is chosen to compare the post-reactor branching process of polypropylene with the *in-situ* polymerization of branched mPE having the same polydispersity as the linear polymer. Precursor S-35L has a Schultz-Zimm distribution (Eq. 6.10 with $\vartheta = 200$), a polydispersity of 1.005, and the same M_n as 35L. For each precursor, branched systems having various values of α were simulated. The upper limit value of α is determined by Eq. 6.22, which corresponds to the gel point. The almost monodisperse nature of precursor S-35L allows us to use the highest possible value of α before reaching the gel point and to get a segment composition curve as complete as possible.

The number fractions of the three types of segments, linear, arm and inner backbone, are shown in Fig. 6.48 and compared with that of metallocene polyethylene. Assuming that on average all of the segments in the same chain have the same length, the weight fractions were calculated and are shown in Fig. 6.49. Figures 6.48 and 49 show that the higher the polydispersity of the linear precursor, the lower the level of branching at which the system reaches the gel point. The curve of the branched systems based on F-35L falls below the curve of mPE, although the linear polymers have the same polydispersity. The differences are due to the different branching mechanisms of metallocene polyethylene and polypropylene. Compared to mPE, branched polypropylenes contain more inner backbones and fewer free arms (Fig. 6.48), while the inner backbones are longer; the free arms are shorter (Fig. 6.49). Free arms enhance the zero-shear viscosity, and broaden the transition zone. Inner backbones cause strain hardening in extension. In order to improve melt strength, it is desirable to have more and longer inner backbones and fewer and shorter free arms. Therefore, the post-reactor branching process is an efficient way to improve the processability of polymers.

As the polydispersity of the linear precursor increases, the weight and number distributions fall further below the mPE curve, which means the branched system contains more and longer inner backbones, and fewer and shorter free arms. However, as mentioned before, the higher the polydispersity of the linear precursor, the lower the branching level at which the branched system reaches the gel point. Therefore, in order to design a branched system having good processability, it is crucial to choose a suitable linear precursor. It is obvious in Figs 6.48-49 that a monodisperse linear polymer such as S-35L would not be an ideal precursor.

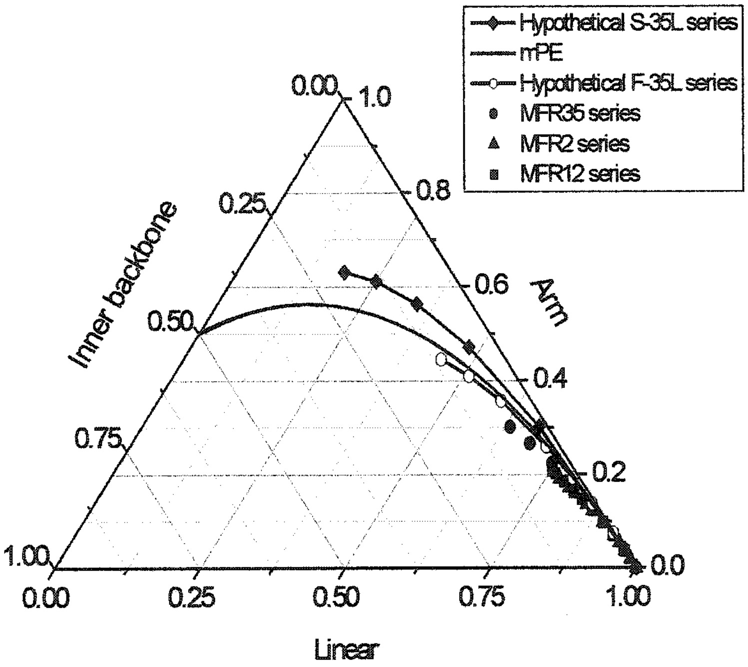

Figure 6-48: Segment type composition in number fraction of branched systems based on five precursors compared with that of mPE

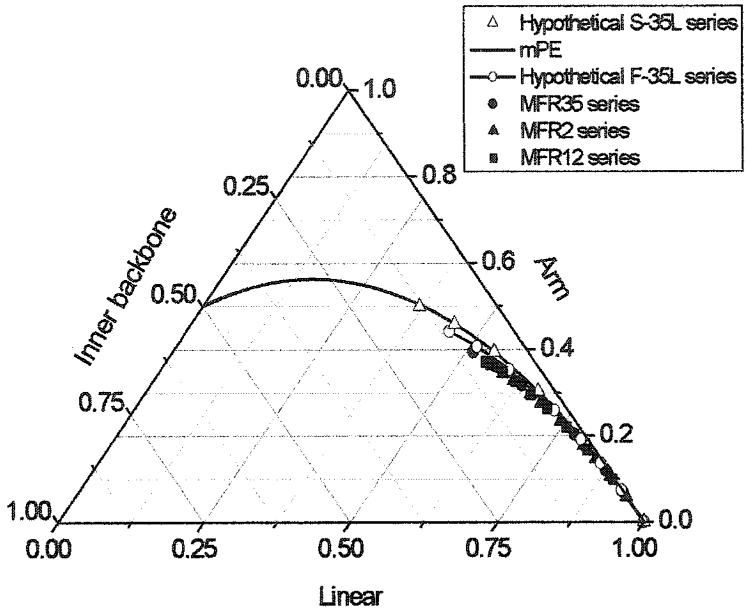

Figure 6-49: Segment type composition in weight fraction of branched systems based on five precursors compared with that of mPE

6.5.6. Relating Engineering Properties to Structural Information

The melt flow rate (MFR), a parameter commonly used in industry to classify polymers, can be related to the molecular weight of the branched system, M_w, as shown in Fig. 6.50. The melt flow rate data were provided by The Dow Chemical Company.

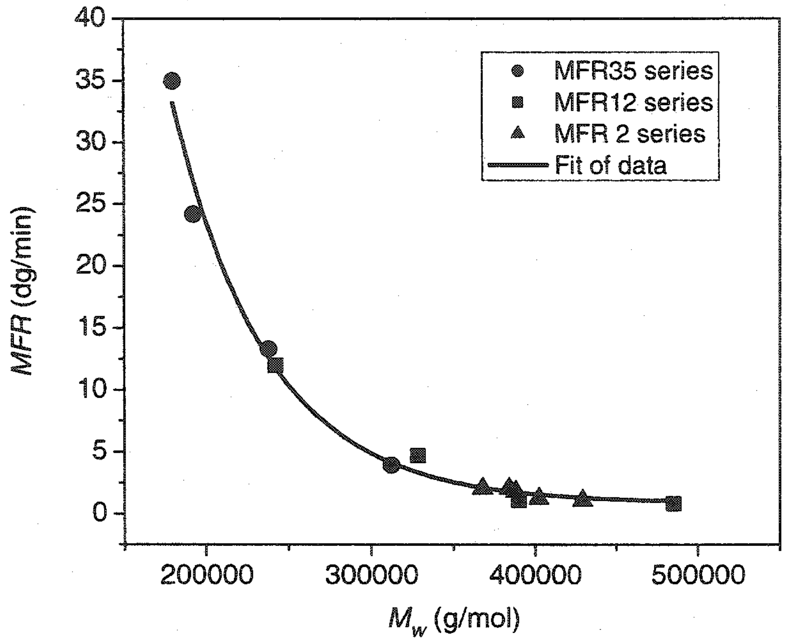

Figure 6-50: Melt flow rate (2.16 kg weight at 230 °C) and weight average molecular weight of the branched polypropylenes

From Fig. 6.50 we see that the melt flow rate decays exponentially with increasing weight average molecular weight. The relationship can be expressed as:

$$MFR = 297.4 \exp\left(-1.32\times10^{-5} M_w\right) \tag{6.24}$$

This relationship does not depend on the polydispersity of the linear precursor, so the melt flow rate of the branched system can be calculated from M_w.

Melt strength, an important parameter that is related to processability in processes where extensional deformation dominates, has a straightforward relationship with the structural parameters as shown in Fig. 6.51. The melt strength data were provided by The Dow Chemical Company.

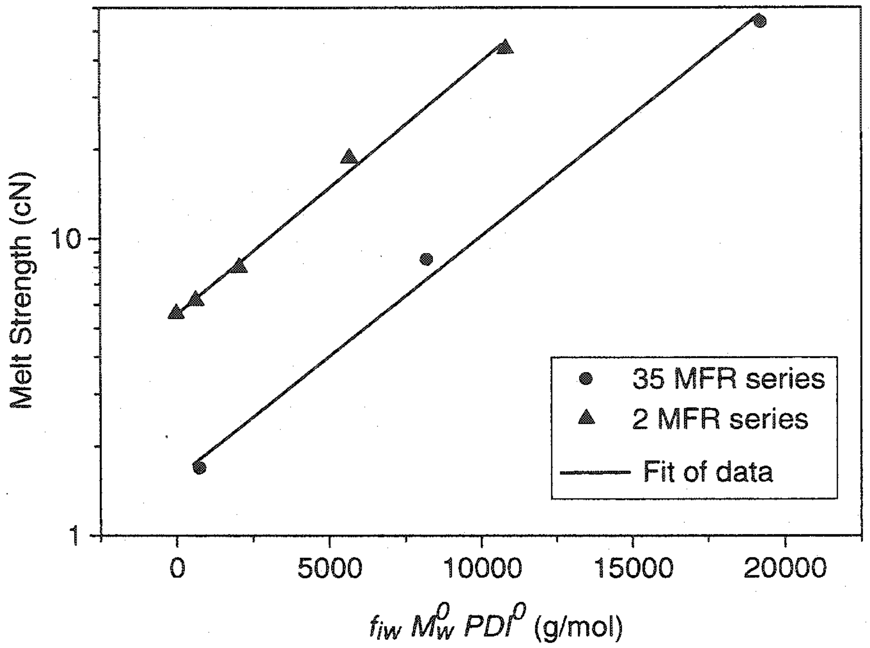

Figure 6-51: Melt strength (190 °C) correlates with ($f_{iw}\ M_w^0\ PDI^0$)

Figure 6.51 shows that the melt strength of a branched polymer depends on the product of the weight fraction of inner backbone f_{iw} and the weight average molecular weight M_w^0, and the polydispersity index PDI^0 of the linear precursor. The logarithm of melt strength has a linear relationship with ($f_{iw}\ M_w^0\ PDI^0$) for samples based on a given linear precursor, but the slope and intercept depend on the linear precursor.

6.5.7. Cyclization

Although the simulation allows cyclization in which a polymer chain reacts with itself to form a ring structure, we do not see ring molecules in the simulation of branched polypropylenes with low levels of branching. However, for the same linear precursor, if α keeps increasing, ring structures will eventually appear. Figure 6.52 shows the number fractions of ring molecules (*n-ring*) in the branched systems up to the gel point. We see that ring molecules only show up very close to the gel point. At a α value below the gel point, there is no ring polymer in the branched system.

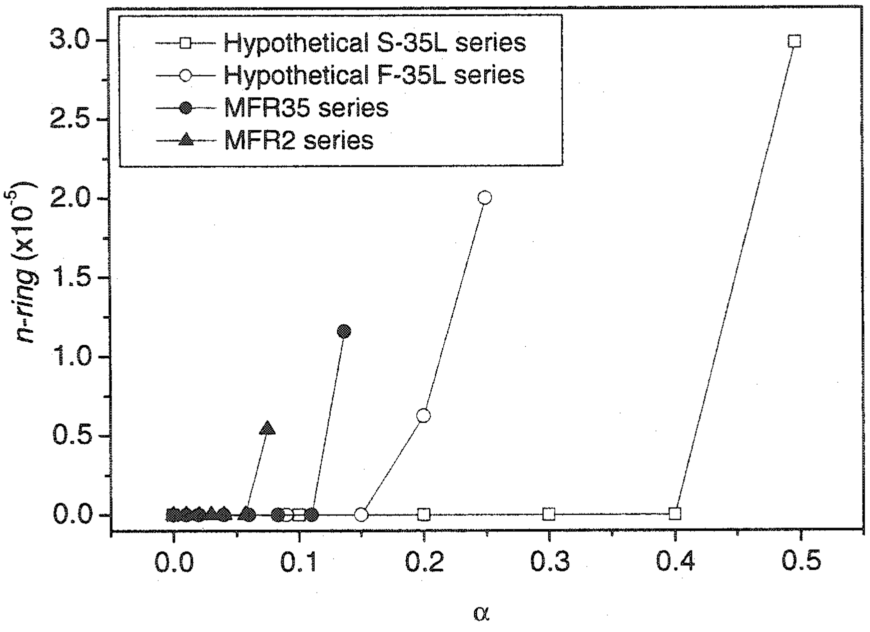

Figure 6-52: Number fractions of ring molecules in branched systems up to gel point

6.6. Conclusions

The Monte Carlo technique developed to simulate the branching process of polypropylenes made it possible to simulate the MWDs of branched materials that are in good agreement with those from GPC measurements.

The polydispersity index of the branched system increases with increasing branching level, while the polydispersity of chains having k_b branch points decreases with increasing k_b and converges to the value of 1. Branching parameters β and λ are calculated from the simulation parameter α. The distributions of β or λ with the molecular weight show that small chains are nearly linear and that most of the branch points are located on the large molecules. This type of branching distribution improves the processability of a polymer without sacrificing its solid-state properties.

By comparing the weight fraction distributions of chains with various numbers of branch points in a polypropylene and a metallocene polyethylene having the same average β value, it is shown that the branched polypropylene has a higher melt strength than the metallocene polyethylene. The branching parameter β is linearly related to the ratio of the number average molecular weights of the branched system and the corresponding linear precursor, and this linear relationship does not depend on the type of distribution of the linear precursor. The branching parameter α is related to the ratio of the weight average molecular weights of the branched system and its linear precursor and to the polydispersity index of the linear precursor.

The branching efficiency is calculable. Knowing the branching efficiency and the value of α at the gel point, the maximum nominal branch points per precursor chain that will not cause gelation can be estimated. Ring molecules are only found in the branched systems at or very close to the gel point.

The melt flow rate decreases exponentially with increasing weight average molecular weight. Melt strength is related to the product of the weight fraction of inner backbone, f_{iw}, and the values of M_w^0 and PDI^0 for the linear precursor. To provide a general picture of the rheological behavior, the branched systems are represented by points in a ternary diagram of segment type composition.

Detailed structural information can be obtained by simulating the branching process and relationships are found between important industrial processing properties and structural parameters. Therefore, this modeling technique makes it possible to calculate the optimal branching level, to select the correct precursor to achieve the desired molecular weight and branching level, and to quickly obtain a general picture of the structure-rheology relationships, which is closely related to melt processability.

References

---

[1] Costeux, S., P. Wood-Adams, D. Beigzadeh, "Molecular Structure of Metallocene-Catalyzed Polyethylene: Rheologically Relevant Representation of Branching Architecture in Single Catalyst and Blended Systems", Macromolecules, 35, 2514-2528, 2002

[2] Weng, W., W. Hu, A.H. Dekmezian, C.J. Ruff, "Long Chain Branched Isotactic Polypropylene" Macromolecules, 35, 3838-3843, 2002

[3] Soares, J.B.P., A.E. Hamielec, "Bivariate Chain Length and Long Chain Branching Distribution for Copolymerization of Olefins and Polyolefin Chains Containing Terminal Double-Bonds", Macromol. Theory Simul., 5, 547-572, 1996

[4] Read, D., T.C.B. McLeish, "Molecular Rheology and Statistics of Long Chain Branched Metallocene-Catalyzed Polyolefins", Macromolecules, 34, 1928-1945, 2001

[5] Tobita, H., "Molecular Weight Distribution in Free-Radical Crosslinking Copolymerisation", Macromolecules, 26, 836-841, 1993

[6] Tobita, H., "Random Sampling Technique to Predict the Molecular Weight Distribution in Nonlinear Polymerization", Macromol. Theory and Simul., 5, 1167-1194, 1996

[7] Macosko, C. W., D. R. Miller, " A New Derivation of Average Molecular Weights of Nonlinear Polymers", Macromolecules, 9, 199-206, 1976

[8] Tobita, H., "Molecular Weight Distribution in Random Crosslinking of Polymers: Modality of the Molecular Weight Distribution", Macromol. Theory Simul. 3, 1033-1049, 1994

[9] Tobita, H., "Molecular Weight Distribution in Random Crosslinking of Polymer Chains", J. Polymer Science: Part B: Polymer Physics, 33, 1191-1202, 1995

[10] Tobita, H., "Molecular Weight Distribution Formed Through Chain-Length-Dependent Crosslinking Reactions", Macromol. Theory Simul., 7, 225-232, 1998

Chapter 7. Structure Determination from Rheology

7.1. Introduction

In polymer science, rheology is used not only to determine the flow properties of a polymer but also to infer molecular structure. The latter application is based on the sensitivity of rheological properties to various aspects of polymer structure such as molecular weight, molecular weight distribution and long-chain branches. To obtain information about a specific aspect of structure, such as long-chain branching, from rheology is difficult because of long-chain branching and molecular weight distribution can have similar effects on rheology. Usually rheological properties are empirically correlated with the level of long chain branching based on certain assumptions, and as a result only averaged branching parameters can be obtained.

7.2. Rheological Method to Determine the Branching Level

Lai *et al.*[1] have introduced a long-chain branching index, the Dow rheology index (DRI), for metallocene polyethylenes (mPE) having approximately the same polydispersity. The DRI is based on the Cross viscosity model:

$$\eta(\dot{\gamma}) = \frac{\eta_0}{1+(\tau_0\dot{\gamma})^m} \tag{7.1}$$

where τ_0 is a characteristic time, and m is related to the power law region behavior. Usually the Cox Merz rule, $\eta(\dot{\gamma}) = \eta(\omega)$, when $\dot{\gamma} = \omega$, was assumed[2] and the complex viscosity was used in Eq. 7.1. By fitting the experimental data for linear mPE to the Cross model, they found Eq. 7.2:

$$\eta_0(Pa \cdot s) = 3.65 \times 10^5 \tau_0(s) \tag{7.2}$$

However, for branched mPE, η_0 and λ did not obey the relationship in Eq. 7.2, and they defined the departure from Eq. 7.2 as a long-chain branching index:

$$DRI = \frac{3.65 \times 10^5 (\tau_0 / \eta_0) - 1}{10} \tag{7.3}$$

As stated by Lai *et al.*, the DRI is only applicable to metallocene polyethylenes having approximately the same polydispersity, and the level of branching is sufficiently low that the Cox Merz rule is still valid.

Vega *et al.*[3] carried out dynamic measurements of metallocene polyethylenes in the temperature range from 130 to 190 °C. The average activation energy was determined by analyzing the effect of temperature on the dynamic viscosity η'. Based on their data, they defined a "LCB index associated to activation energy of flow":

$$I_{LCB} = \frac{(E_a)_{LCB} - (E_a)_l}{(E_a)_l} \tag{7.4}$$

where $(E_a)_{LCB}$ is the activation energy of a LCB polyethylene, and $(E_a)_l$ is the activation energy for flow of a linear polyethylene. Others have demonstrated that long-chain branched mPE is thermorheologically complex[4], and instead of a single value of activation energy, a spectrum of activation energies should be used to describe temperature sensitivity.

Shroff and Mavridis[5] defined a long-chain branching index for essentially linear polyethylenes. They assumed that the zero-shear viscosity depends on molecular weight and long chain branching and is independent of polydispersity. They also assumed that for essentially linear polymers, the mean-square radius of gyration of a branched polymer equals that of a linear polymer having the same molecular weight, and that the intrinsic viscosity of a branched polymer equals that of a linear polymer having the same molecular weight. Based on these assumptions, the long-chain branching index was defined as:

$$LCBI = \frac{\eta_0^{1/a_3}}{[\eta]} \frac{1}{k_3^{1/a_3}} - 1 \tag{7.5}$$

where η_0 and $[\eta]$ are the zero-shear viscosity and intrinsic viscosity of the branched polymer, and a_3 and k_3 are constants that can be determined by fitting experimental data to the following relationship for linear polymers:

$$\eta_0 = k_3 [\eta]_L^{a_3} \tag{7.6}$$

The *LCBI* can be used to rank materials having sufficiently low levels of branching that the assumptions are valid.

These indexes for branched polymers only provide a criterion to rank polymers according to the level of branching but do not provide a quantitative determination of branching level such as λ, the average number of branch points per 1000 carbons.

An empirical long-chain branching evaluation technique was developed by Wood-Adams and Dealy[6] for substantially linear polyethylenes. This technique requires complex viscosity data and a molecular weight distribution determined by gel permeation chromatography. A viscosity MWD for the branched material of interest is calculated from the complex viscosity using the method of Shaw and Tuminello[7]. The difference in the location of the peaks in the two MWD curves is correlated with the level of long chain branching as measured by nuclear magnetic resonance.

$$\lambda = \left\{ \begin{array}{ll} \dfrac{\text{GPC Peak}}{\text{Viscosity Peak}} \le 1, & 0 \\ \dfrac{\text{GPCPeak}}{\text{Viscosity Peak}} \ge 1, & 0.1125 \times \log\left(\dfrac{\text{GPC Peak}}{\text{Viscosity Peak}}\right) \end{array} \right\} \tag{7.7}$$

The technique was shown to be valid for well-defined polyethylenes synthesized using metallocene catalysts with narrow molecular weight distribution ($M_w/M_n \approx 2$) and weight average molecular weights around 90000 g/mol.

Jazen and Colby[8] proposed a semi-empirical method to quantitatively determine the level of long-chain branching in polyethylenes. The method was based on the sensitivity of zero-shear viscosity to molecular weight and branching, which was described by Lusignan *et al.*[9] as:

$$\eta_0 = AM_b \left[1 + \left(\frac{M_b}{M_c} \right)^{2.4} \right] \left(\frac{M_w}{M_b} \right)^{\frac{s}{\gamma}} \tag{7.8}$$

where M_b is the average molecular weight between a branch point and its adjacent vertexes, either other branch points or chain ends, *i.e.*, the average molecular weight of free arms and inner backbones; M_c is the critical molecular weight for entanglement; M_w is the weight average molecular weight; and A is a constant depending on the polymer and temperature. The first two terms on the left side of Eq. 7.8 represent the effect of M_b on the zero-shear viscosity. The last term reflects the exponential effect of the number of free arms and inner backbones on the zero-shear viscosity. The exponent (s/γ) depends on M_b:

$$\frac{s}{\gamma} = max\left[1, \quad \frac{3}{2} + \frac{9}{8} B\, ln\left(\frac{M_b}{90 M_{kuhn}} \right) \right] \tag{7.9}$$

where B and M_{kuhn} are constants for a specific polymer. Therefore, if we know all the constants A, B, M_c, and M_{kuhn}, and have measured η_0 and M_w, the structural parameter M_b

can be calculated from Eq. 7.8. For randomly branched polyethylenes, M_b is related to λ as:

$$\lambda = \frac{14000}{2}\left(M_b^{-1} - M_w^{-1}\right) \qquad (7.10)$$

This method requires knowledge of four constants, and the authors[8] state that there is uncertainty in the values of these constants.

The prediction of zero-shear viscosity by Eq. 7.8 for polyesters at fixed weight average molecular weight (M_w = 200000 g/mol) and varying λ values at 60 °C is presented in Fig. 7.1. The values of the constants, A, B, M_c and M_{kuhn}, are from Table 1 in reference 8. We notice that the zero-shear viscosity is very sensitive to the level of branching, even at a fixed weight average molecular weight. For linear polyethylene (λ = 0), the zero-shear viscosity is 260000 Pa.s. With increasing level of branching, the zero shear viscosity increases, reaching a maximum (λ~0.1 branch points/1000 carbons) and then decreases sharply to values lower than that of a linear polymer when λ is beyond 0.3 branch points per 1000 carbons.

The dependence of the zero-shear viscosity on branch point density, λ, is nonmonotonic. For the same zero-shear viscosity value, there are two corresponding values of the branch point density. Therefore, in using this method to determine the level of branching, one needs to choose the right value of the branch point density for the measured zero-shear viscosity.

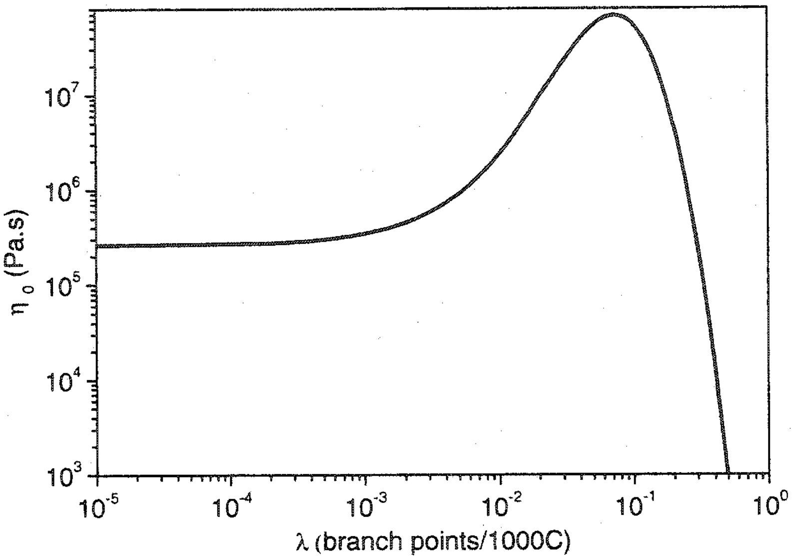

Figure 7-1: Prediction of zero-shear viscosity by Eq. 7.7 for randomly branched polyesters at M_w = 200000 g/mol and various levels of branching λ at 60 °C .

Recently, Tsenoglou and Gotsis[10] proposed a rheological method to estimate the average number of branches per chain, β, in slightly crosslinked polypropylenes. The method is based on the following assumptions: 1) the polymer can be considered as a "blend" of a (1-β) fraction of linear chains and β fraction of nonlinear chains; 2) the structure of the nonlinear chains is a three-arm star, with average molecular weight of an arm being half that of the linear precursor; 3) the weight average molecular weight of a linear component remains the same in the precursor and in the branched system. By using the power law for the zero-shear viscosity dependence on molecular weight for the linear component, the exponential dependency of the zero-shear viscosity of stars on the molecular weight of their arms[11], and the logarithmic sum of the zero-shear viscosity of the linear component and the three-arm star for a branched polymer, the parameter β can be expressed as:

$$\beta \approx \frac{\ln\left(\frac{\eta_B}{\eta_L}\right)}{\alpha\left[\left(\frac{M_L}{M_c}-1\right)\right]-3\ln\left(\frac{M_L}{M_c}\right)} \tag{7.11}$$

where η_B and η_L are the zero-shear viscosities of the branched system and the linear precursor respectively; M_L is the weight average molecular weight of the linear precursor, and M_c is the critical molecular weight at the onset of entangled behavior. By making strong simplifying assumptions about the branching system and the branching structure, the branching parameter β can be obtained from rheological data.

In this study, the relaxation spectrum obtained from experimental data will be correlated to the branching structure. The method involves the careful assignment of each peak in the relaxation spectrum to a corresponding relaxation mechanism. A detailed description of the method is given in the next section; and it is applied to two sets of polypropylene samples, the 35 MFR based series and the 2 MFR based series. The results together with a discussion from the point of view of molecular theory are presented.

7.3. Inferring Branching Information from Rheological Data

7.3.1. Assignment of the relaxation spectrum peaks

By combining small amplitude oscillatory shear and interrupted creep measurements, a complete picture of the linear viscoelastic behavior of branched polypropylenes as well as their linear precursors has been obtained and is presented in Chapter 4. The experimental data presented in Section 4.3 indicate that molecular structure has significant effects on linear viscoelastic properties such as $G'(\omega)$, $G''(\omega)$ and $\eta^*(\omega)$. However, these properties are the sum of all of the various relaxation mechanisms and present only a blurred view of individual mechanisms. Transforming the experimental $G'(\omega)$, $G''(\omega)$ data into a relaxation spectrum amplifies the effects of various relaxation mechanisms. We associate a characteristic relaxation time with the corresponding relaxation mechanism to create a correlation with the branching structure. However, first we need to identify the various characteristic relaxation times. Due to the complexity of the relaxation behavior of branched polymers, only the principal relaxation mechanisms are considered.

The normalized time-weighted relaxation spectra of the MFR 35 set of samples are shown in Fig 7.2 (same as Fig. 4.46).

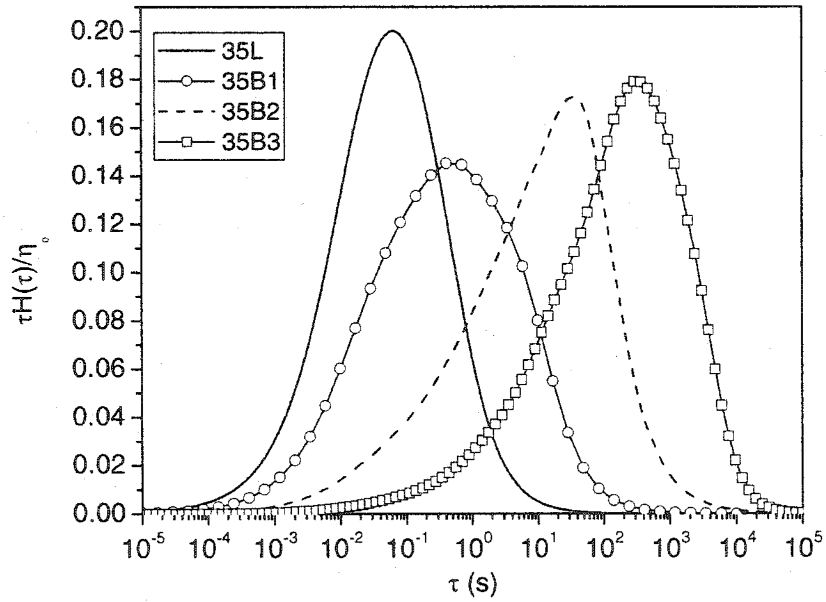

Figure 7-2: Normalized time-weighted relaxation spectra of 35 MFR polypropylenes

Linear sample 35L exhibits only one important relaxation mechanism, reptation. The peak in the relaxation spectrum corresponds to the reptation of molecules having the weight average molecular weight of the polymer.

From the modeling of the branching process of polypropylenes described in Chapter 6, we obtained the weight average molecular weight of the linear portion (M_{wl}) of the branched polymers, and these are listed in Table 7.1.

Table 7-1: The weight average molecular weight of the linear portion in branched polymers and of their linear precursor 35L from modeling described in Chapter 6

Sample	35L	35B1	35B2	35B3
M_{wl}(g/mol)	179,746	165,827	139,283	121,730

From Table 7.1 we see that with increasing level of branching, the weight average molecular weight of the linear portion M_{wl} decreases, which indicates that the location of the reptation peak of the linear portion of branched polymers should shift to the left (to shorter times) of that of the linear precursor. Therefore, we consider that the reptation of the linear portion of branched polymers takes place in the short time tail of the relaxation spectrum, before the peak location of the linear precursor. However, no reptation peaks are present in the spectra of the branched samples other than sample 35B1, because its magnitude is small compared with those of other relaxation mechanisms. For example, for sample 35B1, the relaxation of the linear portion and other relaxation mechanisms related to the branched molecules are comparable in magnitude, resulting in a single broad relaxation peak.

According to molecular theory, after the reptation of the linear portion, the next main relaxation step is the relaxation of free arms. Therefore, we assign the first peak location in branched polymers after the peak location of the linear precursor mainly to the relaxation of free arms. For samples 35B1, 35B2 and 35B3, such peaks are located at t = 0.54 s, 31.6 s and 341.4 s respectively.

Although there is a small amount of inner backbones in the samples, especially in sample 35B3, because of the dynamic dilution effect due to the relaxation of the linear portion and free arms, the relaxation of these portions of the molecules does not generate a peak in the relaxation spectrum and may be located in the long time tail region.

The normalized time-weighted relaxation spectra of the MFR 2 set of samples are shown in Fig. 7.3 (same as Fig. 4.47).

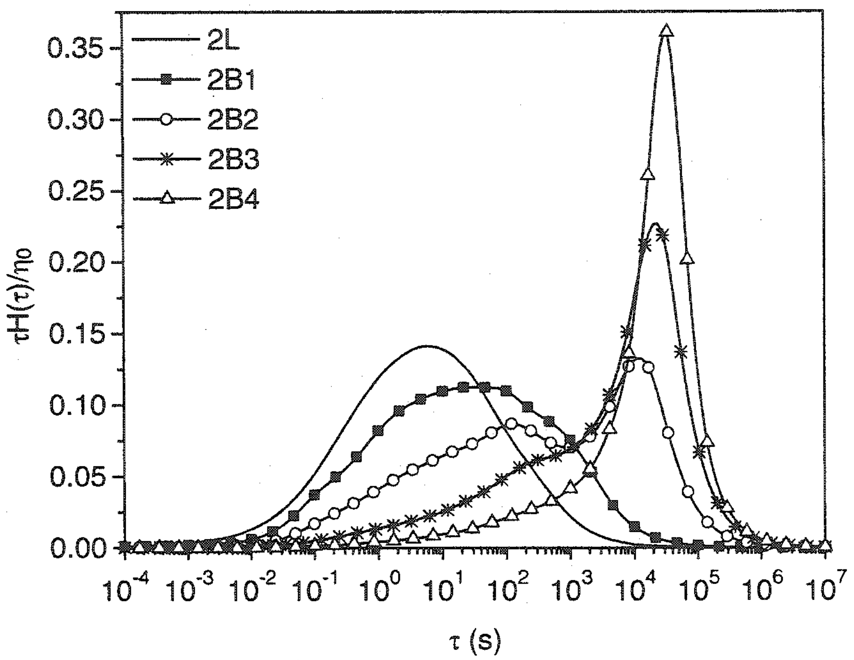

Figure 7-3: Normalized time-weighted relaxation spectra of MFR 2 polypropylenes

The weight average molecular weights of the linear portions in branched samples from the modeling results in Chapter 6 are shown in Table 7.2.

Table 7-2: The weight average molecular weight of the linear portion in branched polymers and of their linear precursor 2L from modeling described in Chapter 6

Samples	2L	2B1	2B2	2B3	2B4
M_{wl} (g/mol)	367,813	337,939	332,288	315,168	288,806

The same tendency of the M_{wl} in the branched samples to decrease with increasing level of branching can be observed in Table 7.2. Therefore, we consider that the reptation of the linear portion of the branched polymers occurs at times shorter than that of the main reptation of the linear precursor 2L. Again, there is no reptation peak in the relaxation spectrum of the branched polymers due to the overwhelming influence of the other relaxation mechanisms in the branched molecules. Sample 2B1 has a very similar relaxation behavior to that of sample 35B1, which has a broad relaxation spectrum. Similarly, we consider that the peak in the relaxation spectrum of sample 2B1 corresponds primarily to the relaxation of arms, which is located at $t = 36.9$ s.

There are two distinct peaks in the relaxation spectrum of sample 2B2. For the reasons stated above, we consider the first peak to be due primarily to the relaxation of free arms, which is located at t = 116.6 s. According to the hierarchical relaxation scheme of the various types of molecular segments, the last type of segment to relax is the inner backbone. Therefore, the second peak (at longer time), which is located at $t = 12589$ s, is assigned to the relaxation of the inner backbones. Despite the strong dynamic dilution effect resulting from the relaxation of the linear portion and the free arms, the contribution due to the relaxation of the inner backbones is still significant due to their long lengths relative to the 35 MFR series. The weight average molecular weight of the linear precursor 2L is twice that of the linear precursor 35L, and we therefore assume that, on average, the length of the inner backbone in the branched samples derived from sample 2L is also twice that of the length of the inner backbone in the branched samples derived from 35L. In sample 2B2, the contribution from the relaxation of the free arms is comparable with that from the inner backbones. Thus, there are two distinct peaks.

With increasing level of branching, the inner backbone fraction increases, and its contribution to the relaxation also increases. In the relaxation spectrum of sample 2B3, the second peak becomes higher, and the first peak becomes a "bump". The locations of the "bump" and second peak are at $t = 316.2$ s and 23263 s respectively. With further increases in the level of branching, in the case of sample 2B4 the first peak is smoothed out and becomes invisible, but the second peak, located at $t = 31622.8$ s, is even higher.

7.3.2. Results and Discussion

Branching parameters can be calculated after the peaks in the relaxation spectrum have been assigned to the corresponding species. It is found that the peak location in the relaxation spectrum is related to the weight fraction of the corresponding species (free arms or inner backbones). The weight fractions of free arms or inner backbones in branched polypropylenes (f_{aw}, f_{iw}) are obtained from the modeling of the branching process presented in Chapter 6. The peak locations and weight fractions of free arms and inner backbones of each branched polypropylene are listed in Table 7.3, where τ_a is the first peak location corresponding to the relaxation of free arms, and τ_i is the second peak location corresponding to the relaxation of inner backbones. The relationships between the weight fractions and the peak locations are presented in Figs. 7.4-7.5.

Table 7-3: Peak locations of the relaxation spectrum (τ_a corresponds to the relaxation of free arms, and τ_i corresponds to the relaxation of inner backbones) and weight fractions of free arms (f_{aw}) and inner backbones (f_{iw}) of each branched polypropylene

Samples	τ_a (s)	τ_i (s)	f_{aw}	f_{iw}
35B1	0.54	NA	0.06	0.001
35B2	31.6	NA	0.184	0.013
35B3	341.4	NA	0.266	0.03
2B1	36.9	NA	0.025	0.00026
2B2	116.6	12589	0.048	0.00084
2B3	316.2	23263	0.079	0.00234
2B4	NA	31622.8	0.105	0.00446

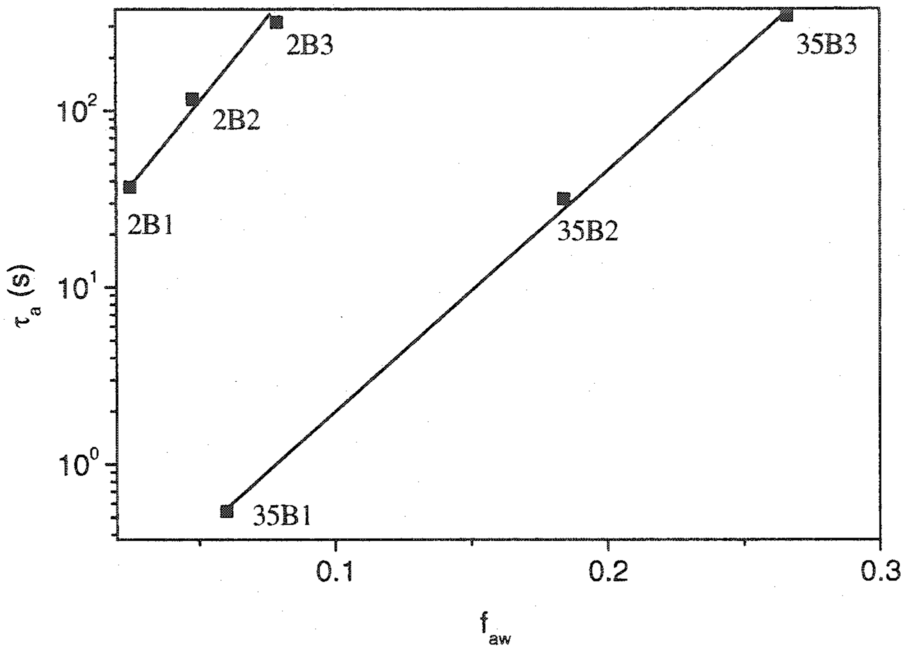

Figure 7-4: The first peak location of the relaxation spectrum versus the weight fraction of free arms of branched polypropylenes (the straight line is an exponential fit of the data)

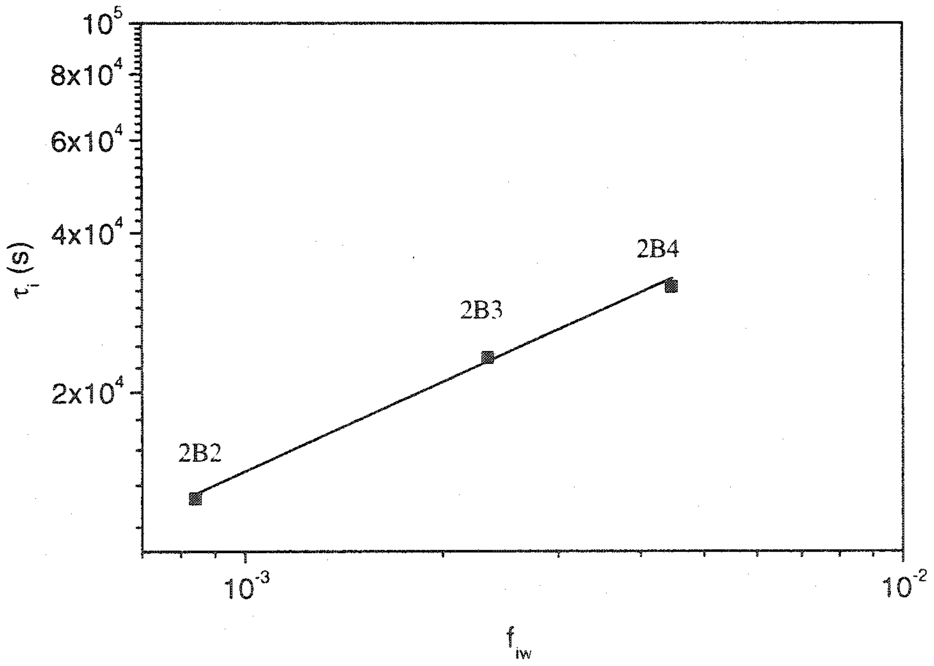

Figure 7-5: The second peak location of the relaxation spectrum versus the weight fraction of inner backbone of branched polypropylenes (the straight line is an exponential fit of the data)

Figure 7.4 is a semi-logarithm plot of the weight fraction of free arms versus the first peak location of the relaxation spectrum. Branched samples based on the same linear precursor follow an exponential relationship, which can be expressed as:

$$\tau_a = \exp(Af_{aw} + B) \qquad (7.12)$$

where A and B are constants that depend on the linear precursor at the same experimental temperature. Equation 7.12 shows the exponential dependency of τ_a on f_{aw}. This dependency can be explained as follows: the relaxation mechanism of free arms is fluctuation, which is a hierarchically activated process. From the free end to the branched point, the relaxation time of an arm increases exponentially.

From the exponential fit of the data in Fig. 7.4, the constants *A* and *B* are obtained. For branched samples based on linear precursor 35L, *A* and *B* have values of 31.45 and –2.45 respectively. For branched samples based on linear precursor 2L, constants *A* and *B* have values of 40.11 and 2.70 respectively. Therefore, for a branched sample based on a given linear precursor, if we know the value of τ_a, the weight fraction of free arms of the sample can be determined from Eq. 7.12.

In the double logarithmic plot Fig.7.5 we see that there is a relationship between f_{iw} and τ_i, which can be expressed as:

$$\tau_i = Df_{iw}^{\,C} \qquad (7.13)$$

where *C* and *D* are constants depending on the linear precursor and experimental temperature. For branched samples based on linear precursor 2L, constants *C* and *D* have values of 0.56 and 658292 (s) respectively.

As mentioned before, the second peak location τ_i is related to the relaxation of inner backbones, which takes place only after all the linear chains and free arms have relaxed. Due to the dilution effect resulting from the relaxation of linear chains and free arms, and the very small amount of the inner backbone, the inner backbones are not entangled and relax as Rouse segments. However, the value of the constant *C* is smaller than that of the Rouse relaxation dependency of time on molecular weight ($\tau \sim M^2$). The decrease in constant C may be due to the strong dilution effect associated with the relaxation of other species.

Therefore, for branched samples based on a sample's linear precursor, knowing the second peak location τ_i, the weight fraction of inner backbones can be determined from Eq. 7.13.

7.3.3. Requirements of the Technique

The previously described technique determines the weight fractions of free arms and inner backbones from the relaxation spectrum. It requires rheological data over a complete relaxation time window, which includes the relaxation of free arms and inner backbones. The experimental procedure for arriving at such a spectrum is described in Chapter 4.

The technique is based on a study of branched polypropylenes. The assignment of peak locations of these polymers was based on a comparison of the relaxation behavior of branched polymers with their linear precursor. Therefore, it is necessary to know the relaxation behavior of the linear precursor. For branched polymers produced by other processes, such as metallocene polyethylenes, the assignment of peak locations may require different criteria.

Because a blend of two linear polymers with very different weight average molecular weight may also have two distinct peaks or a shifted peak location compared to the linear components, it is also important to have knowledge of the GPC molecular weight distributions. For such a blend, a bi-model molecular weight distribution is expected, while the GPC molecular weight distributions of branched samples are usually unimodel. For this study, molecular weight distributions are also important, because the results of the modeling of the branching process are compared with GPC molecular weight distributions. The branching information obtained from the modeling is used to relate the peak location in the relaxation spectrum to branching information.

7.4. Conclusions

A technique to infer the weight fractions of free arms and inner backbones from rheological data is described. The technique requires careful assignments of peak locations of the relaxation spectrum and correlates the characteristic relaxation time with the weight fractions of the corresponding species by using results from Chapter 6 as a calibration. Due to the overlapping relaxation time domains of the several relaxation mechanisms, this technique provides only a rough estimate of branching parameters. Detailed branching information for branched polypropylenes can be obtained by modeling the branching process as explained in Chapter 6.

Reference

---

[1] Lai, S., T.A. Plumley, T.I. Butler, G.W. Knight, C.I. Kao, "Dow Rheology Index (DRI) for Insite Technology Polyolefins (ITP): Unique Structure-Processing Relationships", SPE Antec Technol. 40, 1814-1815, 1994

[2] Wood-Adams, P.M., J.M. Dealy, A.M. deGroot, O.D. Redwine, "Effect of Molecular Structure on the Linear Viscoelastic Behavior of Polyethylene", Macromolecules, 33, 7489-7499, 2000

[3] Vega, J.F., A. Santamaria, A. Munoz-Escalona, P. Lafuente, "Small-Amplitude Oscillatory Shear Flow Measurements as a Tool to Detect Very Low Amounts of Long Chain Branching in Polyethylenes", Macromolecules, 31, 3639-3647, 1998

[4] Wood-Adams, P., S. Costeux, "Thermorheological Behavior of Polyethylene: Effects of Microstructure and Long Chain Branching", Macromolecules, 34, 6281-6290, 2001

---

[5] Shroff, R.N., H. Mavridis, "Long-Chain-Branching Index for Essentially Linear Polyethylenes", Macromolecules, 32, 8454-8464, 1999

[6] Wood-Adams, P., J.M. Dealy, " Using Rheological Data to Determine the Branching Level in Metallocene Polyethylenes", Macromolecules, 33, 7481-7488, 2000

[7] Shaw, M.T., W.H. Tuminello, "A Closer Look at the MWD-Viscosity Transform", Polym. Eng. Sci, 34, 159, 1994

[8] Janzen, J., R.H. Colby, "Diagnosing Long-Chain Branching in Polyethylenes", J. Mol. Struct. 485/486, 569-584, 1999

[9] Lusignan, C.P., T.H. Mourey, J.C. Wilson, R.H. Colby, "Viscoelasticity of Randomly Branched Polymers in the Critical Percolation Class", Phy. Rev. E 52, 6271-6280, 1995

[10] Tsenoglou, C.J., A.D. Gotsis, "Rheological Characterization of Long Chain Branching in a Melt of Evolving Molecular Architecture", Macromolecules, 34, 4685-4687, 2001

[11] Milner, S.T., T.C. B. McLeish, "Parameter-Free Theory for Stress Relaxation in Star Polymer Melts", Macromolecules, 30, 2159-2166, 1997

Chapter 8. Conclusions

1. It is possible to characterize linear viscoelastic properties of polymers with long relaxation time by combining dynamic and creep data;
2. Time-weighted relaxation spectrum reveals clearly the effects of molecular structure on linear viscoelasticity. With increasing level of branching, the range of relaxation spectrum shifts to longer time and the shape and peak location of relaxation spectrum change dramatically;
3. The dual constraint model has a better performance on predicting the linear viscoelastic properties of Ziegler-Natta polypropylene with polydispersity index of 3.6 than the modified double reptation model;
4. It is possible to show the separate effects of polydispersity and branching on linear viscoelastic properties by comparing the relaxation spectrum of a branched sample to that of its linear equivalent;
5. It is possible to see the role of molecular weight on linear viscoelastic properties by comparing the predicted relaxation spectrum of a linear sample to the relaxation spectra of linear equivalents of branched samples based on the same linear sample. In advancing from the linear sample to the linear equivalent corresponding to the branched sample having the highest level of branching, the peak, which is related to M_w, shifts to longer times, and the area under the curve, which is the zero-shear viscosity, increases;
6. Even the dual constraint model has a poor performance on predicting the linear viscoelastic properties of Ziegler-Natta polypropylene with polydispersity index of 6.2;

7. The developed Monte Carlo technique makes it possible to predict the MWDs of branched materials that are in good agreements with GPC data;
8. The polydispersity index of the whole branched system increases with increasing the branching level, and the polydispersity of chains having various branch points decreases with increasing number of branch points and converges to one;
9. Branching parameters β and λ can be calculated from the simulation parameter α. The distributions of β or λ with molecular weight show that small chains are nearly linear and most of the branch points are located on the large molecules;
10. For a given branching parameter β, a branched polypropylene has higher melt strength than a metallocene polyethylene;
11. The branching parameter β is linearly related to the ratio of the number average molecular weights of the branched system and the corresponding linear precursor. This linear relationship does not depend on the type of distribution of the linear precursor. The branching parameter α is related to the ratio of the weight average molecular weights of the branched system and its linear precursor and to the polydispersity index of the linear precursor;
12. The branching efficiency can be estimated. Knowing the branching efficiency and the value of α at the gel point, the maximum nominal branch points per precursor chain that will not cause gelation can be estimated;
13. Ring molecules are only found in the branched systems at or very close to the gel point;
14. The melt flow rate decreases exponentially with increasing weight average molecular weight. Melt strength is related to the product of the weight fraction of inner backbones, and the weight average molecular weight and polydispersity of the linear precursor;
15. It is possible to correlate the weight fraction of free arms and of inner backbones in a polymer with the corresponding peak locations in the relaxation spectrum, and to infer weight fraction of free arms and of inner backbones from rheological data. However, the branching information from rheology is only approximate.

Chapter 9. Contributions to Knowledge

1. Developed a new method to combine dynamic and creep data to extend the experimental window to low frequencies that are not accessible by the traditional dynamic measurements;
2. Demonstrated how the time-weighted relaxation spectrum can reveal clearly the effect of molecular structure on rheology;
3. Evaluated the performance of molecular theory models on predicting the linear viscoelastic properties of Ziegler-Natta polypropylenes with broad molecular weight distributions. Elucidated the effects differing of branches and molecular weight on rheology;
4. Developed a Monte Carlo method to simulate the branching process of Ziegler-Natta polypropylenes;
5. Obtained detailed branching information including the average branching parameters β and λ and their distributions $\beta\ (M)$ and $\lambda\ (M)$;
6. Related branching parameters β and α to the structural characteristics measurable by GPC;
7. Estimated the branching efficiency and the maximum nominal branch points per precursor chain before gelation;
8. Correlated engineering properties of the polypropylenes with the structural information;
9. Developed a technique to obtain weight fraction of free arms and of inner backbones from rheological data. Revealed that the branching information from rheology is only approximate.

Bibliography

Benallal, A., G. Marin, J. P. Montfort, C. Derail, "Linear Viscoelasticity Revisited: The Relaxation Function of Monodisperse Polymer Melts", Macromolecules, 26, 7229-7235,1993

Bersted B.H., Encyclopedia of Fluid Mechanics, Vol.7, Chapter 22, Gulf Publishing Company, Houston, 1988

Borsig E., M. Capla, A. Fiedlerova, M. Lazár, "Crosslinking of Polypropylene using a System Consisting of Peroxide and Thiourea or its Derivatives", Polymer Communications, 31, 293-296, 1990

Carrot, C., P. Revenu, J. Guillet, "Rheological Behavior of Degraded Polypropylene Melts: From MWD to Dynamic Moduli", J. Appl. Polym. Sci., 61, 1887-1897, 1996

Cassagnau, Ph., J. P. Montfort, G. Marin, Ph. Monge, "Rheology of Polydisperse Polymers: Relationship Between Intermolecular Interactions and Molecular Weight Distribution", Rheol. Acta, 32, 156-167, 1993

Chodák I., E. Zimányová, "The Effect of Temperature on Peroxide Initiated Crosslinking of Polypropylene", European Polymer Journal, 20, 81-84, 1984

Constantin, D., "Linear-Low-Density Polyethylene Melt Rheology: Extensibility and Extrusion Defects", Polym. Eng. & Sci., 24, 268-274, 1984

Costeux, S., P. Wood-Adams, D. Beigzadeh, "Molecular Structure of Metallocene-Catalyzed Polyethylene: Rheologically Relevant Representation of Branching Architecture in Single Catalyst and Blended Systems", Macromolecules, 35, 2514-2528, 2002

Davies, A.R. and R.S. Anderssen, "Sampling Localization in Determining the Relaxation Spectrum", J. Non-Newt. F. Mech., 73, 163-179, 1997

Debye, P., A.M. Bueche, "Intrinsic Viscosity, Diffusion, and Sedimentation Rate of Polymers in Solution", J. Chem. Phys. 16, 573-579, 1948

De Gennes, P.G., "Reptation Of A Polymer Chain in The Presence of Fixed Obstacles", J. Chem. Phys. 55, 572-579, 1971

De Gennes, P. G., "Possible Moessbauer or Neutron Experiments on Fluid Interfaces and Smectics", Journal de Physique (Paris), 36, 603-606, 1975

DeNicola A. J. Jr., J. A. Smith, M. Felloni, "High Melt Strength, Propylene Polymer, Process for Making it, and Use Thereof", US Patent 5414027, 1995

Des Cloizeaux, J., "Double Reptation vs. Simple Reptation in Polymer Melts", Polym. Sci. Phys. Ed. 5, 437-442,1988

Doi, M., S.F. Edwards, "Dynamics of Concentrated Polymer Systems", J. Chem. Soc., Farady Trans. II, 74, 1789-1832, 1978

Doi, M., "Explanation for the 3.4 Power Law of Viscosity of Polymeric Liquids on the Basis of the Tube Model", J. Polym. Sci., Polym. Lett. Ed., 19, 265-273, 1981

Doi, M., and S.F. Edwards, "The Theory of Polymer Dynamics", Oxford, 1986

Doi, M., W.W. Graessley, E. Helfand, D.S. Pearson, "Dynamics of Polymers in Polydisperse Melts", Macromolecules, 20, 1900-1906, 1987

Eckstein, A., J. Suhm, C. Friedrich, R.-D. Maier, J. Sassmannshausen, M. Bochmann, R. Mulhaupt, "Determination of Plateau Moduli and Entanglement Molecular Weights of Isotactic, Syndiotactic, and Atactic Polypropylenes Synthesized with Metallocene Catalysts", Macromolecules, 31, 1335-1340, 1998

Ferry J. D., "Viscoelastic Properties of Polymers", New York, Wiley, 1980

Fetters, L. J., A. D. Kiss, D. S. Pearson, G. F. Quack, F. J. Vitus, "Rheological Behavior of Star-Shaped Polymers", Macromolecules, 26, 647-654, 1993

Gabriel, C., J. Kaschta, H. Munstedt, "Influence of Molecular Structure on Rheological Properties of Polyethylenes I. Creep Recovery Measurements in Shear", Rheol. Acta, 37, 7-20, 1998

Gabriel, C., H. Munstedt, "Creep Recovery Behavior of Metallocene Linear Low-Density Polyethylene", Rheol. Acta, 38, 393-403, 1999

Gabriel, C., H. Munstedt, "Influence of Long-Chain Branches in Polyethylenes on Linear Viscoelastic Properties in Shear", Rheol. Acta, 41, 232-244, 2002

Gell, C. B., W. W. Graessly, V. Efstratiadis, M. Pittsikalis, N. Hadjichristidis, "Viscoelasticity and Self-Diffusion in Melts of Entangled Asymmetric Star Polymers", J. Poly. Sci. Part B: Polymer Physics, 35, 1943–1954, 1997

Graebling D., "Synthesis of Branched Polypropylene by a Reactive Extrusion Process", Macromolecules, 35, 4602-4610, 2002

Graessley, W.W., "Entangled Linear, Branched and Network Polymer Systems-Molecular Theories", Adv. Polym. Sci., 47, 67-117,1982

Hingmann, R., B. L. Marczinke, "Shear and Elongational Flow Properties of Polypropylene Melts", J. Rheol., 38, 573-587, 1994

Hoenig, W. D., C. P. Bosnyak, K. Sehanobish, W. Van Volkenburgh, C. Ruiz, L. M. Tau, "New polypropylene for differentiated blown films," SPE ANTEC Proceedings 2, 1843-1846, 2000

Honerkamp, J., J. Weese, " A Nonlinear Regularization Method for The Calculation of Relaxation Spectra", Rheol. Acta, 32, 65-73, 1993

Janzen, J., R.H. Colby, "Diagnosing Long-Chain Branching in Polyethylenes", J. Mol. Struct. 485/486, 569-584, 1999

Kasehagen, L. J., C. W. Macosko, D. Trowbridge, and F. Magnus, "Rheology of Long-Chain Randomly Branched Polybutadiene", J. Rheol., 40, 689-709,1996

Kraft, M., J. Meissner, J. Kaschta, "Linear Viscoelastic Characterization of Polymer Melts With Long Relaxation Times," Macromolecules, 32, 751-757, 1999

Kurzbeck, S., F. Oster, H. Munstedt, T. Q. Nguyen, R. Gensler, "Rheological Properties of Two Polypropylenes with Different Molecular Structure", J. Rheol., 43, 359-374, 1999

Lagendijk, R.P., A.H. Hogt, A. Buijtenhuijs, A.D. Gotsis, "Peroxydicarbonate Modification of Polypropylene and Extensional Flow Properties", Polymer, 42, 10035-10043, 2001

Lai, S., T.A. Plumley, T.I. Butler, G.W. Knight, C.I. Kao, "Dow Rheology Index (DRI) for Insite Technology Polyolefins (ITP): Unique Structure-Processing Relationships", SPE Antec Technol. 40, 1814-1815, 1994

Léonardi, F., J.-C. Majeste, A. Allal, G. Marin, "Rheological Models Based on the Double Reptation Mixing Rule: The Effects of A Polydisperse Environment", J. Rheol., 44(4), 675-692, 2000

Likhtman, A.E., T.C.B. McLeish, "Quantitative Theory for Linear Dynamics of Linear Entangled Polymers", Macromolecules, 35, 6332-6343, 2002

Lu B., T.C. Chung, "Synthesis of Maleic Anhydride Grafted Polyethylene and Polypropylene, with Controlled Molecular Structures", J. Polym. Sci., Part A: Polymer Chemistry, 38, 1337-1343, 2000

Lusignan, C.P., T.H. Mourey, J.C. Wilson, R.H. Colby, "Viscoelasticity of Randomly Branched Polymers in the Critical Percolation Class", Phy. Rev. E 52, 6271-6280, 1995

Macosko, C. W., D. R. Miller, " A New Derivation of Average Molecular Weights of Nonlinear Polymers", Macromolecules, 9, 199-206, 1976

Majesté, J.C., "Propriétés Viscoélastiques de Polymers Linéaires à Très Large Distribution de Masses Molaires", Thèse de l'Université de Pau et des Pays de l'Adour, 1998

McLeish, T. C. B., Chapter 6 "Topology of Polymers: Entangled Dynamics and Melt Flow", of "Chemical Topology Introduction and Fundamentals" Edited by D. Bonchev and D.H. Rouvray, Gordon and Breach Science Publishers, 1999

Marrucci, G., "Relaxation by Reptation and Tube Enlargement: A Model for Polydisperse Polymers", J. Polym. Sci., Polym. Phys. Ed. 23, 159-177, 1985

Mead, D.W., T.J. Van Dyke, R.G. Larson, M. Doi, Private communication, 1997

Milner, S.T., T.C. B. McLeish, "Parameter-Free Theory for Stress Relaxation in Star Polymer Melts", Macromolecules, 30, 2159-2166, 1997

Milner, S. T., T. C. B. McLeish, "Reptation and Contour-Length Fluctuations in Melts of Linear Polymers", Phys. Rev. Lett., 81, 725-728, 1998

Montfort, J.P., G. Marin, P. Monge, "Effects of Constraint Release on the Dynamics of Entangled Linear Polymer Melts", Macromolecules, 17, 1551-1560, 1984

Montfort, J.P., G. Marin, P. Monge, "Molecular Weight Distribution Dependence of the Viscoelastic Properties of Linear Polymers: The Coupling of Reptation and Tube-Renewal Effects", Macromolecules, 19, 1979, 1986

Moore E. P., Jr., Polypropylene Handbook, Hanser/Gardner Publications, 1996

Mourey, T. H., S. T. Balke, ACS Symp. Ser. 521, 231, 1993

Pattamaprom C., R.G. Larson, T.J. Van Dyke, "Quantitative Predictions of Linear Viscoelastic Rheological Properties of Entangled Polymers", Rheol. Acta, 39, 517-531, 2000

Randall, J.C., "A Review of High Resolution Liquid 13Carbon Nuclear Magnetic Resonance Characterizations of Ethylene-Based Polymers", Rev. Macromol. Chem. Phys., C29(2 & 3), 201-317, 1989

Read, D., T.C.B. McLeish, "Molecular Rheology and Statistics of Long Chain Branched Metallocene-Catalyzed Polyolefins", Macromolecules, 34, 1928-1945, 2001

Robertson C. G., C. M. Roland, C. Paulo and J. E. Puskas, "Linear Viscoelastic Properties of Hyperbranched Polyisobutylene", J. Rheol. 45, 759–772, 2001

Roovers, J., "Melt Rheology of H-Shaped Polystyrenes", Macromolecules, 17, 1196-1200, 1984

Roovers, J., "Encyclopedia of Polymer Science and Engineering", Klingsber, A., J. Muldoon, A. Salvatore, Eds.; Wiley: New York, 2, 478-499, 1985

Rubinstein, M., R. H. Colby, " Self-Consistent Theory of Polydisperse Entangled Polymers: Linear Viscoelasticity of Binary Blends", J. Chem. Phys., 89, 5291-5306, 1988

Saito J., S. Kikukawa, K. Makuuchi, F. Yoshii, "Process for Producing a Modified Polypropylene and a Molded Product" US Patent 5560886, 1996

Shaw, M.T., W.H. Tuminello, "A Closer Look at the MWD-Viscosity Transform", Polym. Eng. Sci, 34, 159, 1994

Shroff, R.N., H. Mavridis, "Long-Chain-Branching Index for Essentially Linear Polyethylenes", Macromolecules, 32, 8454-8464, 1999

Shroff, R.N., H. Mavridis, "Assessment of NMR and Rheology for the Characterization of LCB in Essentially Linear Polyethylenes", Macromolecules, 34, 7362-7367, 2001

Soares, J.B.P., A.E. Hamielec, "Bivariate Chain Length and Long Chain Branching Distribution for Copolymerization of Olefins and Polyolefin Chains Containing Terminal Double-Bonds", Macromol. Theory Simul., 5, 547-572, 1996

Stevens J.C. "Constrained Geometry and Other Single Site Metallocene Polyolefin Catalysts: A Revolution in Olefin Polymerization", 11th international congress on catalysis – 40th anniversary studies in surface science and catalysis, vol. 101, 11-20, 1990

Striegel, A.M., M.R. Krejsa, "Complementarity of Universal Calibration SEC and 13C NMR in Determining the Branching State of Polyethylene", J. of Poly. Sci. Part B: Poly. Phys., 38, 3120-3125, 2000

Tackx, P., J.C.J.F. Tacx, "Chain Architecture of LDPE as a Function of Molar Mass Using Size Exclusion Chromatography and Multi-Angle Laser Light Scattering (SEC-MALLS)", Polymer, 39, 3109-3113, 199

Tobita, H., "Molecular Weight Distribution in Free-Radical Crosslinking Copolymerisation", Macromolecules, 26, 836-841, 1993

Tobita, H., "Random Sampling Technique to Predict the Molecular Weight Distribution in Nonlinear Polymerization", Macromol. Theory and Simul., 5, 1167-1194, 1996

Tobita, H., "Molecular Weight Distribution in Random Crosslinking of Polymers: Modality of the Molecular Weight Distribution", Macromol. Theory Simul. 3, 1033-1049, 1994

Tobita, H., "Molecular Weight Distribution in Random Crosslinking of Polymer Chains", J. Polymer Science: Part B: Polymer Physics, 33, 1191-1202, 1995

Tobita, H., "Molecular Weight Distribution Formed Through Chain-Length-Dependent Crosslinking Reactions", Macromol. Theory Simul., 7, 225-232, 1998

Tsenoglou, C., "Molecular Weight Polydispersity Effects on the Viscoelasticity of Entangled Linear Polymers", Macromolecules, 24, 1761-1767, 1991

Tsenoglou, C.J., A.D. Gotsis, "Rheological Characterization of Long Chain Branching in a Melt of Evolving Molecular Architecture", Macromolecules, 34, 4685-4687, 2001

Vega, J.F., A. Santamaria, A. Munoz-Escalona, P. Lafuente, "Small-Amplitude Oscillatory Shear Flow Measurements as a Tool to Detect Very Low Amounts of Long Chain Branching in Polyethylenes", Macromolecules, 31, 3639-3647, 1998

Viovy, J.L., "Tube Relaxation: A Quantitative Molecular Model for the Viscoelastic Plateau of Entangled Polymeric Media", J.Polym. Sci., Polym. Phys. Ed. 23, 2423-2442, 1985

Wang X., C. Tzoganakis, G.L. Rempel, "Chemical Modification of Polypropylene with Peroxide/Pentaerythritol Triacrylate by Reactive Extrusion", J. Appl. Polym. Sci., 61, 1395-1404, 1996

Wasserman, S.H., W.W. Graessley, "Effects of Polydispersity on Linear Viscoelasticity in Entangled Polymer Melts", J. Rheol., 36, 543-572, 1992

Weng W., W. Hu, A.H. Dekmezian, C.J. Ruff, "Long Chain Branched Isotactic Polypropylene", Macromolecules, 35, 3838-3843, 2002

Wilmes G. M., L. Shirley, R. M. Waymouth, "Propylene Polymerization with Sterically Hindered Unbridged 2-Arylindene Metallocenes", Macromolecules, 35, 5382-5387, 2002

Wood-Adams, P.M., J.M. Dealy, A.M. deGroot, O.D. Redwine, "Effect of Molecular Structure on the Linear Viscoelastic Behavior of Polytheylene", Macromolecules, 33, 7489-7499, 2000

Wood-Adams, P., J.M. Dealy, " Using Rheological Data to Determine the Branching Level in Metallocene Polyethylenes", Macromolecules, 33, 7481-7488, 2000

Wood-Adams, P., S. Costeux, "Thermorheological Behavior of Polyethylene: Effects of Microstructure and Long Chain Branching", Macromolecules, 34, 6281-6290, 2001

Yan, D., W. J. Wang, S. Zhu, "Effect of Long-Chain Branching on Rheological Properties of Metallocene Polyethylene", Polymer, 40, 1737-1744, 1999

Yu Q., S. Zhu, "Peroxide Crosslinking of Isotactic and Syndiotactic Polypropylene", Polymer, 40, 2961-2968, 1999

Zimm, B.H, W.H. Stockmayer, "The Dimensions of Chain Molecules Containing Branches and Rings", J. Chem. Phys., 17, 1301-1314, 1949

Zimm, B.H., R.W. Kilb, "Dynamics of Branched Polymer Molecules in Dilute Solution", J. Polymer Sci. 37, 19-42, 1959

Appendix A. Differential Scanning Calorimetry Results

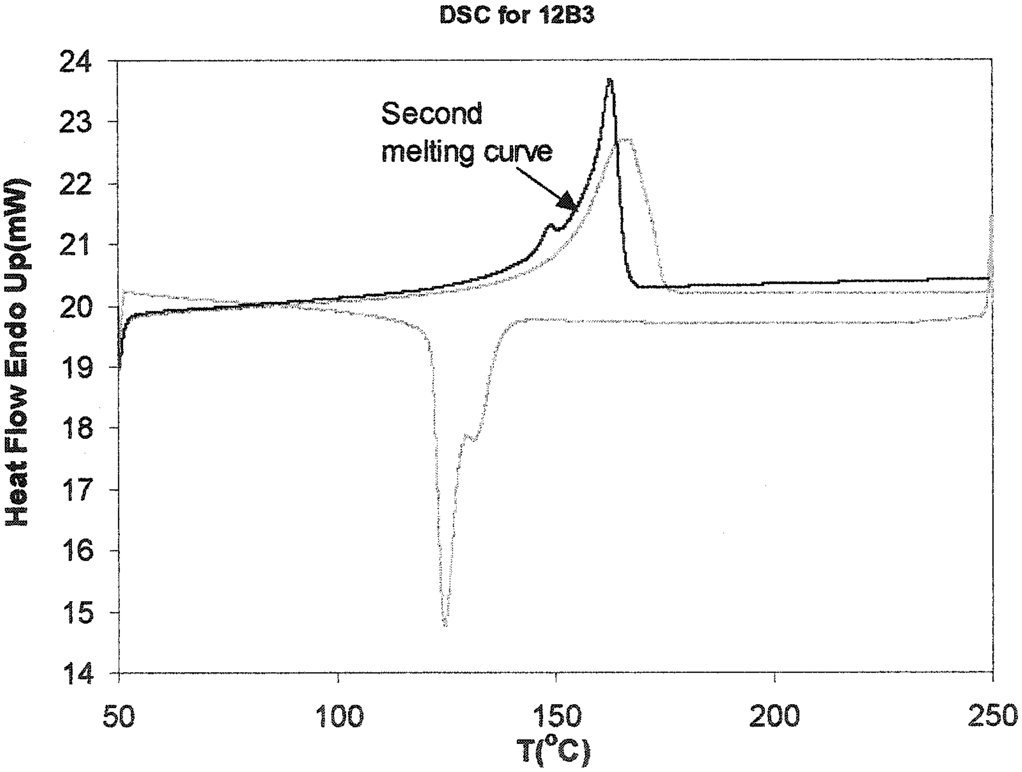

Appendix B: Determine Molecular Weight Corresponding to A Random Number From Cumulative Molecular Weight Distribution Curve

In order to create a large number of chains with the same molecular weight distribution as that of the linear precursor, we make use of the cumulative molecular weight distribution curve of the linear precursor. For example the cumulative molecular weight distribution of 35L is shown in Fig. D-1. The cumulative number fraction *CNM* is in the range between 0 and 1. If we choose a random number R falling in the same range, we can find a corresponding value of chain length X_R by using an iterative technique. The molecular weight of the chain is the chain length multiplied by monomer molecular weight. The technique involves the comparison of *R* and the *CNM* value in the middle of searching chain length range *CNM(mid)*.

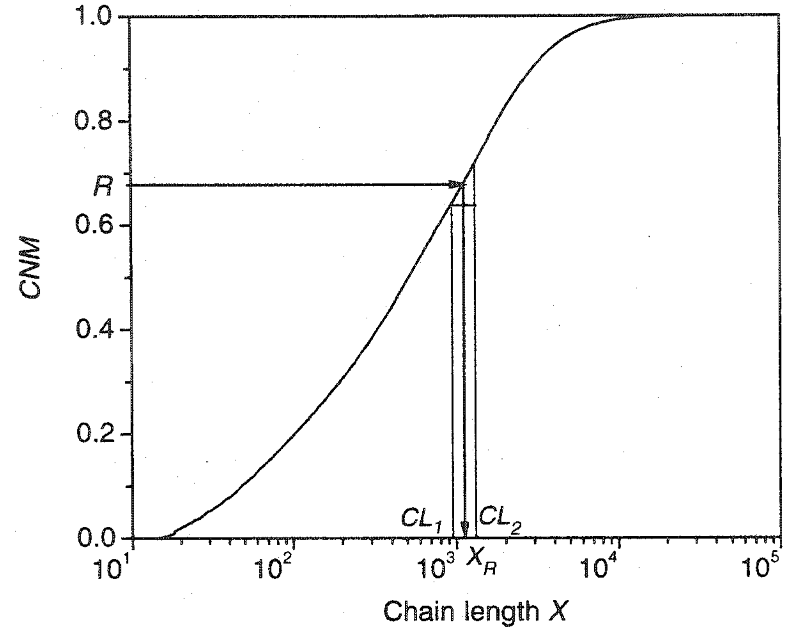

Figure Appendix B-0-1: Cumulative number molecular weight distribution *CNM* along chain length *X* for linear polypropylene sample 35L

First we search in the whole range and assign CL_1 corresponding to *CNM*=0 and CL_2 corresponding to *CNM*=1. The chain length value in the middle of searching range is $CL(mid)=(CL_1+CL_2)/2$, from the cumulative molecular weight distribution curve, we can find the cumulative molecular weight *CNM(mid)* corresponding to *CL(mid)*. Compare *CNM(mid)* with *R*, if *R*> *CNM(mid)*, renew CL_1 value with *CNM(mid)*, otherwise renew CL_2 value with *CNM(mid)*. By doing so, we narrow the searching range of chain length. In the defined new range, calculate the new *CL(mid)* and compare the corresponding *CNM(mid)* with *R* again. This procedure is repeated until the difference between CL_2 and CL_1 equals 1. Thus the chain length corresponding to *R* can be determined as:

$$X_R = CL_1 + \frac{R - CNF_1}{CNF_2 - CNF_1} \times (CL_2 - CL_1) + 0.5 \qquad \text{(B-1)}$$

The additional 0.5 is used to round the X_R value to the closest integer number.

Nomenclature

α	the number of branch points per precursor chain
α_{nom}	the nominal number of branch points per precursor chain
β	the average number of branch points per molecule
c	the concentration of the solution
CNM	the cumulative number distribution
CTA	chain transfer agent
D^{+}	a saturated dead chain,
$D^{=}$	a vinyl-terminated dead chain
D_i	the curvilinear diffusion coefficient
ε	the Debye-Bueche viscosity shielding constant
E_{bran}	the branching efficiency
f_{aw}	the weight fraction of free arms
f_{iw}	the weight fraction of inner backbones
$F(t,M)$	kernel function describing the relaxation behavior of a monodisperse species of molecular weight M
$\phi(t)$	the average survival probability of the chains
$\phi'(t)$	the average survival probability of the constraints surrounding a chain
$\phi_i(t)$	the survival probability of chain i at time t
g	the ratio of the mean-square radius of gyration of the branched molecule to that of a linear molecule having the same molecular weight
$\langle g_3 \rangle_w$	the weight average g ratios for branch functionalities of 3

g'	the ratio of the intrinsic viscosities of the branched molecule to that of a linear molecule having the same molecular weight
$G(t)$	the relaxation modulus
$G'(t)$	the storage modulus
$G''(t)$	the loss modulus
$G^*(t)$	the complex modulus
G_N^0	the plateau modulus
$[\eta]$	the intrinsic viscosity
η_1	the viscosities of the pure solvent
$\eta_{1,2}$	the viscosities of the solution
η_0	the zero-shear viscosities
η^*	the complex viscosity
$\left\|\eta^*\right\|$	the absolute value of the complex viscosity
H	the continuous relaxation spectrum
$J(t)$	shear creep compliance,
J_s^0	steady-state compliance
J'	the storage compliance
J''	the loss compliance
$J^*(\omega)$	the complex compliance
$J_r(t)$	recoverable compliance
J_g	the instantaneous compliance
k_b	number of branch points in a chain
k_{ce}	the rate coefficient for the crosslinking reaction
L	the continuous retardation spectrum
L_i	the averaged contour length of the tube
λ	the number of branch points per 1000 carbons

λ_{reg}	regularization parameter
M_c	the critical entanglement molecular weight
M_e	the molecular weight between entanglement points
M_w	weight average molecular weight,
M_n	number average molecular weight
M_z	z-average molecular weight
M_0	the monomer molecular weight
M_{min}	the low limiting molecular weights of the molecular weight distribution
M_{max}	the high limiting molecular weights of the molecular weight distribution
M_n^0	the number average molecular weight of the linear precursor
M_w^0	the weight average molecular weight of the linear precursor
M_b	the average molecular weight between a branch point and its adjacent vertexes
M_{wl}	the weight average molecular weight of the linear species of the branched polymers
n_w	the weight average number of branch points per molecule
N	the number of monomers per chain,
N_e	the number of monomers between two successive entanglement points
$N_{en,i}$	the number of entanglements of chain i
$N_p(r)$	number fraction of segments with length r
ω	frequency
PDI	the polydispersity index
PDI^0	the polydispersity index of the linear precursor
P_r	a living chain of polymerization degree r with active catalyst attached at one end
$\overline{P}_{np}$	the number average length of segments
$\overline{P}_w$	the weight average chain length
$\overline{P}_{wp}$	the weight average chain length of the linear precursor

ρ	the crosslinking density
$\overline{P}_n$	the number-average chain length
$\overline{P}_{np}$	the number-average chain length of the linear precursor
$\langle R_g^2 \rangle$	the mean-square radius of gyration
γ_0	a small step strain
γ_r	recoil strain
s_i	contour length
T	temperature
τ	relaxation time
$\tau_d(M)$	the longest relaxation time of the chain having molecular weight M
τ_{mon}	an elementary monomer time scale
$\tau_{\xi,i}$	the time constant for contour length fluctuations
$\tau_{R,i}$	the longest Rouse relaxation time of chain i
τ_e	the characteristic Rouse relaxation time of an entanglement segment
τ_t	tube renewal time
$\langle \tau_{obs} \rangle$	the average lifetime of a constraint
σ_0	a small step stress
τ_0	elementary relaxation time
τ_a	the first peak location of relaxation spectrum corresponding to the relaxation of free arms,
τ_i	the second peak location of relaxation spectrum corresponding to the relaxation of inner backbones
ϑ	a parameter governing the narrowness of the distribution
θ	a constant that represents the degree of chain-length dependence
$U_{eff}(s,t)$	the effective activation energy for chain fluctuation
χ	a mixing exponent in relaxation modulus based on reptation concept